

Air Force Institute of Technology

AFIT Scholar

Theses and Dissertations

Student Graduate Works

3-2006

Evaluation of Factors Contributing to Damping of Coated and Uncoated Titanium Plates

Dustin W. Lee

Follow this and additional works at: <https://scholar.afit.edu/etd>



Part of the [Aerospace Engineering Commons](#), and the [Mechanics of Materials Commons](#)

Recommended Citation

Lee, Dustin W., "Evaluation of Factors Contributing to Damping of Coated and Uncoated Titanium Plates" (2006). *Theses and Dissertations*. 3520.

<https://scholar.afit.edu/etd/3520>

This Thesis is brought to you for free and open access by the Student Graduate Works at AFIT Scholar. It has been accepted for inclusion in Theses and Dissertations by an authorized administrator of AFIT Scholar. For more information, please contact AFIT.ENWL.Repository@us.af.mil.



**EVALUATION OF FACTORS CONTRIBUTING TO DAMPING
OF COATED AND UNCOATED TITANIUM PLATES**

THESIS

Dustin W. Lee, Second Lieutenant, USAF
AFIT/GA/ENY/06-M06

DEPARTMENT OF THE AIR FORCE
AIR UNIVERSITY

AIR FORCE INSTITUTE OF TECHNOLOGY

Wright-Patterson Air Force Base, Ohio

APPROVED FOR PUBLIC RELEASE; DISTRIBUTION UNLIMITED

The views expressed in this thesis are those of the author and do not reflect the official policy or position of the United States Air Force, Department of Defense, or the United States Government.

AFIT/GA/ENY/06-M06

EVALUATION OF FACTORS CONTRIBUTING TO DAMPING
OF COATED AND UNCOATED TITANIUM PLATES

THESIS

Presented to the Faculty

Department of Aeronautics and Astronautics

Graduate School of Engineering and Management

Air Force Institute of Technology

Air University

Air Education and Training Command

In Partial Fulfillment of the Requirements for the
Degree of Master of Science in Astronautical Engineering

Dustin W. Lee, BS

Lieutenant, USAF

March 2006

APPROVED FOR PUBLIC RELEASE; DISTRIBUTION UNLIMITED

EVALUATION OF FACTORS CONTRIBUTING TO DAMPING
OF COATED AND UNCOATED TITANIUM PLATES

Dustin W. Lee, BS
Lieutenant, USAF

Approved:

Prof. Anthony N. Palazotto (Chairman)

date

Dr. Richard Cobb (Member)

date

Dr. Tommy George (Member)

date

Abstract

High Cycle Fatigue (HCF) is the leading cause of component failure in gas turbine engines today, which poses great risk to aircraft, engines, and their crews. Mitigation of HCF effects has become a priority topic, and the damping benefits of hard coatings are being reevaluated for this purpose. Research was conducted to further understanding of damping measurements on these coatings.

This study continues work to characterize the damping effects of a magnesium aluminate spinel (mag spinel) coating applied to a titanium plate via vibration testing. Two different plate sizes were evaluated in a clamped-free-free-free condition and a free-free-free-free condition, respectively. In both the clamped and free studies, the second bending and two-stripe mode shapes were identified and studied. Clamped specimens were tested in order to determine various factors affecting damping. Using these factors, it was shown that air damping has a statistically significant impact on damping, where the impact is dependent on mode shape. The amount of damping introduced by the air was, however, minute compared to the losses introduced by the constraint blocks. Testing on free condition specimens explored another possible method to obtain a damping comparison between coated and uncoated samples with fewer damping losses.

Acknowledgments

When I started working on this thesis, I didn't have a clue how to begin. I was an aspiring astro major who knew a lot about orbits, but very little about titanium plates. Dr. Palazotto, you showed incredible patience and skill in helping me throughout this project. I feel I have learned a great deal about the topic, and without your assistance it would not have been possible. You were a constant source of encouragement and reassurance.

I also owe a great debt of gratitude to everyone in the TEFF lab. The guidance and advice of Dr. Tommy George, Dr. Brian Runyon, Dr. Herman Shen, John Justice, and Angie Smith was absolutely invaluable. If I had this project to do again, I would chose to work with you all again in a heartbeat. Your friendship made this project enjoyable, and I couldn't help but feel, throughout this project, that having an entire lab willing to lend a hand gave me a tremendous advantage in both learning the material and performing the experiments.

I would like to thank my family and friends for their support as well. Life would have been much tougher if I couldn't run over to my parents' to relax, and possibly steal some leftovers from the fridge. Movie Night with my friends was always a highlight, and our amity made the AFIT experience something which I will always think of fondly.

Table of Contents

	Page
Abstract.....	iv
Acknowledgments	v
List of Figures.....	viii
List of Tables	xiv
I: Introduction	1
Fatigue	1
Damping	2
Mag Spinel Coating.....	4
Damping Factors, Considerations, and Mechanisms.....	6
Air Damping.....	7
Damping Characterization and Comparison.....	9
Strain Relationships	12
Related Work	16
Objective of Thesis.....	20
General Approach.....	21
II: Finite Element Analysis for Samples and Baseplate Re-Design	27
Test Specimens	27
Finite Element Analysis.....	31
Titanium Plate Modeling	32
Modal Verification.....	39
Baseplate Re-Design.....	43
Baseplate Finite Element Analysis	45
Clamping Fixture and Pressure Vessel Concerns.....	55
III: Test Set-Up and Procedures.....	58
Electrodynamic Shaker Testing of Cantilevered Set-Up.....	59
Clamping Fixture	63
Data Collection Location	65
Initial Repeatability Testing.....	66
Single Clamping Repeatability Testing	69
Constraint Block Movement Testing.....	70
Temperature Effect and Repeatability Testing	72
Accelerometer Location and Bungee Cord Testing.....	74
Ping Testing	78
Analysis of Variance (ANOVA).....	80
ANOVA Testing.....	82

	Page
Air Horn Testing of Free-Free-Free-Free Condition Set-Up.....	92
Free Condition Mounting Fixture.....	94
Symmetric Data Collection Locations.....	96
Damping Evaluation Testing.....	98
IV: Results and Discussion.....	102
Electrodynamic Shaker Testing Results.....	103
Initial Repeatability Testing Results.....	103
Single Clamping Repeatability Testing Results.....	115
Constraint Block Movement Testing Results.....	121
Temperature Effect and Repeatability Testing Results.....	133
Accelerometer Location and Bungee Cord Testing Results.....	155
Ping Testing Results.....	161
ANOVA Testing Results.....	165
Conventional Analysis of ANOVA Testing Results.....	186
Air Horn Testing of Free-Free-Free-Free Condition Results.....	192
Damping Evaluation Testing Results.....	193
V: Conclusions and Recommendations.....	202
Conclusions.....	202
Recommendations.....	206
Appendix A: ANOVA Theory.....	209
Appendix B: Peak Frequency Plots from Air Pressure Testing.....	229
Appendix C: Combined Coated and Uncoated Plots from Air Pressure Testing.....	231
Appendix D: Typical Response Plots from ANOVA Testing.....	232
Appendix E: Data from ANOVA Testing with Strain Error.....	234
Appendix F: Comparison of Strain Calculation Techniques.....	236
Appendix G: Additional Ping Testing Results.....	238
Bibliography.....	239
Vita.....	242

List of Figures

Figure	Page
Figure 1. Half-Power Bandwidth Method (13).....	10
Figure 2. Previous Set-Up Showing Old Baseplate [adapted from (2)]	23
Figure 3. 4.5” x 4.5” x 0.125 Ti Test Specimen (2).....	25
Figure 4. 9” x 4.5” x 0.125” Ti Specimen [adapted from (2)].....	26
Figure 5. Uncoated (Left) and Coated (Right) Ti-6Al-4V 4.5” x 4.5” x 0.125” Specimens	29
Figure 6. Uncoated (Left) and Coated (Right) Ti-6Al-4V 9” x 4.5” x 0.125” Specimens	30
Figure 7. Solid45 Element	33
Figure 8. Predicted Mode Shapes for Cantilevered Sample	35
Figure 9. Predicted Mode Shapes for Free Sample (continued from previous page).....	37
Figure 10. Mode Shape Comparison between Sample Sizes.....	38
Figure 11. Predicted vs. Experimental Mode Shape Comparison for Free Samples.....	42
Figure 12. Original 1” Thick Aluminum Baseplate.....	43
Figure 13. Orthogonal and Side View of Mesh Pattern.....	45
Figure 14. FEA Results for 1” Aluminum Baseplate with Constraint Blocks.....	47
Figure 15. FEA Results for Aluminum and Steel Baseplates with Constraint Blocks...	49
Figure 16. New 2.5” Thick Aluminum Baseplate, no Constraint Blocks.....	51
Figure 17. FEA Results for 2.5” Aluminum Baseplate on 6,000 lbf Shaker	52
Figure 18. Side View of Pressure Vessel Support on Both Shaker Tables.....	53
Figure 19. New Wires Providing Data from Inside Pressure Vessel.....	56
Figure 20. Overall Experimental Design	59

	Page
Figure 21. Basic Diagram of Shaker Table Operation.....	61
Figure 22. Constraint Blocks with Bolts Labeled (2)	63
Figure 23. Laser Vibrometer Data Collection Location on Specimen (2).....	65
Figure 24. Clamp Movement Testing Laser Locations	71
Figure 25. Window in Top of Pressure Vessel	76
Figure 26. Ping Hammer.....	79
Figure 27. Vacuum Pump and Pressure Gauge	83
Figure 28. Experimental Set-Up on 18k lbf Shaker.....	83
Figure 29. Test Set-Up for Coated and Uncoated Free Samples	94
Figure 30. Symmetric Measurement Locations on Free Sample.....	97
Figure 31. Laser Plane Point Locations on Free Sample	98
Figure 32. Laser Scanning Each Point on Sample.....	99
Figure 33. Damping vs. Sample Strain, Mode 3 1g 18k Shaker.....	105
Figure 34. Damping vs. Sample Strain, Mode 4 1g 18k Shaker.....	107
Figure 35. Damping vs. Sample Strain, Mode 3 8g 18k Shaker.....	108
Figure 36. Damping vs. Sample Strain, Mode 4 8g 18k Shaker.....	108
Figure 37. Damping vs. Sample Strain, Mode 3 1g 6k Shaker.....	111
Figure 38. Damping vs. Sample Strain, Mode 4 1g 6k Shaker.....	112
Figure 39. Damping vs. Sample Strain, Mode 3 4g 6k Shaker.....	112
Figure 40. Damping vs. Sample Strain, Mode 4 4g 6k Shaker.....	113
Figure 41. Q Value versus Run Order, mode 4 1g.....	117
Figure 42. Q Value versus Run Order, mode 4 4g.....	117
Figure 43. Q Value versus Run Order, mode 3 1g.....	118

	Page
Figure 44. Q Value versus Run Order with Cooling Time, mode 4 1g	119
Figure 45. Q Value versus Run Order with Cooling Time, mode 4 4g	120
Figure 46. Q Value versus Run Order with Cooling Time, mode 3 1g	120
Figure 47. Jack Bolts vs. No Jack Bolts at Sample– 1st Clamping, Mode 3	123
Figure 48. Jack Bolts vs. No Jack Bolts at Blocks– 1st Clamping, Mode 3	123
Figure 49. Jack Bolts vs. No Jack Bolts at Sample– 1st Clamping, Mode 4	125
Figure 50. Jack Bolts vs. No Jack Bolts at Blocks– 1st Clamping, Mode 4	125
Figure 51. Jack Bolts vs. No Jack Bolts at Sample–2nd Clamping, Mode 3	127
Figure 52. Jack Bolts vs. No Jack Bolts at Blocks– 2nd Clamping, Mode 3	127
Figure 53. Jack Bolts vs. No Jack Bolts at Sample– 2nd Clamping, Mode 4	128
Figure 54. Jack Bolts vs. No Jack Bolts at Blocks– 2nd Clamping, Mode 4	129
Figure 55. Jack Bolts vs. No Jack Bolts at Sample– 3rd Clamping, Mode 3	130
Figure 56. Jack Bolts vs. No Jack Bolts at Blocks– 3rd Clamping, Mode 3	130
Figure 57. Jack Bolts vs. No Jack Bolts at Sample– 3rd Clamping, Mode 4	132
Figure 58. Jack Bolts vs. No Jack Bolts at Blocks– 3rd Clamping, Mode 4	132
Figure 59. Temperature vs. Q Value, Multi-Clamping, Mode 3, 1g	135
Figure 60. Temperature vs. Velocity, Multi-Clamping, Mode 3, 1g	135
Figure 61. Temperature vs. Q Value, Single Clamping, Mode 3, 1g	136
Figure 62. Temperature vs. Velocity, Single Clamping, Mode 3, 1g	136
Figure 63. Strain vs. Q Value, Single Clamping, Mode 3, 1g	137
Figure 64. Temperature vs. Q Value, Multi-Clamping, Mode 3, 4g	138
Figure 65. Temperature vs. Velocity, Multi-Clamping, Mode 3, 4g	139
Figure 66. Temperature vs. Q Value, Single Clamping, Mode 3, 4g	139

	Page
Figure 67. Temperature vs. Velocity, Single Clamping, Mode 3, 4g	140
Figure 68. Strain vs. Q Value, Single Clamping, Mode 3, 4g	141
Figure 69. Temperature vs. Q Value, Multi-Clamping, Mode 4, 1g	142
Figure 70. Temperature vs. Velocity, Multi-Clamping, Mode 4, 1g	142
Figure 71. Temperature vs. Q Value, Single Clamping, Mode 4, 1g	143
Figure 72. Temperature vs. Velocity, Single Clamping, Mode 4, 1g	143
Figure 73. Strain vs. Q Value, Single Clamping, Mode 4, 1g	144
Figure 74. Temperature vs. Q Value, Multi-Clamping, Mode 4, 4g	145
Figure 75. Temperature vs. Velocity, Multi-Clamping, Mode 4, 4g	146
Figure 76. Temperature vs. Q Value, Single Clamping, Mode 4, 4g	146
Figure 77. Temperature vs. Velocity, Single Clamping, Mode 4, 4g	147
Figure 78. Strain vs. Q Value, Single Clamping, Mode 4, 4g	147
Figure 79. Sine Sweep Results for Various Temperature Changes	149
Figure 80. Comparison of Rescaled Temperature Change Sweep Results	150
Figure 81. Comparison of Linearity in Sweep Results	150
Figure 82. ΔT vs. Q value for Mode 4, 4g with Trend Line	151
Figure 83. ΔT vs. Q value for Mode 3, 1g with Trend Line	151
Figure 84. Temperature vs. Run on 3 November	153
Figure 85. Temperature vs. Run on 8 November	153
Figure 86. Pressure Vessel Handle Sine Sweep Response	159
Figure 87. Ping Testing Between Constraint Blocks and Baseplate	163
Figure 88. Ping Testing Between Pressure Vessel Window and Baseplate	164
Figure 89. Ping Testing Between Pressure Vessel Handle and Baseplate	165

	Page
Figure 90. Ishikawa Diagram of Factors Affecting Damping	166
Figure 91. Uncoated Sample ANOVA Design and Response	169
Figure 92. Uncoated Sample Normal Plot of Residuals	171
Figure 93. Uncoated Sample Residuals vs. Predicted and Residuals vs. Run	172
Figure 94. Coated Sample Half Normal Plot	174
Figure 95. Coated Sample Normal Plot of Residuals	175
Figure 96. Coated Sample Residuals vs. Predicted and Residuals vs. Run	176
Figure 97. Coated Sample Mode 4 Experiment Design and Response	177
Figure 98. Coated Sample Mode 4 Experiment Half Normal Plot	177
Figure 99. Coated Sample Mode 4 Experiment Diagnostic Plots	179
Figure 100. Coated Sample Mode 4 Experiment (New Strain Levels) Half Normal Plot	180
Figure 101. Coated Sample Mode 4 Experiment (New Strain Levels) Diagnostic Plots	182
Figure 102. Coated Sample Mode 3 Experiment (New Strain Levels) Half Normal Plot	183
Figure 103. Coated Sample Mode 3 Experiment (New Strain Levels) Diagnostic Plots	185
Figure 104. Uncoated Sample Mode 3 Damping at two Pressure Levels	187
Figure 105. Uncoated Sample Mode 4 Damping at two Pressure Levels	188
Figure 106. Coated Sample Mode 3 Damping at two Pressure Levels	189
Figure 107. Coated Sample Mode 4 Damping at two Pressure Levels	190
Figure 108. Rigid Body Effect in Uncoated Free Condition Sample	194
Figure 109. Rigid Body Effect in Coated Free Condition Sample	195
Figure 110. Example Experimental Result for Uncoated Sample, Mode 7	196

	Page
Figure 111. Free Condition Damping Results, Mode 4	196
Figure 112. Free Condition Damping Results, Mode 7	197
Figure 113. Free Condition Damping Results, Coated Sample, Mode 4.....	198
Figure 114. Free Condition Damping Results, Coated Sample, Mode 7.....	198
Figure 115. Free Condition Damping Results, Coated Sample, Mode 4, Color Coded	200
Figure 116. Free Condition Damping Results, Coated Sample, Mode 7, Color Coded	200

List of Tables

Table	Page
Table 1. Thickness Measurements of Ti-6Al-4V Specimens	31
Table 2. Material Properties for Ti-6Al-4V (12)	33
Table 3. Predicted Frequencies for Cantilevered Sample	34
Table 4. Predicted Frequencies for Free Sample	36
Table 5. FEA Derived Max Strain/Displacement Relationships	39
Table 6. FEA Predicted vs. Experimental Frequencies for Coated Free Sample	41
Table 7. FEA Predicted vs. Experimental Frequencies for Uncoated Free Sample	41
Table 8. Predicted Frequencies for 1” Aluminum Baseplate with Constraint Blocks.....	47
Table 9. Predicted Frequencies for Aluminum and Steel Baseplates with Constraint Blocks	50
Table 10. Predicted Frequencies for 2.5” Baseplate on 6,000lbf Shaker	52
Table 11. Settings and Test Sequence for Repeatability Testing Clampings	68
Table 12. Clamp Movement Testing Sequence and Settings	72
Table 13. Temperature Repeatability Testing Sequence and Settings.....	74
Table 14. Factors and Settings for ANOVA Testing	86
Table 17. ANOVA Experiment Design for Uncoated Sample	87
Table 18. ANOVA Experiment Design for Coated Sample	88
Table 19. Modified Factors for Additional Testing Mode 4, Coated	89
Table 20. Experiment Design for Additional Testing Mode 4, Coated	89
Table 21. Modified Factors for Additional Strain Testing Mode 4, Coated.....	90
Table 22. Experiment Design for Additional Strain Testing Mode 4, Coated	90

	Page
Table 23. Experiment Design for Additional Strain Testing Mode 3, Coated	91
Table 24. Settings Used for Free Condition Experiment	100
Table 25. Runs Completed for Free Condition Experiment	100
Table 26. Repeatability Results, Mode 3 1g 18k Shaker	105
Table 27. Repeatability Results, Mode 4 1g 18k Shaker	107
Table 28. Repeatability Results, Mode 3 8g 18k Shaker	107
Table 29. Repeatability Results, Mode 4 8g 18k Shaker	108
Table 30. Overall Variation Comparison, 18k Shaker	109
Table 31. Repeatability Results, Mode 3 1g 6k Shaker	111
Table 32. Repeatability Results, Mode 4 1g 6k Shaker	111
Table 33. Repeatability Results, Mode 3 4g 6k Shaker	112
Table 34. Repeatability Results, Mode 4 4g 6k Shaker	113
Table 35. Overall Variation Comparison, 6k Shaker	114
Table 36. Like Runs With and Without Bungee Cords	157
Table 37. Like Runs With and Without Bungee Cords	158
Table 38. Uncoated Sample ANOVA Design and Response	168
Table 39. Uncoated Sample ANOVA Table	170
Table 40. Coated Sample ANOVA Design and Response	173
Table 41. Coated Sample ANOVA Table	175
Table 42. Coated Sample Mode 4 Experiment ANOVA Table	178
Table 43. Coated Sample Mode 4 Experiment (New Strain Levels) Design and Response	179
Table 44. Coated Sample Mode 4 Experiment (New Strain Levels) ANOVA Table ...	181

	Page
Table 45. Coated Sample Mode 3 Experiment (New Strain Levels) Design and Response	182
Table 46. Coated Sample Mode 3 Experiment (New Strain Levels) ANOVA Table ...	184

EVALUATION OF FACTORS CONTRIBUTING TO DAMPING OF COATED AND UNCOATED TITANIUM PLATES

I: Introduction

Fatigue

High Cycle Fatigue (HCF) is the leading cause of failure for all modern gas turbine engines (6). HCF failures are not limited to any particular engine component or manufacturer, and a single failure can destroy an engine or an entire aircraft. HCF has, in fact, resulted in the loss of aircraft and cost billions of dollars in damage over the last two decades. Specifically, it is estimated that up to 50% of all aircraft engine failures can be attributed to HCF, while the U.S. Navy and Air Force spend upwards of \$400 million annually on HCF related problems (8).

Fatigue is typically termed either High Cycle Fatigue or Low Cycle Fatigue (LCF). While LCF was at one time a concern, it has been largely negated due to design requirements which emphasize damage tolerance and a retirement-for-cause philosophy (2). This leaves HCF as the dominant cause of fatigue failure, and a primary source of concern.

The HCF life expectancy of a high energy device, such as the blades within a turbine engine, can be compromised due to adverse vibratory conditions (22). Resonant

responses in the blades, encountered through normal engine operations, will eventually lead to HCF if they impart sufficient strain levels. For example, resonant responses in blades can occur in a non-uniform flow field operating environment, where unsteady aerodynamic loading causes an excitation frequency which is coincident with a blade's natural frequency (21). The sources of excitation leading to HCF are generally placed into one of three categories: aerodynamic excitation, airfoil flutter, and acoustic excitation (6).

Efforts to lessen the effect of HCF by eliminating the causes mentioned above have proven to be impractical (2). Instead, research has focused on attenuating the resonant peaks seen by the engine blades via damping, in hopes of greatly increasing the operational lifespan of these blades. In aircraft engines, even a small amount of damping can have a pronounced effect, so this is a very real possibility (4).

Moving beyond this scope, the HCF life of any high energy device can be compromised by adverse vibratory conditions (22). Therefore, a method by which these vibrations can be attenuated has implications which stretch out far beyond turbine engines. For example, high cycle fatigue is a consideration when designing space systems (29). Technology derived today could some day help to attenuate unwanted resonant movement on spacecraft (9).

Damping

Damping is the conversion of mechanical energy into heat (7). In the case of turbine engine blades, this conversion translates into attenuated oscillation of the blade when undergoing resonance. This reduced movement, in turn, leads to a lower

accumulation of damage to the structure over time and an attenuation of the HCF problem.

Damping can be achieved through passive or active means, as well as through hybrid techniques. Damping is typically determined through experimentation, as it has proven more difficult to arrive at accurate measurements through analytical techniques (2). Even through experimentation, however, damping is often a difficult quantity to measure (7). Damping measurements can be taken in any of three general ways: measuring how damping conditions limit the amplitude of peak resonance, directly measuring energy absorbed, and measuring reductions in structural vibrations (7).

These damping measurement techniques may not be applicable, depending on the experiment being performed. In the case of this study, higher modes of flat plates are being observed. Directly measuring the energy absorbed is not feasible. Measuring reductions in structural vibrations can be extremely effective technique at dominant modes, but is extremely difficult at higher modes which quickly damp out. As such, measuring how damping limits the amplitude of peak resonance is the technique used in this study's plate excitation (2). This is instituted through the half-bandwidth method, which is sometimes referred to as the half-power method.

The reader may be aware that the half-bandwidth method was developed for determining damping in systems which display a linear response. However, it is also useful in the study of nonlinear systems. The response curves used to determine damping in this method allow the experimenter to spot nonlinear behavior and visualize trends in the data. The relative height and width of response curves can still be used to make damping comparisons, even though they lack the symmetry indicative of linear behavior.

Further, sweep direction can be altered due to strain hardening or strain softening in order to reduce the effects on data collection. This technique of measuring damping has been used in previous studies which characterized damping behavior of coated materials (21). Because this study deals with strain softening, down sweeps are used in order to better capture the response.

Mag Spinel Coating

Hard ceramic coatings are applied to the outer surface of a material in order to provide damping. The usefulness of such hard coatings as a passive damping material has been known to engineers for roughly forty years, though it has only recently become an area of great interest within the engineering community (19). This renaissance in interest is due to the fact that ceramic coatings offer several advantages over other damping methods.

Attempts to design around, and thus avoid exciting, the resonant frequencies of turbine engine blades have proven impractical, as the operating envelope of turbine engines necessarily encompasses those frequencies (2). Much work has been done with viscoelastic materials as well, but this approach also has drawbacks.

The term “viscoelastic” is derived from the fact that such a material has both energy dissipating and energy storing properties (28). That is to say, it is both “viscous” and “elastic”. The damping is introduced by the relaxation and subsequent recovery of a polymer network which is deformed by the excitation. As one would suspect, these materials are highly effective dampers, but only over a small temperature and frequency range. Viscoelastics show considerable variation in damping properties as temperature

and frequency are varied (4). Additionally, the addition of viscoelastics and milled cavities to a structure raises durability, as well as cost, concerns (21).

Ceramic coatings have drawbacks of their own, but manage to sidestep the vices of viscoelastics by virtue of being inexpensive, easily applied, and effective over a greater range of temperatures and frequencies. Magnesium aluminate spinel ($\text{MgO}+\text{Al}_2\text{O}_3$) is of particular interest because it has been shown to have a higher intrinsic damping capacity than other ceramic materials (22). Research has also shown that mag spinel's damping characteristics are highly dependent on both strain within the specimen and the mode shape in question. Due to the strain softening it displays, the coating is considered to have nonlinear damping characteristics. This makes the determination of its exact damping properties problematic.

The microstructure of mag spinel applied to a material is similar to a substantial array of parallel plates situated perpendicular to the plane of the substrate (22). The microstructure forms this way because mag spinel coating is applied in layers via an air plasma spray. Plasma spraying provides a stronger coating than many other spray processes and allows materials with high melting points to be applied to a surface (4). The plasma spray works by injecting a powdered coating into a high temperature plasma gas and spraying it at high velocity onto the substrate, where the molten powder then cools and bonds to the surface.

The energy dissipation vehicle within mag spinel is regarded to be internal friction. During testing of greater than 10 million cycles, a performance drop of approximately 15% was seen in mag spinel (22). The reason for this performance drop is believed to be internal friction mechanisms "wearing out." The energy dissipation effect

of mag spinel is also a volume effect, meaning that the unit volume enclosed by the coating dissipates energy according to the local strain level (25). The nonlinear stress distribution within the coating is the source of mag spinel's non-linear behavior (21).

Damping Factors, Considerations, and Mechanisms

In any experiment, it is necessary to understand the environment affecting the test in order to interpret the results. Damping makes this task particularly difficult, as there are a myriad of factors at work which affect the result. Temperature, strain level, mode shape, test apparatus resonant frequencies, air pressure, and the boundary condition are all factors which may have a significant impact on damping. In the case of this study, variations in either the clamped or free boundary condition could be significant. In order to experimentally determine damping, these factors must be monitored or the results will be meaningless. Each of these factors affects the overall damping of the specimen and must be taken into account in some manner. Air pressure is of central significance in this study, and is explained in some detail in the next section.

Beyond these factors, there are other considerations which must be realized. First, the clamped condition may vary every time a sample is reloaded into constraint blocks. This "reclamping" necessarily changes the clamped condition, and thus the damping introduced by the clamp. Similarly, the free condition is highly dependent on the positioning of the excitation device relative to the way the sample is hung. Repositioning the sample forces a repositioning of the excitation device. In the clamped condition, the boundary condition is ideally immobile. In actuality, small movements of the clamp along this boundary may impart some damping.

Strain levels are also important because the effectiveness of both the clamp and the mag spinel coating are strain dependent. Therefore, it is pointless to make comparisons unless the strain values are known. The positioning of the free condition, of course, lacks a clamp and therefore exhibits no strain dependence in the boundary condition.

Temperature is, in the case of this study, an uncontrollable factor which could alter damping through two mechanisms. Temperature changes cause metal to expand or contract, which affects the effectiveness of the clamp. Temperature changes may also alter the ability of the sample to dissipate heat, its dimensions, and its material properties, thus altering damping.

Air pressure, or aerodynamic damping, may introduce damping through an apparent mass effect. The details of air damping are described in the next section, as it is an area of primary interest in this study.

Air Damping

Air damping, as mentioned, is suspected to be a culprit in increasing the damping of a cantilevered plate. Past analytical studies indicate the air damping should be a concern when attempting to determine damping, and it has been suggested that damping values should be determined inside a vacuum environment (2). The idea behind this consideration certainly makes sense. A vibrating plate in air would have its vibration attenuated by that medium. Therefore, the maximum displacement would be reduced, thus reducing the resonant peak and increasing the apparent damping. Since the plate is apparently moving more mass than expected, this effect is sometimes known as apparent

mass damping. It is well known that varying air pressure causes a frequency shift in the response; however, the true effect on damping in plates has proven difficult to show. Factors such as the amplitude of sample oscillation and the geometry of the specimen, logically, should also have an effect (2).

In his related work, Allen discusses five mechanisms by which air damping are thought to occur. These further explore the concept of “apparent mass” and take into account the movement of a medium, friction, and heating. They are: axial-shear, transverse-shear, transverse-displacement, axial-displacement, and flow-induced oscillation (2). It is important to note that these mechanisms are not universally applicable, as they are dependent on the environmental conditions and the specific geometry of the sample. Each of these methods is discussed in detail in Allen’s work.

Several of the damping methods discussed above were not applicable to this study. For example, flow-induced oscillation occurs when a medium, such as air, is moving across the surface of a sample. Depending on the flow conditions, the vibration of the sample may be either reduced or enhanced (2). That is, the movement of the flow field may either supply or remove energy to the sample depending on relative velocity, mode shape, sample geometry, *et cetera*. Flow-induced oscillation is certainly applicable to the purpose of this study (*i.e.* damping in turbine engine blades), but was not a consideration in this study or closely related studies (2). In all cases observed, the medium was considered motionless and this mechanism was, therefore, also a non-issue.

Other methods of air damping do apply to the situation in this study, however. The applicable methods of air damping amount to two possible scenarios. First, traveling pressure waves moving across the sample may impart some measure of damping. These

air waves move both axially and transversely along a boundary layer and dissipate energy. Second, the oscillation of the sample could force air up and down, with the resistance of the air imparting some measure of damping on the sample. In this study, the latter option is considered to be the primary source of air damping.

In discussing pressure waves and air movement, it is important to note that air pressure testing done in this study was performed using a pressure vessel placed over the sample. Therefore, there was another consideration. Pressure waves could reverberate off the side of the pressure vessel, or moving air could be turned back on to the sample, thus further influencing the air damping mechanisms at work.

The study of air damping is important for two reasons. First, it is a potential source of system damping in laboratory study. In order to properly study and characterize damping within a system, factors affecting damping must be understood. Second, changing air pressures, and thus changing air damping, occur in the operational environment. In order to characterize the damping abilities of a material, one must understand how it performs at the various pressures it may encounter when in service (23).

Damping Characterization and Comparison

In this study, total damping between numerous different tests were compared. In order to do this, a method by which to compare damping levels had to be chosen. The logical choice is the half-bandwidth, or half-power, method. As mentioned previously, it is the preeminent method due to its relative simplicity to implement. A log decrement

approach would have been impractical because the modes of interest for this study would damp out too quickly for accurate measurements.

When using the half-bandwidth method, a sine sweep or slow chirp is performed over a frequency range of interest and the response is recorded. This response could be displacement, velocity, or acceleration. The peak amplitude of the resulting curve occurs at the resonant frequency. The amount of damping present is determined based on the bandwidth of the peak at its half-power point. That is, the width of the peak at approximately 0.707 times the peak amplitude, in relation to the resonant frequency, determines damping. This is shown in the figure below.

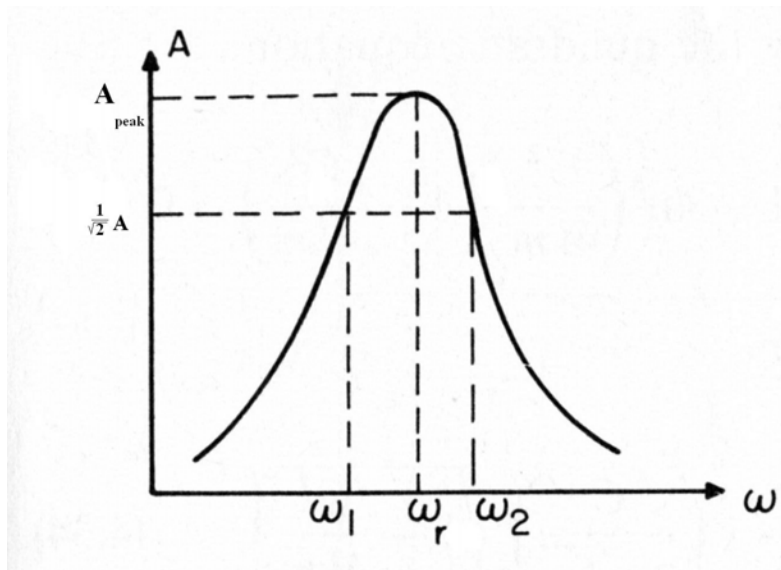


Figure 1. Half-Power Bandwidth Method (13)

The resonant frequency, or peak frequency, is labeled ω_r . The lower and upper frequencies at the half-power mark are annotated by ω_1 and ω_2 , respectively. These values are used to determine the damping ratio, as in the below equation.

$$\zeta = \frac{\Delta\omega}{2\omega_r} \tag{1.1}$$

where

ζ = damping ratio

$\Delta\omega$ = bandwidth ($\omega_2 - \omega_1$)

ω_r = resonant frequency

The quality factor (Q) can trace its lineage to the electrical engineering community. This quality factor, or Q value, is a useful value in expressing the damping present within a system. It is inversely related to the damping ratio, such that as Q value increases the damping ratio decreases. Therefore, a system with a high Q value would have very little damping. A system with a low Q value would be represented by a short, wide resonant peak and thus high damping. The equation for Q value in terms of the damping ratio is shown below.

$$Q = \frac{1}{2\zeta} \quad (1.2)$$

The system loss factor, η , is also commonly used to describe the damping present within a system. It is equal to the inverse of Q, as shown below.

$$\eta = \frac{1}{Q} \quad (1.3)$$

In addition to methods for determining damping, one must also determine a standard method for comparing these values. Throughout this study, all percent differences were defined via the relationship below. For ease of comparison to previous related results, this is the same formulation used by Allen.

$$\% \text{ Diff} = \frac{\text{HighValue} - \text{LowValue}}{\text{HighValue}} * 100\% \quad (1.4)$$

In observing damping, it is also important to keep in mind some fundamentals. For a linearly damped uncoated material, the Q value or damping ratio should remain constant regardless of the force input. That is, the damping properties of such a material do not change due to increases or decreases in the amplitude of the displacement imparted. When materials display nonlinear behavior, such as strain-dependence, it becomes important to track the strain levels in order to make valid comparisons. The strain-dependence issue is discussed throughout this study.

In this study, the second bending and two-stripe modes were observed on all samples. While the sequence in which the modes appear necessarily changes with the sample geometry, they were present in each case. The two-stripe mode shape is also sometimes referred to as “first chord wise.” These particular mode shapes occur within the frequency range of interest for turbine blades currently in service, and were thus of interest for this and related studies. In using these particular mode shapes, the results of this analysis can be more easily compared to previous work and applied to real-world situations.

Strain Relationships

Maximum strain values were used in order to make comparisons between experimental runs in this study. This had to be done due to strain dependence in the mag spinel coating, as well as in the constraint blocks. Variations between runs, due to environmental factors, also necessitated the use of strain as a means of comparison.

Several methods were available for determining strain levels in the samples. The first option was to place strain gauges at the point of maximum strain for each mode. For

the second bending mode, the position of maximum strain was at the specimen root. For the two-stripe mode, this position was instead at the specimen tip. Placement of strain gauges here would have allowed maximum strain to be read and recorded for each run. However, the use of strain gauges would have been intrusive. Attaching a strain gauge on the sample would alter the damping of the sample, and make the task of determining damping sources even more complicated. While the equipment used in this study was capable of supporting strain gauge readings, it was desired to find a more elegant solution to the problem.

The technique chosen instead of a strain gauge involved several steps. First, finite element analysis (FEA) was used to determine a proportional maximum strain/displacement relationship for the samples. The results of an FEA model produced strain and displacement data for all nodes on a modeled sample. By using a tight mesh of data points, strain versus displacement data could be analyzed for virtually any point in the model. These results allowed the experimenter to determine a ratio of maximum strain per inch displacement ratio for the point of interest on the sample. All ratios were double-checked by finding the maximum strain/displacement proportion from each of the calculation methods available within the FEA software. Different strain/displacement proportions were, of course, found for each different sample size and mode of interest.

In the case of this experiment, the point of interest point was always 0.7" from the plate tip and 0.1" from the side of the sample. The strain/displacement proportion was a linear one, with the ratio holding true throughout the linear region for the material in question. The same strain/displacement relationship was used for both the coated and

uncoated samples. This could be done because the samples shared the same mode shapes, and derived their physical properties, in this respect, from an identical material.

The FEA-derived proportional relationship between maximum strain and the displacement of the point of interest, for each sample and mode, was then applied to experimental data. The FEA program delivered this ratio using arbitrarily scaled values, and the original units were in terms of strain per inch. This was converted to a more useful proportion, in terms of microstrain per millimeter of displacement.

A laser vibrometer was used throughout the experiment. This vibrometer returned the velocity measured at the point of interest on the sample in millimeters per second. In order to apply the maximum strain/displacement proportion, the displacement experienced by the sample had to be determined from this velocity. This was done via the equation below, which simply relates the observed sample peak velocity, at the corresponding peak frequency, to the peak displacement. For all testing with cantilevered samples in this experiment, displacement had to be calculated after testing in this manner. The software used was incapable of converting a velocity curve into a displacement curve. In testing with samples in a free condition, computer software was able to make the displacement calculations.

$$\delta_{Peak} = \frac{V_{Peak}}{2\pi f_{Peak}} \quad (1.5)$$

where

δ = displacement

v = measured velocity

f = frequency, in 1/sec (or cycles/sec, or Hertz)

One can see from the equation above that the maximum displacement experienced by a sample will occur at the largest velocity. Velocity and displacement are, for a given mode, both directly and linearly related. The maximum displacement (and maximum velocity) thus corresponds to the peak of the frequency response function for the mode in question.

This leaves the experimenter with the maximum displacement experienced by the sample during an experimental run at the point of interest, for a given sample and mode. This can then be multiplied by the maximum strain/displacement proportion for that same point of interest, sample, and mode. The result is the maximum strain experienced by the sample for that given run.

The maximum strain/displacement relationships determined by FEA modeling are shown in Chapter II. They are shown for each sample geometry and mode of interest. In Appendix F of this document, strains determined via FEA-derived proportions are compared to strains calculated from a set of experimental strain/displacement relationships. This is done for several experimental runs from each mode of interest, representing a broad range of displacements. The experimental strain relationships were obtained by Blackwell in a previous study, using the same uncoated cantilevered sample used in this study (4). The difference in strain values calculated between the two methods did not exceed 7.6% for the entire range of displacements compared. As such, the practice of using FEA-derived proportions to determine strain was considered acceptable for all portions of this study.

Related Work

Numerous studies have been undertaken which attempt to characterize the damping qualities and performance of hard damping coatings. Their applicability as passive dampers makes them valuable, but nailing down their exact damping performance characteristics has, at times, proven to be an elusive quest. Edwins, in discussing damping measurements, points out that calculating damping is a tricky undertaking. That is certainly a prescient statement, and the inherent difficulty only increases when dealing with a strain-dependent material. In a study of finite element predictions for hard coatings, the difficulty in determining damping for materials with strain-dependent coatings is specifically mentioned (18).

One coating which has seen attention is mag spinel. Studies often produce varying results for this material, making it difficult to say exactly what damping values should be accepted (or, for that matter, excepted). The non-linearity observed is certainly a large part of the reason there are varying conclusions regarding the exact damping properties, while another reason may be the sheer number of different approaches taken to this problem (26). Sample geometry, sample composition, method of coating application, boundary conditions, and strain levels are just a few of the factors affecting the outcome of these studies. The net result is that many excellent experiments have been done, but any conclusions drawn regarding mag spinel's damping attributes should be written in pencil, not stone. There is no exact set of damping values, though several clear trends have emerged and great progress has been made in understanding the factors which affect damping.

It has been shown that the way in which mag spinel is applied to a sample has a significant impact on its damping effectiveness. Specifically, altering factors in the application process has resulted in differences of greater than 60% (17). In that study, spray application angle, spray distance, substrate temperature, and coating rate were all factors used to derive an optimal technique for applying the coating. Results indicated that spray application angle and pre-heating of the substrate had the greatest effect on the damping capability of the coating.

Mag spinel coatings consistently show an ability to generate damping. Shen, using beams, and Blackwell, using plates, both demonstrated that a mag spinel coating attenuated resonant peaks when a sample was excited. Further, the study undertaken by Allen, though not primarily aimed at showing the effectiveness of the coating, further supports these results. These studies also clearly demonstrated the strain softening effects of mag spinel. That is, the coating reacts differently at different strain levels. As strain increases, the modal frequencies shift downward.

Blackwell used 4.5”x4.5”x0.125” samples, both coated with mag spinel and uncoated, in the cantilevered position. His experimentation plotted the effect of the coating versus the bare plate at various strain levels at and below 500 microstrain. Blackwell looked at the second bending and two-stripe modes, which correspond to modes 3 and 4, respectively, for the sample size given. At 10 microstrain, he found the Q value for the uncoated sample was 16% and 63% higher for modes 3 and 4, respectively, compared to the coated plate (4). When testing at 500 microstrain, he determined that the Q value for the uncoated sample increased by 31% and 82%, again respectively, for those same modes.

Blackwell's study produced interesting results, but there were still questions surrounding the details. The damping values produced were much more consistent than previous studies, but still showed unexpected variation (11). Further, the damping levels recorded for the bare plate specimens were noted to be too high according to accepted material properties for Ti-6Al-4V (4). That is, Q values for the uncoated plate were unexpectedly low. The results were therefore deemed unreliable. They hint at some very interesting conclusions, though, and the study was therefore continued in an attempt to remedy these inconsistencies. The undamaged samples used by Blackwell, and the clamping blocks he designed, were used in both this study and that of Allen.

Air damping was suggested as a contributor to the high damping levels, and not without good reason. A NASA study in air damping has long shown that air damping could outpace the structural damping within a system (23). These findings applied when the area to mass ratio was sufficiently large, such as in the plates used by Blackwell. This study indicated that air damping varied linearly with pressure and non-linearly with the amplitude of sample oscillation, and was carried out between atmospheric and near-vacuum pressures. In a different study, it was also shown that vibrating thin beams were affected by a drag force proportionate to pressure (3).

While these conclusions clearly support the idea that air damping is significant, it has also been shown that it can be less significant than material damping. The study that showed this analyzed small brass plates in a wind tunnel (24). While the focus of that study aimed at air flows moving parallel to the displacement of an oscillating sample, data was also taken in stationary air. It again indicated that air damping varied linearly with pressure, despite the fact that the damping observed was relatively small (24). In

that study, absolute pressure had a very small effect on damping. The study in question also indicated that flow velocity had a much greater effect on results than absolute pressure.

The disparity in results is almost certainly due to differences in the samples used and the details of the set-up. This situation shows that conclusions could not be arbitrarily drawn in regard to air damping's true effect or significance. In light of this, Allen set out to quantify the effect of air damping at various strain and pressure levels for both coated and uncoated samples.

The study carried out by Allen is the most relevant to the study presented in this document. He recreated Blackwell's experiment and again found inordinately high damping levels for the same specimens (2). In determining how much the coating increased damping, he tested at numerous strain levels. In using the uncoated sample, he found that Q values were 59.5% and 72.4% higher, respectively, for modes 3 and 4, than the values found for the coated sample. Modes 3 and 4 once again corresponded to the second bending and two-stripe modes. Allen's testing showed that, when examining mode 4, air pressure had a definitive impact on damping for a bare plate. As pressure increased, damping generally increased. He also demonstrated a peak frequency shift associated with pressure. Specifically, frequency shifted down as absolute pressure increased for both modes under examination.

While Allen's testing yielded quality results, there were many questions left unanswered. Due to modal interference issues with the baseplate, none of the data regarding the effect of air damping on the coated sample could be used. Since the constant control inputs used produced varying strains in the samples, it was difficult to

establish clear trends in the results when making comparisons between runs. Further, when looking at the bare plate sample in mode 3, no definitive conclusion could be drawn as to the effect of air pressure. Numerous factors were considered as suspects in the skewing of these results (2). Some of these factors affecting damping have already been addressed in this chapter, while others will be discussed in more detail later.

Allen also tested a 9.5"x4.5"x0.125" uncoated Ti-6Al-4V sample suspended in a free-free-free-free condition. This specimen was tested at mode shapes corresponding to the second bending and two-stripe modes, which equate to modes 4 and 7 for this particular sample. It was by excited magnets and tested inside a large stationary vacuum chamber, allowing pressure to vary (2). While this test also showed a clear change in modal frequency as a function of pressure, it did not yield any definitive results as to the effect of air damping. No coated free-free-free-free specimen was tested.

Objective of Thesis

The objective of this investigation was to determine factors affecting the clamped condition, perform tests to show these effects, and then show, via careful experimental design, whether air damping has a statistically significant effect on the damping of a coated and uncoated cantilevered 4.5"x4.5"x0.125" Ti-6Al-4V plate in the second bending and two-stripe modes. This investigation also used observed data to show the significance of damping introduced by a mag spinel coating in order to draw comparisons to previous studies. Determination of factors affecting the damping of the sample was necessary in order to complete the statistical analysis.

A secondary objective of this thesis was to study the effect of a mag spinel coating applied to a 9"x4.5"x0.125" plate of the same material in a free-free-free-free condition. This was done in order to better understand the true influence of the mag spinel coating by altering the boundary condition and eliminating other potential sources of damping. The second bending and two-stripe modes were used for these experiments as well.

General Approach

This portion of the introduction is designed to yield an overview of the experiments performed and the reasoning behind their selection, while further chapters in this thesis entertain all the details of this work. The results are also presented in a separate chapter.

As alluded to by the thesis objectives, this thesis endeavored to compare coated and uncoated samples, determine what factors were affecting damping, and show conclusively whether air pressure has an effect on damping in the modes under consideration. In order to do this in an efficient and effective manner, a specific set of experiments were adopted. These experiments were broken up into two set-ups, corresponding to either the primary or secondary objectives of this study. A cantilevered set-up, using a clamped sample on an electrodynamic shaker table, was used to study air damping and other factors in accordance with this study's primary objective. A free-free-free set-up, using larger samples hanging in a free condition, was used to study the effects of mag spinel coating in a different boundary condition.

In previous testing, Allen used a cylindrical pressure vessel mounted over a sample and baseplate, which was in turn mounted onto an electrodynamic shaker table. This was done in order to evacuate air and thus determine the effects of air damping at various pressures. The constraint blocks holding the sample were originally designed by Blackwell.

In order to complete testing on the cantilevered set-up, the hardware initially used by Blackwell and Allen were re-used. However, modifications had to be made to the equipment in order to complete air pressure testing. The existing baseplate and pressure vessel, designed by Kyle Allen, were outstanding. These pieces of equipment are shown and labeled in the picture below. However, modifications had to be made to the baseplate design, accelerometer mounting position, and, subsequently, the pressure vessel cabling. These changes were necessary to counteract modal interference experienced during prior testing, which will be described more fully in Chapter II.

Next, a set of experiments were run to determine nuisance factors in damping other than air pressure. The next phase of the study involved a determination of whether air pressure, and its interaction with other factors, was significant. The testing technique used in this phase required some degree of repeatability as it determined statistical significance through an analysis of variance (ANOVA). As such, the determination of factors which could affect variability was absolutely vital. After statistical testing was completed, the results were re-formatted into standard plots in order to show the trends observed and proven. Suspected trends in plotted data were “backed-up” by statistics which asserted, with a minimum of 95% certainty, the effects were actually occurring.

Thus, ANOVA was used to remove a layer of ambiguity surrounding experimental results.

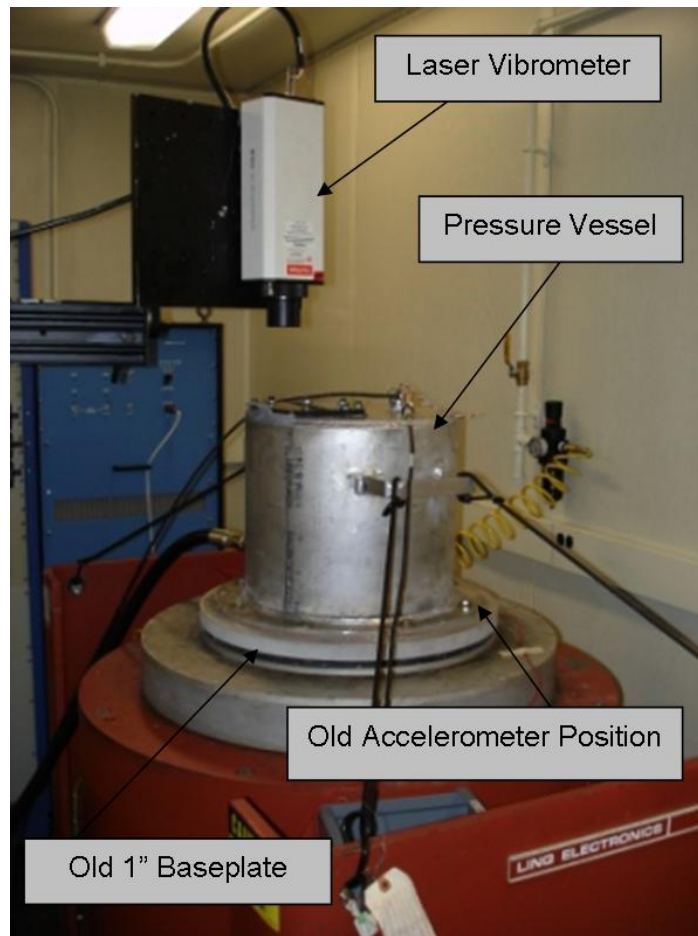


Figure 2. Previous Set-Up Showing Old Baseplate [adapted from (2)]

In testing for the free condition set up, the samples first had to be designed and ordered. Afterward, the samples were mounted in a free condition and their mode shapes were verified using a scanning laser vibrometer. This was necessary, obviously, to ensure that the study determined damping for the correct modes. Using the same scanning laser, the investigator then determined damping values over a range of strain

values for the modes of interest on both coated and uncoated samples. Conventional plots were used to compare damping performance between the samples.

The cantilevered set-up consisted of a 4.5"x4.5"x0.125" sample of Ti-6Al-4V mounted in the cantilevered position on top of either an 18,000 lbf or 6,000 lbf electrodynamic shaker table. Both tables were controlled using the exact same equipment. The cantilevered condition, achieved via constraint blocks, is designed to approximate the condition seen in aircraft turbine blades. This testing used the same uncoated sample (sample T4) as both Allen and Blackwell, though the coated sample was switched to an unused sample (sample T2) because sample T1 had been damaged in the interim. Testing was carried out both with and without a pressure vessel installed in order to streamline testing and in order to make comparisons to previous work. A single point laser was used to measure the velocity of the sample throughout each test. In this set-up, modes 3 and 4 corresponded to the second bending and two-stripe modes, respectively. The point of measurement was always 0.1" from the tip of the sample, and 0.7" from the edge.

The second set-up consisted of a 4.5"x9"x0.125" sample of Ti-6Al-4V hanging in a free-free-free-free condition. Though sized differently, these coated and uncoated samples were otherwise designed to the same specifications of the original cantilevered specimens. The sample was suspended by a string at its centerline, which also corresponded to a node line for both modes of interest. This second set-up was excited via an air horn, and modes 4 and 7 corresponded to the mode shapes studied in the cantilevered samples. As in the first set-up, Q values were calculated and used to determine damping.

The second set-up was interesting in that it produced mode shapes which were very similar to those of the first set-up. The samples in the second set-up were double the size of the first, but produced anti-symmetric mode shapes which were reflected about their center node line for both the second bending and two-stripe modes. The node line was a rough approximation of an ideal clamped condition despite some differences, most notably shear running down the centerline. Because of this, the net effect was a sample in a different boundary condition with very similar, equally scaled mode shapes.

All testing was performed at the Turbine Engine Fatigue Facility (TEFF), located at Wright-Patterson Air Force Base (WPAFB), Ohio. Diagrams of the samples used are presented in the below figures, while actual pictures are provided in Chapter II. The first figure represents the sample used in the first set-up, or cantilevered testing. The figure below that represents the sample used for the second set-up, or all free-free-free-free testing.

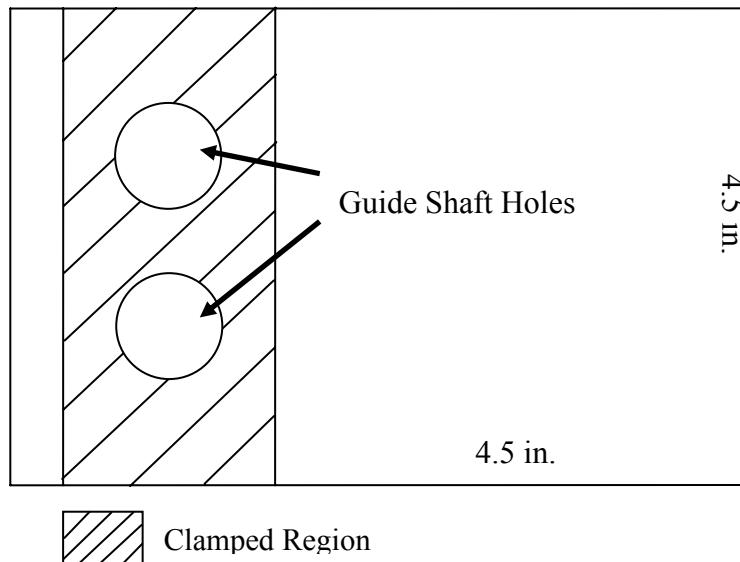


Figure 3. 4.5" x 4.5" x 0.125 Ti Test Specimen (2)

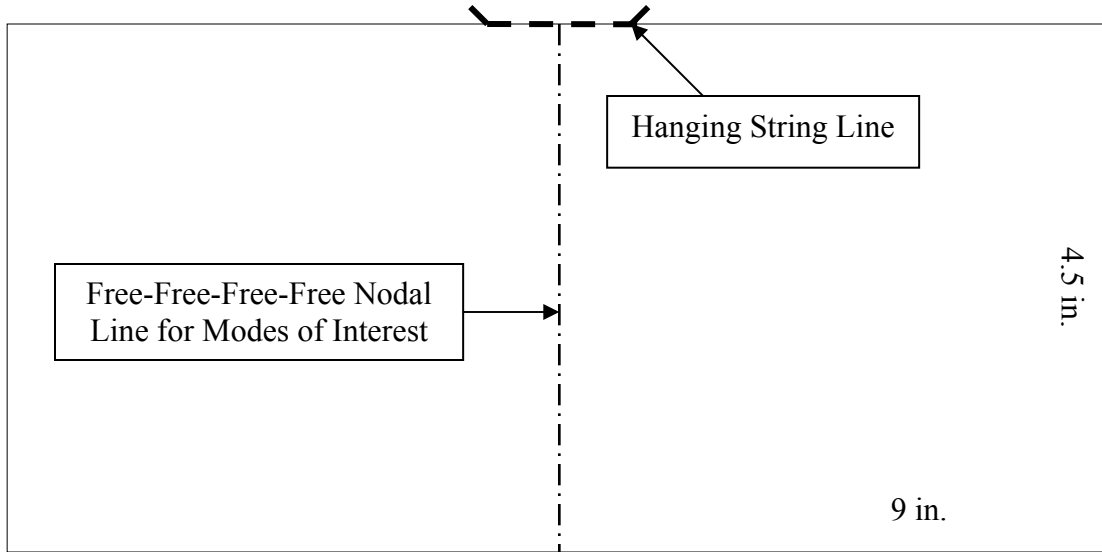


Figure 4. 9" x 4.5" x 0.125" Ti Specimen [adapted from (2)]

II: Finite Element Analysis for Samples and Baseplate Re-Design

This chapter evaluates the expected modal frequencies and mode shapes for all samples used within this study. For both specimen sizes used, the coated and uncoated specimens shared a common geometry. They were cut from the same material and shared the same mode shapes. As such, the finite element analysis (FEA) models derived for each sample geometry were applied to both the coated and uncoated samples.

Due to modal interference issues in the prior studies, it was necessary to design a new baseplate for the cantilevered set-up and complete minor modifications to the pressure vessel. The details of this re-design are also included in this chapter.

Test Specimens

The testing included four test specimens composed of Ti-6Al-4V, as discussed previously. Ti-6Al-4V is an alloy commonly used in turbine engine blades (20). The rectangular shape of the samples, and the boundary conditions applied, were meant to further simulate operational turbine blades, allowing for a better understanding of how results would impact a real-world environment (14)

The 4.5"x4.5"x0.125" cantilevered specimens were each cut from the same sheet of Titanium, while the 9"x4.5"x0.125" free-free-free-free specimens were each cut from another sheet of Titanium. While the cantilevered specimens were from the same stock as those originally used by Blackwell, the larger specimens for the free condition testing were made especially for this study. An attempt was made to find the original sheet from

which the cantilevered samples were born, in order to make any results more comparable, but that sheet was no longer available.

It is prudent to note here that the cantilevered samples in question actually measure 4.5"x7"x0.125". The dimension 4.5"x4.5"x0.125" represents their effective dimension in testing, when they are placed within a clamp. That is, the excess 2.5" of length in the sample is used to secure it to the test fixture, allowing for guide shaft holes and a 0.5" tail in the back. The tail is necessary as a means for removing the tight fitting sample from the clamp. The diagram at the end of Chapter I yields further insight into the dimensionality of these samples. Blackwell performed further exact dimension measurements using a caliper.

Both cantilevered specimens were cut from the same piece of 0.125" titanium sheet using a 55,000 psi water jet (2). Mag spinel came in powder form, and was applied to the coated sample via a high temperature air plasma spray process. This process is detailed in the study written by Blackwell (4). The coating was applied to both the top and bottom surfaces of the sample to a thickness of 0.01", or 10 thousandths. The edges of the sample were not coated, and the coating was only applied to the non-clamped portion of the sample (*i.e.* the coating was applied only to the portion of the sample representing the effective size).

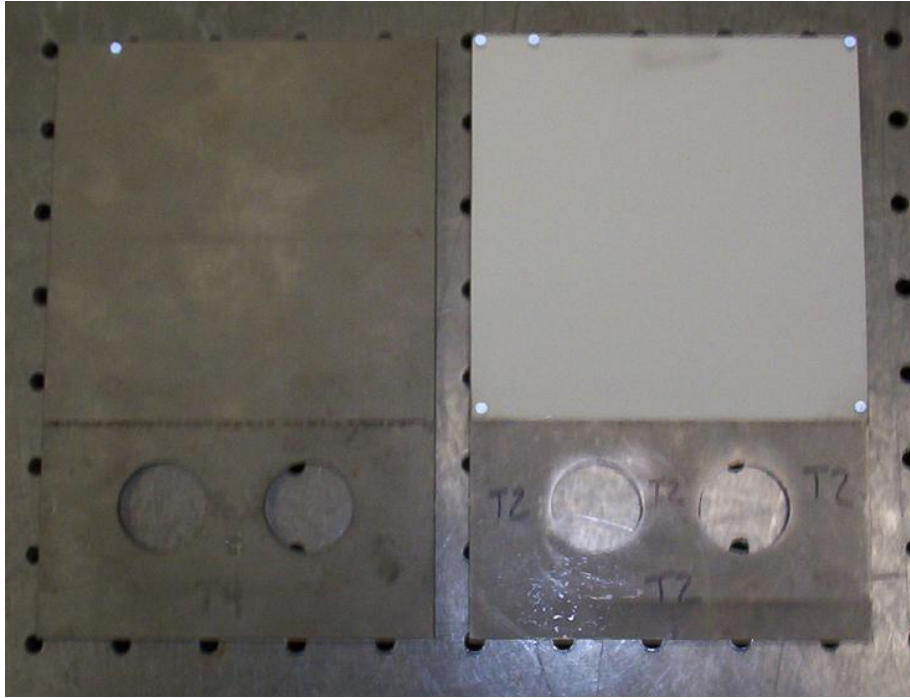


Figure 5. Uncoated (Left) and Coated (Right) Ti-6Al-4V 4.5” x 4.5” x 0.125” Specimens

The test specimens for the free-free-free-free condition testing were cut and coated in the same manner as the cantilevered samples. One coated sample and one uncoated sample were made. They were cut from a sheet of annealed Ti-6Al-4V as similar to the original piece as possible. The mag spinel coating was applied to the coated sample via air plasma spray to a thickness of 0.01”, as before, leaving the edges uncoated. This coating was applied by the same company which coated the original samples. Since the entire 9”x4.5” surface on each side of the samples represents the effective area in this case, this entire area was coated on both sides.

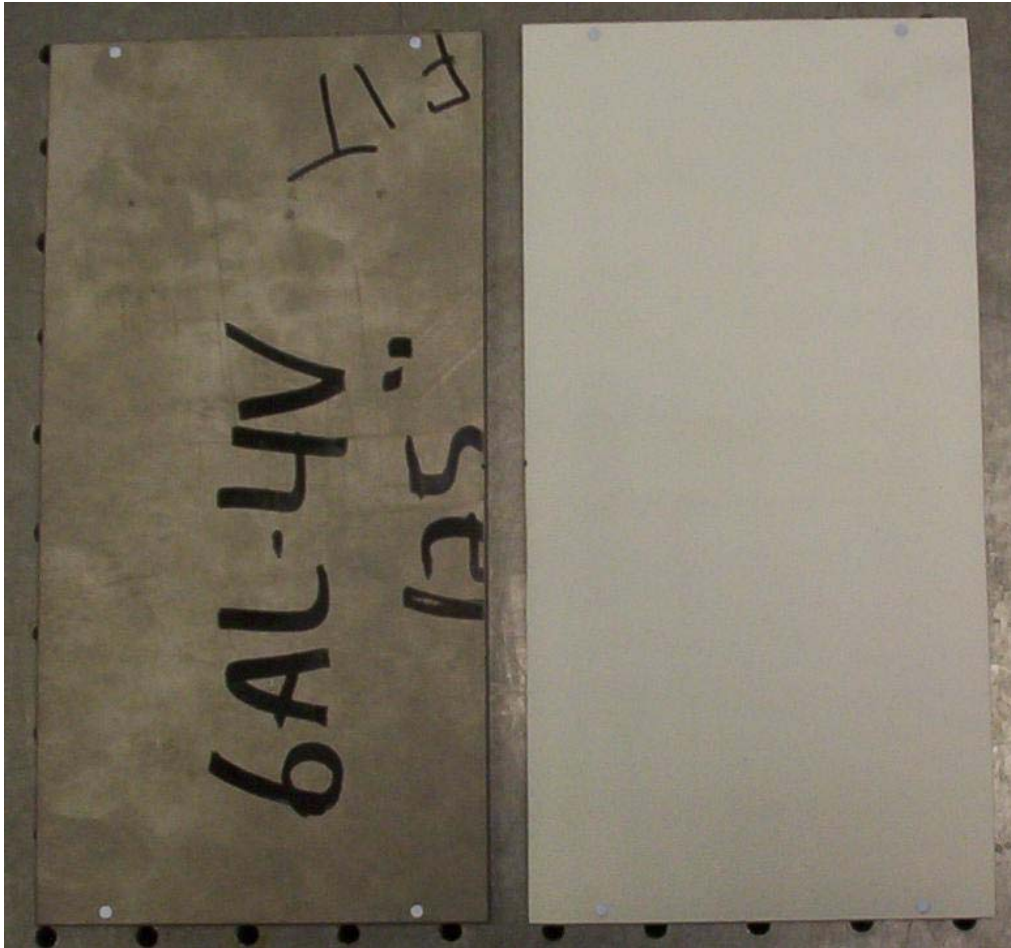


Figure 6. Uncoated (Left) and Coated (Right) Ti-6Al-4V 9" x 4.5" x 0.125" Specimens

The actual thickness of each of the free condition and cantilevered plates was measured using a Starrett® caliper. Measurements were taken at each of the 4 corners for each specimen. This was done in order to ensure that there existed no apparent difference in thickness across the surface of the samples. The four measurements were averaged for each plate and are presented in the table below. The reader should keep in mind that the coated samples will have a greater thickness, as they are coated on both sides with the mag spinel ceramic coating. At 0.01" per side, this coating should add 0.02" to the overall thickness of the coated samples over the uncoated samples.

Table 1. Thickness Measurements of Ti-6Al-4V Specimens

COATING	SIZE	TESTING	MEASURED THICKNESS (in)
Uncoated	4.5"x4.5"	Cantilevered	0.128
Coated	4.5"x4.5"	Cantilevered	0.150
Uncoated	9"x4.5"	Free	0.123
Coated	9"x4.5"	Free	0.146

Finite Element Analysis

All materials and structures have an infinite set of frequencies at which they will resonate. When subjected to an input at one of these resonances, or modal frequencies, they respond by amplifying the input signal and its oscillations increase in magnitude, thus increasing the displacement experienced by a material. The force of the input signal will ultimately determine the magnitude of displacements for a particular natural frequency, and the magnitude of the oscillation for a particular input force will be attenuated by damping. All materials have at least some intrinsic damping ability, and this damping is ideally at a minimum for uncoated specimens (2).

Plates, such as this study's samples, can be forced to oscillate at one of these frequencies via a sinusoidal input. The frequency of this input will determine which modal frequency is being excited, while the force input will determine the degree to which it is excited. Each particular modal frequency causes the sample to resonate in a different shape, and this shape is referred to, quite intuitively, as a modal shape. At each modal frequency, the samples displace so as to form different shapes. The portions of the sample which display no displacement, at a given frequency, are referred to as nodal lines. These lines are used to define the shape created.

There are many different techniques used to determine the modal shapes for a material. For example, this can be done via experimentation with a scanning laser

vibrometer, or a set of accelerometers with corresponding phase data. The modes can also be derived analytically via FEA. FEA is especially useful when designing a structure or sample which is not yet physically available. As mentioned, FEA is also highly useful for acquiring close approximations of strain/displacement relationships where strain gauges are impractical.

Titanium Plate Modeling

Because of the versatility offered by finite element modeling, it was used somewhat extensively throughout this study. All models were created using ANSYS® software, which served as both a pre and post processor for the data. In all cases, sequential runs of the models with increases in the number of elements, and consequently the mesh density, were run until the model clearly converged. The results of finite element analysis for the cantilevered samples were also compared with those produced by Allen in order to ensure consistency (2).

The nominal thickness for all samples was 0.125". This value necessarily varied from the norm for the samples. For example, the thickness of titanium portion of the cantilevered samples was actually 0.127". Despite this variance, the nominal thickness of 0.125" was used in creating the model. The nominal thickness of 0.125" was used in the design of the as-yet-unordered free-free-free-free samples, so it only made sense to create all of the FEA models using the same nominal thickness for better comparability. It could also be assumed that the difference in thickness of 0.002" between the model and reality for the cantilevered samples was negligible. The table below summarizes the material properties entered for the finite element code. These values were used every

time the sample was modeled. In creating an FEA model, the density below was converted to a mass density, as required by the software used.

Table 2. Material Properties for Ti-6Al-4V (12)

Property	Ti-6Al-4V
Modulus of Elasticity (E)	$1.65 \times 10^7 \text{ lb/in}^2$
Poisson's Ratio (ν)	0.33
Density (ρ)	$.160 \text{ lb/in}^3$

Using these material properties, the samples were modeled using the appropriate element type. Solid45 elements were chosen, as the rectangular plate shape of the samples lent itself to the rectangular element shape. Solid45 elements have 8 nodes, with three degrees of freedom at each node. An example Solid45 element is shown below.

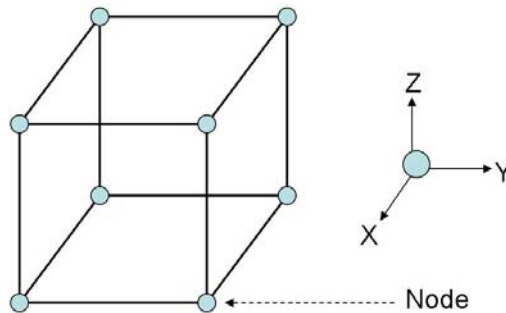


Figure 7. Solid45 Element

The mesh densities used were sufficient to ensure model convergence and correlation to the results found by Allen. The mesh densities were also the same for each sample modeled. All of the Solid45 elements used had a length of 0.1” and a height of

0.042". In all, 10,368 elements and 15,987 nodes defined the cantilevered sample, while 21,888 elements and 33,507 nodes defined the free-free-free-free sample.

In analyzing the two sample geometries, the first 10 eigenvectors were modeled for each. These eigenvectors each corresponded to a physical mode shape, while their individual eigenvalues corresponded to that shape's modal frequency. It is imperative to note that different sample geometries, and samples with differing boundary conditions, had different mode shapes. The shapes also appeared in a different order, despite the fact that the samples were made of the same material. For example, the second bending and two stripe modes occurred as mode shapes 3 and 4, respectively, for the cantilevered sample. In modeling the free-free-free-free sample, they appeared as modes 4 and 7, respectively. The frequency range of interest for each sample was determined by the location of these modes.

The table below shows the predicted peak frequencies for the first 8 modes analyzed in the cantilevered sample, while the following figure shows the corresponding mode shapes. In the images below, the clamped end is on the left. The second bending mode (mode 3) gains its name from being the second shape where the plate is in bending motion. The first bending mode has all displacements in phase, while this second bending mode reveals a more sinusoidal-esque motion. The two stripe mode (mode 4) is so named because of its two axial node lines, which form two stripes as they move toward the sample tip.

Table 3. Predicted Frequencies for Cantilevered Sample

MODE	FREQ (Hz)	MODE	FREQ (Hz)
1	207	2	498
3	1261	4	1612
5	1815	6	3164
7	3636	8	3777

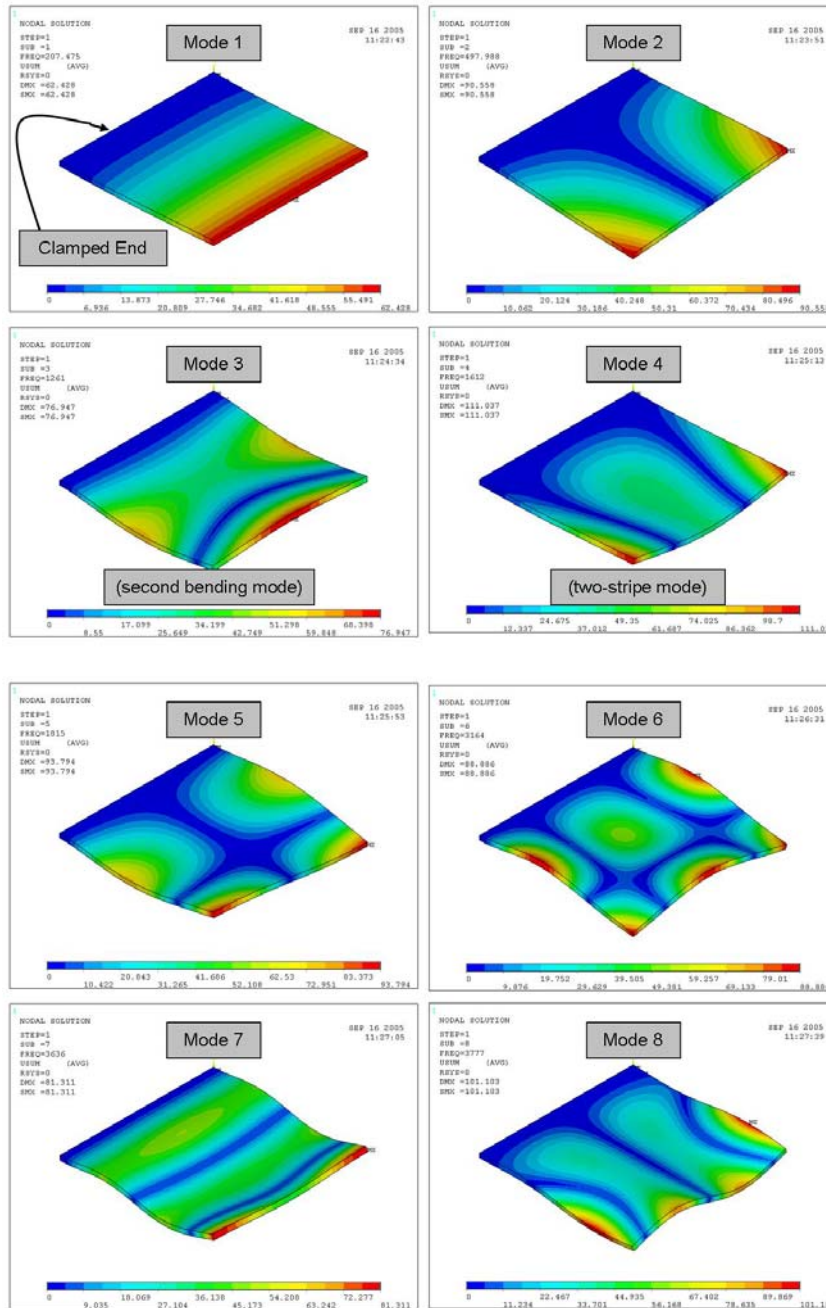


Figure 8. Predicted Mode Shapes for Cantilevered Sample

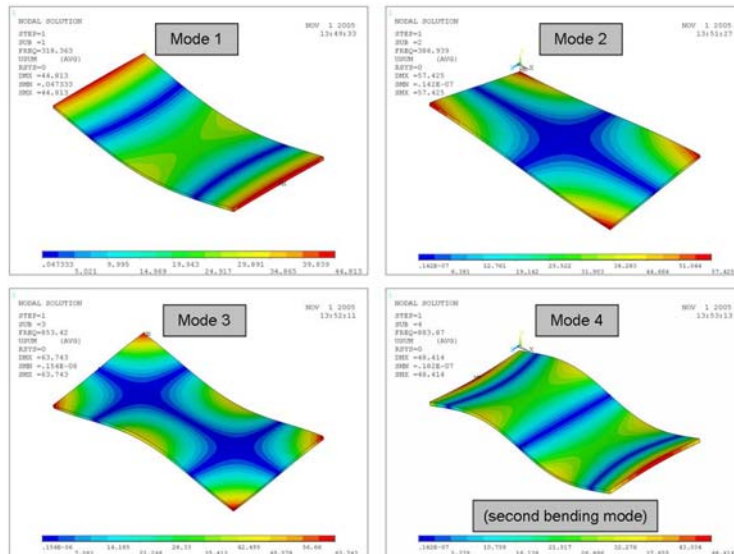
This next table shows the modal frequencies analyzed for the free condition sample. The first 10 modes are presented for this sample, and the following figure again

shows their corresponding mode shapes. The second bending and two stripe modes can be clearly spotted below occupying the 4th and 7th mode positions. It is interesting to note that modes 3 and 4 were very close on the frequency spectrum. Because of this proximity, the position of the two modes could have been switched during actual experimentation. Due to this situation, it was especially important to experimentally verify mode shapes.

It should also be noted that the free condition samples used in this study were 0.5” shorter than the one used by Allen. His sample measured 9.5”x4.5”x0.125”. As such, his modal frequencies, and, to some extent, the shapes should not be expected to correspond to the values determined by this investigator.

Table 4. Predicted Frequencies for Free Sample

MODE	FREQ (Hz)	MODE	FREQ (Hz)
1	318	2	387
3	853	4	884
5	1310	6	1485
7	1539	8	1763
9	2119	10	2349



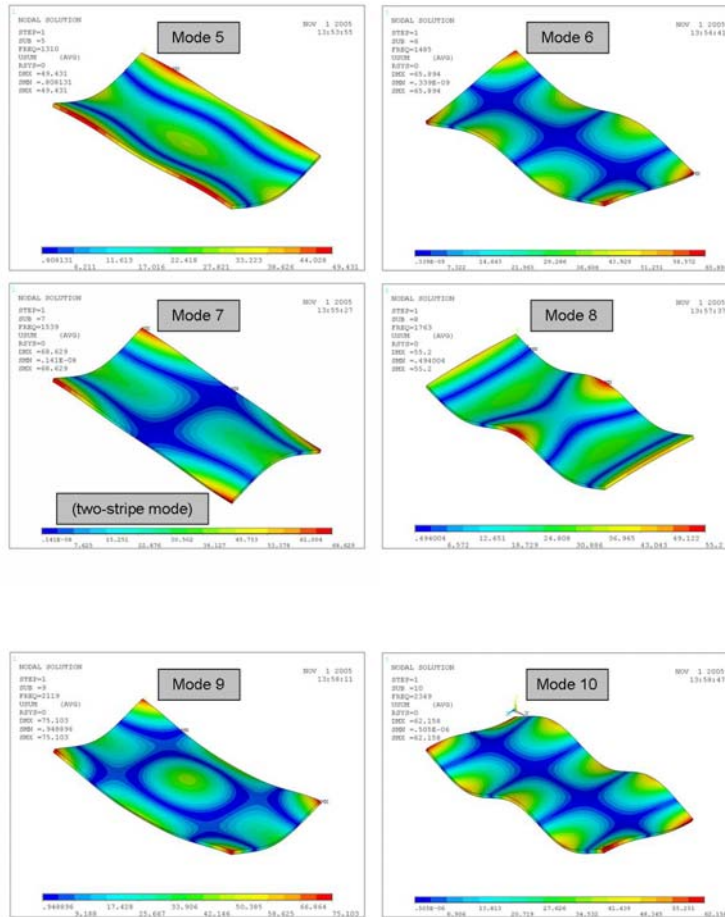


Figure 9. Predicted Mode Shapes for Free Sample (continued from previous page)

The figure below shows how modes 4 and 7 in the free condition samples compared to modes 3 and 4 in the cantilevered samples. Note that the mode shape on one half of the free condition samples is very similar the shape seen in the cantilevered samples, as mentioned in the introduction. This similarity was important because it implied the results from the free condition testing could be related back to an engine blade undergoing similar mode shapes.

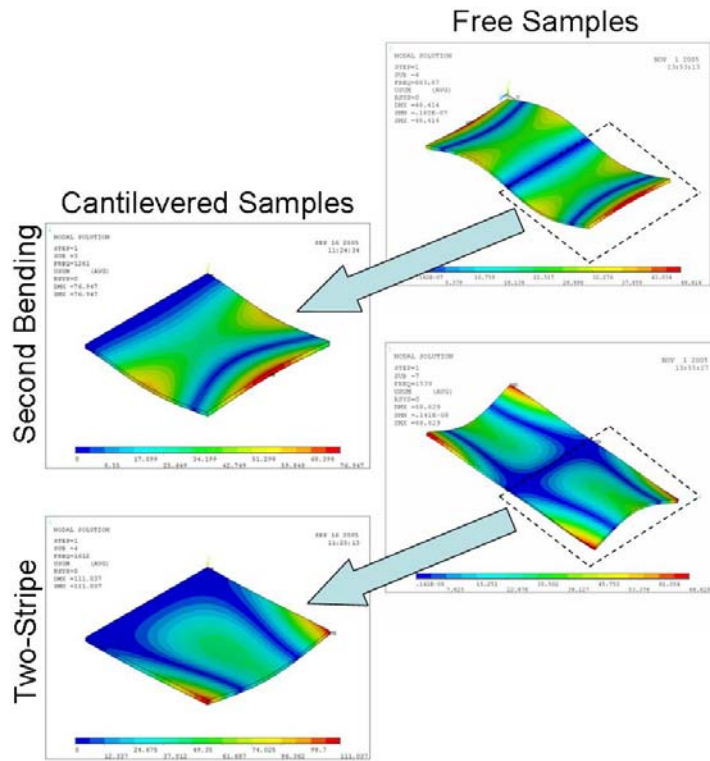


Figure 10. Mode Shape Comparison between Sample Sizes

When analyzing both samples, the displacement to maximum strain/displacement proportion was taken at the point where all measurement on the samples would be done. For both samples, this represented a point 0.1” from the tip and 0.7” from the edge of the sample. This value was used to determine the strain in the actual samples during experimentation based on the actual displacement, as determined through the measured velocity. There is a different strain/displacement relationship for each mode, as different mode shapes have different strain relationships and locations. Previous testing has shown the strain/displacement relationship remains linear for the cantilevered samples. In both the cantilevered and free-free-free-free cases, experimental performance which closely

approximated FEA predictions solidified the assumption that the strain/displacement relationship predicted was valid.

The strain/displacement relationships used in this study are given below for both modes of interest in the two different set-ups. The values highlighted are those supplied directly by the FEA model, which represented the strain produced for an arbitrary displacement. Dividing these values provided the maximum strain/displacement proportions.

Table 5. FEA Derived Max Strain/Displacement Relationships

Cantilevered Sample -- Mode 3 (Second Bending)					
Disp (in)	Disp (mm)	Strain	Disp/Strain (in/strain)	Disp/Strain (mm/strain)	Strain/Disp (strain/mm)
47.1379	1197.30	4.712	10.0038	254.10	0.003936
Cantilevered Sample -- Mode 4 (Two-Stripe)					
Disp (in)	Disp (mm)	Strain	Disp/Strain (in/strain)	Disp/Strain (mm/strain)	Strain/Disp (strain/mm)
43.6288	1108.17	5.639	7.7370	196.52	0.005089
Free Sample -- Mode 4 (Second Bending)					
Disp (in)	Disp (mm)	Strain	Disp/Strain (in/strain)	Disp/Strain (mm/strain)	Strain/Disp (strain/mm)
36.4952	926.98	1.69147	21.5760	548.03	0.001825
Free Sample -- Mode 7 (Two-Stripe)					
Disp (in)	Disp (mm)	Strain	Disp/Strain (in/strain)	Disp/Strain (mm/strain)	Strain/Disp (strain/mm)
22.9246	582.28	3.84332	5.9648	151.51	0.006600

Modal Verification

The modal shapes and frequencies of interest for the cantilevered samples have been clearly established by both Blackwell and Allen. As such, these shapes were not again experimentally verified. The free condition samples were brand new, though, and therefore another matter entirely. The accuracy of the FEA modal had to be experimentally verified for two reasons. First, the experimenter had to be sure he was, in fact, studying the correct mode shapes. Second, the accuracy of the model had to be established in order to justify the application of the analytical strain/displacement relationships shown immediately above.

The FEA results for the free condition sample were compared to scanning laser vibrometer results for both the coated and uncoated sample. In each case, the mode shapes were as expected and the frequencies remained close to the model. The laser vibrometer was used to scan the entire surface of each sample, which was suspended via a string attached to the centerline, and excited by an air horn. A chirp signal excited the sample as the laser scanned each point on a virtual rectangular grid covering the surface of the sample. Analysis of the sample's movement at each point on the grid allowed the software to interpolate the mode shapes the entire structure underwent.

The following tables show the modal frequencies predicted by the FEA model, as well as those experimentally determined for the coated and uncoated samples. The percent difference is shown in each case. For the coated sample, the values match the basic FEA prediction more closely than expected, with no percent difference exceeding 1%. More disparity between the predicted and experimental frequencies was observed for the uncoated sample, with the difference in mode 4 approaching 4%. The modes of interest, modes 4 and 7, have been highlighted in both tables for easy reference. Because the same FEA model was used for both samples, the predicted resonant frequencies are the same for each table.

The disparity in modal frequencies between the samples and the FEA model is at least partially explainable. FEA produces models which are stiffer than reality, due to the finite number of nodes in the model. This means the FEA model should have predicted resonant frequencies which were consistently higher than those for an actual, bare sample. In the case of the mag spinel coated sample, the addition of the coating afforded the sample more stiffness. This, in turn, caused the performance of the sample to more

closely match the FEA prediction. The differences seen may also be due, in part, to uncertainties in material properties. This analysis is fully consistent with the results below and, given this explanation, the investigator considered the differences between the predictions and reality acceptable.

Table 6. FEA Predicted vs. Experimental Frequencies for Coated Free Sample

MODE	PREDICTED FREQ (Hz)	COATED EXP FREQ (Hz)	% DIFFERENCE
1	318	318.2	0.06285
2	387	384.4	0.67183
3	853	850	0.35170
4	884	884.4	0.04523
5	1310	1322	0.90772
6	1485	1484	0.06734
7	1539	1547	0.51713
8	1763	1766	0.16988
9	2119	2128	0.42293
10	2349	2344	0.21286

Table 7. FEA Predicted vs. Experimental Frequencies for Uncoated Free Sample

MODE	PREDICTED FREQ (Hz)	UNCOATED EXP FREQ (Hz)	% DIFFERENCE
1	318	305	4.08805
2	387	365	5.68475
3	853	806.3	5.47479
4	884	848.8	3.98190
5	1310	1299	0.83969
6	1485	1413	4.84848
7	1539	1510	1.88434
8	1763	1706	3.23313
9	2119	2060	2.78433
10	2349	2241	4.59770

The following figures compare the FEA prediction to the mode shapes actually seen for both of the free condition samples. Note that even when the attachment point for the string was not coincidental with a node line, the experimental samples closely matched the prediction. Modes 3 and 4 did not switch places, although that switch did occur when Allen studied his slightly larger sample (2). Note that all of the mode shapes, including the modes of interest, match the FEA prediction.

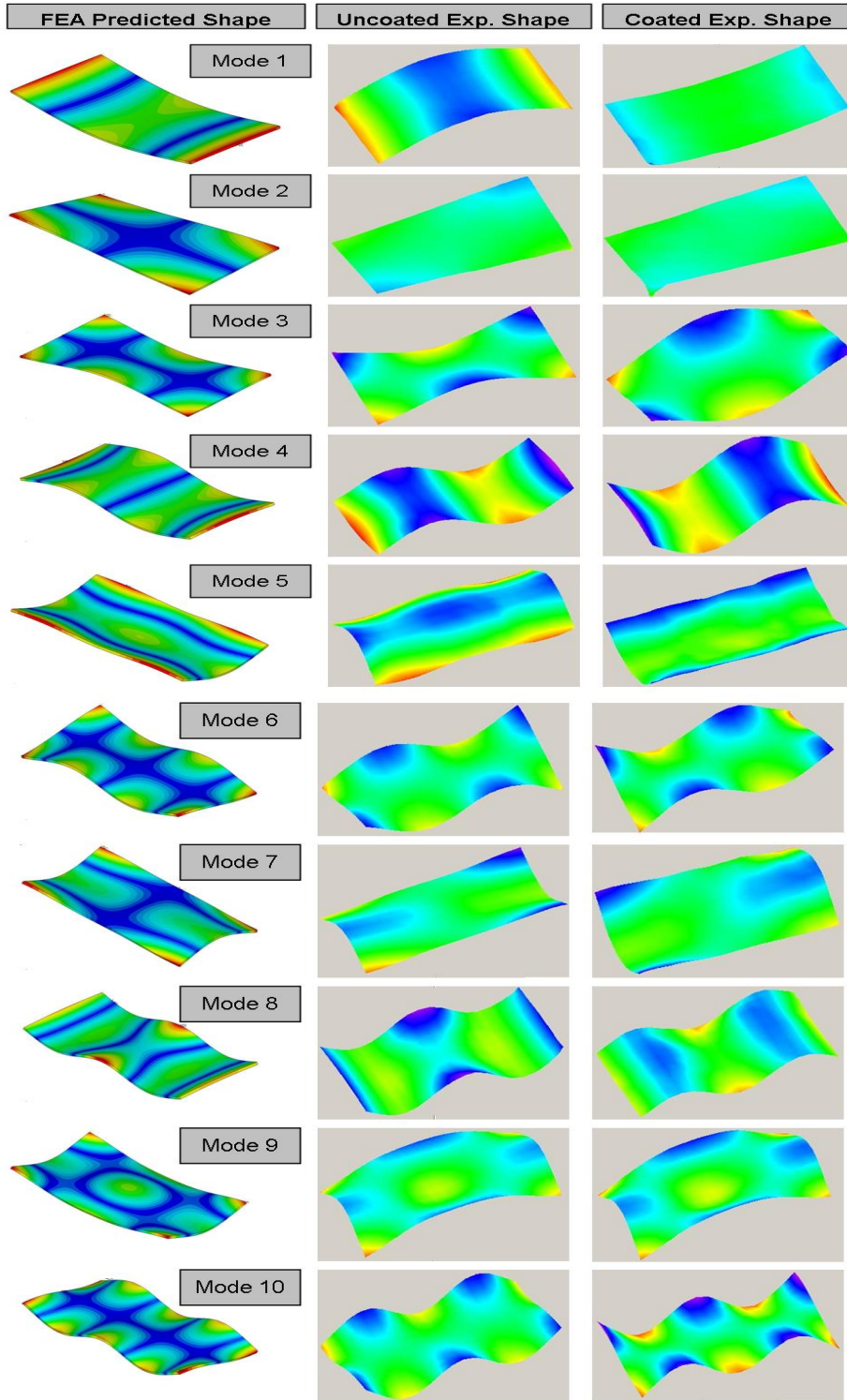


Figure 11. Predicted vs. Experimental Mode Shape Comparison for Free Samples

Baseplate Re-Design

The design process required to develop a new baseplate for cantilevered testing did not present any specific technical challenge, but was overall a time-consuming and detailed process. The design of a cylindrical baseplate may seem mundane, and certainly did not push the envelope of science as we know it, but it was a vital step in the completion of this study. As such, considerable effort was expended in order to design a plate that would satisfy a multitude of requirements.

The original baseplate was a 1" thick disc cut from a piece of aluminum and measuring 20" in diameter. It had threaded holes inset in the top for use in mounting the clamping blocks, as well as 16 clearance holes for a 3/8" screw at radii of 4" and 8" for mounting the baseplate to the shaker. A picture of the original set-up with this baseplate was shown earlier in this document. The picture below shows the original 1" baseplate by itself.

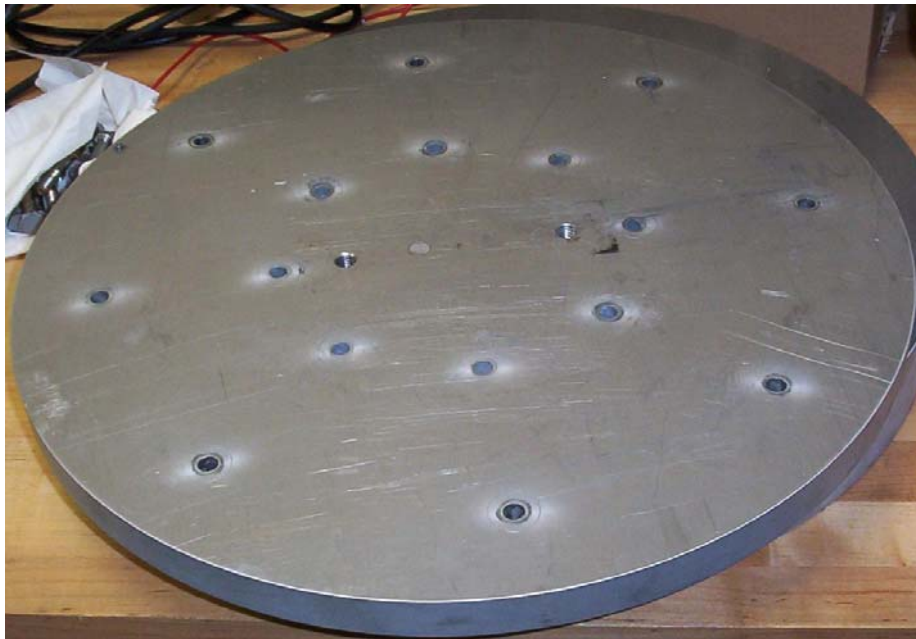


Figure 12. Original 1" Thick Aluminum Baseplate

At the time this original baseplate was made, modal interference was not considered an issue. The highly constrained condition of the plate, being attached by 16 screws to the shaker head, was assumed sufficient to negate the effect of modal interference. Unfortunately, experimental testing using the pressure vessel on this baseplate revealed that modes experienced by the plate had a significant impact on the result. As such, a new baseplate had to be designed.

The main requirement of this design was that it had to be rigid enough to stave off the oscillations which had been the curse of its predecessor. It also, however, had to meet several constraints. It had to be capable of being mounted on two different shaker tables: both a 6,000 lbf and an 18,000 lbf electrodynamic shaker. This was done so that testing could be performed on either of the machines.

Due to this constraint, and several others, the baseplate had to be kept as light as possible. The 6,000 lbf shaker could handle less mass than the 18,000lbf shaker, so the plate was designed to this level. It had to remain light enough that higher g-level tests could be run on it if required. While this study was not intended run at high g-levels, it made sense not to preclude the possibility of such testing at the outset. It also made sense to keep the baseplate light for other reasons. Namely, the plate would have to be useful for other investigators who might use it in future studies. Whatever size was chosen would also, obviously, have to be light enough to be moved around the lab with some semblance of ease. Compatibility with the existing pressure vessel was also a concern for the new baseplate. Conveniently, the requirement to fit on the 18,000 lbf shaker already took this dimensionality into account.

Baseplate Finite Element Analysis

As with the design of the free condition samples, ANSYS® software was used in order to model all potential designs for the baseplate. The mesh density used in modeling the sample was initially set low for a fast run time, then doubled and run again until the model converged. The baseplate was, in all cases, modeled as a homogenous plate. The locations of the bolt holes were modeled as 0.375” holes extending through the thickness of the plate. All nodes around the perimeter of these holes, through the entire thickness of the baseplate, were set to 0 degrees of freedom. This simulated the presence of the mounting bolts which would be used on the actual baseplate by restraining their movement. An example layout of the FEA model grid and constraints is shown in the figure below, representing a 2.5” baseplate. Note that the cantilevered sample constraint blocks have been included in the model. This is represented by the rectangular block attached to the top of the baseplate in the figure below, and in all subsequent FEA pictures of the baseplate.

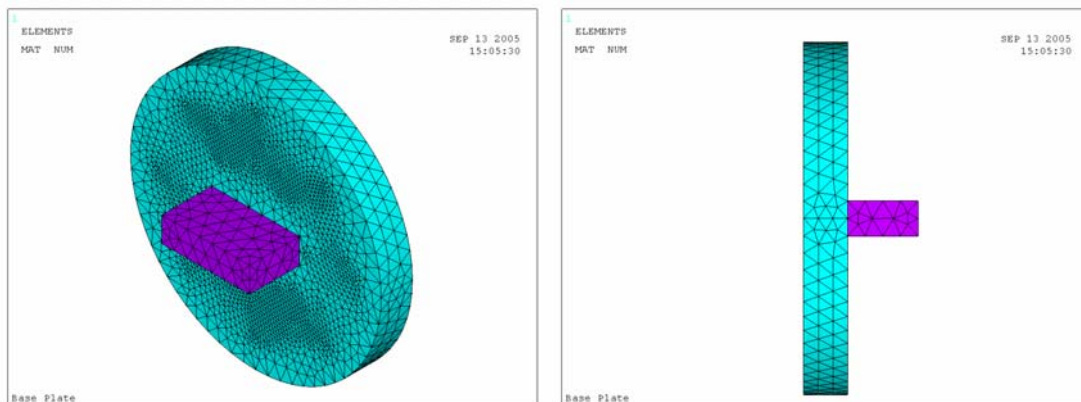


Figure 13. Orthogonal and Side View of Mesh Pattern

Initially, the steel constraint blocks were omitted from the model, but they were later added in order to better approximate reality and improve the results. When these blocks were added, they were modeled as one solid steel piece fused to the baseplate. This addition to the model put modal responses of the system closer to the frequencies of interest for the sample. Because these results were acceptable, no future modifications to this basic baseplate/bolts/clamp system model were made in the FEA model. Further modifications would surely have pushed the modal response of the model to more accurate levels, but this was sufficient for the purposes of designing a new plate. With this reasonable degree of accuracy, one could ensure that the modes of the baseplate were pushed further away from the modes of interest in the samples.

In keeping with the same general technique as mentioned in the previous section, this analysis attempted to recreate the modal responses of the 1” thick baseplate first. Then, the FEA code could be used to modify the thickness, and perhaps the material used, in an attempt to find an ideal design for the replacement baseplate. The modal results for the modeled 1” Aluminum plate and constraint blocks are shown below. In creating the model, material properties for 6061 aluminum were used.

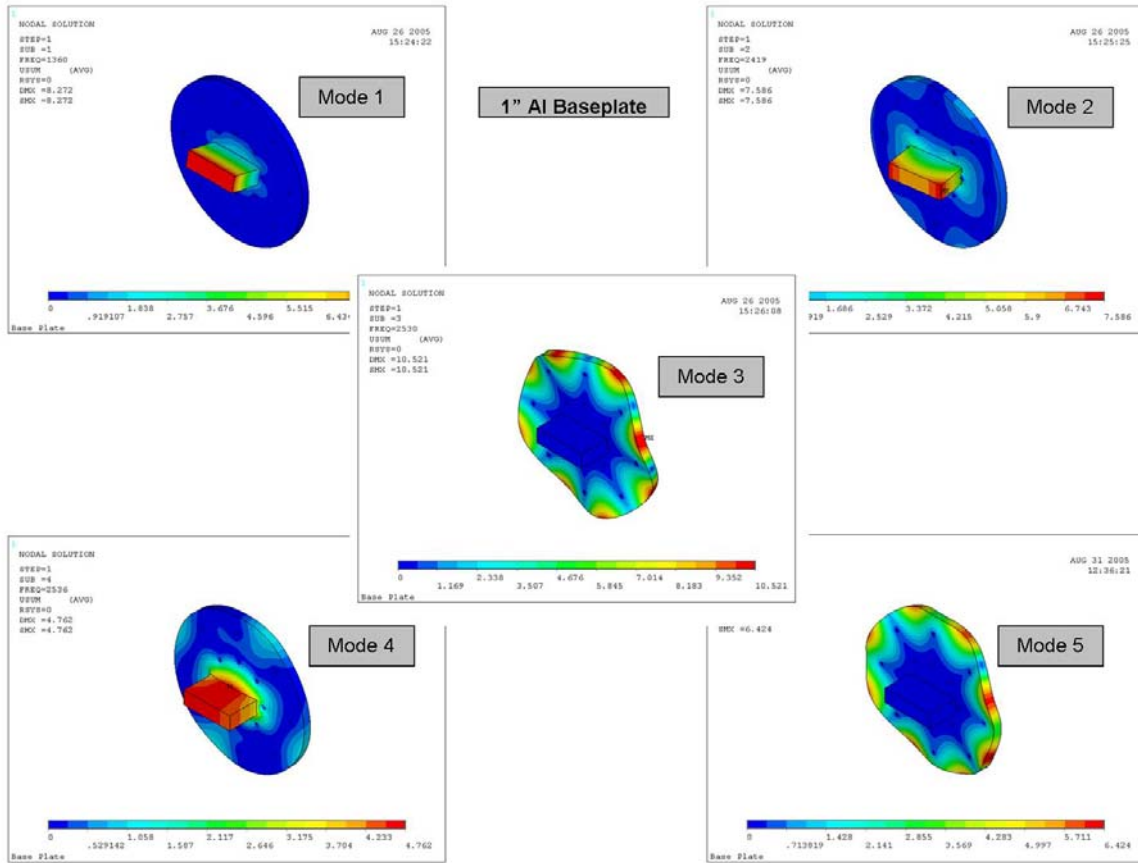


Figure 14. FEA Results for 1" Aluminum Baseplate with Constraint Blocks

Table 8. Predicted Frequencies for 1" Aluminum Baseplate with Constraint Blocks

MODE	FREQ (Hz)
1	1360
2	2419
3	2530
4	2536
5	2897

The FEA results from the 1" baseplate show that the constraint blocks go into a bending mode at 1360 Hz, while baseplate oscillations begin to appear at 2419 Hz. In a prior study, baseplate interference occurred at mode 4 for the coated cantilevered sample.

Mode 4 for that sample was known to occur at a frequency of approximately 1660 Hz, depending on strain. Given the approximate nature of the model, the modes found at both 1360 Hz and 2419 Hz were initially considered candidates for causing the interference. The attachment of the pressure vessel to the baseplate could add mass and rigidity to the system, forcing these frequencies to move closer to mode 4 for the sample. In order to avoid this problem, the new baseplate had to possess modal frequencies which were farther removed from frequency ranges of interest in the samples.

Alterations in both thickness and material were both principal considerations in designing the new baseplate. Steel was denser than aluminum and had a higher modulus of elasticity (29). This meant that more mass could be squeezed into the same size plate. However, no increase in modal frequencies would be seen. For many metals, including steel and aluminum, the ratio of modulus elasticity to density is relatively constant. As such, aluminum was chosen. A 2.5" aluminum plate would weigh over 8 pounds less than a 1" steel plate, and also benefit from the rigidity afforded it by the increased thickness. This rigidity offset the higher modulus of the steel, and presented an ideal trade-off in mass for performance. FEA models also showed that the 2.5" aluminum baseplate was better suited to this study. Both the 2.5" aluminum and 1" steel baseplates are shown below in these modal response predictions

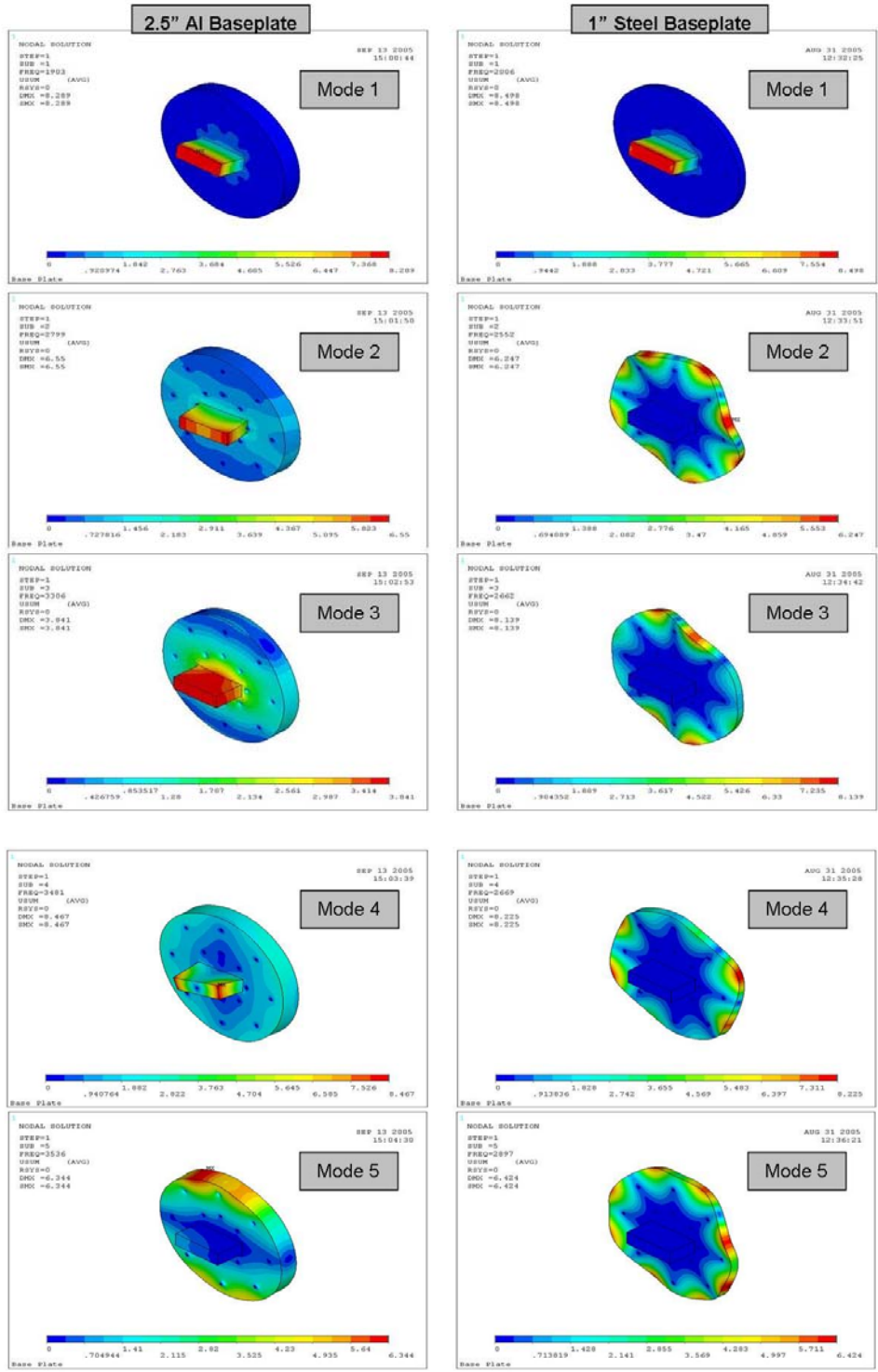


Figure 15. FEA Results for Aluminum and Steel Baseplates with Constraint Blocks

Table 9. Predicted Frequencies for Aluminum and Steel Baseplates with Constraint Blocks

MODE	2.5" Al FREQ (Hz)	1" STEEL FREQ (Hz)
1	1903	2006
2	2799	2552
3	3306	2662
4	3481	2669
5	3536	2897

The figures given above may require some interpretation. In both the aluminum and steel designs, the modal frequencies were an improvement over the 1" baseplate. The location of the bending mode in the blocks increased by well over 500 Hz in each case, moving it further from sample modes of interest. Modal movement of the baseplate itself also occurred at higher frequencies in both models. However, the aluminum shows a distinct advantage in this respect. The rigidity afforded to the aluminum by its thickness allowed it to resist modal oscillations. The oscillations that occur in the 2.5" aluminum plate itself are at much higher frequencies than those in the 1" steel plate, and the movements themselves are far less pronounced. The frequency of mode 1, representing bending in the constraint blocks, was over 100 Hz higher for the steel baseplate. However, the movement of the baseplate itself was considered a larger threat than the bending of the blocks.

As a side note, it is important to highlight that the movement of the constraint blocks was a very interesting result. The possibility that modal oscillations of the clamping blocks themselves were a factor in influencing the results of tests was not previously considered.

The final design for the baseplate was an aluminum cylinder 2.5" thick and 20" in diameter. It had two inset threaded holes for mounting the clamping blocks, as well as

numerous through holes for mounting to the shaker tables. Sixteen clearance holes for $\frac{1}{2}$ " bolts were placed at radii of both 4" and 6" from the center to accommodate the 6,000 lbf shaker head. In order to accommodate the 18,000 lbf shaker head, an additional set of eight clearance holes for $\frac{3}{8}$ " bolts were added at a radius of 8" from the center. The set of holes at the 8" radius would also be used for mounting the pressure vessel to the baseplate. The outer circumference of the baseplate was cut from a 2.5" thick slab of Aluminum via high pressure waterjet, and is pictured below.



Figure 16. New 2.5" Thick Aluminum Baseplate, no Constraint Blocks

Because the 2.5" Aluminum baseplate would have to be usable on both shaker tables, it was also modeled using the bolt patterns at radii of 4" and 6" as constraint locations. This represents the baseplate mounted to the 6,000 lbf shaker table. FEA modeling in this condition revealed that the frequencies of the baseplate shifted downward. Though the modal frequencies were lower, they were still out of the frequency range of interest for the specimens. The results of the FEA modeling representing the plate mounted on the 6,000 lbf shaker are shown below.

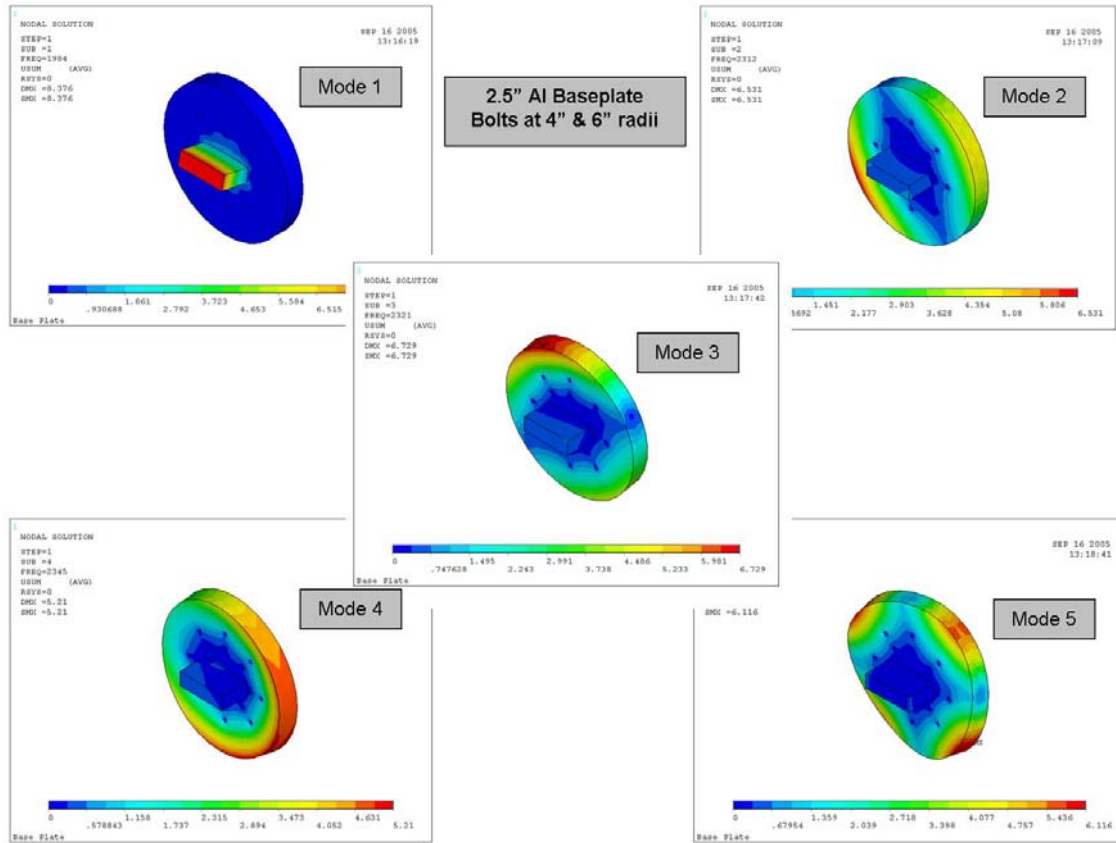


Figure 17. FEA Results for 2.5" Aluminum Baseplate on 6,000 lbf Shaker

Table 10. Predicted Frequencies for 2.5" Baseplate on 6,000lbf Shaker

MODE	FREQ (Hz)
1	1984
2	2312
3	2321
4	2345
5	2471

As can be seen in the figure and table above, mounting the baseplate to the 6,000 lbf shaker was perfectly feasible. The investigator was less certain about mounting the pressure vessel to the baseplate when it was mounted to the 6,000 lbf shaker. The additional mass, and its distribution along the plate, could create modal interference

issues all over again. The figure below illustrates a side view of the pressure vessel mounted on the baseplate on the 6,000 lbf shaker, as well as the 18,000 lbf shaker.

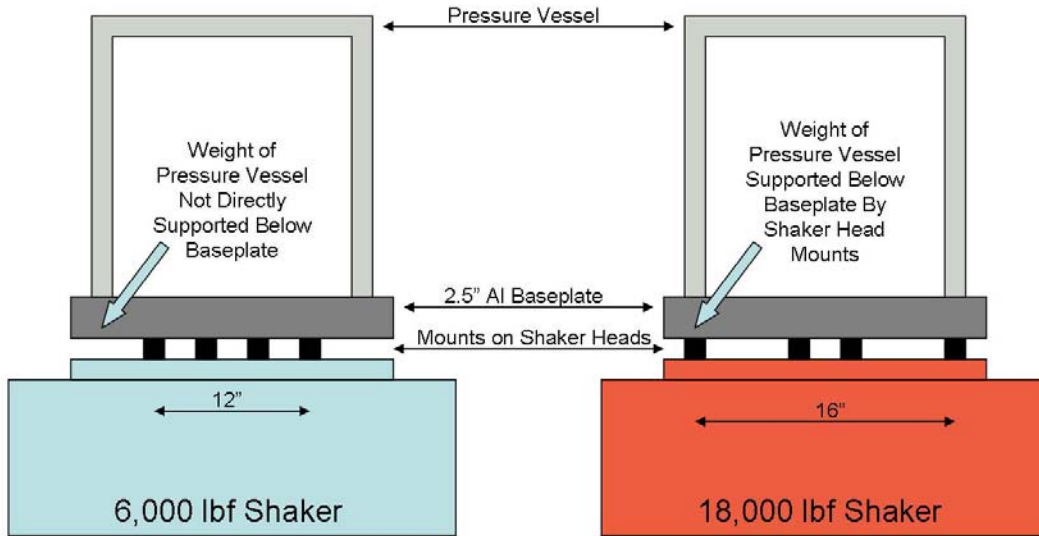


Figure 18. Side View of Pressure Vessel Support on Both Shaker Tables

The pressure vessel was mounted at a radius of 8” from the center of the baseplate. On the 18,000 lbf shaker, the baseplate was mounted to the shaker head at a radius of 4” and 8”. Because the bolt pattern on the shaker head, baseplate, and pressure vessel aligned at the 8” radius, they all attached together there with a single set of bolts. Further, the weight of the pressure vessel was largely supported by the shaker head underneath the baseplate. The extra mass was expected to lower frequencies on the 18,000 lbf shaker, but the effect of the added mass would be tempered by the support of the shaker head.

The situation on the 6,000 lbf shaker was different, though. The bolt pattern for mounting the baseplate was positioned at 4” and 6”. In this case, the pressure vessel sat on a baseplate which was not directly supported underneath. As such, when the pressure vessel was attached to the baseplate, the cantilevered circumference of the baseplate

supported the entire weight of the pressure vessel. The pressure vessel weighed over 40 lbs.

There was no way to avoid this mounting configuration on the 6,000 lbf shaker table. Throughout much of the testing in this study, the 18,000 lbf shaker was down for maintenance. Due to the size of the sample and the need to align the constraint blocks with the center of the shaker head, the pressure vessel could not be replaced with a smaller one. For example, a pressure vessel with attachments at a radius of 6" would impinge upon the specimen in the constraint blocks.

No FEA models were run which represented the pressure vessel on top of the baseplate. This decision was made for good reason. The FEA models already completed showed that the new baseplate would perform significantly better than its predecessor. Given these models, it could be seen that any modes in the baseplate itself would be nowhere near the modes of interest in the samples. Their drastic increase over the previous plate made interference, at least on the 18,000 lbf shaker, seem very unlikely.

Interference on the 6,000 lbf shaker, wherein the weight of the mounted pressure vessel was unsupported, seemed far more likely than on the larger shaker. As already mentioned, though, the pressure vessel mounting location could not be changed without significant redesign of the entire experiment, to include the samples themselves. Increasing thickness would make an already hefty baseplate even heavier. Therefore, even if a model was run and showed modal interference was likely due to this arrangement, nothing could be done. Given these facts, it was wiser to simply test the actual behavior of this particular configuration once the new baseplate arrived. Details

concerning the testing of the new baseplate-pressure vessel system are given in Chapter III, and the results of this testing are presented in Chapter IV.

Clamping Fixture and Pressure Vessel Concerns

The clamping fixture, also known as the constraint blocks, was inherited from previous investigators. The center threaded rods, which attach the top constraint block to the bottom, were of different length. In order to correct this potential problem, new threaded rods of equal length were used to replace these. The difference in length was great enough that the number of threads engaged in the bushings could have differed. It was thought that perhaps the different length of these rods was causing the clamping force to be non-uniformly distributed once the nuts were tightened.

Some concern also surrounded whether the pressure vessel itself could be contributing to the modal interference observed in previous cantilevered set-up testing. Indeed, Allen documented in his research that the handles welded to the pressure vessel were a matter of concern. It was believed that they resonated near the frequency of interest for the titanium specimens (2). Allen took great pains to model the pressure vessel before construction, and the handles were an unexpected addition.

The design of the pressure vessel allowed for data to be passed from the interior to the outside while it was in operation. Strain gauge wires, a thermocouple wire, and strain gauge wire soldered to a BNC were all present. As the reader may be aware, a BNC is a bayonet connection device commonly used on coaxial cables. The acronym BNC (Bayonet Neill-Concelman) pays homage to its inventors.

In order to mitigate any possible modal interference issues, it was desired to place the control accelerometer inside the pressure vessel and as close to the sample as possible. This could have been done using the existing BNC-wire connection, but it was decided to replace the wire with a coaxial cable and BNC. This was done in order to improve signal fidelity to the control accelerometer by reducing the number of connections required and increasing the quality of the cable. The thermocouple wire, as well as the soldered BNC connection, remained in the wiring bundle through the pressure vessel top. At the same time, additional strain gauge wiring was added in case they would be needed. This increased the overall capability of the pressure vessel, both for this and future studies.

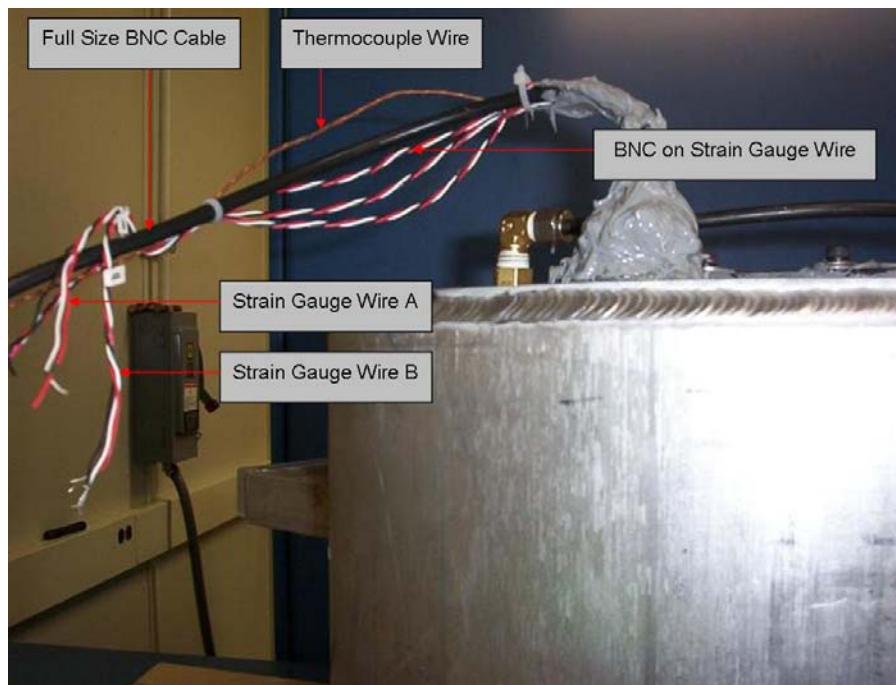


Figure 19. New Wires Providing Data from Inside Pressure Vessel

The baseplate, pressure vessel, blocks, and sample were never modeled together using FEA. As such, the modal frequencies to be expected through the interaction of the whole system were not known. Ping tests on the set-up were used to gain insight into this

interaction. As the reader may know, ping tests do not yield a complete picture of how every part of the system responds unless extensive ping testing is performed. However, ping tests are very useful as a means to gain a basic understanding of how areas of interest in a structure respond to an input force.

III: Test Set-Up and Procedures

This chapter fully details the tests run in order to obtain experimental vibration data. It also includes further descriptions of the techniques used to both design experiments and interpret the resulting data. The results of each set of experiments are shown in Chapter IV. Overall conclusions about those results are presented in Chapter V.

The chart given graphically depicts the overall design of this study, showing all experiments performed. Because many of the experiment designs were dependent on previous results, they were performed in a specific order. This order is indicated by the arrows within the diagram.

The bulk of the research focused on the cantilevered set-up, which was run on two different electrodynamic shaker tables. In order to prove the air damping effect, the system had to be well understood. Thus, numerous tests on various factors which could affect the system were performed before air pressure testing was completed. The effect of these additional factors had to be recognized so that they could be mitigated to the largest extent possible.

In the free condition testing, an air horn was used as the source of excitation. Instead of a clamped condition, the free-free-free-free condition was used. As demonstrated earlier in this document, the new boundary condition closely approximates the clamped condition testing through clever design of the free condition samples. The new boundary condition was used to eliminate many of the nuisance factors plaguing the cantilevered condition.

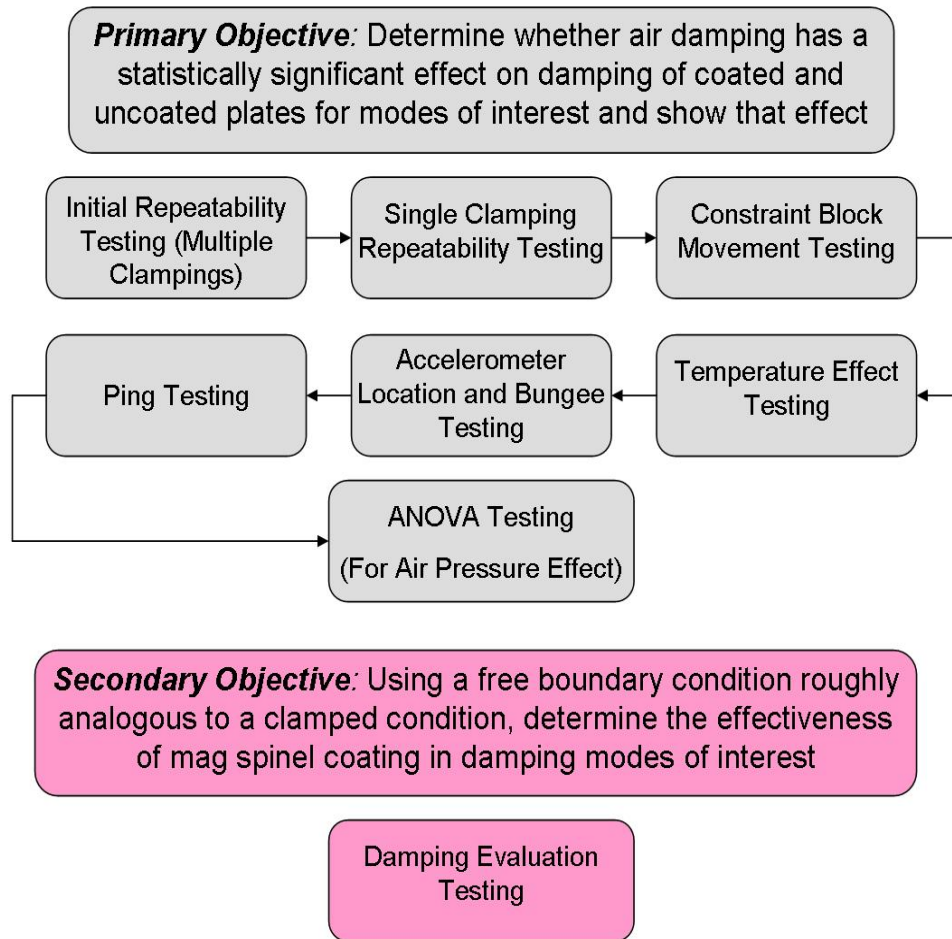


Figure 20. Overall Experimental Design

Electrodynamic Shaker Testing of Cantilevered Set-Up

All testing of the cantilevered samples was performed using one of two electrodynamic shaker tables. Though each table differed in its maximum capacity, both were sufficient to handle all tests required for this study. The capacity of an electrodynamic shaker is typically given in pounds force. That value represents the maximum force the shaker can handle in accordance with Newton’s second law.

Assuming the mass in question is not changing, this reduces to the well known equation below.

$$F = ma \tag{3.1}$$

F = Force (lbf)

m = mass (lbm)

a = acceleration in g's

If the force F is the maximum capacity of the table, the maximum acceleration achievable by the table can be determined if the mass m is known. This mass represents the sum of the mass of the shaker armature, the test sample, and the entire test fixture. The resulting acceleration a , determined from the equation above, will reduce to g's. That is, given the units above, the value for a represents the number of g's at which the shaker is run. Inputs controlling a shaker are entered in terms of g's. In this study, a "g" refers to an acceleration equal to Earth's sea-level gravitational acceleration. Thus, for each g at which the shaker is run, the machine is moved at an acceleration of 9.81 m/s^2 (or 32.2 ft/s^2). The number of g's used as an input acceleration is referred to as the g-level in this study. Due to the nature of the set-up, the input acceleration is not necessarily the same acceleration seen by the sample. Rather, it is the acceleration at the location of a control accelerometer.

Both shakers were run by the same controller, which utilized PC based Unholtz-Dickie software. The use of the same controlling and data recording system on both the 6,000 lbf and 18,000 lbf shakers allowed for better consistency and comparability between results. The diagram below outlines how the set-up on both shaker tables operated.

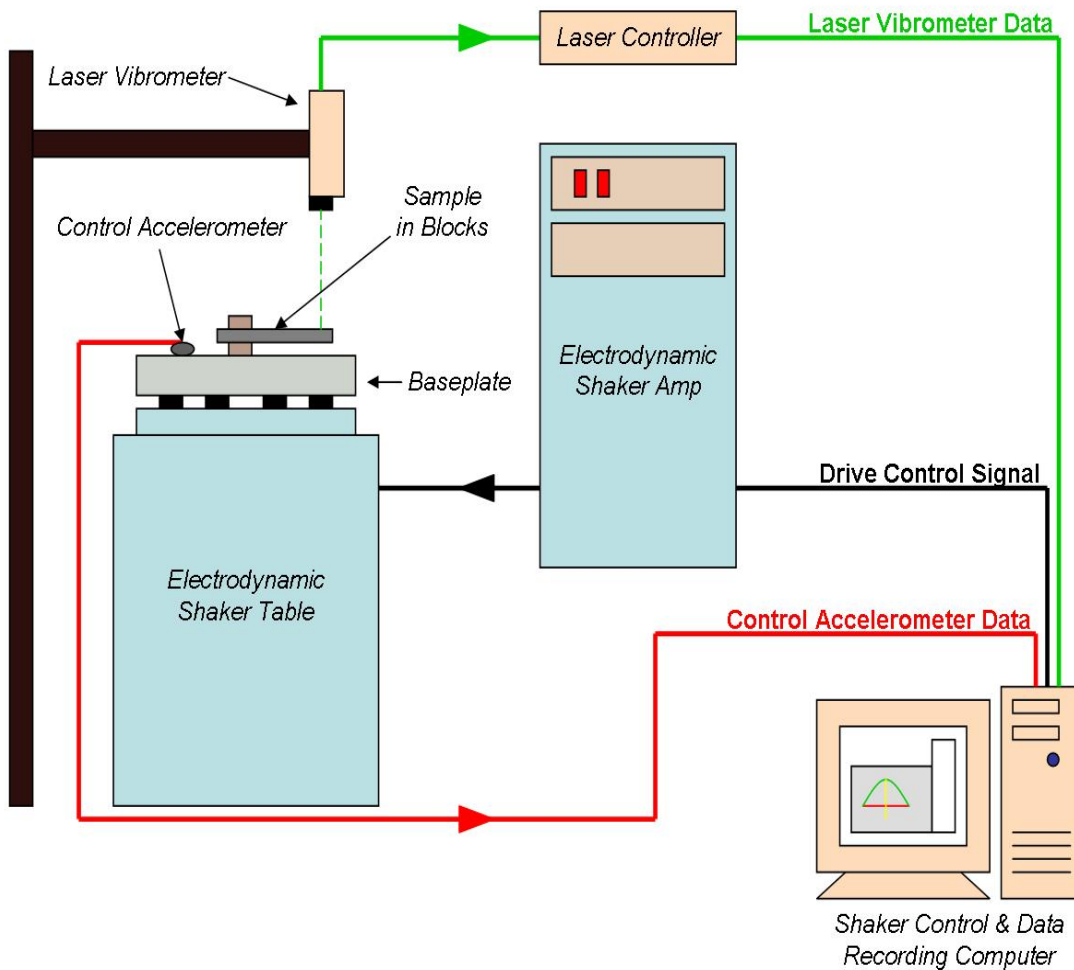


Figure 21. Basic Diagram of Shaker Table Operation

The above figure shows that a laser reads the velocity of the sample movement and feeds that information back to the controller, which records the data. The acceleration applied to the table was a sinusoidal input at a constant g-level. This input had a constantly changing frequency, thus making it a sine sweep. The rate of change of the frequency across the range of the test is referred to as the sweep rate. Sweep rates which are too high sacrifice resolution and lead to inaccurate results, while sweep rates which are very low make each test run excessively long (10). A sweep rate must be able

to capture the true bandwidth of a response in order to accurately determine damping (27). For this study, a sweep rate of 5 Hz per minute was used in all shaker testing. This sweep rate was sufficiently slow to satisfy the accuracy requirements of the material, and was the same rate used by Allen in his related study (2).

All tests run for this set-up were sine sweeps. Because of the nonlinear strain softening characteristics of the mag spinel coating, all of these sine sweeps run on the shakers were down sweeps. That is, the sweeps were run from high to low frequency. While linear resonant response peaks are symmetrical, nonlinear peaks bear a resemblance to ocean waves. They can bend over themselves, and in this bend three possible response amplitudes exist at one frequency. This leads to misshapen peaks where, in the case of mag spinel, down sweeps capture far more of the true curve and is thus closer to reality. Essentially, down sweeps record the top of the ocean wave. The down sweeps were a necessity in order to produce usable results, and also kept the experiment consistent with previous studies. It is important to note that down sweeps yield only an approximation of the actual damping, but this is an accepted method.

Prior research suggests that exceeding 750 microstrain can permanently damage the mag spinel coating (2). Because of this, all testing was done below this level. It has been noted that high strain memory effects in mag spinel coating can alter the results as well (22). That is, experimental runs at high strain levels may temporarily alter the behavior of the material and yield anomalous results in subsequent tests. The randomized nature of the testing required did not permit this investigator to run tests in increasing magnitude of input in order to mitigate this effect, as had previously been done (2).

Instead, results were closely monitored for inconsistencies which might indicate the presence of this phenomenon.

Clamping Fixture

The constraint blocks used to secure cantilevered specimens were the same blocks used by Blackwell and Allen. They were designed to better approximate the ideal boundary condition by reducing the movement of the sample within the blocks. They also increased consistency by making it easy to align the sample in precisely the same way each time it was placed within the blocks (4). The sample fit snugly over twin bushings in the center of the bottom block. Each of the two blocks was 7" long, 2" tall, and 2" deep. These blocks can be seen in the figure below.

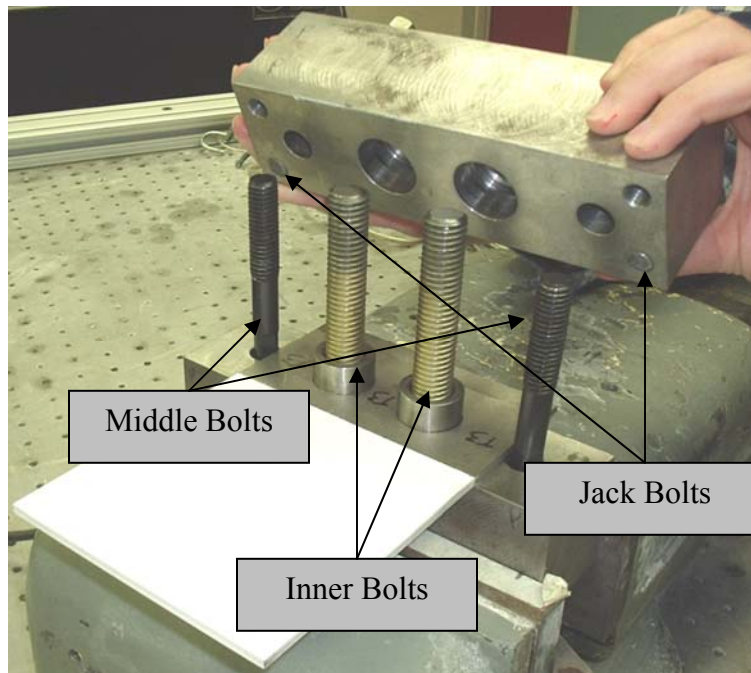


Figure 22. Constraint Blocks with Bolts Labeled (2)

The top block was placed on top of the sample and secured in place with large nuts over both the middle and inner bolts. The middle bolts connected the constraint blocks to the baseplate, while the inner bolts secured the sample in place within the blocks. The jack bolts were threaded through the top block and impinged on the lower block. This forced the top block to cant forward slightly onto the clamped edge of the sample, creating an improved boundary condition.

Throughout this study, the bolts were tightened in the exact same manner. Previous experimentation showed that alterations to the torque to which each bolt was tightened had no discernable effect in improving the damping values (2). Therefore, no consideration was given to optimizing the bolt torques. The bolts in this study were always tightened in the same order to their specified torque value by the same person using the same tools.

All torques were determined through the use of a torque wrench, and the same torque wrenches were used consistently. For the middle and outer bolts, a USAPro® Proto 6014 torque wrench performed the tightening. The smaller torque requirements of the jack bolts were fulfilled by a 1502 DI, manufactured by Consolidated Systems, Inc.

The bolt tightening sequence was logical and straightforward. First, the middle bolts were secured to a torque of 120 ft-lbs. Next, the inner bolts were tightened to 125 ft-lbs. Finally, the jack bolts, if used, were tightened to 120 in-lbs. In each case, each bolt pair was tightened together. The torque wrench was alternated between bolts, starting with the left one, so that each pair reached their desired torque at the same time. All bolts and nuts were labeled. They were used consistently in the same location after it was determined that total system damping was affected by the position of specific bolts.

Data Collection Location

The figure below shows the data collection location, or point of interest, which has been discussed previously. It sits at a point 0.1” from the tip of the specimen and 0.7” from the edge. This point was used for all tests run in this set-up. On all samples, a small reflective sticker was used to mark the measurement point. This sticker improved the return signal for the laser vibrometer, while also simplifying the task of consistently aiming the laser at the same point. Several of these stickers are visible on the sample in the figure below. These stickers are approximately 1/8” in diameter and are extremely lightweight.

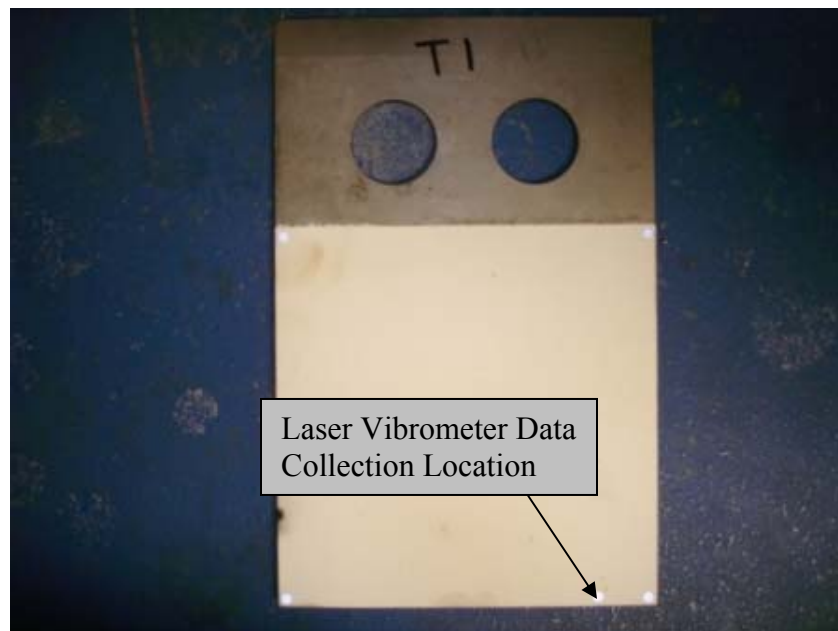


Figure 23. Laser Vibrometer Data Collection Location on Specimen (2)

This measurement location was chosen because it did not lie on or near a node line for either mode 3 or mode 4 (2). Keeping the measurement point away from node lines was vital to consistency. If a measurement point is away from a node line, it and the

surrounding area present a more forgiving target to the laser. This target will displace with relatively low velocity gradients nearby, which means that if the laser position varies slightly over the course of experimentation the results will not be skewed. If a measurement point is over a node, though, no displacement will be seen and there may be higher velocity gradients nearby. If the laser is shifted slightly in this case, repeatability will be lost. The results will show a relatively high variation in the velocity when the laser is repositioned, and the results themselves will not be indicative of the expected measurement point. The maximum strain/displacement relationship derived from the FEA model would be impossible to apply in this case as well, since this relationship varies greatly along the nodes.

Initial Repeatability Testing

The first sets of tests were used to determine variance between clampings for the uncoated sample mounted in the constraint blocks. Each time the sample was loaded into the constraint blocks and the bolts are torqued down, the boundary condition was slightly altered. Efforts were made to keep the configuration and torque of the constraint blocks as consistent as possible, and this portion of testing was dedicated to determining the effectiveness of those efforts.

The coated sample was not used in this testing because it was assumed that the effect of reclamping would be the same as for the uncoated sample. The portion of the sample which rested within the constraint blocks was uncoated and dimensionally identical for both the coated and uncoated samples. Further, the strain dependence of the

coated sample would have introduced another variable and made it more difficult to interpret the results.

This testing was performed using both the 18,000 lbf and the 6,000 lbf shaker tables. The original intention was to use the 18,000 lbf shaker exclusively, but it was out of commission for a large portion of the testing required. Both modes 3 and 4 were evaluated in this experiment. These modes were each tested at input levels of 1 and 8 g's on the 18,000 lbf shaker, and 1 and 4 g's on the 6,000 lbf shaker. These g-levels were constant inputs for a sine sweep. The previously given sweep rate of 5 Hz/min was used throughout this experiment. The control accelerometer used on each shaker was an Endevco ® 2271.

Due to the differing bolt patterns on the shaker heads, different baseplates were used on each shaker. The new 2.5" aluminum baseplate was under construction at the time, and therefore not available. Differences between the baseplates meant that the accelerometer was in a different position relative to the sample on each shaker. During testing on the 18,000 lbf shaker, the inner bolts were not of equal length. Testing on the 6,000 lbf shaker, and all tests in following sections, utilized new inner bolts, which were of equal length.

The test regime used on each shaker was very straightforward. The sample was clamped in to the constraint blocks, a sequence of 4 runs were completed, and then the constraint blocks were removed. The blocks were then reattached in the exact same manner as before and the experiment continued for 10 iterations. The four runs consisted of modes 3 and 4, each at two different g-levels. A table showing the specific test sequence and settings on each shaker is shown below.

Table 11. Settings and Test Sequence for Repeatability Testing Clampings

<i>Test Sequence on 18,000 lbf Shaker Table</i>			<i>Test Sequence on 6,000 lbf Shaker Table</i>		
g LEVEL INPUT	FREQ RANGE SWEPT (Hz)	MODE	g LEVEL INPUT	FREQ RANGE SWEPT (Hz)	MODE
1	1225-1275	3	1	1195-1235	3
1	1600-1650	4	1	1605-1645	4
8	1225-1275	3	4	1195-1235	3
8	1600-1650	4	4	1605-1645	4

Differences between the set-up and input levels on the two shakers meant the data from each could not be combined. Combining them would yield an incorrect assessment of variance due to reclamping. Because the experiments' data could not be combined into one set, they would have to stand alone and be compared as a whole. In order to take advantage of this situation, it was decided to run the 6,000 lbf shaker tests without jack bolts in order to see if the overall variance suffered. This would show if the jack bolts were indeed necessary, since their usefulness had been under discussion.

In addition, 2 runs on the 18,000 lbf shaker were added to experimentally verify the effectiveness of the 5 Hz/min sweep rate. It has been shown that the maximum sweep rate can be determined mathematically by employing the accepted Q value for a material, or by halving the sweep rate and verifying that the Q value observed does not change (26). For the 2 runs in question, the sweep rate was lowered to 2.5 Hz/min. Modes 3 and 4 were each tested at an input level of 1 g, and no appreciable difference in damping was found.

In each run, the frequency response curve for the sample, peak frequency (Hz), Q value, and peak velocity (mm/s) were recorded. Displacement values were determined using the peak velocity and peak frequency, and strain was then determined using the FEA derived strain/displacement proportion. There were a total of 42 runs on the 18,000

lbf shaker, where the sample was clamped into the blocks 10 times. On the 6,000 lbf shaker, there were 40 runs and the sample was clamped in to the blocks 10 more times.

Single Clamping Repeatability Testing

It was also desired to determine the variance between subsequent runs on a sample which had not been resealed into the constraint blocks. Therefore, all runs in this portion of the study were run using the same clamping. That is, the sample was never removed from the blocks. Prior research indicated that subsequent runs in the same clamping for this set-up could yield varying results (2). This effect was investigated using bookend tests in the past, but was not specifically studied before. Investigation between subsequent runs in the exact same clamped condition was designed to provide a baseline condition for how the results varied between tests. This would allow for a better understanding of how much variance was introduced by resealed the sample when results from this experiment were compared with those of the previous section.

In this portion of the study, only the unsealed sample was used. This was done for the same reasons quoted in the previous section. All testing for this experiment was performed on the 6,000 lbf shaker table. Mode 4 was studied at input g-levels of 1 and 4 g's, while a cursory examination of mode 3 was done at 1 g only.

Overall, 24 runs were performed for this experiment. Of these 24 runs, 20 of them investigated Mode 4, while only 4 of them were devoted to Mode 3. More runs were planned for this portion of the study, but unexpected results indicating a clear temperature and strain dependence in the constraint blocks demanded alterations to this

portion of the investigation. This realization would also lead to changes in the way future experiments would be performed. Chapter IV provides a full analysis of the testing from this section and highlights the implications of those results.

Constraint Block Movement Testing

In his work, Allen studied the possibility that different portions of the constraint blocks move differently during testing (2). This would imply that the boundary condition supporting the sample in the blocks is non-uniform. He measured movement at three locations across the top of the blocks for several different input g-levels in order to make comparisons. Indeed, his results indicated that different portions of the blocks moved differently for identical sine sweeps. Based on these findings, it was decided that differing conditions along the constraint blocks were a likely cause of variation between clampings. Further, it illustrated how the boundary condition along the root of the plate was non-ideal. In order to gain a fuller understanding of this situation, a more robust analysis of the block movement was designed.

This part of the investigation sought to show how the top constraint block moved as the sample swept through resonance. In each run of this study, the velocity of a particular point was recorded as frequency varied. In order to maintain comparability with Allen's work, the top block was measured at the exact same locations he used. These locations corresponded to the "right", "left", and "center" of the top block, with each point shifted toward the side of the blocks clamping the sample. The point of the interest on the sample itself was also measured, and is referred to as "sample." The

figure below shows the measurement locations and their respective orientations on the top of the blocks and the sample.

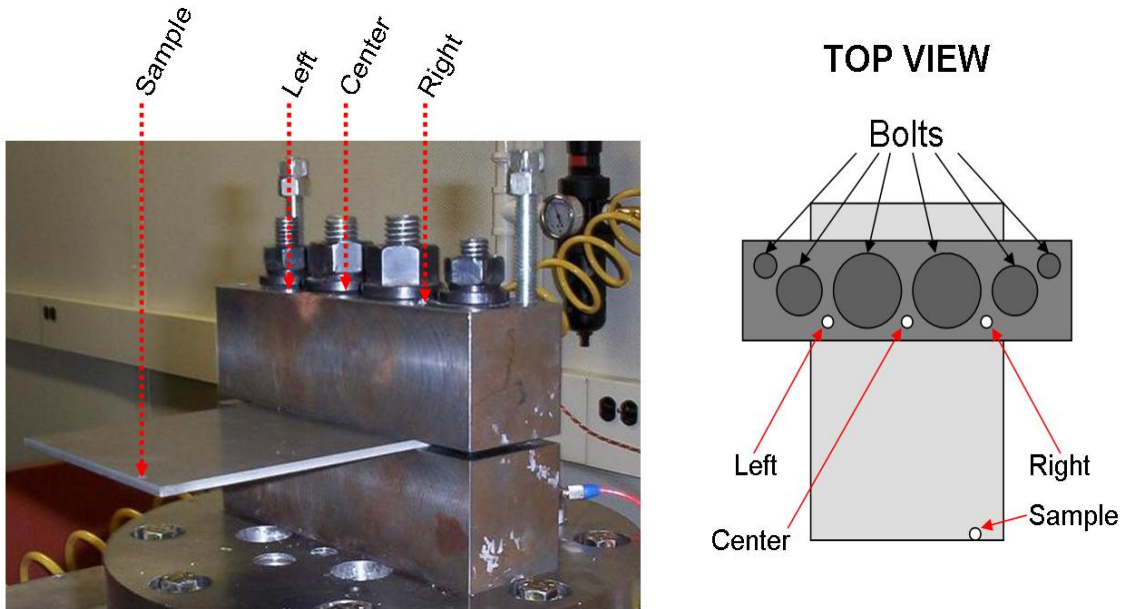


Figure 24. Clamp Movement Testing Laser Locations

Because the usefulness of jack bolts was still in question, they were included as the single varying factor in this experiment. The experiment design consisted of 16 runs each time the sample was clamped in place and tightened to the specified torques. At each of the 4 measurement locations, modes 3 and 4 were investigated both with and without jack bolts in place. This was done for 3 different clampings, producing an experimental design of 48 runs. Once again, this study only investigated the uncoated sample. The table below shows the run sequence used for the first clamping. This run sequence was later reversed in order to confirm that run order was not the driving factor in the results. All runs in this experiment were performed at an input level of 1 g.

Table 12. Clamp Movement Testing Sequence and Settings

FREQ RANGE SWEPT (Hz)	MODE	LASER LOCATION	JACK BOLTS (Y/N)
1210-1240	3	SAMPLE	NO
1615-1645	4	SAMPLE	NO
1210-1240	3	RIGHT	NO
1615-1645	4	RIGHT	NO
1210-1240	3	CENTER	NO
1615-1645	4	CENTER	NO
1210-1240	3	LEFT	NO
1615-1645	4	LEFT	NO
1210-1240	3	LEFT	YES
1615-1645	4	LEFT	YES
1210-1240	3	CENTER	YES
1615-1645	4	CENTER	YES
1210-1240	3	RIGHT	YES
1615-1645	4	RIGHT	YES
1210-1240	3	SAMPLE	YES
1615-1645	4	SAMPLE	YES

There was only one single point laser vibrometer available at the time of testing. Because of this, each time the measurement location changed the laser had to be moved. While simultaneous measurements of multiple points would have been highly preferable in observing the movement of the blocks, this was not a viable option. Instead, efforts had to be made to mitigate the variation between runs in one clamping. Several additional runs were performed in order to verify that data remained consistent.

Temperature Effect and Repeatability Testing

Because prior testing in this study indicated temperature was a major concern, it was decided to run a large series of tests investigating the effect of temperature on experimental results. This portion of the study evaluated temperature effect for multiple

runs of a single clamping, as well as runs where the sample had been reclamped. Only the uncoated sample was used in this experiment, which was also carried out on the 6,000 lbf shaker table.

For each run performed, the temperature of the blocks was recorded immediately before and after the sine sweep. This temperature was read through a thermocouple which had been spot welded to the blocks and used in Allen's study. Peak frequency, Q value, peak velocity, and the response curve as function of velocity versus frequency were also recorded for each run. Throughout this portion of the study, both modes 3 and 4 were analyzed. These modes were each tested at input levels of 1 g and 4 g.

An important consideration in designing this test was that temperature in the shaker rooms was not controllable. It was observed that temperature begins at ambient levels for the building, then increases when the shaker is turned on. The rate of temperature increase slowly drops off over time, until temperature reaches an approximate steady state. The temperature versus time curve would appear logarithmic in nature. Temperature in the shaker room could also be affected by changes in building configuration, such as someone leaving an exterior door open. Because of this, the experiment had to be designed to take advantage of temperatures as they occurred, rather than a regimen that specified which temperatures were to be evaluated.

In this section, a total of 96 experimental runs were completed. That breaks down into 24 runs for each permutation of mode and input g-level. A total of 44 runs were completed for the single clamping portion (corresponding to 11 sets of the 4 permutations, or 11 runs per permutation). The remaining 52 runs were performed with a reclamping of the sample after each set of 4 permutations were run (corresponding to 13 runs per

permutation). The table below shows the 4 permutations and the order they were run for this experiment.

Table 13. Temperature Repeatability Testing Sequence and Settings

g LEVEL INPUT	FREQ RANGE SWEPT (Hz)	MODE
1	1225-1255	3
1	1615-1645	4
4	1215-1245	3
4	1610-1640	4

This section produced interesting results which both built on prior testing for this study, and contributed directly to the understanding required to determine the significance of air damping.

Accelerometer Location and Bungee Cord Testing

The new 2.5” thick Aluminum baseplate was used for the temperature effect and repeatability testing described in the previous section. In that application, it worked quite well. However, in that configuration there was no pressure vessel installed. The attachment of the pressure vessel to the system would show whether modal interference issues would be a problem on the 6,000 lbf shaker. It was expected that the pressure vessel and baseplate combination would perform well on the 18,000 lbf shaker table, but there were questions surrounding whether the set-up would work well mounted on the 6,000 lbf shaker head. As discussed in Chapter II, the weight of the pressure vessel rested on an unsupported circumference of the baseplate when the baseplate-pressure vessel system was mounted on the 6,000 lbf shaker.

Instead of relying on an FEA model, it was decided to experimentally determine whether it would be possible to use the pressure vessel on the 6,000 lbf electrodynamic

shaker table. This was an important determination because the 18,000 lbf shaker was broken at the time. If the larger shaker could not be repaired, testing would have to be completed on the 6,000 lbf shaker. Further, the data taken regarding the use of the pressure vessel on the smaller table could have held applications to future research, or other investigators designing a similar system.

In this portion of the investigation, all testing was done at full atmospheric pressure. The pressure vessel was not attached to a vacuum pump or pumped down in any way, and the valve was left open. The uncoated sample was used in the majority of testing for this section. The coated sample was only loaded and tested in order to determine how susceptible it was to modal interference in this baseplate-pressure vessel-6,000 lbf shaker configuration. Testing of the coated sample consisted of 12 experimental runs, while all other testing utilized the uncoated sample. The uncoated sample was used primarily because it would not introduce any nonlinearity on its own, making it easier to recognize when the baseplate-pressure vessel system was creating interference. The configuration used in this testing is the same as that shown in Chapter I. Namely, the laser vibrometer can “see” the sample through an acrylic window in top the pressure vessel. It measures the sample just as before, reading velocity from the point of interest on the sample. The figure below shows this window in top of the pressure vessel.



Figure 25. Window in Top of Pressure Vessel

The first step was to evaluate what resonant frequencies, Q values, peak velocities, and frequency response curves were returned for the baseplate-pressure vessel system holding the sample. A total of 8 experimental runs, testing modes 3 and 4 at inputs of 1 and 4 g's, were performed. These were slow 5 Hz/min sweeps run over the frequency range of interest for each mode. The 8 runs used worked out to a total of 2 runs per permutation of mode and input level.

Because these tests showed modal interference, bungee cords were secured from the handles of the pressure vessel to the shaker table platform. The previous study suggested that a possible source of the interference was vibration of the pressure vessel handles. In fact, experimental runs in that study were carried out with bungee cords in place, restraining the pressure vessel handles (2). In this study, a total of 3 runs were performed with bungee cords in place. With the bungee cord testing, this investigator was looking for any evidence that the addition of the bungee cord altered the results. Such evidence, if found, would suggest that the pressure vessel handles were a factor in

generating modal interference. In both this bungee cord testing and the 8 runs discussed in the previous paragraph, the control accelerometer used was an Endevco® 2271. It was super glued onto the baseplate directly behind the constraint blocks, and connected to a coaxial cable passing through the top of the pressure vessel.

The next step in this section was to evaluate the accelerometer location. This was done because the placement of the accelerometer can have a profound effect on the results if modal interference in the baseplate is occurring. In order to ascertain whether this accelerometer placement was adequate, the pressure vessel was removed and a smaller accelerometer was placed directly on top of the constraint blocks. This smaller accelerometer was a PCB® 352B10. A different accelerometer had to be used because the Endevco® model was too large to place on top of the blocks. The proximity of the nuts on the top block left only enough real estate for a relatively small accelerometer to be attached and later removed. It was also mounted using superglue, to ensure that it would not fall out of place when the pressure vessel was reattached. Once the pressure vessel was reinstalled, 10 runs were performed with the small PCB® accelerometer in control. These were performed at input g-levels ranging from 1 to 5 g's for both modes 3 and 4. Runs representing modes 3 and 4 with 1 and 4 g inputs were directly comparable to runs performed with the larger Endevco® accelerometer in its position behind the blocks, while the other runs were meant to better highlight how the modal interference observed changed with increasing input acceleration.

The additional runs obtained using the small accelerometer did yield some interesting insight into how the modal interference was affected by the magnitude of the input signal. In order to capitalize on this finding, a series of broader sine sweeps were

run on the sample. These sweeps were run at a range of 120 to 150 Hz, centered at the peak frequency for either mode 3 or mode 4 of the sample. Due to the broader range of frequencies, and the fact that the Q value was not of primary interest in these sweeps, the sweep rate was increased to 30 Hz/min. Input g-levels of 1, 3, and 5 g's were run for mode 3, while inputs of 1, 3, 5, 6, 7, and 8 were run for mode 4. Intense shrieking, due to a strong resonance in the experimental set-up, meant that testing above 5 g's near mode 3 was inadvisable. This would have produced an intolerably loud noise.

Data pertaining to this section of testing is presented and evaluated in detail in Chapter IV. This data is complimented by the next section, which details the ping testing performed on the same set-up.

Ping Testing

In order to better understand the baseplate-pressure vessel system in place on the 6,000 lbf shaker, ping testing was performed. The goal of this testing was to experimentally determine, to the best extent possible, the modal frequencies in the entire system.

Ping testing works by imparting an impulse on a system, then measuring the response over time via an accelerometer placed somewhere on the system. The impulse is provided by a ping hammer strike, which is ideally as instantaneous as possible. The accelerometer reads a response over time. This time response, coupled with the input acceleration read by the hammer, allows the response data to be transformed into the frequency domain. There it represents the frequency response function (FRF) over a predetermined frequency range. This FRF represents the transfer function for the

locations of the accelerometer and the ping hammer strike. Therefore, using a ping hammer, one could theoretically find the modal frequencies at some location on the system relative to any input location. Additionally, if the positions of the accelerometer and hammer strike were swapped, the resulting frequency response would not be changed. Ping testing shows the frequency response between two points, and it does not matter which point is struck with a hammer and which is read with an accelerometer.

When testing equipment, desired ping locations may not be accessible. Take the baseplate-pressure vessel set-up in question as one example. When in operation, the shaker table moved the entire set-up up and down (*i.e.* vertically) in accordance with the sinusoidal input it was given. The best way to represent this input would have been to “ping” the center of the baseplate. However, when it was attached to the shaker head, it was inaccessible from the bottom to a ping hammer. When the pressure vessel was attached, the entire middle area of the baseplate inside an 8” radius was also inaccessible from the top by a hammer. Accelerometers could be placed at either the top or bottom of the baseplate at or near this location, but there was still no way to ping them from the ideal location.



Figure 26. Ping Hammer

Given this limitation, the ping testing performed for this study was done in such a way as to get the best results possible. The ping hammer could not strike the ideal location, so it instead was used to strike the outer edge of the baseplate. All ping testing was performed with the pressure vessel and uncoated sample in place on the 6,000 lbf shaker. Ping testing accelerometer locations included a pressure vessel handle, the top of the constraint blocks, the outer edge of the baseplate, the pressure vessel flange, and the acrylic window on the pressure vessel. The results of this testing show the modal frequencies expected from the structure in question.

Analysis of Variance (ANOVA)

It was desired to determine with a degree of certainty whether air pressure has an effect on damping for the cantilevered samples. This was the primary objective of this study, as stated previously. In order to accomplish this task, a statistical method for experimental design had to be employed. The method chosen was Analysis of Variance, which is commonly referred to as ANOVA. In ANOVA, each factor the experimenter wishes to evaluate is divided into treatments. After a series of runs, the ratio of variation between treatments to the variation within treatments is evaluated. If this ratio is adequately high, depending on the degree of certainty desired, the factor in question is said to be significant.

ANOVA is useful for showing which factors in an experiment have a significant impact on the result. It also allows for the interactions between factors to be tested for significance. In ANOVA, the significance found for a factor or interaction represents

that probability that the results obtained were due to their effect. ANOVA allows for testing of interactions, whereas experiments which modify only one factor at a time can not determine what happens when multiple factors are altered.

In ANOVA, the randomization of run order is important. This helps to mitigate the effects of time trends, which could be caused by any number of variables in the lab environment. If specific variations between sets of runs cannot be avoided, then groups of runs with homogenous conditions may be grouped together in blocks. These blocks allow results obtained under various conditions to be compared without unduly increasing the experimental noise. Ideally, they also prevent testing conditions from aliasing with the factors being studied.

ANOVA designs test each factor at a high (+) and low (-) level, and these levels are used in creating a standard experimental design. An ANOVA experimental design at two levels typically referred to as a 2^k design, where k represents the number of factors tested. Each time a full experimental design is repeated, it is termed a replicate. Increasing the number of replicates is, obviously, a good way to improve the certainty within the results and allow significant factors to shine through.

After an ANOVA experiment is completed, significant factors can be determined by using a half-normal plot. This plot charts the contrasts for each factor and interaction versus their linearized normal probability. Factors which do not fall in line with normal probability are assumed significant, and this significance is verified through the use of an ANOVA table. An ANOVA table shows the probability that each factor or interaction selected is significant in determining the response of a system, based on experimental data. The reliability of ANOVA results should be verified through the use of several

diagnostic plots, as well. These plots verify a normal distribution within the results, while also checking for unwanted time or measurement trends in the data.

The above explanation of ANOVA is obviously greatly simplified and does not impart any in depth understanding of how the process works. For those readers unfamiliar with ANOVA, the procedure is explained in far greater detail in Appendix A. In this section, the statistical theory is discussed first. This is followed by a discussion of ANOVA experimental design, and, finally, an explanation of how results are evaluated. The section in the appendix details terms associated with ANOVA, as well as several important experimental considerations, such as blocking, and randomization. The next section, titled “ANOVA Testing,” details how ANOVA was employed in this study.

ANOVA Testing

In this section, the actual testing carried out on the cantilevered specimens using ANOVA is described. All testing in this section was carried out on the 18,000 lbf shaker table, utilizing the newly designed baseplate and the pressure vessel. The pressure vessel-baseplate -18,000 lbf shaker configuration was used for all ANOVA testing. In this section of testing, a vacuum pump was used to evacuate air from the pressure vessel when necessary. This vacuum pump is shown below, along with a picture set-up on top of the 18,000 lbf shaker table.



Figure 27. Vacuum Pump and Pressure Gauge **Figure 28. Experimental Set-Up on 18k lbf Shaker**

The main objective was to determine whether air damping had a significant effect on damping for coated and uncoated plates. It was also desired to know if interactions with strain and mode shape played a role in the significance of this damping. Because damping, mode shape, and strain level were all important considerations which could be controlled, they were all picked as factors. These 3 factors were each set at two levels, making this a 2^3 experiment. Mode shape was a categorical factor, meaning the options for that factor were either “two-stripe” or “second bending”. Both strain and air pressure were based on numerical values, though, and were therefore entered as numerical factors. These factors were used throughout all ANOVA testing.

These factors were tested in such a manner as to produce the best results possible. As such, the results obtained from all previous sections of this study were put to use in order to design an effective ANOVA experiment. These results enabled the investigator

to eliminate or lessen many potential nuisance factors and design around others. Because reclamping the sample proved to cause changes in the measured damping and constraint block movement, it was decided to not remove a sample from the constraint blocks for the duration of its ANOVA testing. Day to day variations observed in the lab during previous testing meant that ANOVA testing would have to be blocked by day. That is, the testing carried out each day was grouped in to its own block. Jack bolts were used in all ANOVA testing because they had proven valuable in reducing unwanted movement of the top block. In order to combat temperature change in the room, all testing was performed only after the shaker table room had reached an approximate steady state temperature. This both removed a potential temperature related trend and made it easier to produce consistent strain values.

Several other factors were considered for this experiment, but could not be used due to practicality concerns. Ideally, the coating on the sample (either coated or uncoated) could have been included as a factor as well. However, this would have required the investigator to continually insert and remove these samples from the blocks. This would have certainly been tedious, but it would have also meant changing the clamped condition. The changes to the clamped condition meant the results would vary and perhaps cloud the significance of the factors being studied. Any change observed for the different samples would also, obviously, be aliased with the concurrent changes in the blocks.

It was initially desired to test foam under the blocks as well. The “foam” versus “no foam” factor could have indicated whether there were pressure wave effects on the interior walls of the pressure vessel. However, removing and replacing the foam would have required the experimenter to continually remove and replace the pressure vessel as

well. This would have made the testing process very long, and possibly made it impossible to complete a single replicate in one working day. Further, the effect of the foam would be aliased with the removal and replacement of the pressure vessel. Since the pressure vessel and baseplate shared constraint bolts, this reattachment had the potential to change the configuration of the system during testing as well. In order to protect the integrity of the overall experiment, these factors were not included. The coated and uncoated samples were tested in separate experiments, while foam testing had to be ignored.

Ideally, the ANOVA design used would have incorporated centerpoints as well. Several centerpoints could have been added to each block in order to check for curvature. This was, however, not a practical solution. An imperfect seal in the pressure vessel meant that testing could not be performed at partial pressures, so only near vacuum and full atmospheric pressures could be tested. Further, the categorical factor for mode shape meant that it had no centerpoint. Even if this factor was numerical, a frequency in between the two mode shapes would not be at a resonance, and would be meaningless. In light of this, no centerpoints were used in ANOVA testing.

The uncoated sample was tested using 3 replicates, where each replicate corresponded to a block. Each block in turn represented a different day of testing. Given the 3 factors mentioned, this corresponded to $2^3 \times 3 = 24$ experimental runs, in blocks of 8 runs each. Though there were only 8 ANOVA runs used from each day, many more runs were actually performed. In most cases, attaining the desired strain values took several tries. Only those runs who strain values closely matched the desired values were used in ANOVA analysis. The factors used and their respective high(+) and low(-)

settings are given here. The value of 500 microstrain was consistent with the testing limit imposed by Allen in order to avoid any possible damage to the sample. This was well below the suspected coating damage threshold of 750 microstrain. The air pressure levels were set so that they spanned the greatest range possible. This was done so that any air damping effect would be more likely to show up in the results. If pressure differences between the high and low settings were small, their effect might be lost in the noise.

Table 14. Factors and Settings for ANOVA Testing

Factor	Units	High (+)	Low (-)
Mode Shape	--	two stripe	second bending
Air Pressure	mm Hg	741	5
Strain	microstrain	500	150

In testing the uncoated plate, the response was Q value. ANOVA analysis was used to determine the significant factors affecting this response in this experiment, as well as all other ANOVA testing. The table below shows the experiment design used for the uncoated sample testing. The standard run order has been randomized within blocks, producing a randomized run order for experimentation. Standard run order refers to the run order which would be generated through the use of a design matrix.

Table 15. ANOVA Experiment Design for Uncoated Sample

Std	Run	Block	Factor 1 A:mode	Factor 2 B:air pressure torr	Factor 3 C:strain microstrain
13	1	Block 1	2nd Bend	5	500
22	2	Block 1	Two Stripe	741	500
16	3	Block 1	Two Stripe	5	500
4	4	Block 1	Two Stripe	5	150
10	5	Block 1	Two Stripe	741	150
1	6	Block 1	2nd Bend	5	150
7	7	Block 1	2nd Bend	741	150
19	8	Block 1	2nd Bend	741	500
11	9	Block 2	Two Stripe	741	150
8	10	Block 2	2nd Bend	741	150
20	11	Block 2	2nd Bend	741	500
17	12	Block 2	Two Stripe	5	500
14	13	Block 2	2nd Bend	5	500
5	14	Block 2	Two Stripe	5	150
23	15	Block 2	Two Stripe	741	500
2	16	Block 2	2nd Bend	5	150
15	17	Block 3	2nd Bend	5	500
18	18	Block 3	Two Stripe	5	500
9	19	Block 3	2nd Bend	741	150
24	20	Block 3	Two Stripe	741	500
6	21	Block 3	Two Stripe	5	150
12	22	Block 3	Two Stripe	741	150
21	23	Block 3	2nd Bend	741	500
3	24	Block 3	2nd Bend	5	150

The first experiment conducted on the coated sample was conducted in the exact same manner. The same factors at the same high and low settings were used, and the same experimental design was followed. The experiment design for testing of the coated sample is shown below. Note that the only difference between it and the uncoated design is that randomization has produced a different run order.

Table 16. ANOVA Experiment Design for Coated Sample

Std	Run	Block	Factor 1 A:mode	Factor 2 B:air pressure torr	Factor 3 C:strain microstrain
10	1	Block 1	two stripe	741	150
19	2	Block 1	2nd bend	741	500
16	3	Block 1	two stripe	5	500
7	4	Block 1	2nd bend	741	150
4	5	Block 1	two stripe	5	150
13	6	Block 1	2nd bend	5	500
1	7	Block 1	2nd bend	5	150
22	8	Block 1	two stripe	741	500
17	9	Block 2	two stripe	5	500
8	10	Block 2	2nd bend	741	150
11	11	Block 2	two stripe	741	150
14	12	Block 2	2nd bend	5	500
5	13	Block 2	two stripe	5	150
2	14	Block 2	2nd bend	5	150
20	15	Block 2	2nd bend	741	500
23	16	Block 2	two stripe	741	500
24	17	Block 3	two stripe	741	500
21	18	Block 3	2nd bend	741	500
3	19	Block 3	2nd bend	5	150
18	20	Block 3	two stripe	5	500
9	21	Block 3	2nd bend	741	150
15	22	Block 3	2nd bend	5	500
6	23	Block 3	two stripe	5	150
12	24	Block 3	two stripe	741	150

In order to better characterize the coated sample, more experiments were designed and run on the individual mode shapes. Specifically, two 2^2 designs were completed on the two-stripe mode, and one 2^2 design was completed for the second bending mode. These additional experiments studied different high and low strain levels, while continuing to use the same treatments for air pressure. Mode shape was fixed for all three of these additional experiments, and therefore removed as a factor.

The first of these additional experiments looked at the two stripe mode. Because this mode proved interesting in the initial coated plate ANOVA experiment, it was decided to pursue a further test which dealt only with this mode. Air pressure was shown to have a significant effect, and results indicated it had a much greater effect in the

two stripe mode. This was further supported by the significant interaction between mode and air pressure. It was thought that removing mode as a factor would further show how air pressure was significant. The factors, levels, and design used for this experiment are shown below. Note that the high and low settings remain the same here for both factors. This was done so that data from both experiments could be combined, if required.

Table 17. Modified Factors for Additional Testing Mode 4, Coated

Factor	Units	High (+)	Low (-)
Strain	microstrain	500	150
Air Pressure	mm Hg	741	5

Table 18. Experiment Design for Additional Testing Mode 4, Coated

Std	Run	Block	Factor 1 A:pressure torr	Factor 2 B:strain microstrain
10	1	Block 1	741	500
11	2	Block 1	741	500
4	3	Block 1	741	150
5	4	Block 1	741	150
1	5	Block 1	5	150
2	6	Block 1	5	150
6	7	Block 1	741	150
12	8	Block 1	741	500
3	9	Block 1	5	150
9	10	Block 1	5	500
7	11	Block 1	5	500
8	12	Block 1	5	500

The second additional experiment performed also focused on the two stripe mode on the coated sample. The goal of this experiment was to look at different strain levels and determine if air pressure remained a significant factor. The factor settings and experimental design for this experiment are shown here as well.

Table 19. Modified Factors for Additional Strain Testing Mode 4, Coated

Factor	Units	High (+)	Low (-)
Strain	microstrain	350	20
Air Pressure	mm Hg	741	5

Table 20. Experiment Design for Additional Strain Testing Mode 4, Coated

Std	Run	Block	Factor 1 A:pressure torr	Factor 2 B:strain microstrain
10	1	Block 1	741	325
12	2	Block 1	741	325
9	3	Block 1	5	325
8	4	Block 1	5	325
3	5	Block 1	5	20
1	6	Block 1	5	20
7	7	Block 1	5	325
5	8	Block 1	741	20
6	9	Block 1	741	20
2	10	Block 1	5	20
4	11	Block 1	741	20
11	12	Block 1	741	325

Finally, the last additional ANOVA experiment was run on the second bending mode of the coated sample. This test was also performed at different strain levels than the main experiment. The objective of this experiment was to gain data for different strain values at this mode while simultaneously determining if air pressure had a significant effect on this mode. The factor settings for this experiment are the same as for the experiment described immediately above. The experimental design is shown in the table below.

Table 21. Experiment Design for Additional Strain Testing Mode 3, Coated

Std	Run	Block	Factor 1 A:pressure torr	Factor 2 B:strain microstrain
8	1	Block 1	5	325
12	2	Block 1	741	325
1	3	Block 1	5	20
5	4	Block 1	741	20
7	5	Block 1	5	325
3	6	Block 1	5	20
10	7	Block 1	741	325
2	8	Block 1	5	20
11	9	Block 1	741	325
4	10	Block 1	741	20
6	11	Block 1	741	20
9	12	Block 1	5	325

In producing the experimental designs shown, Design Expert ® software was used. This software was programmed to utilize ANOVA theory, and saved time both in designing experiments and analyzing the results. The results and analysis of ANOVA testing, presented in Chapter IV, were produced using this software as well.

Overall, ANOVA testing produced valuable results. These results are expressed in the following chapter. The results are given in terms of ANOVA analysis, indicating statistical significance, as well as in standard plots. The standard plots show the results of all runs performed in the course of this testing, while the runs used for ANOVA were only those where strain values achieved were sufficiently close to those desired. Inconsistency in strain values would skew the results of the statistical analysis required by ANOVA, but all the runs performed are still valid experimental data. The ANOVA analysis shows the statistical significance of the factors in question, while a more standard analysis of the data allows the reader to see the effects quantitatively.

The ANOVA results show which factors and interactions included in the experiment are at least 95% certain to have affected the results. ANOVA shows conclusively that changes are imparted on the system and which of the experimental factors are causing those changes. It is left to the standard plots to show this effect, though, and allow for interpretation as to the magnitude and direction of these changes. ANOVA thus works well in conjunction with a standard presentation of the data, as seen in Chapter IV.

Air Horn Testing of Free-Free-Free-Free Condition Set-Up

In addition to the series of tests run on the shaker table, a series of tests was also performed using different samples and a different excitation method. As previously mentioned, these samples were the 9"x4.5"x0.125" specimens. They were designed to hang in a free-free-free-free condition, which would avoid many of the loss mechanisms and repeatability issues present for the cantilevered sample. This sample was also designed to produce nearly identical mode shapes to the cantilevered sample. The goal of this testing was to gain further perspective into the effectiveness of mag spinel coating in damping an oscillating plate. It was also hoped that, given the similarities in mode shape and size, some comparisons could be drawn between the cantilevered and free-free-free-free sample.

An acoustic air horn would have yielded the same excitation levels as magnetic excitation, but offered key advantages. When using a magnet, magnetically attracted discs must be attached to the titanium samples in order to allow it to excite the structure. The addition of these discs to the samples, understandably, alters the samples.

Additionally, air horns produce more repeatable results than magnets. Slight misalignments of the air horn between tests have less effect on the final results than slight misalignment of magnets. Because of these considerations, it was decided to use an air horn for this testing.

No air pressure testing was performed on the free condition samples. Previous work in determining air pressure effects on a free-free-free-free plate of similar dimensions proved inconclusive (2). It is likely that any air pressure effects present were lost in the noise, as the displacements involved in that testing were miniscule. Since similar displacements (on the order of nanometers) would be achieved with these samples, it was decided to forgo air pressure testing in this study.

In this section, references are once again made to a slow chirp and windows. A chirp test is typically a quick burst of sinusoidal signal which increases or decreases in frequency during its execution, and covers a specified frequency range. In this study, a slow chirp refers to a chirp signal which has been increased in duration in order to attain better resolution in the results. While a chirp is ideal for scanning numerous points and determining modal shapes, more resolution is required in order to determine damping in the manner prescribed by this study. This is discussed in more detail later in this section.

As the reader may know, windows are a set of constants multiplied over data in order to produce cleaner results. In each segment of data, they may multiply data in the center by higher factors than data at the edges. The multipliers used vary in their distribution depending on the application. Windowing alleviates leakage, or discontinuities caused by non-periodic data at the edges of a segment of data (5).

ANOVA was not used in this part of the study because only the effect of mag spinel coating on the sample's damping was being studied, and it was already assumed that this factor would be significant.

Free Condition Mounting Fixture

This testing was performed using a high frequency acoustic air horn as the excitation source, which was controlled via Polytec® software. The velocity of the sample was measured via a Polytec® scanning laser vibrometer. The laser vibrometer scanned the “front” side of the sample, or the side without the air horn. The set-up used for testing is shown in the picture collage below.

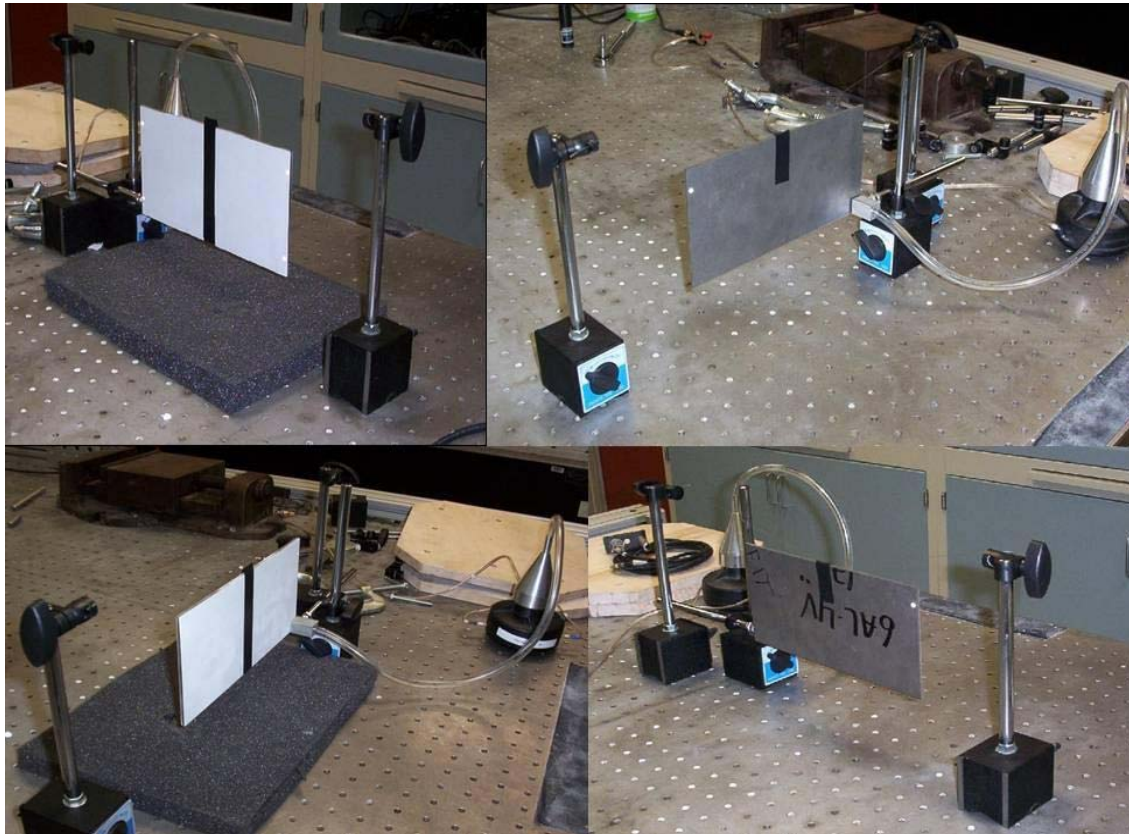


Figure 29. Test Set-Up for Coated and Uncoated Free Samples

Both the coated and uncoated sample were set up in the same manner. The sample was suspended from the centerline via a length of Spyderwire® string, which had been attached to the sample via electrical tape. Spyderwire® was used because it possessed strength, yet also did not stretch. Either end of the Spyderwire® was tied to the tops of poles, which were screwed into magnetized bases. The sample was always positioned perpendicular to the scanning laser vibrometer and level with the table. The table itself was level and self-damped. The air horn was always placed so that it lined up precisely with the lower corner of the sample, as shown in the picture above.

In all testing, the top of the sample was 7" from the surface of the table. A small portion of electrical tape was required to secure the Spyderwire® to the uncoated sample. However, a frustrating series of tests revealed that electrical tape does not adhere well to mag spinel coating. As such, a much longer piece of electrical tape was required to secure the mag spinel coating to the wire. Because this tape still lay along a node line, and the coated sample was already more massive than the uncoated sample, this extra tape was considered to be a non-issue. Electrical tape was used because it possessed both a good tack and strength for a relatively small width. The strength of the tape was essential, as a lesser tape would allow the Spyderwire® support string to tear through, or would have required width that would have extended past the center node line. A small block of foam was placed under the sample in order to cushion its fall if the support, tape, or string failed.

The use of electrical tape is not believed to have significantly altered the results of the experiment. The mode shapes found for both the coated and uncoated sample in mode shape verification appeared unaltered by the tape. Even shapes which crossed the

center line, where the tape was located, appeared unaffected. When modal verification tests were performed, equally sized pieces of tape were used on each sample. This negates the possibility that differing tape sizes caused the different modal frequencies seen in the samples, as discussed in Chapter II.

In this experimentation, it was found that placement of the acoustic air horn was key in producing repeatable results. A slight variation in the alignment of the air horn with the corner of the sample could produce varying results for damping. Some tests were run before the key nature of this placement was realized, and those runs had to be thrown out. None of those runs are included in this study. The air horn distance to the sample was adjusted throughout testing in order to attain varying strain levels in the samples.

Symmetric Data Collection Locations

In testing the free condition samples, four data collection locations were always used. These locations each corresponded to a position 0.1” from the end of the sample and 0.7” from the edge. That is, 0.1” from the short side and 0.7” from the long side. Because both modes of interest were symmetric about the sample, these measurement locations were all also assumed to be symmetric. They would all displace in the same way. The measurement location was chosen because it was the same location used on the cantilevered samples. The measurement locations of the free-free-free-free samples are shown below. The same locations were used on the coated and uncoated samples. Note that each of the measurement locations has been marked by a reflective sticker, which made it easier to aim the laser at the same location consistently.

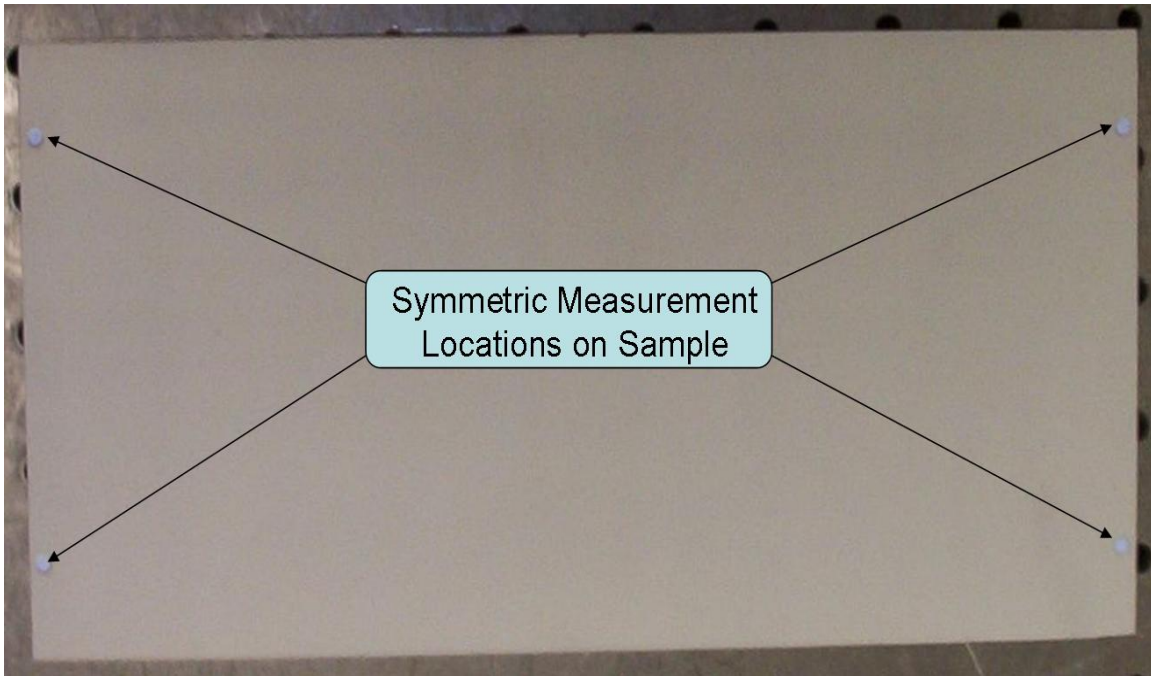


Figure 30. Symmetric Measurement Locations on Free Sample

The use of a scanning laser meant that more than one point on the sample could be measured during an experimental run. The measurement of 4 separate points in each run minimized the chances of error. For example, if the laser was slightly misaimed from time to time, the averaging of data at 4 symmetric points would help to cancel out that small error. If only one point was measured, there would be no way to counteract the error arising from a misaimed laser, or any other source of error. Averaging multiple points, which all show the same displacement, introduced redundancy into the experiment. This was especially important when measuring small displacements, because small errors can have big consequences in the damping calculated if left unchecked.

Damping Evaluation Testing

Because small displacements were expected from the air horn excitation, strict attention to detail was a vital part of the experiment set up. The set up had to be the same every time, otherwise the results would be extremely inconsistent. The same was true for the data collection required.

Data collection began by establishing a plane of reference for the laser. In order to establish this plane, the laser was sequentially targeted at arbitrary points chosen by the user. This plane of reference represented the position of the sample when it was hanging still. It allowed the laser to coordinate with the software and establish relative positions on the surface of the sample. Every time the sample set up was altered in any way, the plane of reference had to be reset. Failure to do this resulted in unusable results. In order to maximize consistency, multiple points in the same pattern were always used to establish this plane. Five points were used in a vertical row near each data collection location for a total of 20 points. The points were taken near the data collection locations to ensure the software accurately understood the equilibrium position of the plate in these locations. This pattern is shown here.



Figure 31. Laser Plane Point Locations on Free Sample

Data was collected by performing slow chirps over specific frequency ranges. A signal generator within the software created this signal, which was then amplified and sent to the acoustic air horn. Because these chirps were performed slowly, they were essentially sine sweeps. In each test run, multiple slow chirps were performed at each of the 4 data collection points. The scanning laser vibrometer recorded the velocity of each plate as it was being scanned. Windows were not used in any of the test runs. The use of windowing would have introduced a bias into the results and altered the shapes of the response peaks, making an accurate determination of damping and displacement impossible. The figure below shows a diagram of the scanning laser and each of the points on the sample which were individually measured using these settings.

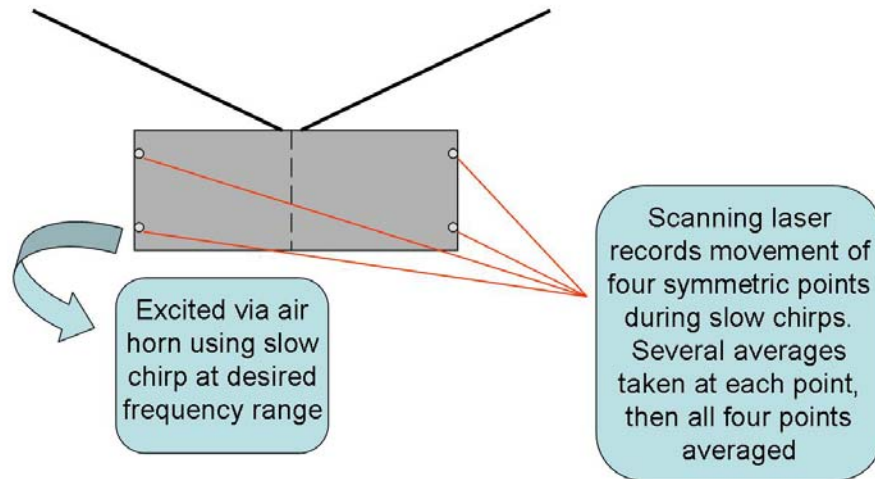


Figure 32. Laser Scanning Each Point on Sample

The results from all chirps at each of the points were averaged together to produce an overall response plot. This response plot was viewed in the form of displacement vs. frequency in order to find the maximum displacement, peak frequency, and Q value. Q

value, or damping, had to be calculated by hand. The specific number of averages used, frequency ranges, and resolution for each mode shape and sample are all shown in the table below. In all cases, the maximum resolution and slowest chirp allowed by the software were used. This was achieved by zeroing in on the desired peak frequency for each mode, and setting the bandwidth as small as possible.

Table 22. Settings Used for Free Condition Experiment

SAMPLE	MODE	RESOLUTION	TIME PER CHIRP	CENTER FREQ	BANDWIDTH OF CHIRP	AVERAGES PER POINT
Uncoated	4	20 mHz	50 sec	848.64 Hz	1 Hz	3
Uncoated	7	40 mHz	25 sec	1510 Hz	2 Hz	5
Coated	4	20 mHz	50 sec	884.48 Hz	1 Hz	3
Coated	7	40 mHz	25 sec	1547 Hz	2 Hz	5

In order to calculate the strain values achieved, the strain/displacement relationships discussed in Chapter II were used. Separate strain relationships were used for each mode shape. While displacement in the cantilevered testing had to be calculated by hand, the software used in this testing was able to calculate displacement using the acquired velocity data. As with the cantilevered sample, the same strain/displacement relationships were used for both the coated and uncoated samples.

The number of valid runs performed for each permutation of mode shape and sample is given here. The reader may note that a much greater number of runs were completed for the second bending mode of the coated sample. This was done in order to establish a clear trend in the results, which had initially proven difficult in that particular case.

Table 23. Runs Completed for Free Condition Experiment

SAMPLE	MODE	# VALID RUNS COMPLETED
Uncoated	4	19
Uncoated	7	18
Coated	4	39
Coated	7	18

All measures of displacement were determined inside the software through integration of the velocity signal, while all values for damping were calculated by hand using the results of each run. All damping was calculated in terms of Q value. This Q value, or quality factor, was calculated using the half-bandwidth method. The response curve for a mode of interest was plotted by the software, and the values required to calculate Q value were pulled from this plot. The software used to gather data was incapable of calculating damping given a response curve. A sample response plot is shown in Chapter IV along with the other results from this experiment. Chapter IV also shows how rigid body motion was avoided in this set-up.

IV: Results and Discussion

This chapter details the results obtained from all experiments in this study. The set-up for each of the experiments is detailed in Chapter III, and the results are given in the same order in which the tests are presented in that chapter. Both the results from the cantilevered testing on the electrodynamic shaker table and the free condition testing using air horn excitation are included in this chapter.

Comparisons were made between strain levels rather than the g-level of the input when analyzing damping results. Due to changing conditions in the lab and variations in different experimental set-ups, input g-level was not a valid means of comparison. Given different set-ups, the actual force felt by the sample varied and the strain felt by the samples was different. Differences in the set-up arose from such factors as the use of a different shaker table, baseplate, sample, or accelerometer position. The input g-level also produced different levels of strain within the sample given different laboratory conditions. This was true even if the set-up of the experiment had not been changed.

The use of strain levels for comparison was followed strictly throughout this chapter. The only exception is in repeatability testing, where the variation between tests is being analyzed. There, comparisons are made between g-levels in order to better understand how the results changed between runs. Even in these experiments, though, results are also presented in terms of strain wherever possible.

Damping values in this chapter and associated appendices are presented as a Q value, as defined in Chapter I. All strain values are given in terms of microstrain, where 1 microstrain is equal to 1×10^{-6} strain (in/in).

In this chapter, plots and tables summarizing the resulting data are presented. Plots showing the frequency response functions of the raw data are presented as well. The additional results in the appendices are referenced when appropriate. While this chapter does discuss the results obtained and immediate conclusions, conclusions regarding the entire scope of this study are drawn in Chapter V.

Electrodynamic Shaker Testing Results

The results of testing on cantilevered samples are detailed in the following subsections. This testing was successful, and has yielded new understanding of the constraint blocks used to hold the sample. It has also highlighted some of the numerous factors affecting the total damping of the system.

Initial Repeatability Testing Results

It was desired to know whether reclamping the uncoated sample in the blocks had an impact on the damping values recorded. That is, the experimenter wanted to know whether reloading the sample into the constraint blocks caused changes in the results of sine sweeps at given force levels. In this testing, the experimenter endeavored to minimize the differences introduced in subsequent clampings by standardizing the routine for attaching the sample.

Repeatability between clampings was an important consideration in the way ANOVA testing would be carried out. If there proved to be no significant variation between the results for each time the sample was loaded, then ANOVA experiments could be carried-out over numerous reclampings of the samples without the use of statistical blocks. This would yield more significant results, and allow a greater number

of factors and interactions to be studied. For example, if the constraint blocks proved highly repeatable, plate coating (*i.e.* coated vs. uncoated) could be studied as a factor within a statistical experiment, and the interactions introduced would have yielded further insight into how the entire system responded to air pressure.

Unfortunately, the results showed that repeatability between clampings for the blocks was unacceptably low. This meant that the sample coating could not be used as an ANOVA factor. The variation between clampings on the constraint blocks would coincide with the change in samples if that factor was used.

The results of this multiple clamping repeatability testing are given both in terms of the strain seen in the sample, and the input force applied to the sample. On each of the 2 shaker tables, testing was carried out at 2 input levels for both modes 3 and 4 of the uncoated sample, as shown in the previous chapter.

Testing was first conducted on the 18,000 lbf shaker table. The input g-levels used were 1g and 8g. In this experiment, Modes 3 and 4 were tested at each of these levels, then the sample was reclamped and the tests were repeated. This testing was carried out over several days. The results for testing on mode 3 at an input of 1g are shown below.

Table 24. Repeatability Results, Mode 3 1g 18k Shaker

Date	Torque Down	Control Accel (g)	Mode	Peak Freq (Hz)	Q Value	Velocity (mm/s)	MicroStrain
24-Aug	TD1A	1	3	1245.840	139.53	114.60	57.62
26-Aug	TD2A	1	3	1246.177	119.53	98.62	49.57
26-Aug	TD3A	1	3	1244.877	116.33	91.72	46.15
26-Aug	TD4A	1	3	1243.502	117.58	93.09	46.89
31-Aug	TD5A	1	3	1245.577	83.17	63.13	31.75
31-Aug	TD6A	1	3	1244.552	86.57	63.14	31.78
31-Aug	TD7A	1	3	1244.452	102.41	73.12	36.80
1-Sep	TD8A	1	3	1245.052	129.68	97.11	48.85
1-Sep	TD9A	1	3	1244.527	107.74	80.74	40.64
1-Sep	TD10A	1	3	1244.102	116.81	86.27	43.43
				AVG	1244.866	111.94	43.35
				STD DEV	0.819	17.60	8.24

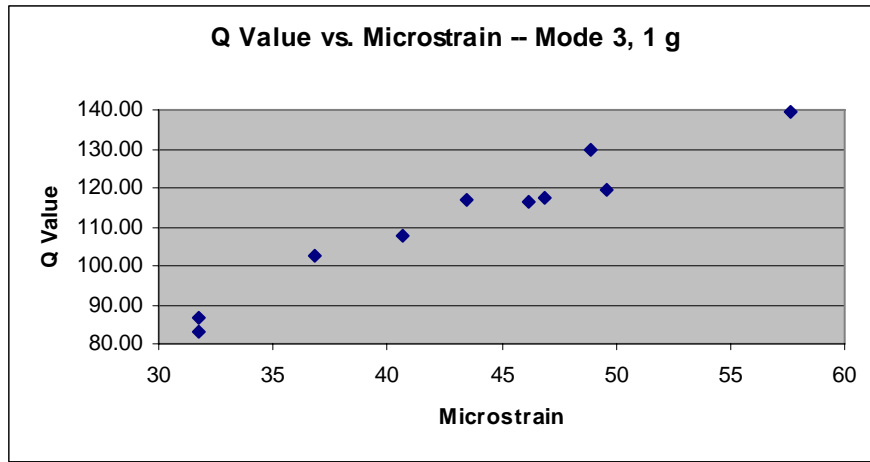


Figure 33. Damping vs. Sample Strain, Mode 3 1g 18k Shaker

In the table above, “Torque Down” refers to each time the sample was reclamped into the constraint blocks. Each time the sample was loaded, that clamping was assigned a successive number designator. This made it easier to analyze results by simplifying the task of tracking each clamping. These designator numbers were used throughout this entire study.

As with all testing in this experiment, the results above show that the variation between peak frequencies for the successive clampings was quite small. Thus, the resonant frequencies found were very consistent throughout testing in this section. The

maximum velocity of the sample varied between tests, however. This was not unusual, though it did necessarily mean that the displacement varied between runs and that the strain, as shown, changed between runs as well.

The results at mode 3 and 1g showed clear strain dependence. The figure above illustrates that as strain increases, Q value increases in a roughly linear fashion. That is, as strain increases damping decreases. In an ideally clamped bare sample, damping would be independent of strain. The change in damping relative strain indicates that the clamp itself was strain dependent.

The results of the mode 3 1g testing also alluded to other characteristics of the system. First, the resulting Q values were more consistent within the same day. Despite the reclampings between all tests, variation between runs on the same day was smaller than the overall variation. This phenomenon held true for all repeatability testing, and was the reason blocks in ANOVA testing were built around different days in the lab. Second, the variation between clampings was not negligible. Though potentially overshadowed by constraint block strain dependence and day to day variations, the changes in results due to reclamping were still evident in the results. This was evidenced in the above figure, where results at nearly identical strain levels still produced different results for damping.

The remainder of the results for testing on the 18,000 lbf shaker table further illustrated the variation between runs. Much of this variation was due to the strain dependence of the blocks. However, the figures clearly showed that even at the same strain level, different runs, and thus different clampings, produced different values for damping. If clamping had no effect on the damping measured, subsequent clampings

would have lead to the same results at the same strain levels. In the following figures and tables, the results for repeatability testing on the 18,000 lbf shaker at the three remaining mode and input level combinations are given.

Table 25. Repeatability Results, Mode 4 1g 18k Shaker

Date	Torque Down	Control Accel (g)	Mode	Peak Freq (Hz)	Q Value	Velocity (mm/s)	MicroStrain	
24-Aug	TD1A	1	4	1625.952	878.85	216.70	107.94	
26-Aug	TD2A	1	4	1626.302	783.69	185.30	92.28	
26-Aug	TD3A	1	4	1625.027	764.63	202.90	101.12	
26-Aug	TD4A	1	4	1624.352	792.30	226.70	113.03	
31-Aug	TD5A	1	4	1625.602	756.00	185.20	92.27	
31-Aug	TD6A	1	4	1624.602	746.88	195.40	97.41	
31-Aug	TD7A	1	4	1623.827	729.74	196.40	97.95	
1-Sep	TD8A	1	4	1625.277	755.85	192.40	95.87	
1-Sep	TD9A	1	4	1624.152	746.68	195.00	97.24	
1-Sep	TD10A	1	4	1623.752	746.49	192.50	96.01	
				AVG	1624.885	770.11	198.85	99.11
				STD DEV	0.891	42.44	13.31	6.64

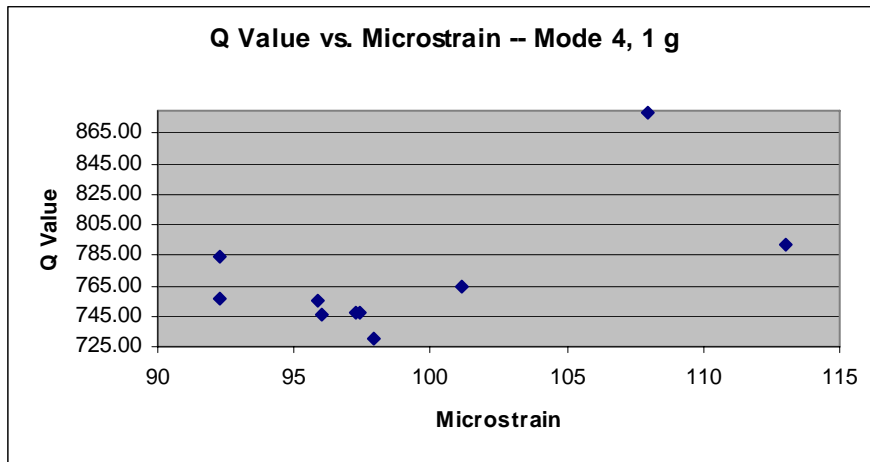


Figure 34. Damping vs. Sample Strain, Mode 4 1g 18k Shaker

Table 26. Repeatability Results, Mode 3 8g 18k Shaker

Date	Torque Down	Control Accel (g)	Mode	Peak Freq (Hz)	Q Value	Velocity (mm/s)	MicroStrain	
24-Aug	TD1A	8	3	1239.201	130.43	1062.00	536.79	
26-Aug	TD2A	8	3	1239.126	138.05	1042.00	526.71	
26-Aug	TD3A	8	3	1238.676	138.78	997.00	504.15	
26-Aug	TD4A	8	3	1238.426	139.14	1015.00	513.35	
31-Aug	TD5A	8	3	1238.376	125.71	885.40	447.83	
31-Aug	TD6A	8	3	1237.951	119.31	832.50	421.21	
31-Aug	TD7A	8	3	1236.776	122.44	855.80	433.41	
1-Sep	TD8A	8	3	1237.426	125.94	930.30	470.90	
1-Sep	TD9A	8	3	1237.551	123.74	884.40	447.62	
1-Sep	TD10A	8	3	1236.901	124.30	900.20	455.85	
				AVG	1238.041	128.78	940.46	475.78
				STD DEV	0.864	7.37	82.03	41.23

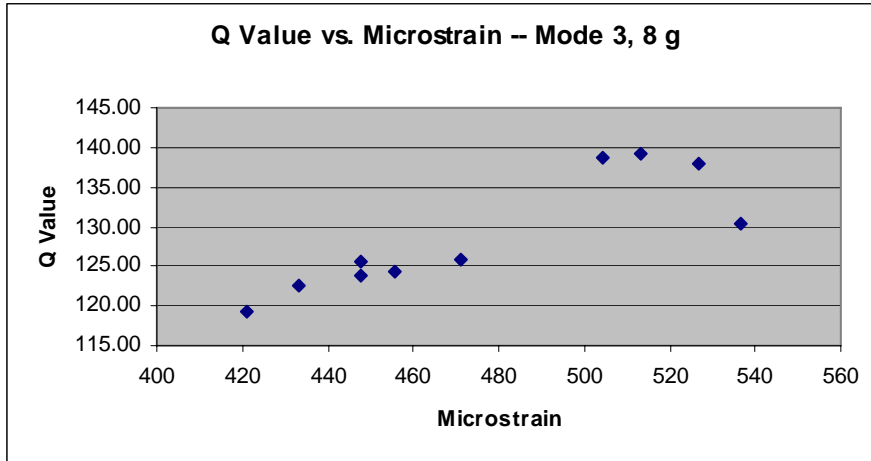


Figure 35. Damping vs. Sample Strain, Mode 3 8g 18k Shaker

Table 27. Repeatability Results, Mode 4 8g 18k Shaker

Date	Torque Down	Control Accel (g)	Mode	Peak Freq (Hz)	Q Value	Velocity (mm/s)	MicroStrain	
24-Aug	TD1A	8	4	1623.552	460.55	1151.00	574.15	
26-Aug	TD2A	8	4	1623.802	515.47	1118.00	557.60	
26-Aug	TD3A	8	4	1622.877	477.28	1143.00	570.40	
26-Aug	TD4A	8	4	1622.377	429.74	1183.00	590.54	
31-Aug	TD5A	8	4	1622.902	491.74	1127.00	562.40	
31-Aug	TD6A	8	4	1622.102	466.76	1132.00	565.18	
31-Aug	TD7A	8	4	1621.627	469.99	1135.00	566.84	
1-Sep	TD8A	8	4	1622.527	480.70	1126.00	562.03	
1-Sep	TD9A	8	4	1622.202	460.15	1136.00	567.14	
1-Sep	TD10A	8	4	1621.727	491.41	1121.00	559.81	
				AVG	1622.570	474.38	1137.20	567.61
				STD DEV	0.721	23.07	18.90	9.44

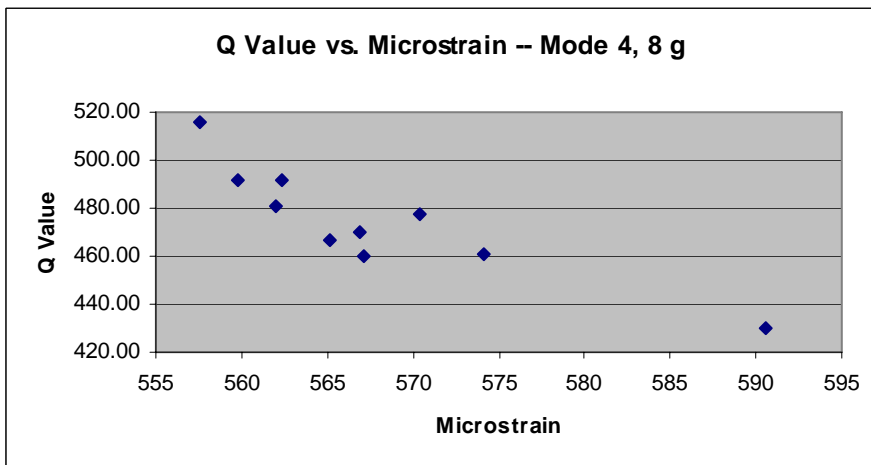


Figure 36. Damping vs. Sample Strain, Mode 4 8g 18k Shaker

The standard deviations seen between successive runs at each mode and input g-level on the 18,000 lbf shaker were collected in the table below. This table shows that variations were far more rampant in mode 4 than mode 3. Further, these variations were decreased for both modes at higher input g-levels. This implies that as strain in the sample increased, the variations within the system decreased.

Table 28. Overall Variation Comparison, 18k Shaker

	Peak Freq(Hz)	Q Value	Velocity
Mode 3, 1g mean	1244.866	111.935	86.154
Mode 4, 1g mean	1624.885	770.111	198.850
Mode 3, 8g mean	1238.041	128.784	940.460
Mode 4, 8g mean	1622.570	474.379	1137.200
Mode 3, 1g stdev	0.819	17.601	16.407
Mode 4, 1g stdev	0.891	42.439	13.313
Mode 3, 8g stdev	0.864	7.370	82.027
Mode 4, 8g stdev	0.721	23.075	18.902

Next, a similar set of tests were conducted on the 6,000 lbf shaker table. This was done to provide further insight into the effects of reclamping the sample, as well as to provide more data in order to bolster any conclusions drawn. In this testing, an even greater variation between clampings was seen. Reclamping a sample could cause very different results in the subsequent runs. Day to day variations in the results were less evident in the 6,000 lbf shaker repeatability testing, though. This could be the case because this portion of testing was performed over a period of only 2 days. Thus, there was no real opportunity for day to day trends to emerge.

In this initial repeatability testing on the 6,000 lbf shaker, the baseplate configuration and control accelerometer location were different than those used on the 18,000 lbf shaker due to the configuration of the shaker head. The jack bolts were not

used either. They were removed in order to determine if repeatability suffered when they were not used. Further, testing was performed at 1g and 4g inputs. A level of 8g could not be used because the resonant response was too loud. Because the 6,000 lbf shaker room did not have the acoustic baffling of the 18,000 lbf shaker room, the noise produced by the tests run became a limiting factor in determining input levels.

Though not shown in the results, it should be noted that the attachment of the outer bolts to the baseplate played a significant role in determining the frequency responses found, as briefly mentioned earlier in this document. Reversing the positions of these bolts or adjusting how tightly they screwed into the baseplate had an obvious effect on the peak frequencies found in test runs. In order to combat this effect, all bolts and nuts were labeled and always installed in the same position. The outer bolts were screwed tight into the baseplate, so as to minimize any movement or undue influence on the resonant frequencies observed in the sample. In addition to these measures, the middle bolts were replaced with new bolts of equal length beginning with this 6,000 lbf shaker testing.

The results of testing on the 6,000 lbf shaker table are shown below. The tables showing comparison between g-levels cannot be related back to the testing on the 18,000 lbf shaker. Due to all the differences in the set-up and the shaker tables themselves, a g-level comparison between the results for different shakers would be meaningless. The sample experienced different strains, and thus behaved differently. The charts showing strain versus damping relationships at each mode can be compared between the set-ups, however.

Table 29. Repeatability Results, Mode 3 1g 6k Shaker

Date	Torque Down	Input Accel (g)	Mode	Peak Freq (Hz)	Q Value	Peak Velocity (mm/s)	MicroStrain	
22-Sep	TD1B	1	3	1217.105	214.76	256.50	132.00	
22-Sep	TD2B	1	3	1217.961	174.49	268.10	137.87	
22-Sep	TD3B	1	3	1225.295	173.48	211.80	108.27	
22-Sep	TD5B	1	3	1216.733	119.91	133.80	68.88	
23-Sep	TD6B	1	3	1220.336	167.34	247.30	126.93	
23-Sep	TD7B	1	3	1223.399	181.23	233.90	119.75	
23-Sep	TD8B	1	3	1222.315	181.06	213.80	109.56	
23-Sep	TD9B	1	3	1218.357	182.16	249.20	128.11	
23-Sep	TD10B	1	3	1223.003	189.35	239.60	122.71	
23-Sep	TD11B	1	3	1221.274	182.03	243.20	124.73	
				AVG	1220.578	176.58	229.72	117.88
				STD DEV	2.949	23.65	37.93	19.50

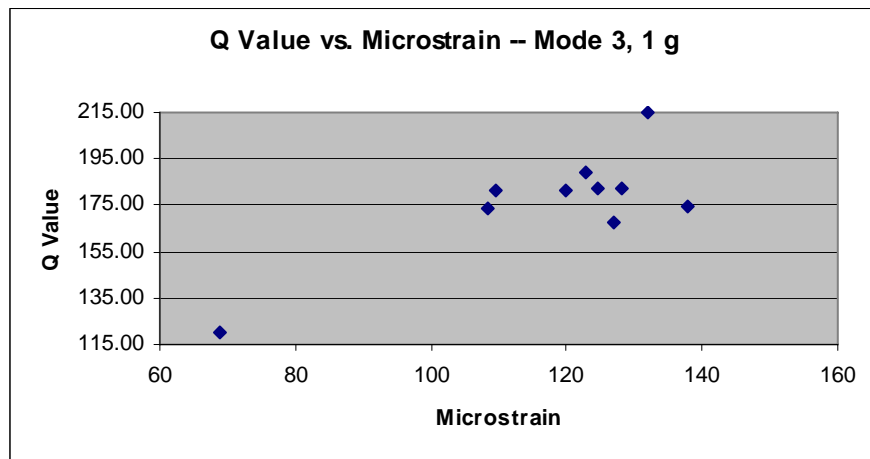


Figure 37. Damping vs. Sample Strain, Mode 3 1g 6k Shaker

Table 30. Repeatability Results, Mode 4 1g 6k Shaker

Date	Torque Down	Input Accel (g)	Mode	Peak Freq (Hz)	Q Value	Peak Velocity (mm/s)	MicroStrain	
22-Sep	TD1B	1	4	1626.627	629.59	250.50	124.72	
22-Sep	TD2B	1	4	1627.148	697.30	234.30	116.62	
22-Sep	TD3B	1	4	1627.252	729.92	171.60	85.40	
22-Sep	TD5B	1	4	1626.211	645.04	141.60	70.52	
23-Sep	TD6B	1	4	1627.294	679.14	271.50	135.12	
23-Sep	TD7B	1	4	1626.981	673.14	190.70	94.93	
23-Sep	TD8B	1	4	1626.398	667.17	175.20	87.24	
23-Sep	TD9B	1	4	1627.482	424.52	122.60	61.01	
23-Sep	TD10B	1	4	1627.002	691.06	214.00	106.52	
23-Sep	TD11B	1	4	1627.151	681.30	234.90	116.92	
				AVG	1626.955	651.82	200.69	99.90
				STD DEV	0.412	84.47	48.49	24.13

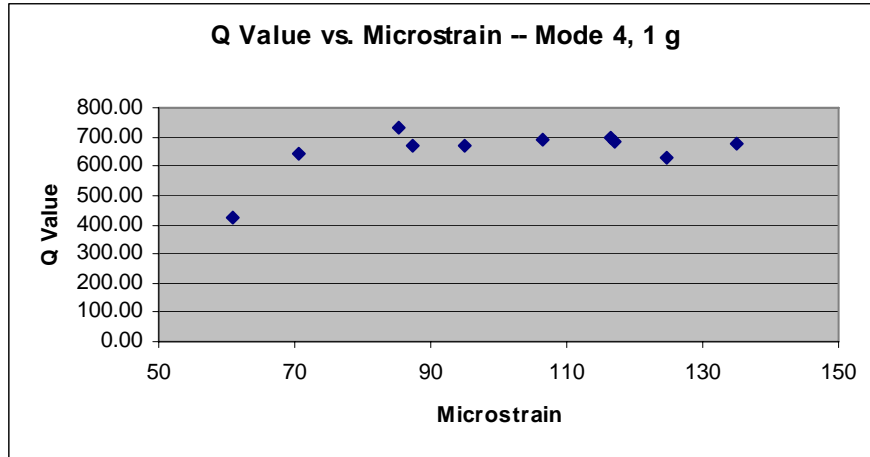


Figure 38. Damping vs. Sample Strain, Mode 4 1g 6k Shaker

Table 31. Repeatability Results, Mode 3 4g 6k Shaker

Date	Torque Down	Input Accel (g)	Mode	Peak Freq (Hz)	Q Value	Peak Velocity (mm/s)	MicroStrain	
22-Sep	TD1B	4	3	1213.335	160.87	861.50	444.73	
22-Sep	TD2B	4	3	1211.668	145.38	865.40	447.36	
22-Sep	TD3B	4	3	1218.211	136.93	684.40	351.89	
22-Sep	TD5B	4	3	1205.209	44.12	271.50	141.10	
23-Sep	TD6B	4	3	1213.231	135.42	785.80	405.69	
23-Sep	TD7B	4	3	1216.836	134.57	741.10	381.48	
23-Sep	TD8B	4	3	1215.565	141.26	700.00	360.70	
23-Sep	TD9B	4	3	1211.877	143.26	793.40	410.07	
23-Sep	TD10B	4	3	1217.231	136.18	716.30	368.59	
23-Sep	TD11B	4	3	1215.002	137.86	765.00	394.37	
				AVG	1213.817	131.59	718.44	370.60
				STD DEV	3.765	31.69	168.71	86.91

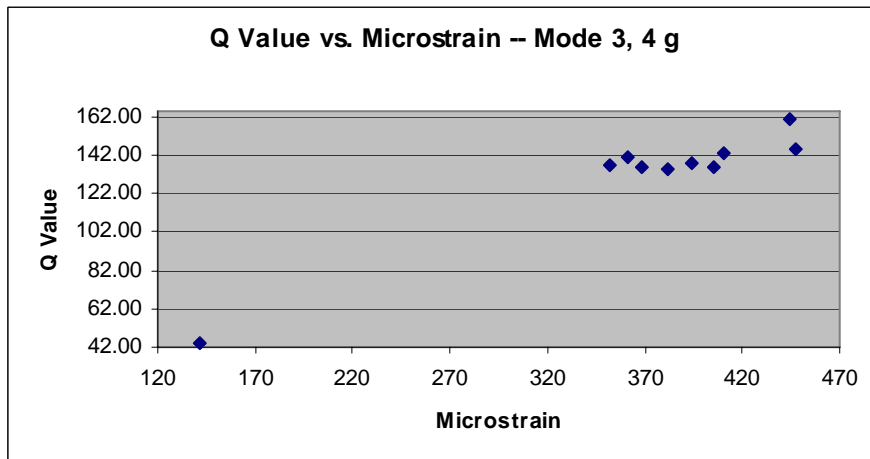


Figure 39. Damping vs. Sample Strain, Mode 3 4g 6k Shaker

Table 32. Repeatability Results, Mode 4 4g 6k Shaker

Date	Torque Down	Input Accel (g)	Mode	Peak Freq (Hz)	Q Value	Peak Velocity (mm/s)	MicroStrain	
22-Sep	TD1B	4	4	1625.440	553.27	668.30	332.98	
22-Sep	TD2B	4	4	1624.710	573.37	783.50	390.55	
22-Sep	TD3B	4	4	1625.065	595.37	570.90	284.51	
22-Sep	TD5B	4	4	1624.127	506.18	493.10	245.88	
23-Sep	TD6B	4	4	1625.210	549.31	740.00	368.75	
23-Sep	TD7B	4	4	1624.669	581.90	652.90	325.46	
23-Sep	TD8B	4	4	1624.169	586.11	605.20	301.77	
23-Sep	TD9B	4	4	1625.044	553.14	590.90	294.49	
23-Sep	TD10B	4	4	1625.148	569.35	706.10	351.88	
23-Sep	TD11B	4	4	1625.273	561.19	773.10	385.23	
				AVG	1624.886	562.92	658.40	328.15
				STD DEV	0.454	25.16	94.42	47.02

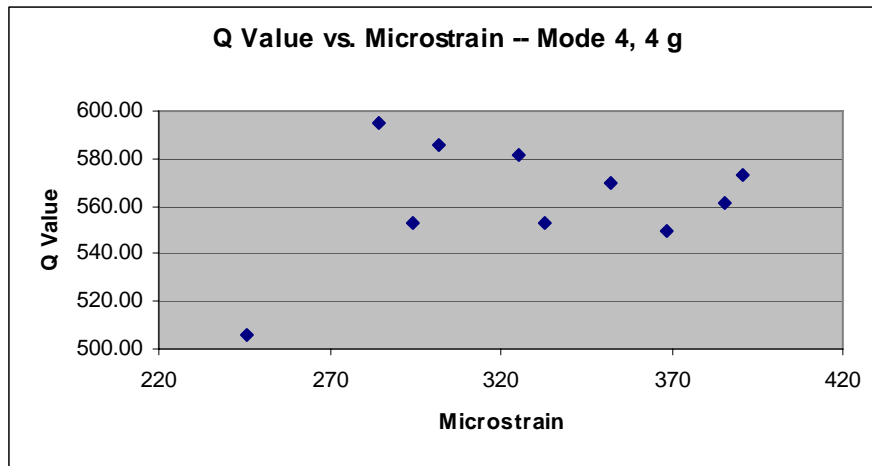


Figure 40. Damping vs. Sample Strain, Mode 4 4g 6k Shaker

These results differ from those found for the 18,000 lbf shaker. The variation seen between runs was greater than that observed in the set-up on the larger shaker table. This can be seen in the charts above, where large variations in observed damping occurred at the nearly the same strain levels. In the charts for 18,000 lbf testing shown previously, the charts did not portray such a large disparity in results between similar runs.

The charts for 6,000 lbf testing displayed not only the inconsistencies between clampings, but also the strain dependence within the constraint blocks. This effect was not as apparent as it was in the 18,000 lbf testing, but it was present. In each of the 4

charts, outlying runs at lower strain values produced results with lower Q values. This suggests that runs with less tip displacement were more highly damped by the constraint blocks.

The table below summarizes the means and standard deviations for this experiment on the 6,000 lbf shaker table. It is interesting to note that the variations in peak frequency were still small, but much more prevalent in this section of testing. This could be due to small changes in the tightness of the outer bolts. As mentioned, this was known to be a factor in testing, and the effect was readily apparent on the 6,000 lbf machine. While peak frequency variations were roughly the same as 18,000 lbf testing for the 4th mode, the variation is an order of magnitude higher for the 3rd mode.

Table 33. Overall Variation Comparison, 6k Shaker

	Peak Freq(Hz)	Q Value	Velocity
Mode 3, 1g mean	1220.578	176.581	229.720
Mode 4, 1g mean	1626.955	651.818	200.690
Mode 3, 4g mean	1213.817	131.585	718.440
Mode 4, 4g mean	1624.886	562.919	658.400
Mode 3, 1g stdev	2.949	23.651	37.934
Mode 4, 1g stdev	0.412	84.471	48.486
Mode 3, 4g stdev	3.765	31.694	168.707
Mode 4, 4g stdev	0.454	25.162	94.419

As in testing on the 18,000 lbf shaker, this experiment also showed that variations were greatest for the 4th mode at lower g-levels. The overall variation between clampings decreased as g-level increased for both modes again as well. In fact, the similarities and differences between both experiments in this section allowed the experimenter to draw several preliminary conclusions about the set-up. These are summarized below, and all of them were used to design experiments in following sections.

- 1) The constraint blocks display strain dependence, which causes greater damping at lower strain levels.
- 2) Mode 4 generally shows more variation between successive reclampings of the sample than mode 3.
- 3) Because of the larger variations in results seen for 6,000 lbf testing, it is likely that jack bolts do increase repeatability. They were used on 18,000 lbf testing, which showed much cleaner results.
- 4) Positioning of the bolts attaching the constraint blocks will have a significant impact on the results, especially for mode 3.
- 5) Standard deviation between reclampings for both modes 3 and 4 decreases as the input g-level, and thus the strain induced, increases.

Single Clamping Repeatability Testing Results

The next task was to complete testing on the variability between runs for a single clamping. The uncoated sample would be clamped in to the constraint blocks only once, and the variation in damping between subsequent runs would be recorded. However, this testing did not fulfill that original purpose. Instead, it turned up another factor influencing the results of damping testing. A time trend was at work affecting the results. As the experimental runs progressed, the results for Q value increased. This made determining variations for a single clamping impossible to determine, but yielded further insight into the temperamental nature of the constraint blocks. This testing was done on the 6,000 lbf shaker table, and all runs were performed at an input level of 1g.

This time trend was assumed to be due to temperature. In his research, Allen noted that temperature changes were recorded during his study. He also noted that temperature could increase by as much as 20 degrees Fahrenheit during a single day of testing (2). His testing showed that temperature changes could cause changes in both the shape and peak frequency of a frequency response curve.

The behavior of the time trend in the results made it reasonable to assume that temperature changes were the culprit in this single clamping experiment as well. This temperature effect was likely present in the previous section of testing too. However, it may have been masked by the variations between subsequent clampings. That is, changes in results due to temperature could just as easily be attributed to changes due to reclamping the sample in the blocks. In the previous section there was, therefore, no way to see the effect of temperature on the damping recorded.

The figure below shows the results of single clamping testing at an input level of 1g for mode 4. In the figure, Q value is plotted versus the run order of the testing. Testing for 2 different days of testing is shown in the plot. Note that the Q-value observed increases quickly between runs at first, then “levels out” on each day. This is consistent with the idea of the shaker room reaching a steady state temperature. Temperature was not initially a consideration in this testing and was, unfortunately, not recorded. The different starting points between the two days might have occurred because the ambient temperature in the lab varied from day to day. The difference seen below between identical runs on separate days supports the idea that day to day variations in the environment played a significant role in determining damping for this set-up.

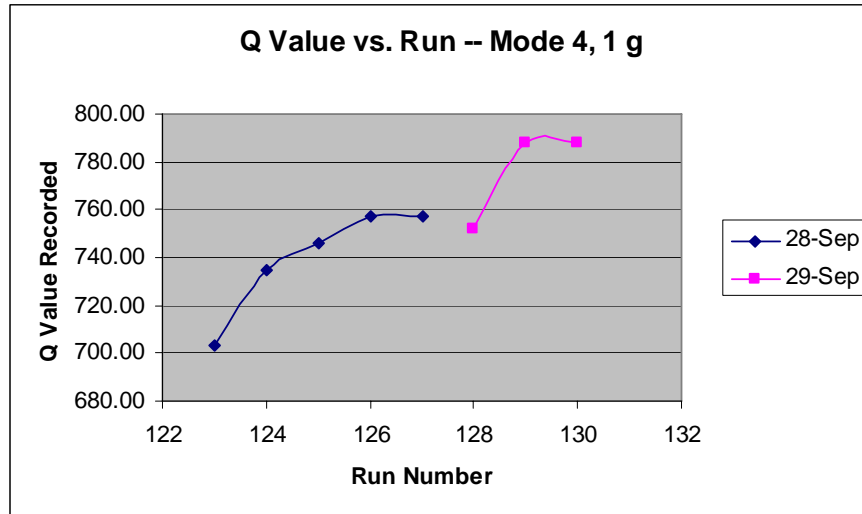


Figure 41. Q Value versus Run Order, mode 4 1g

The next figure shows the resulting Q value versus run order plot for mode 4 at an input g-level of 4g's. Testing at this mode and g-level was carried out over one day only. Once again, the plot shows that Q value increases as the runs progress. It also shows that the Q value increases flatten out over the course of several runs, where the shaker room is likely reaching a steady state temperature.

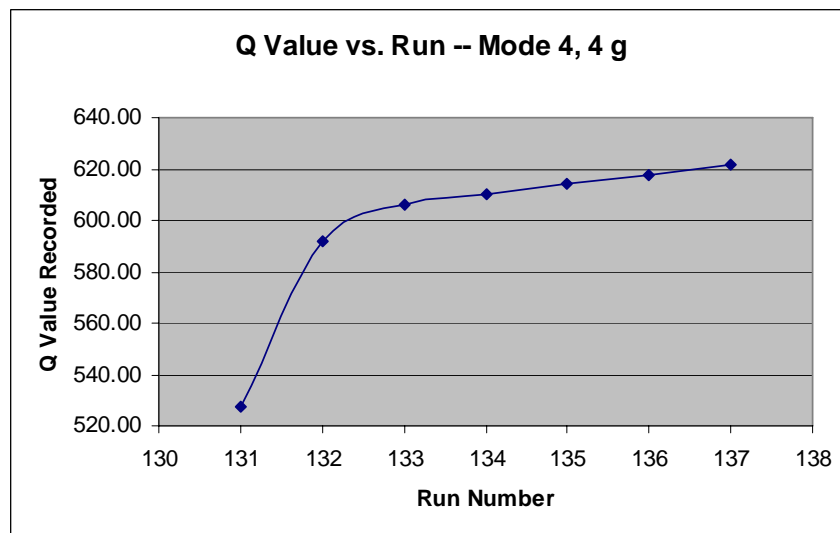


Figure 42. Q Value versus Run Order, mode 4 4g

The temperature time trend was not limited to mode 4. Limited testing on mode 3, at an input g-level of 1g, showed that Q increased over time in this mode as well. Only three runs were performed at this point, and these runs were completed after the runs in the figure above on the same day. As such, the room had already begun to approach a steady state temperature when mode 3 testing was performed. This figure shows the increase in Q value expected, while the small increases presented conform to the idea that temperature was changing little by this point.

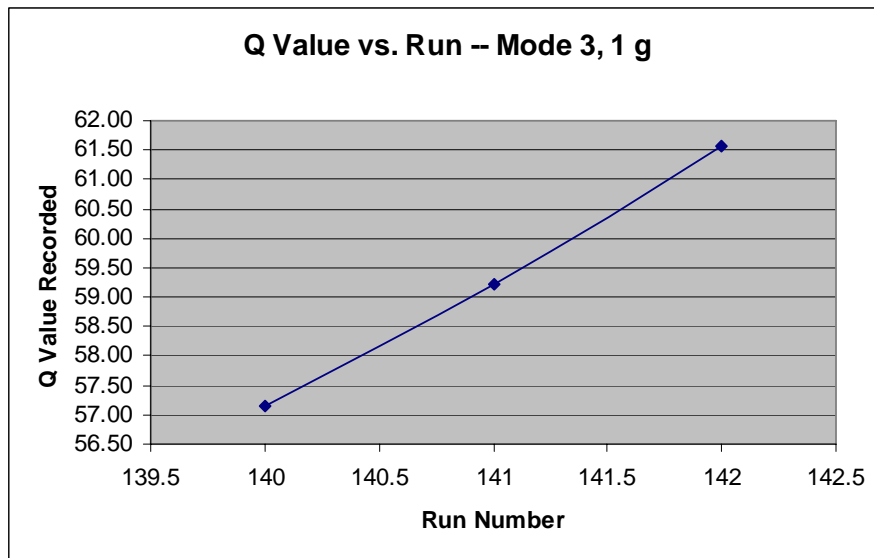


Figure 43. Q Value versus Run Order, mode 3 1g

It seemed logical that temperature was causing the changes in the results. However, this assumption had to be further supported. In order to verify whether temperature was having an effect, the door to the shaker room was opened between tests for a series of runs. The door was left open for 2 minutes between runs, allowing air at room temperature to mix with the hotter air in the shaker room. Because temperature was uncontrollable, this was the only means available for altering the temperature in the room.

While decidedly low-tech, this approach did allow the experimenter to determine that temperature was truly the cause of these variations. When “open door cooling” was introduced between tests, the increasing trend of Q values was interrupted.

The figures below clearly illustrate how temperature has an effect. When the shaker room was allowed to cool slightly between tests, the increasing Q trend was broken. Therefore, altering the temperature in the room had a direct effect on the damping results achieved. In the figures below, the original Q value versus run data form above is combined shown with the results for runs where the door to the shaker room was opened between runs. In all cases, Q value was reduced from the original runs. The data in each plot was taken during the same test session, so that day to day variations were not a factor in these results.

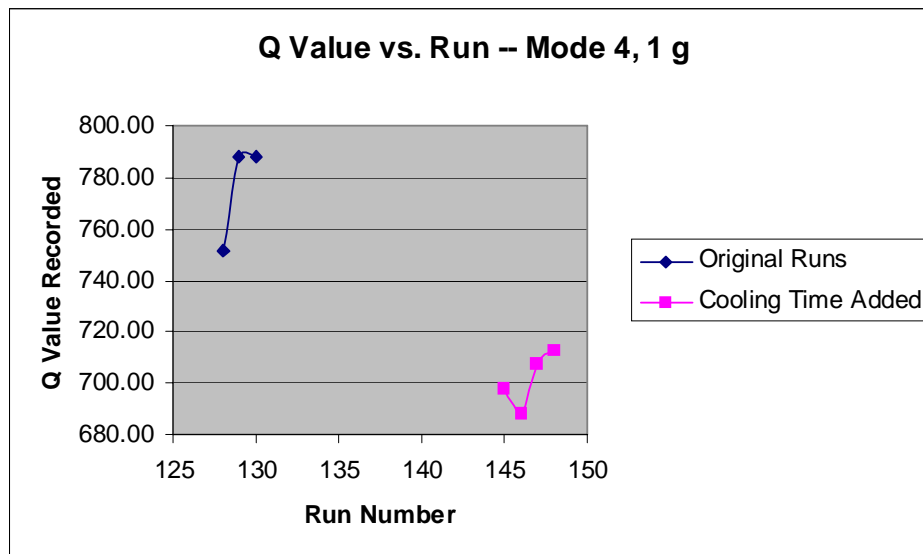


Figure 44. Q Value versus Run Order with Cooling Time, mode 4 1g

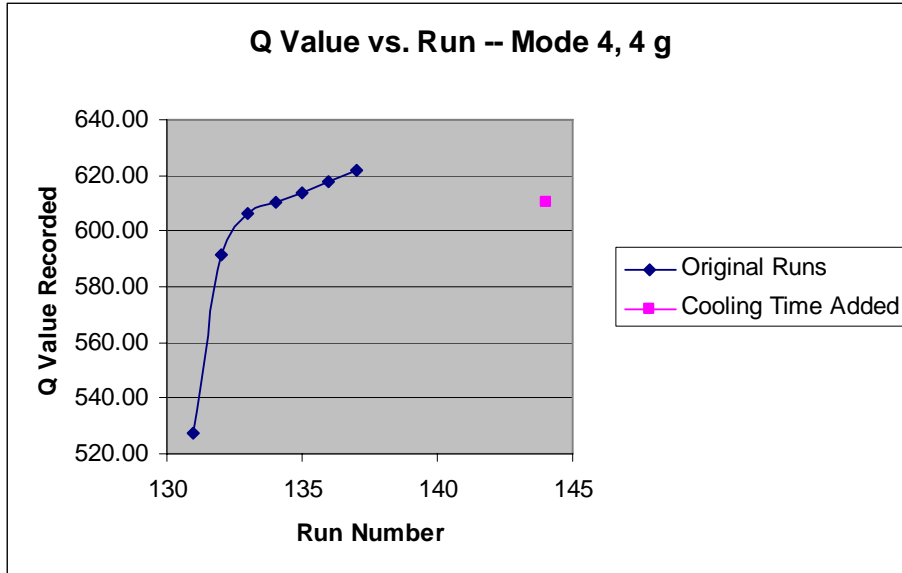


Figure 45. Q Value versus Run Order with Cooling Time, mode 4 4g

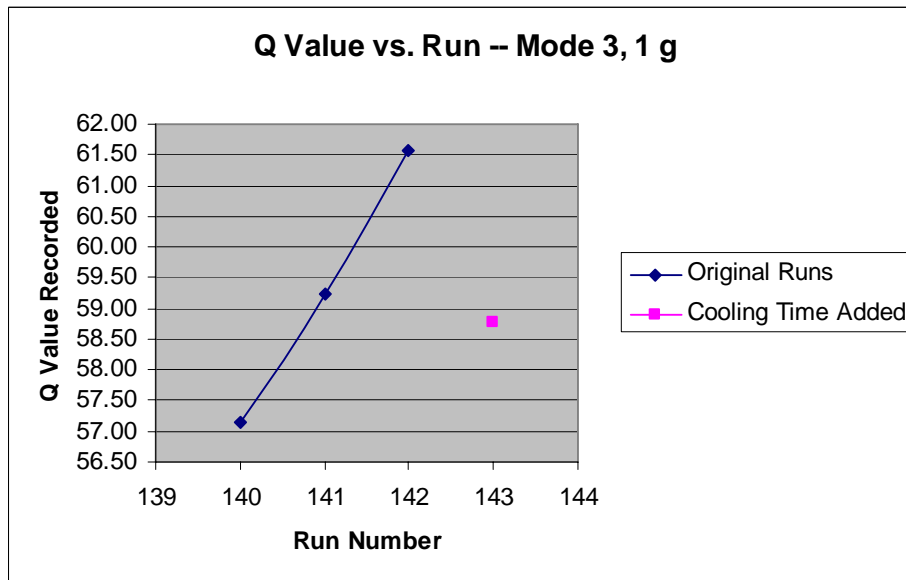


Figure 46. Q Value versus Run Order with Cooling Time, mode 3 1g

In analyzing the results from this testing, it could also be seen that the strain in the sample changed slightly as run order progressed. However, no clear trend regarding

strain over time emerged in this testing. Because temperatures were not known, it was not possible to draw any conclusions regarding strain versus temperature at this time. The effects of temperature on strain for a given input were analyzed in a later section of this study.

This section of testing allowed several conclusions to be drawn. They are:

- 1) Given the use of constraint blocks in damping measurements, temperature is an important consideration
- 2) Temperature may increase quickly in a shaker table room, then this rate of increase may slow over time
- 3) If temperature cannot be controlled, experiments must be designed with this factor in mind.

Given the conclusions above, it made sense to perform further testing on the effect of temperature. In this follow-on testing, which will be discussed later, a thermocouple was used to measure the temperature at the constraint blocks.

Constraint Block Movement Testing Results

Another area of concern was the movement of the constraint blocks themselves. Prior testing by Allen indicated that movement in the constraint blocks might be non-uniform across the top of the blocks. A non-uniform movement in the constraint blocks would indicate a non-ideal clamped condition. Non-uniform movement of the blocks would also be an indicator of inconsistencies in the clamping of the blocks. If one side of the blocks were tighter than the other, the blocks would move differently when the set-up

was excited. Different movement of the blocks would explain the variations seen between successive reclampings of the sample in previous sections of this study.

The results of this section show how three different positions of the top constraint block moved for identical test runs. These runs were all completed using the uncoated sample. They show that the movement of the blocks was related to the movement of the sample, which was undergoing either mode 3 or mode 4 throughout this experiment. The movement of the blocks varied for each of the block positions tested. Additionally, this section revealed that the jack bolts played a role in reducing this variation.

The plots below summarize the results from the first set of runs in this experiment for mode 3. The first plot shows data taken at the point of interest in the sample, both with and without jack bolts in place. The run with jack bolts produced a response curve which attained a higher velocity. That is, the curve in the plot is slightly taller. The second plot below shows the response read from the left, right, and center positions on top of the constraint blocks when sweeping through the sample's 3rd mode. In this plot, it can be seen that the velocity of the blocks went through its inflection point at the same point where the sample reached its peak velocity. The plot shows that for an identical since sweep, each point on the top of the blocks performed differently.

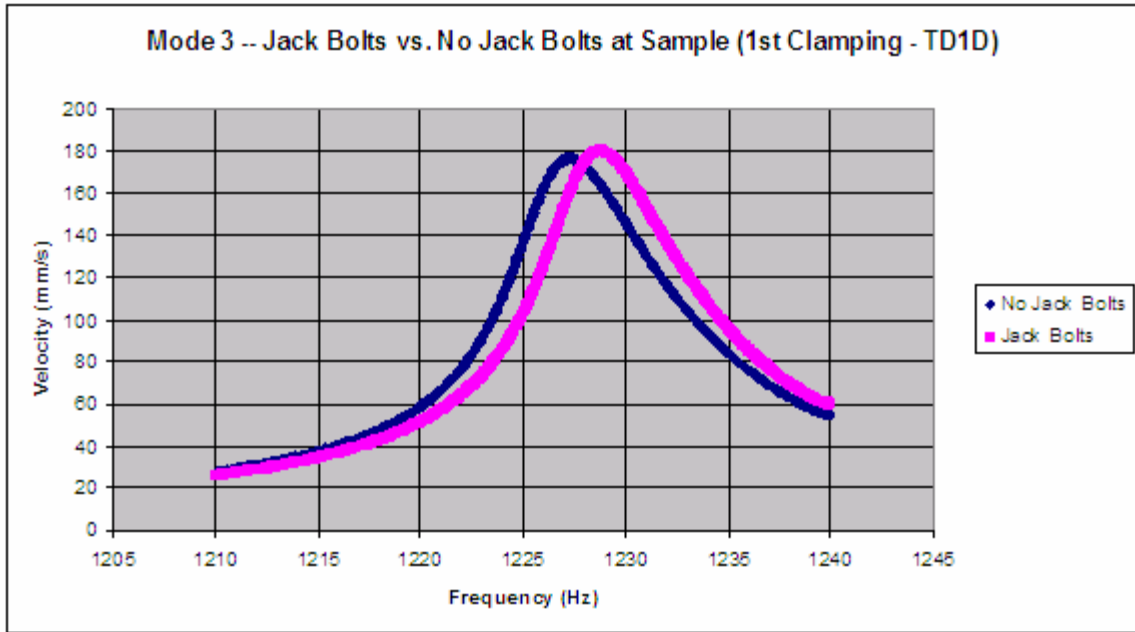


Figure 47. Jack Bolts vs. No Jack Bolts at Sample– 1st Clamping, Mode 3

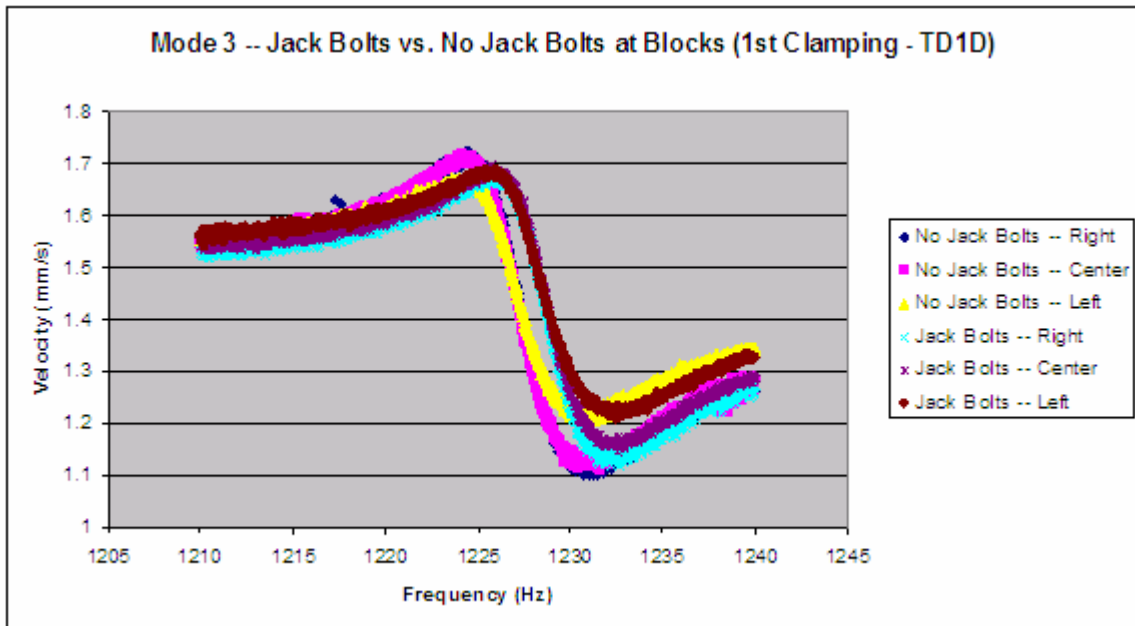


Figure 48. Jack Bolts vs. No Jack Bolts at Blocks– 1st Clamping, Mode 3

It is also important to look at how the movement of each position on the blocks changed when the jack bolts were added. When these bolts were added, the differences in velocities seen across the top of the blocks was reduced, albeit slightly. The plot shows how the spread in velocity across the right, left, and center positions was reduced when the jack bolts were added. With the jack bolts used, the velocities of each point on top of the blocks come closer to overlapping. This acted as further evidence that the jack bolts were useful. They reduced the disparity in movement across the top of the blocks, providing an improved clamped condition.

The figures below detail the results for mode 4 in this first clamping. The results from this mode are consistent with the mode 3 sweeps above. Testing at mode 4 showed that the jack bolts improved the shape of the response peak, making it appear more symmetrical, and thus more linear. The jack bolts also increased the maximum velocity of the sample, as evidence by the increased height of the response peak. In testing the positions on top of the blocks, the use of jack bolts reduced disparities in block movement for this mode as well. The plot shows that the magnitude of the block velocity was roughly the same as for mode 3. As in mode 3, this plot shows the jack bolts caused a slight reduction in the magnitude of the block movement and a reduction in the spread between positions. The inflection point in the block movement once again occurred at the peak frequency for this mode.

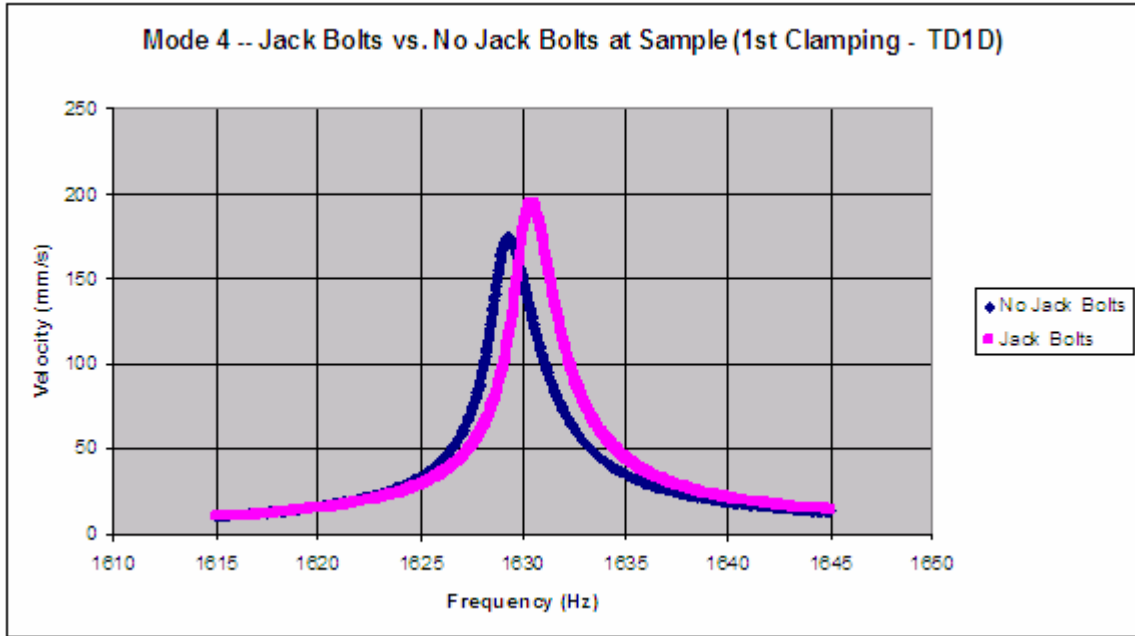


Figure 49. Jack Bolts vs. No Jack Bolts at Sample– 1st Clamping, Mode 4

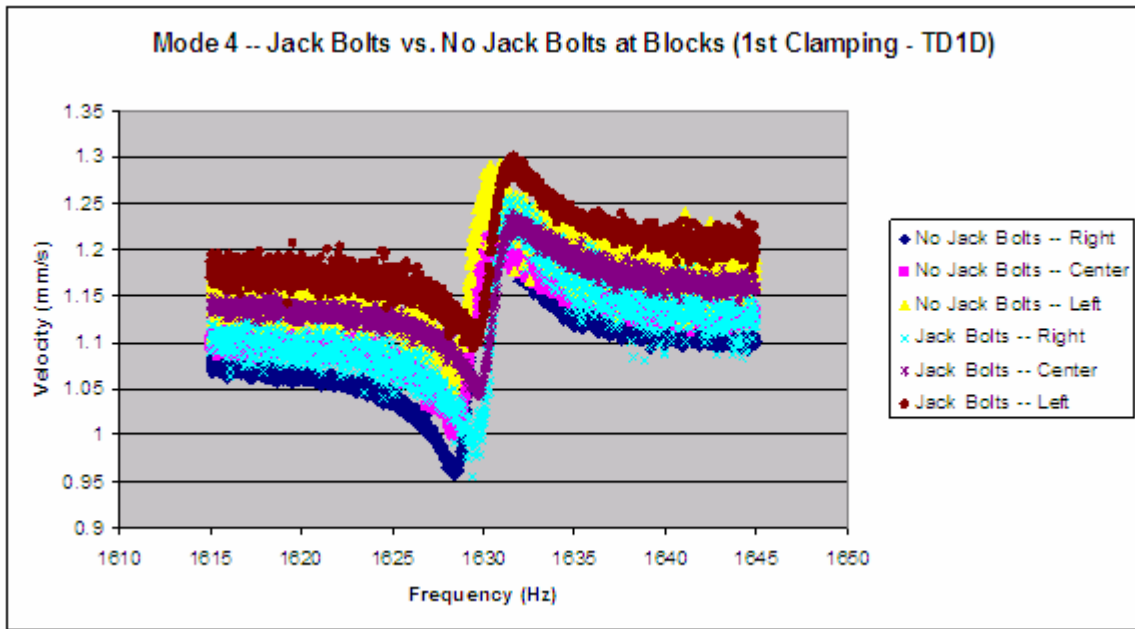


Figure 50. Jack Bolts vs. No Jack Bolts at Blocks– 1st Clamping, Mode 4

In order to verify these results, the entire set of test runs was repeated two more times. The sample was reclamped before each additional set of runs. This was done in order to determine if reclamping the sample changed the movement recorded across the top of the blocks. A change in top block velocity, or in which position displayed greater movement, would show that reclamping the sample had an observable effect on the clamped condition. This was, in fact, the case. When the sample was reloaded in to the blocks and retested, the relative movement displayed by the constraint blocks changed. The general trends indicating the usefulness of the jack bolts, however, remained evident.

The results below show the response for mode 3, after the sample was reloaded and the tests run again. The comparison of sweeps with and without jack bolts in the first figure below indicates the run with the bolts in place produced better results. The pink line, representing the run with jack bolts in place, reached a higher peak and is slightly more symmetrical. The difference between the peaks was less evident in this case than in the first clamping, though. The chart showing movement across the top of the blocks shows that the jack bolts once again reduced the disparity in velocity between measurement points. When the jack bolts were used, the difference in velocities between the three measurement points on the blocks was reduced. As mentioned, this figure shows that the movement of the blocks changed significantly from the 1st clamping in this experiment at the same mode.

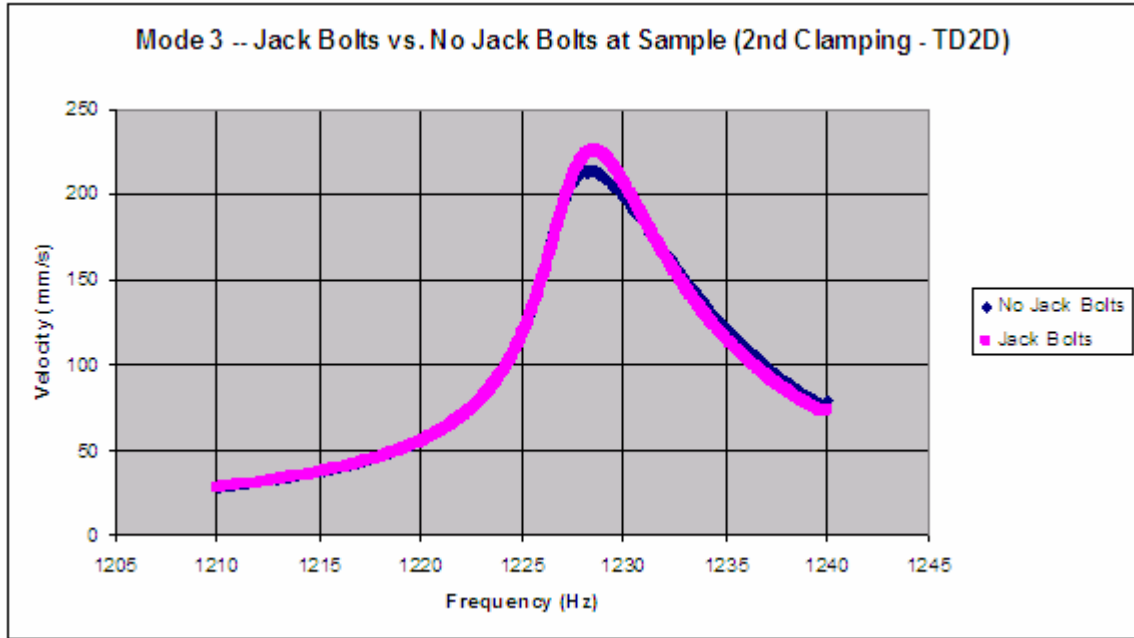


Figure 51. Jack Bolts vs. No Jack Bolts at Sample–2nd Clamping, Mode 3

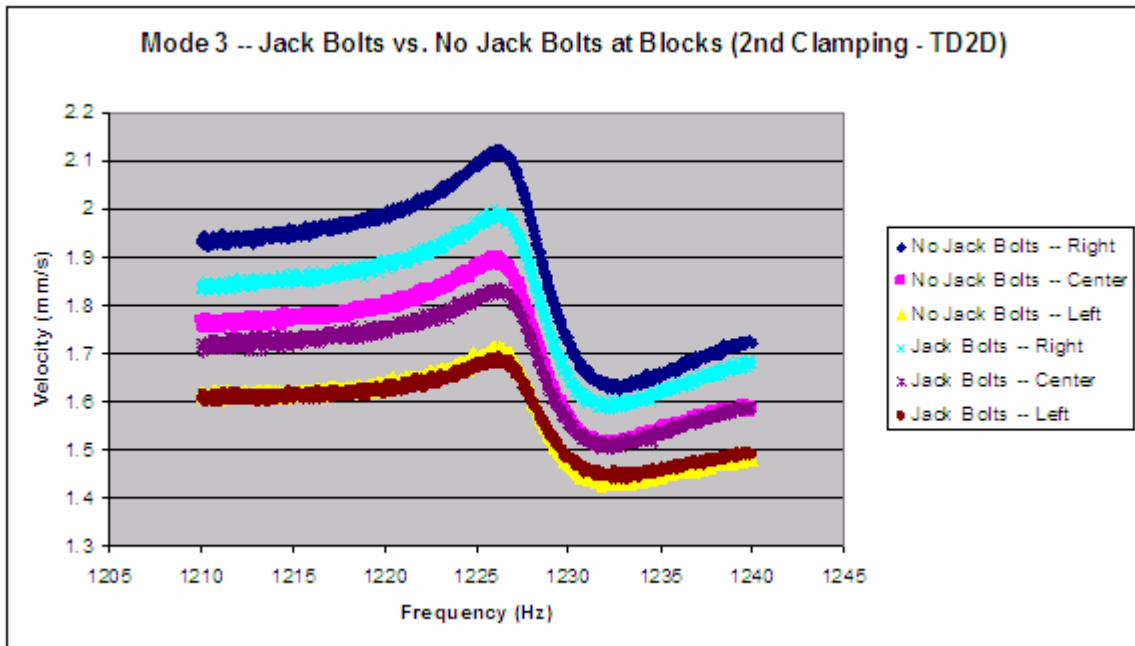


Figure 52. Jack Bolts vs. No Jack Bolts at Blocks– 2nd Clamping, Mode 3

Testing for this 2nd set of runs at mode 4 yielded results consistent with those already shown in this section. When recording data at the sample's point of interest, the run with the jack bolts appeared to be an improvement over the run without the jack bolts. In measuring the movement of the blocks at this mode, the block movement was different for 4th mode movement in the 1st clamping. Additionally, the attachment of the jack bolts once again reduced both the magnitude of, and the disparity between, the movement across the top of the blocks. In fact, the velocity of each measurement point was brought much closer together in this plot, and the effectiveness of the jack bolts can easily be seen.

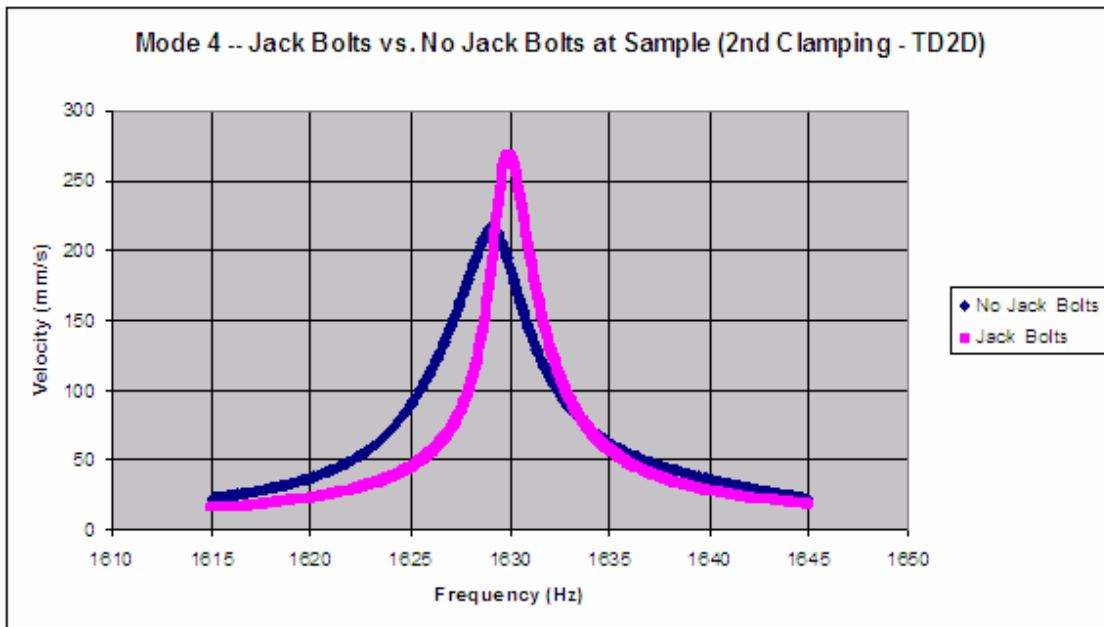


Figure 53. Jack Bolts vs. No Jack Bolts at Sample– 2nd Clamping, Mode 4

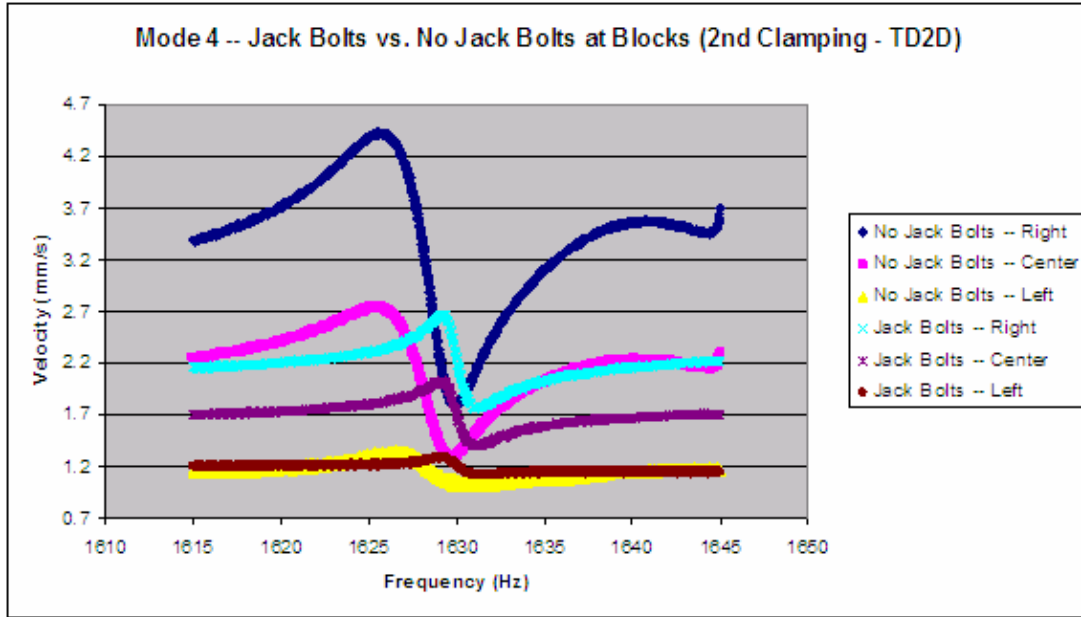


Figure 54. Jack Bolts vs. No Jack Bolts at Blocks– 2nd Clamping, Mode 4

Finally, the sample was clamped in place for a third time and the set of runs was performed again. This time, however, the run order was reversed. As shown in Chapter III, the first two clampings had runs without jack bolts performed first. In this set of runs, however, runs with the jack bolts in place were used first. This was done in order to experimentally verify that run order was not having an effect on the results. Temperature time trends, as discussed in the previous section, were of particular concern.

The figures below show the results for mode 3 in the third clamping. The results of this testing were consistent with the results from the previous two sets of runs. The response peak at the sample was more linear with the use of jack bolts, as before. In the plot showing movement across the constraint blocks, the use of jack bolts still brought the velocities from each measurement point closer together. Once again, re-clamping the

sample into the constraint blocks changed the behavior of the blocks at each of the 3 measurement locations.

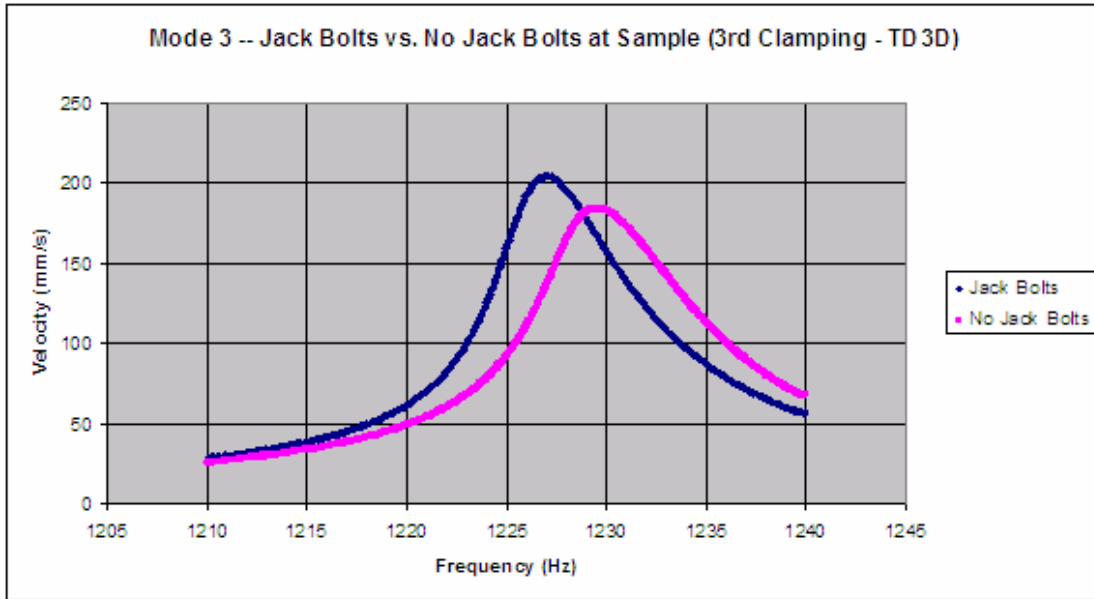


Figure 55. Jack Bolts vs. No Jack Bolts at Sample–3rd Clamping, Mode 3

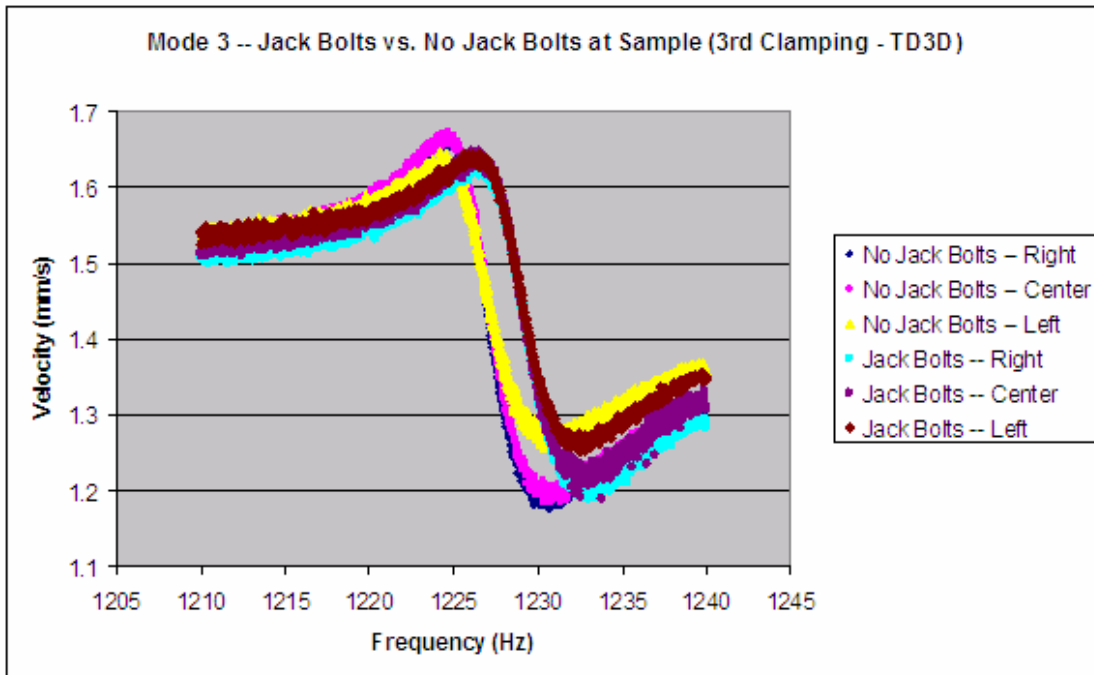


Figure 56. Jack Bolts vs. No Jack Bolts at Blocks– 3rd Clamping, Mode 3

When mode 4 was tested for this third clamping, the results broke with the trend. Interestingly, testing at the sample's point of interest showed that the response improved when the jack bolts were not used. This is a contradiction to all other results obtained in this section. This result could have been a fluke, but it more likely shows that temperature trends were, indeed, at work. Testing using jack bolts was performed first in this set of runs. Testing in later portion of this set of runs, performed without jack bolts, could have benefited from increasing temperature in the room. It has already been shown in the previous section that as run order progressed, Q value and peak velocity increased. These increases are representative of the improvements seen in peak response in this section, where the peak became thinner and taller.

The results for this set of runs at mode 4, therefore, further suggested that temperature played a large role in determining the response of the system. Further, it called into question whether the peak response plots in this section truly showed the influence of the jack bolts, or just highlighted the temperature trend. Mode 3 testing for this third clamping defied the temperature trend and supported the theory that the jack bolts improved results, while mode 4 testing supported the idea that the temperature trend was dominant. Unfortunately, there was insufficient data to draw a definite conclusion in this case.

Mode 4 testing at the constraint block measurement locations was, however, consistent with all other results. It once again showed that the overall spread in block movement was decreased when the jack bolts were used. Plots of the results from mode 4 testing for the 3rd clamping are shown below.

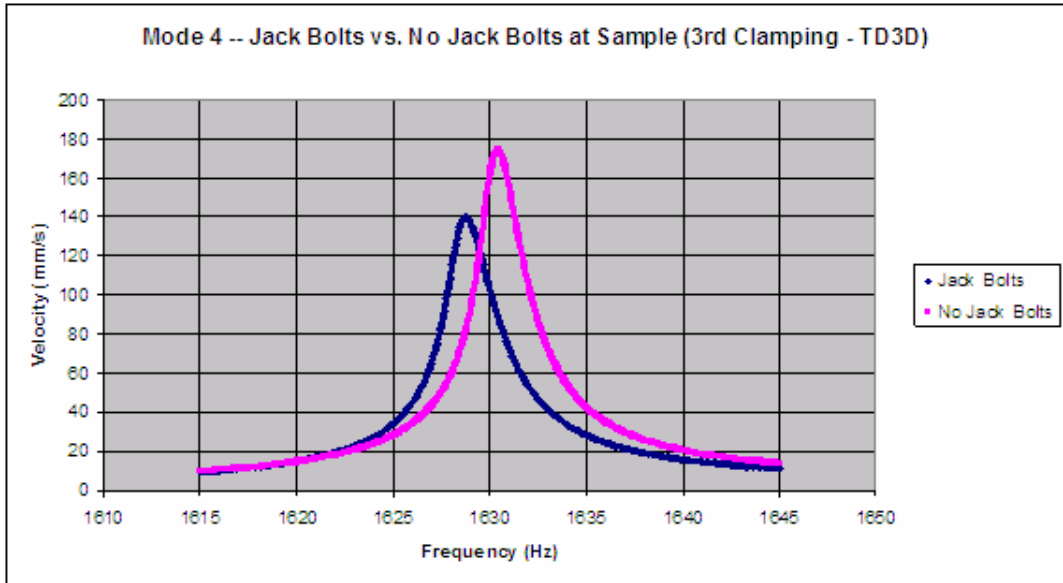


Figure 57. Jack Bolts vs. No Jack Bolts at Sample– 3rd Clamping, Mode 4

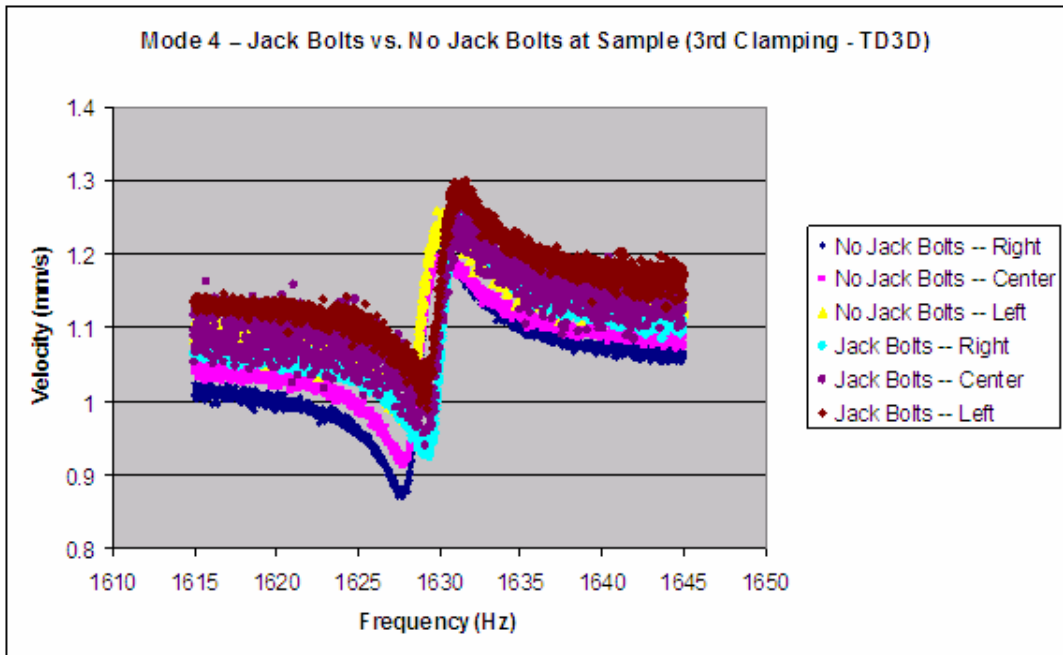


Figure 58. Jack Bolts vs. No Jack Bolts at Blocks– 3rd Clamping, Mode 4

The results from this section supported the following conclusions:

- 1) Jack bolts are useful in better constraining the sample. They force movement across the top of the blocks to be more uniform, and thus increase repeatability. They do this by reducing variations in velocity for different points across the top of the constraint blocks while the sample is undergoing a sine sweep.
- 2) The presence of a temperature trend made it impossible to show definitively whether jack bolts improved the shape of the sample response, though the results imply this is the case.
- 3) Reclamping the sample alters the condition of the blocks, as evidenced by changes in their relative movement. This in turn affects how they hold the sample, and the overall damping measured.

Temperature Effect and Repeatability Testing Results

In this section, the effect of temperature on the response of the sample was tested. Because temperature could not be controlled, it was recorded as the experiment progressed. Testing was performed both for single and multiple clampings (or multiple torques) of the sample. This data was used to create multiple plots showing temperature trends in the response for both modes 3 and 4 of the uncoated sample. Additionally, the effect of temperature change over the course of an experimental run was analyzed in this section.

Testing was performed at input g-levels of 1g and 4g. Both an initial and final temperature were recorded for each run. The temperature shown for each run in the resulting plots is the average of these temperatures.

The results plots below represent findings for mode 3 excited at 1g. The results for the single clamping tests represent runs where the sample was secured into the blocks only once. The results for multi-clamping tests were obtained by reloading the sample into the blocks for each of the runs shown. The single clamping tests provide a more clearly defined time trend, while the multi-clamping tests were performed in order to insure that the results obtained were not due to the peculiarities of one set-up. That is, the multi-clamping tests made sure the results regarding temperature trends were repeatable, and not simply the result of the clamped condition caused by the way the bolts were attached to the blocks in a single case.

These results show a definite trend in regards to temperature. As temperature increased, both the maximum velocity of the sample and its Q value increased. This increase occurred in fashion which was roughly linear. Both the plots below display a large degree of randomness, though the positive slope of the data is unmistakable. The randomness seen in the data would not be present if temperature were the only factor at work. Therefore, the presence of the randomness suggests that other factors were at work affecting the sample. One such factor, as already mentioned, was considered to be the day to day variations in the lab environment. Another contributor could have been the way in which temperature changes affected the shape of the response curve. A large temperature swing over the course of a sine sweep could alter the shape of the response, and thus yield a different response. This is discussed in further detail later in this section.

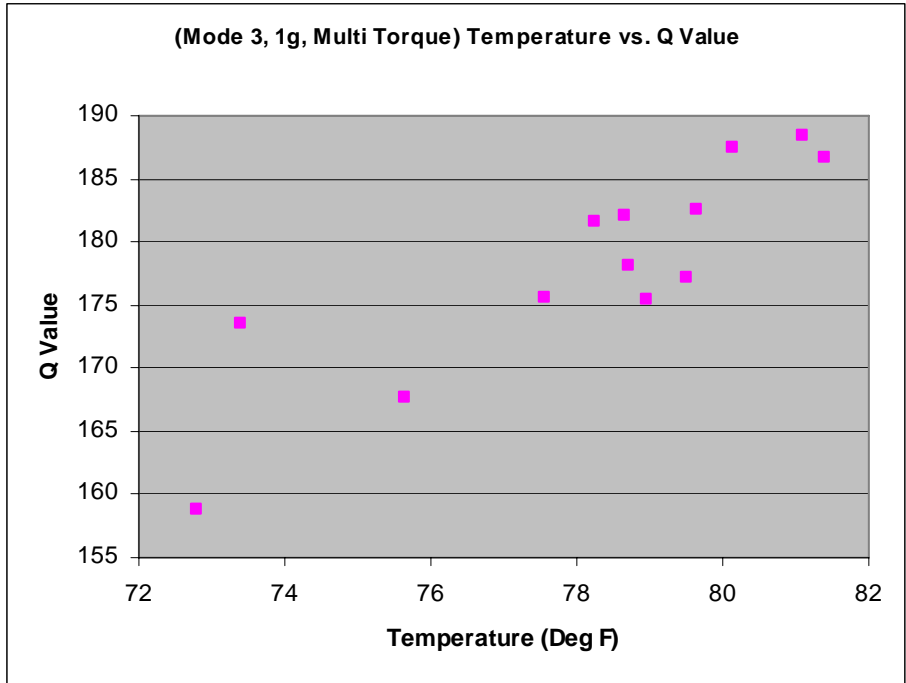


Figure 59. Temperature vs. Q Value, Multi-Clamping, Mode 3, 1g

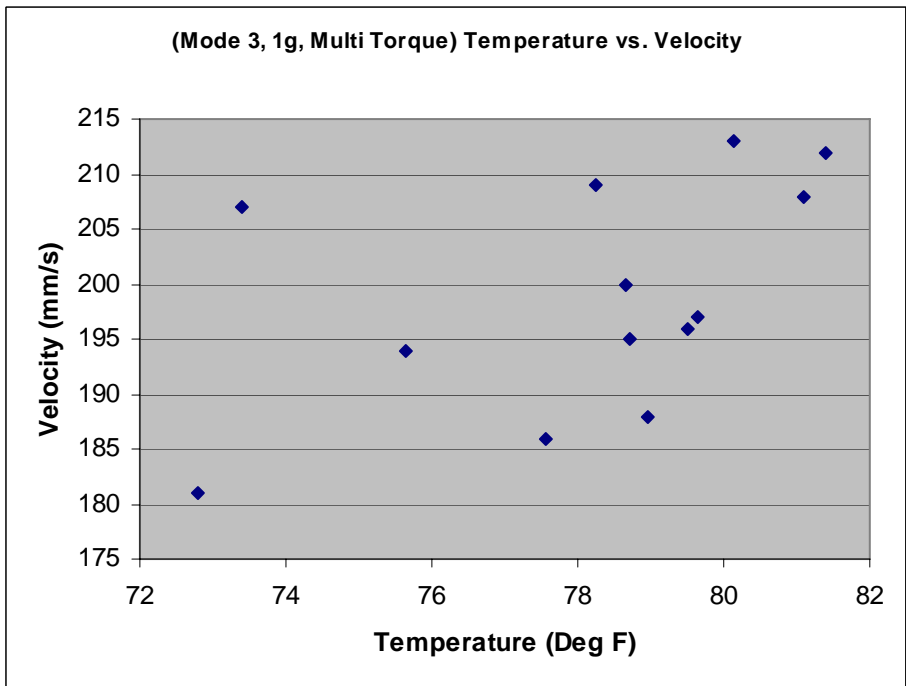


Figure 60. Temperature vs. Velocity, Multi-Clamping, Mode 3, 1g

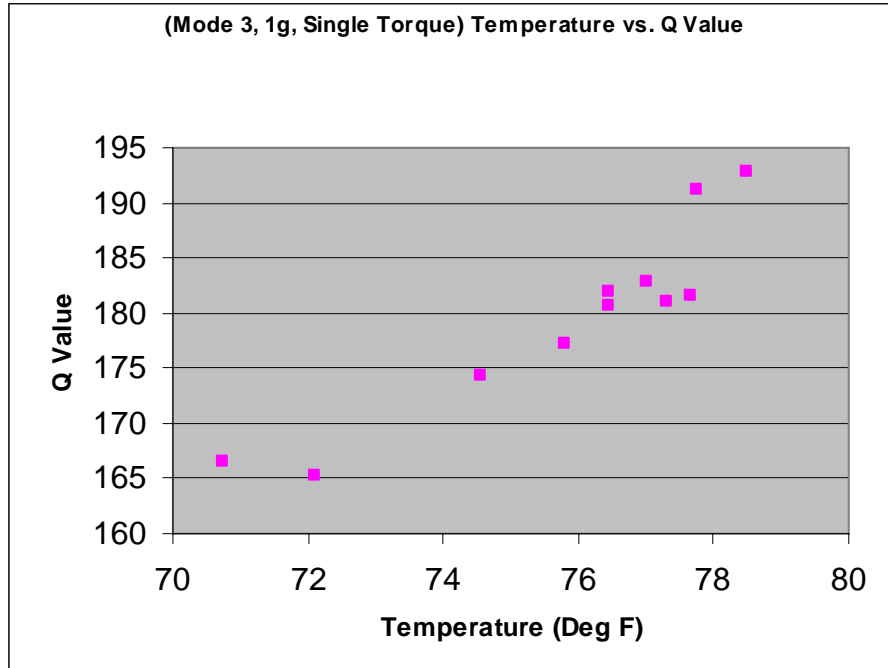


Figure 61. Temperature vs. Q Value, Single Clamping, Mode 3, 1g

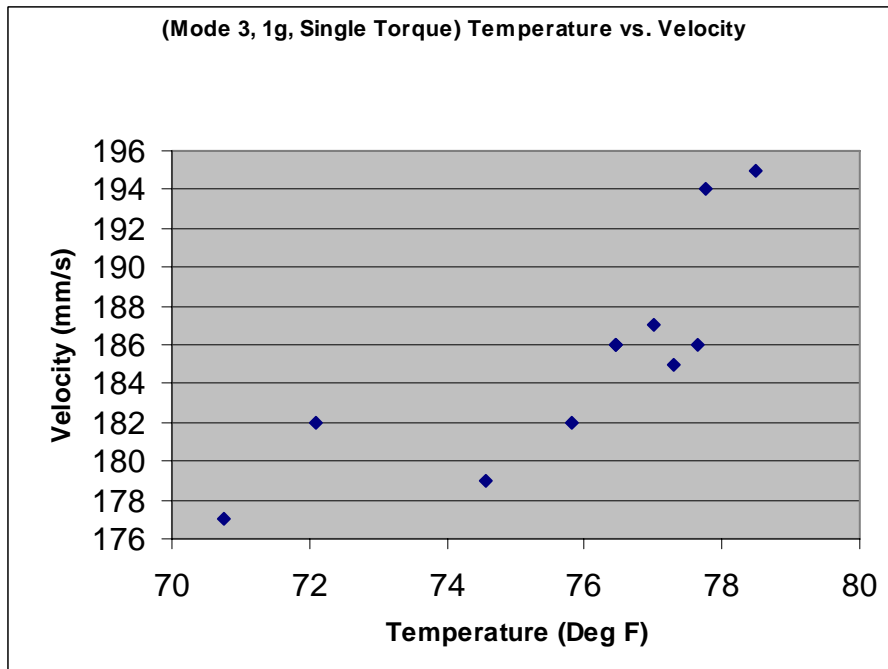


Figure 62. Temperature vs. Velocity, Single Clamping, Mode 3, 1g

As expected, there is more random variation in the multi-clamping plot than in the single clamping plot. The extra variation was introduced by reclamping the sample between runs. This changed the condition of the constraint blocks, and thus the results had to differ. The interesting point is that even as the constraint block condition changed, the general temperature trend persisted.

Both of the plots above show that as temperature increased, the clamp became more effective. The sample was able to reach a higher peak velocity and do so with less damping. The increase in velocity for a given peak frequency implied that strain would also increase. This is shown in the figure below. In this figure, Q value was plotted as strain increased. The figure below shows data from the single clamping testing, which clearly illustrates the trend. In this figure, it is easy to see that as the strain increased, Q value increased. The implication is that increasing temperature allowed for a better clamped condition, leading to greater movement in the sample and lower overall damping.

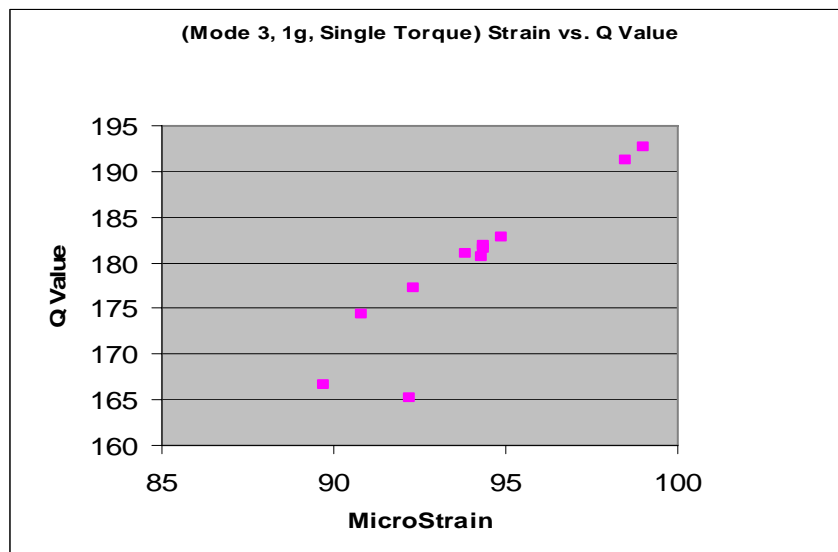


Figure 63. Strain vs. Q Value, Single Clamping, Mode 3, 1g

The results for mode 3 at an input excitation of 4 g's are presented below.

Testing at a higher level of excitation was designed to show how greater movement in the sample affected the temperature trend for the same mode. The plots below indicate that the same linear trend seen at 1g excitation, characterized by increasing velocity and Q value with temperature, occurred here. The results below are once again presented for both single clamping and multi-clamping experiments, where far greater variation is the multi-clamping plots.

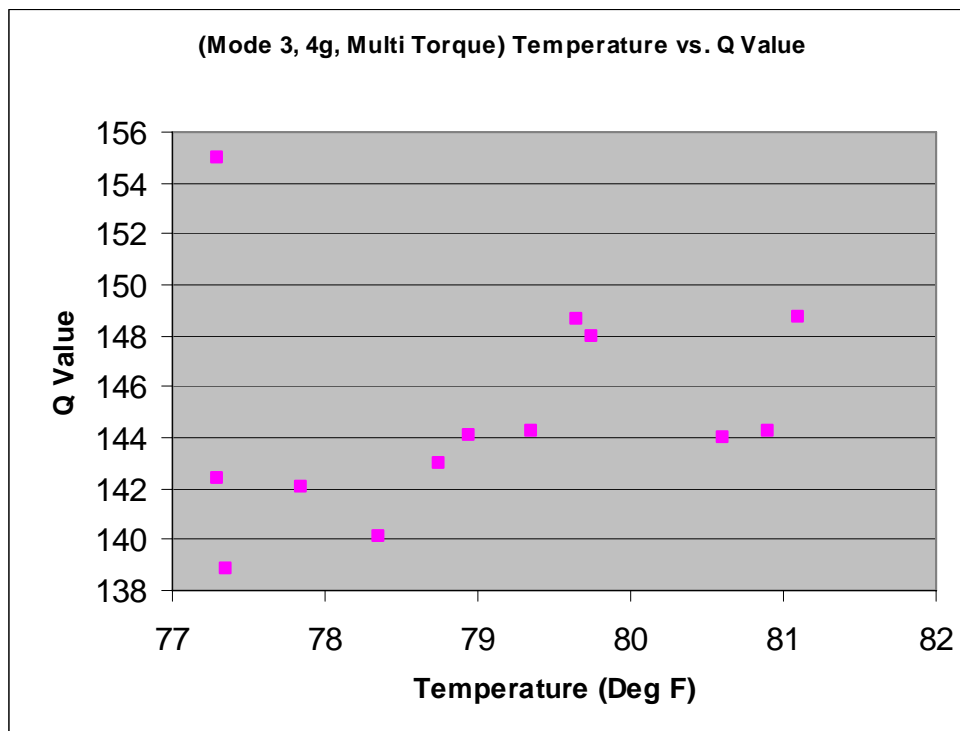


Figure 64. Temperature vs. Q Value, Multi-Clamping, Mode 3, 4g

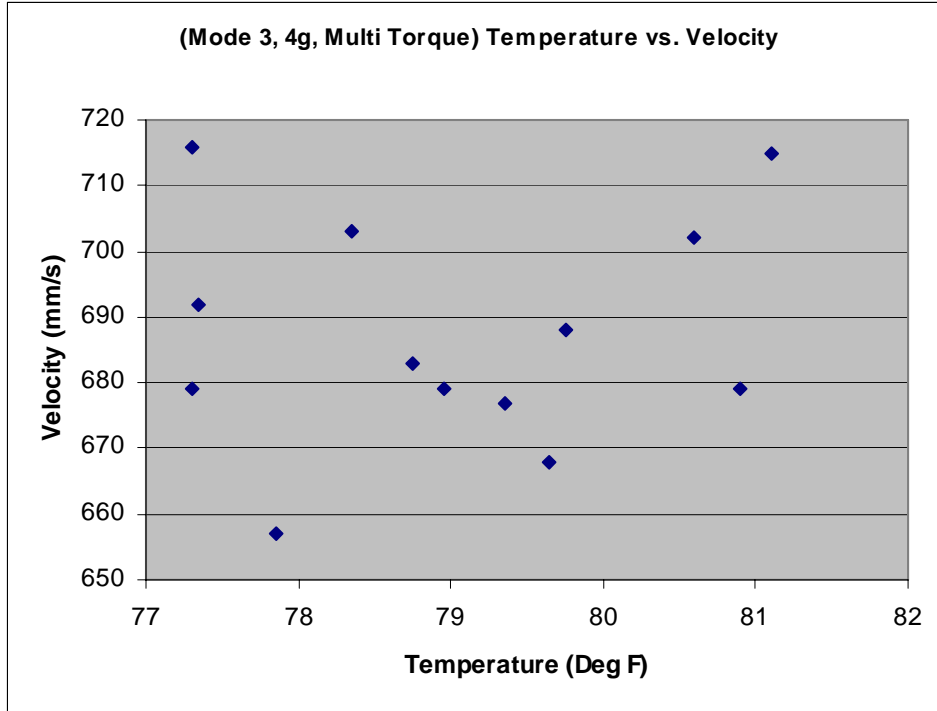


Figure 65. Temperature vs. Velocity, Multi-Clamping, Mode 3, 4g

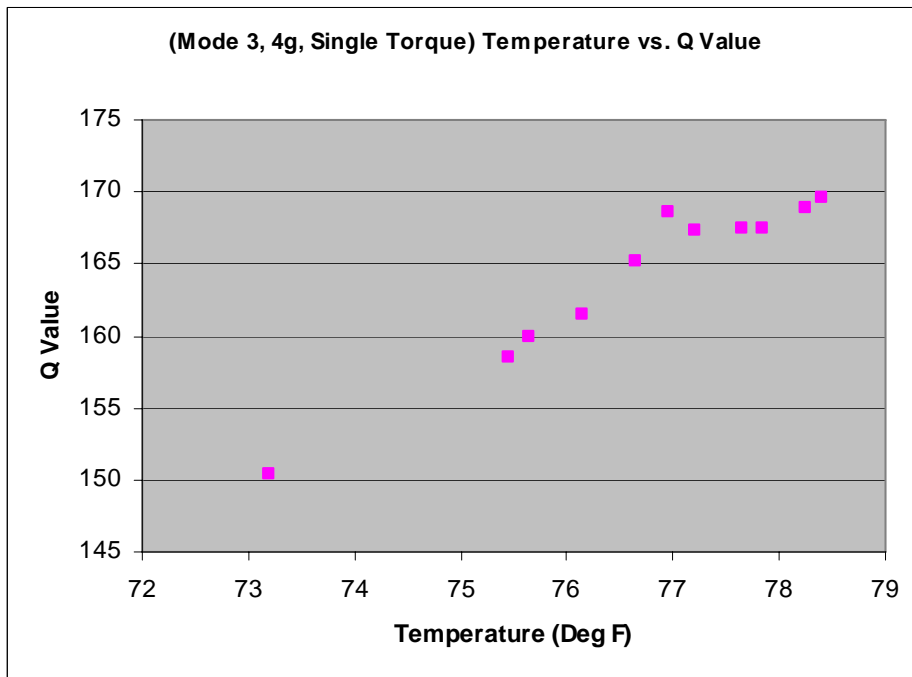


Figure 66. Temperature vs. Q Value, Single Clamping, Mode 3, 4g

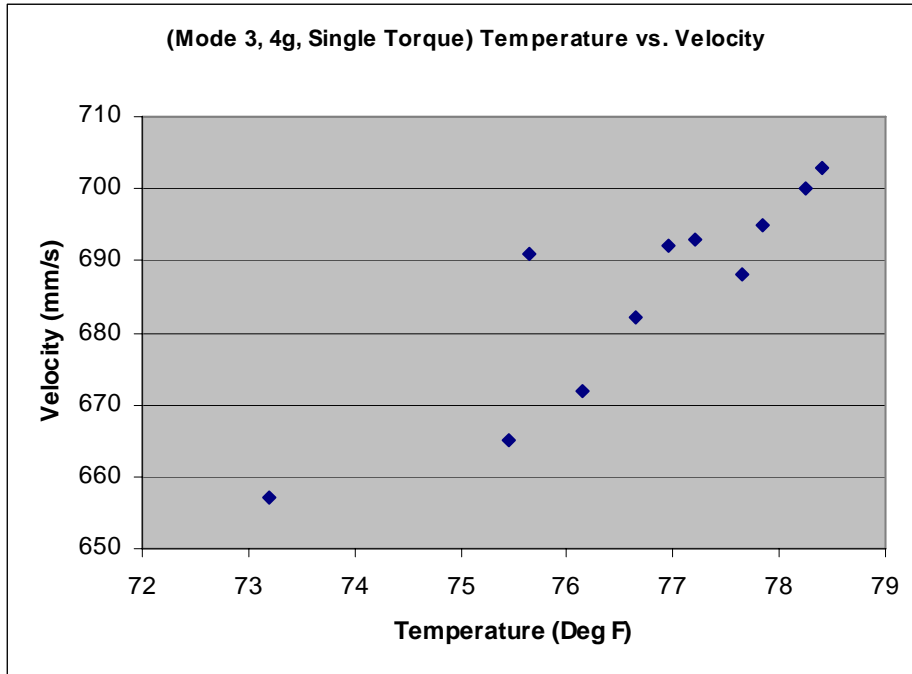


Figure 67. Temperature vs. Velocity, Single Clamping, Mode 3, 4g

In this case, the increase in Q value with strain also held true. The figure below shows a plot of strain versus Q value for mode 3 at an excitation level of 4g's. Data from the experiment using a single clamping is once again presented in order to more clearly show the trend in the data. The effect of temperature on damping measurements was once again shown for mode 3, using the increased input g level of 4 g's. The increase in temperature caused the performance of the clamp to increase, highlighting the strain dependence inherent in the device.

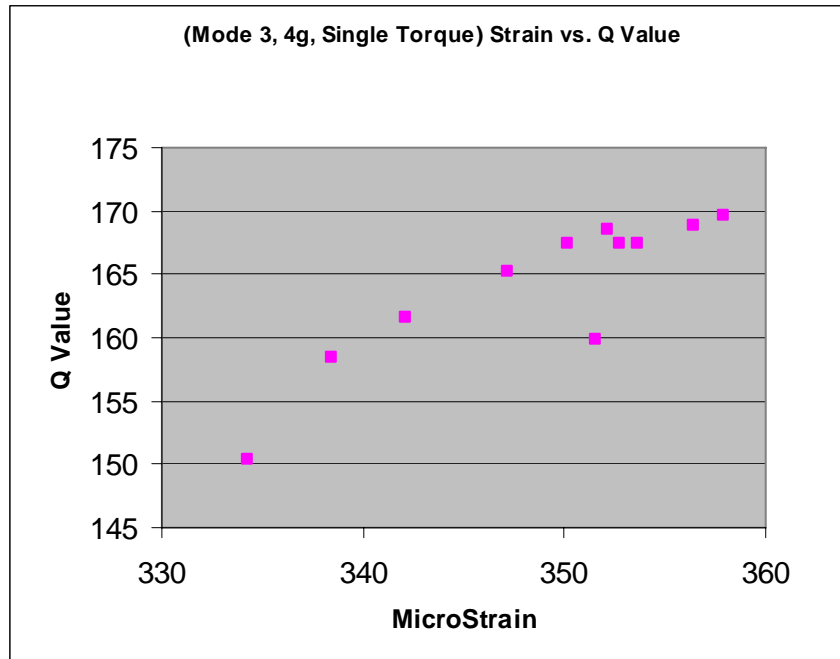


Figure 68. Strain vs. Q Value, Single Clamping, Mode 3, 4g

Testing was conducted at mode 4 to determine whether the temperature trend affected this mode as well. The results below, obtained for an excitation level of 1g, show that temperature did have an effect. However, the effect on this mode was apparently lesser than the effect on mode 3. The data shows far more variation, and the temperature trends are only vaguely present. That is, the data shows that increasing temperature lead to an increase in Q value, but the trends are rough. The nearly linear results obtained for mode 3 are seen in mode 4. Plots of the results for both single clamping and multi-clamping testing are once again shown.

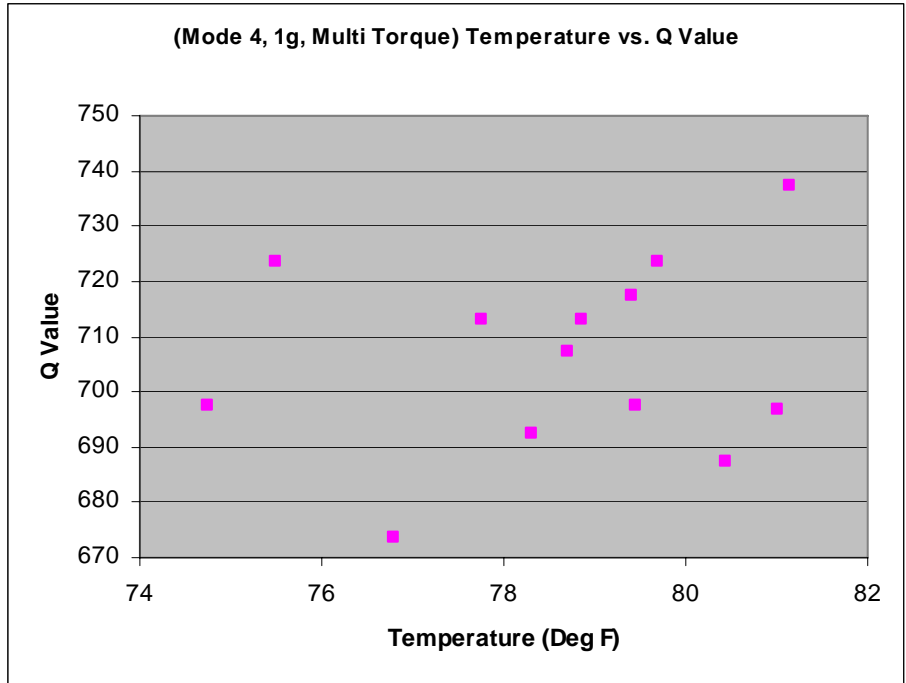


Figure 69. Temperature vs. Q Value, Multi-Clamping, Mode 4, 1g

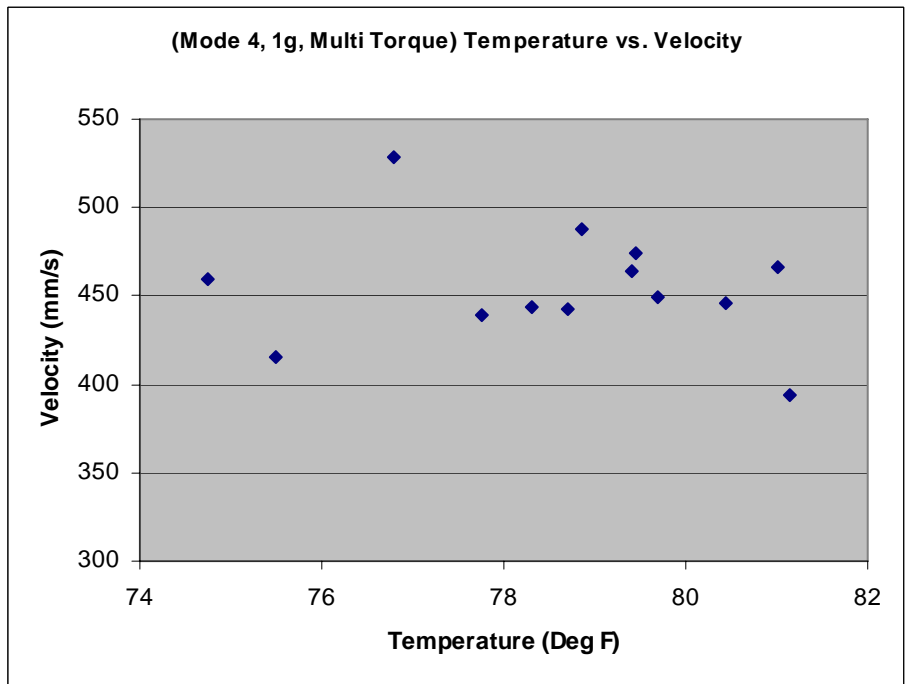


Figure 70. Temperature vs. Velocity, Multi-Clamping, Mode 4, 1g

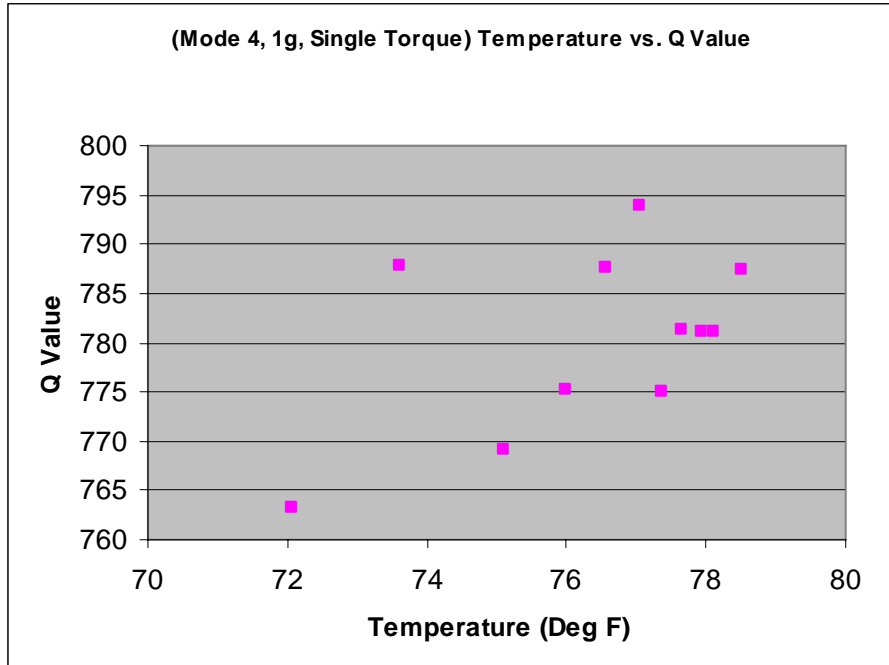


Figure 71. Temperature vs. Q Value, Single Clamping, Mode 4, 1g

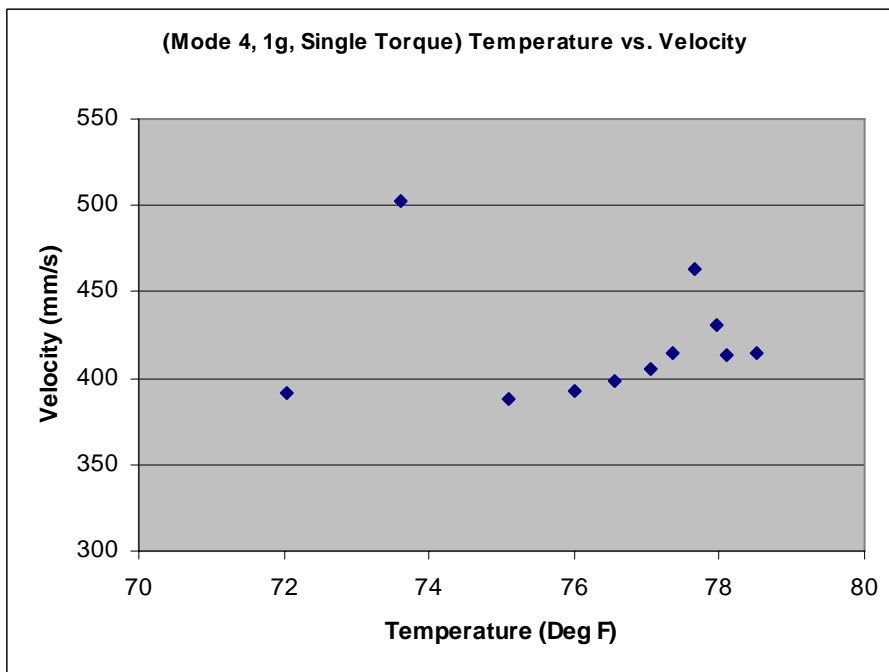


Figure 72. Temperature vs. Velocity, Single Clamping, Mode 4, 1g

The temperature trend observed had a lesser effect on mode 4 due to a change in maximum strain location. For mode 3, the location of maximum strain in the sample was at the root, where the sample was clamped in place. In the case of mode 4, the maximum strain location was instead at the specimen tip. Therefore, when the sample was undergoing mode 4, the constraint blocks did not have to work as hard to hold the sample in place. As such, an improvement in the performance of the clamp through an increase in temperature would have had a reduced impact on the results. This is further evidenced in the plot below, which shows strain versus Q value. The plot shows that Q value lacks a clearly defined trend with regards to the strain in the sample. In mode 4, the performance of the blocks must have played a smaller role in determining the response of the system.

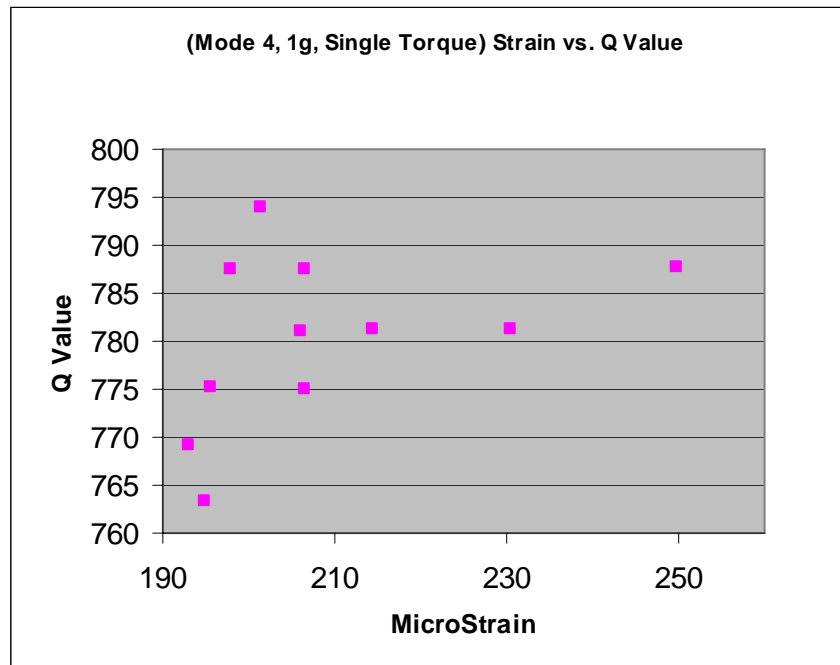


Figure 73. Strain vs. Q Value, Single Clamping, Mode 4, 1g

Finally, mode 4 was tested at an excitation level of 4g's. This was done, once again, in order to determine whether the magnitude of excitation had an impact on temperature trend dependence. The plots below indicate that temperature still had only a minimal impact on mode 4. The single clamping plots show the increase in Q value with temperature, while multi-clamping plots make this trend barely recognizable. It is interesting to note that that the effect of reclamping the sample has almost completely masked the temperature effect for this portion of the study. This certainly emphasizes the impact that reattachment of the blocks had on an experiment.

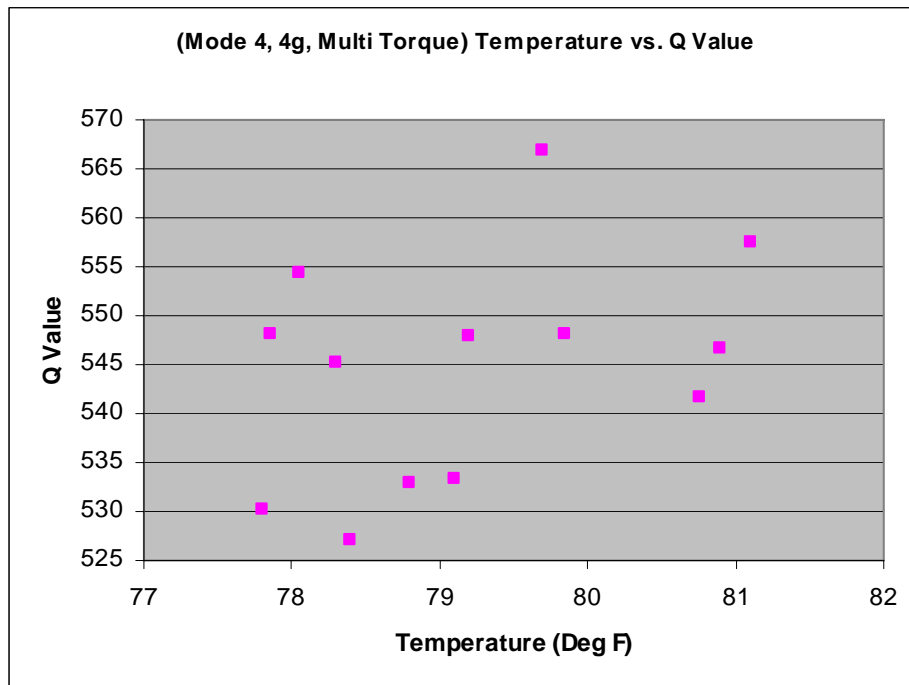


Figure 74. Temperature vs. Q Value, Multi-Clamping, Mode 4, 4g

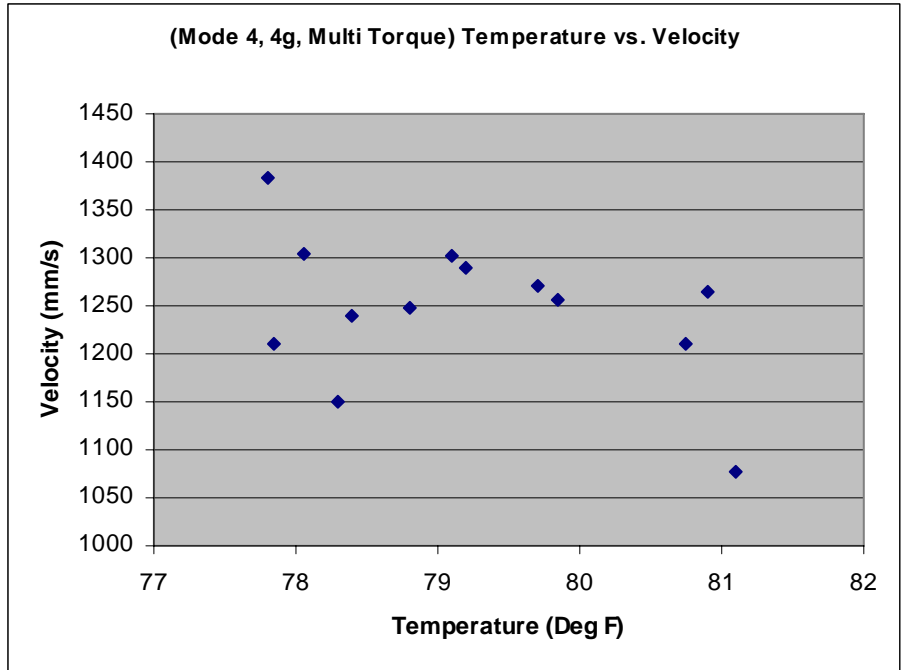


Figure 75. Temperature vs. Velocity, Multi-Clamping, Mode 4, 4g

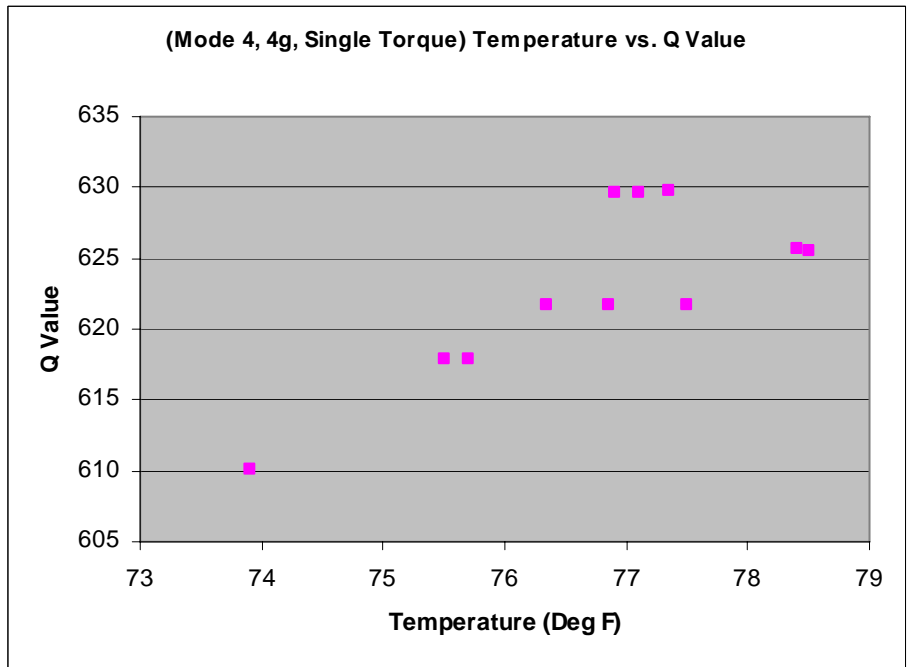


Figure 76. Temperature vs. Q Value, Single Clamping, Mode 4, 4g

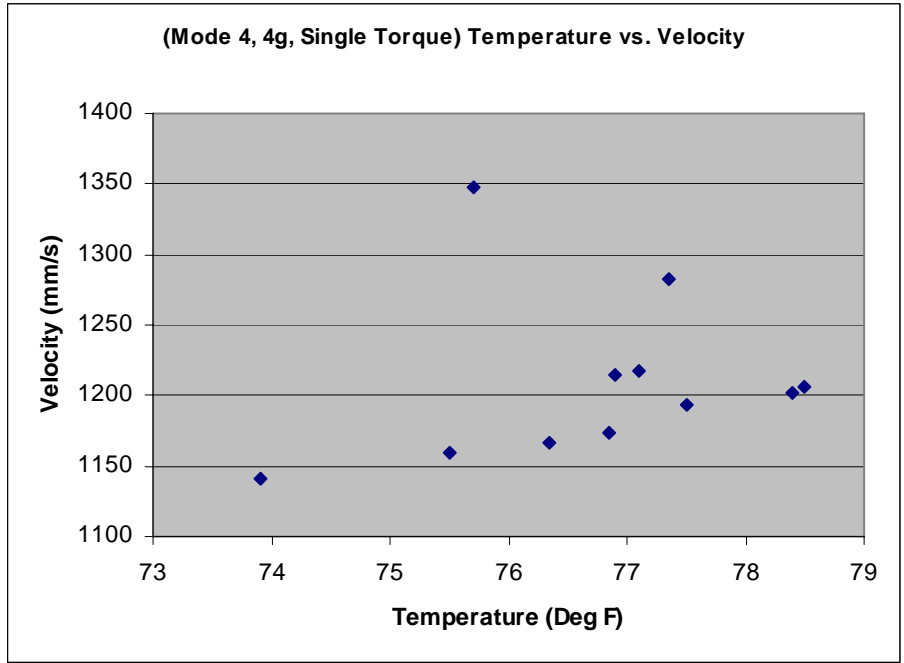


Figure 77. Temperature vs. Velocity, Single Clamping, Mode 4, 4g

The plot below shows Q value versus strain for mode 4 at an input of 4 g's. This plot was, once again, generated using data from the single clamping experiment. It shows no discernable trend in strain versus Q value for mode 4 either. This supports the theory that temperature variations and strain dependence had a lesser impact on mode 4 of the sample.

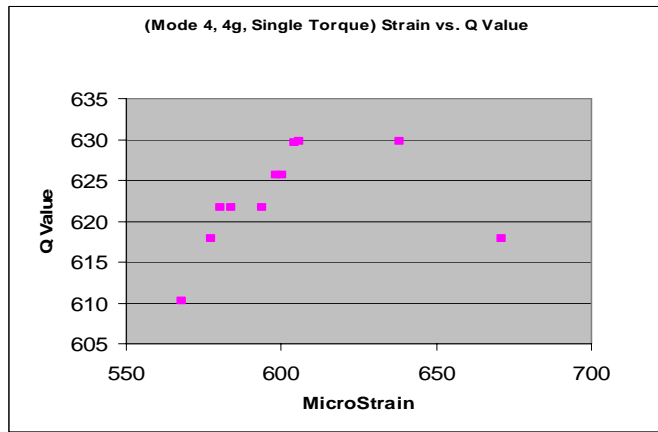


Figure 78. Strain vs. Q Value, Single Clamping, Mode 4, 4g

Further analysis of the results of this testing dealt with the possibility that temperature changes during the course of a sine sweep altered the results. It has been shown in numerous plots that temperature had an effect on the damping and peak velocity of the sample. This means that temperature changes must have had some effect on the shape of the response peak. The question becomes, then, whether temperature changes during the span of a single experimental run could have caused changes in the response. As mentioned earlier in this section, this is a possible reason why so much variation was seen between various tests, even when the sample was not reclamped into the blocks.

The temperature repeatability testing in this section was not designed to look at this “ ΔT effect.” As such, the analysis of the results was simply performed after the fact. This analysis of the results regarding this effect was inconclusive, though it invites further study.

In this analysis, a group of 4 experimental runs from the single clamping portion of the experiment were compared. These 4 runs each corresponded to mode 4 at an excitation level of 1g. For two of these runs, the change in temperature recorded across the run was 1.4 and 1.5 degrees Fahrenheit. These were the highest recorded temperature changes across a single run. In the other two runs, the temperature changes were 0.0 degrees and 0.1 degrees. These runs are shown together in the figure below.

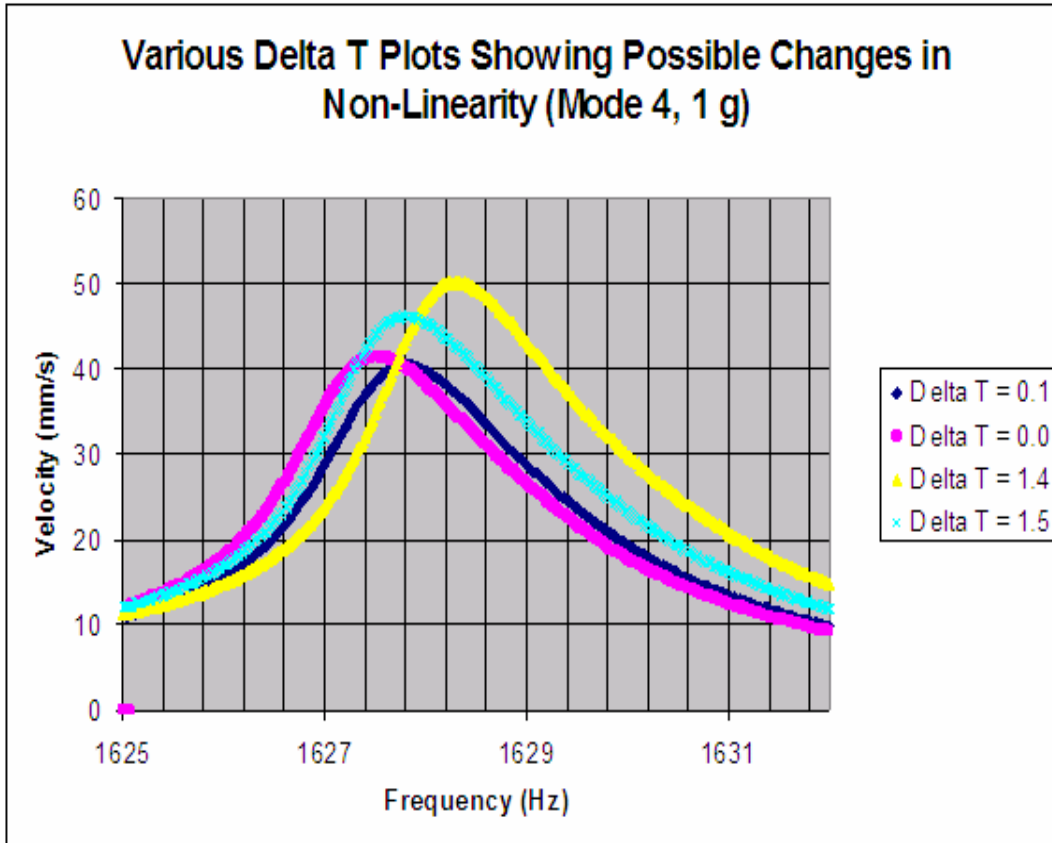


Figure 79. Sine Sweep Results for Various Temperature Changes

In the figure above, it is difficult to tell whether the runs with very low change in temperature (ΔT) are more linear than those with a much higher ΔT . In order to make a comparison, the individual peaks were first rescaled to the same size, then overlaid onto a new figure. In drawing a line of symmetry down the center of the peaks, it can be seen that the peaks with smaller ΔT come slightly closer to being symmetrical. As in the plot above, these peaks represent the portion of a sine sweep between 1625 and 1632 Hz.

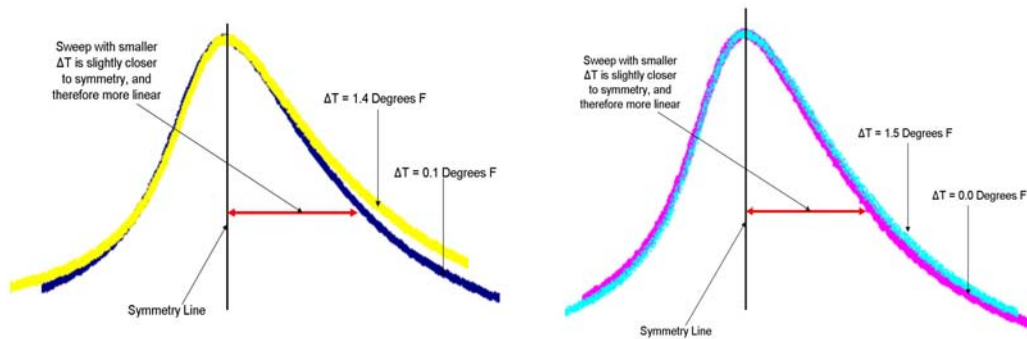


Figure 80. Comparison of Rescaled Temperature Change Sweep Results

The plot below shows the same information about the relative symmetries, but with a different technique. In this case, the right side of the response curve has been reflected onto the left and washed out, allowing the reader to see how close the curves come to symmetry about themselves. In the figure below, the relative scale of the response curves has been preserved. Once again, it appears as though the curves with lower ΔT are more symmetrical. That conclusion is, however, only based on a cursory examination of available data.

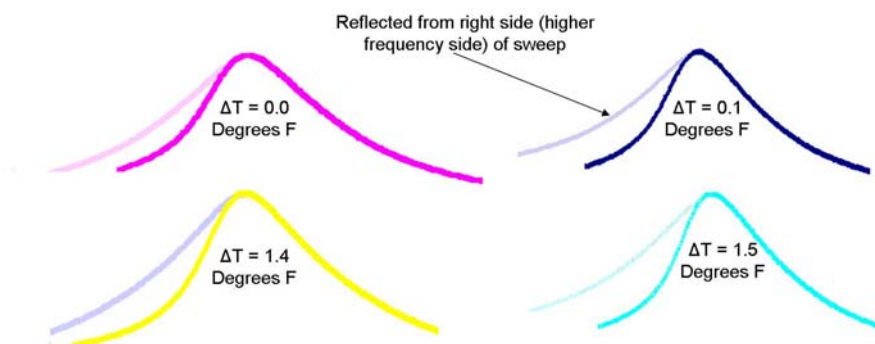


Figure 81. Comparison of Linearity in Sweep Results

In order to better understand the impact of temperature changes within a sine sweep, the temperature changes within each sweep performed were plotted versus the Q values found. This was done for the data on both modes, in both the single clamping and multi-clamping testing. The plots developed were by no means conclusive, but did highlight an interesting trend. In 5 of the 8 plots, Q value clearly appeared to decrease as the ΔT for each run increased. In the remaining 3 plots, the data showed no strong trend or was randomly distributed. The plots below show ΔT versus Q value for single clamping tests. The plots were obtained using data from tests at mode 4 with a 4g input and mode 3 with a 1g input, respectively. In order to highlight the trend in the data, a linear trend line has been added to each.

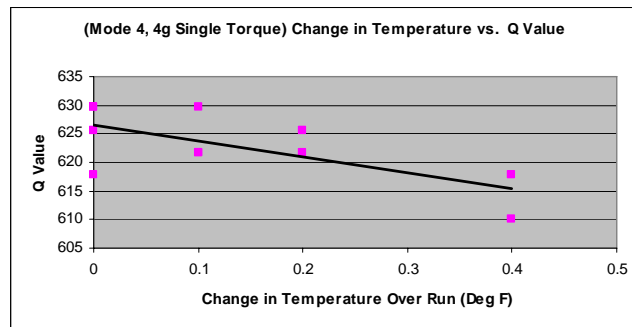


Figure 82. ΔT vs. Q value for Mode 4, 4g with Trend Line

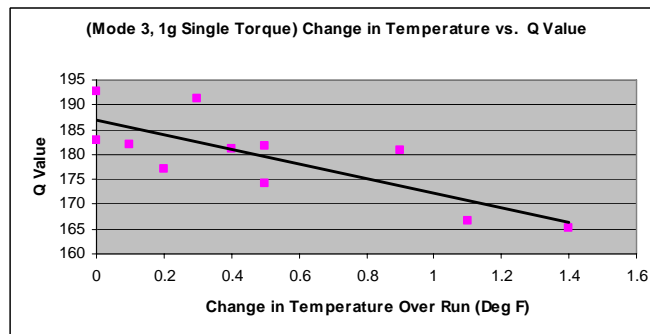


Figure 83. ΔT vs. Q value for Mode 3, 1g with Trend Line

As stated before, while these results are interesting, no hard conclusions could be drawn regarding the effects of change in temperature across a sine sweep. The analysis of temperature testing data indicated that temperature fluctuations would lower Q values in both modes 3 and 4. It also suggested that nonlinearities in response curves may have been partially caused by temperature variations, which affect the clamping ability of the constraint blocks in the middle of a test. More testing would be required in order to confirm these theories, however.

In this section, it was determined that temperature trends had an undeniable effect on the response from the sample. Increased temperature enhanced the performance of the constraint blocks and lowered damping. It also allowed for increases in sample peak velocity for a given input g-level. Further, the temperature variations within runs themselves added another wrinkle into an already complicated problem. The ANOVA experiment would have to contend with variation introduced by a temperature which was not controllable.

The temperature time trend could have been incorporated into the ANOVA experiment. Research in the effect of time trends in ANOVA has been performed, and techniques for minimizing their effects have been analyzed (1). Therefore, a time trend was not an insurmountable obstacle. However, the experimenter decided it would be best to find a way to eliminate the time trend, if possible, in order to produce more robust results. The figures below show plots of average temperature versus run for two different testing dates.

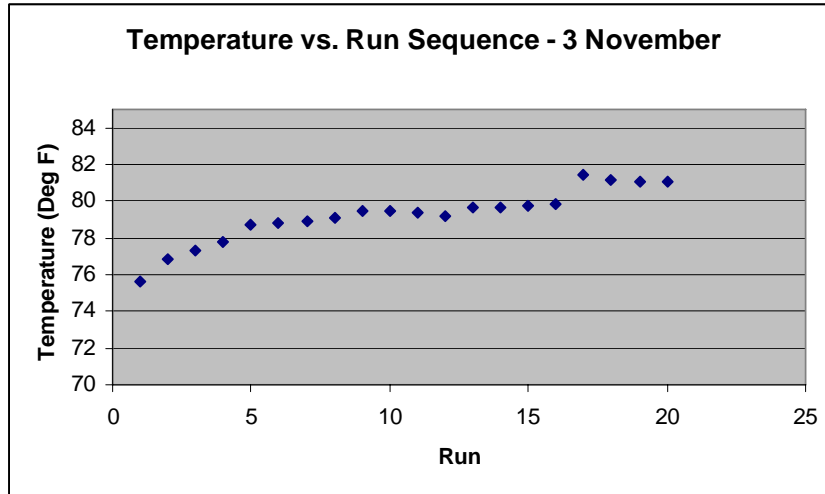


Figure 84. Temperature vs. Run on 3 November

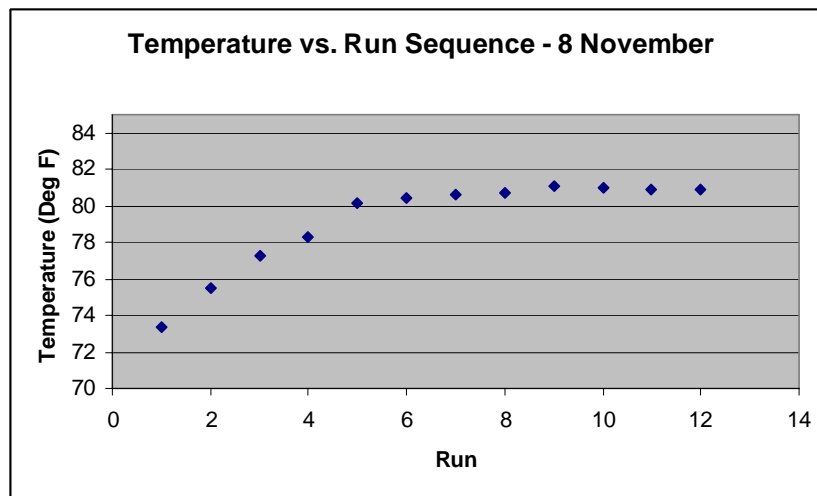


Figure 85. Temperature vs. Run on 8 November

The above plots show that temperature leveled out over the course of testing. The operation of the shaker table heated the room, but the room eventually reached an approximate steady state temperature. At this steady state condition, the temperature experienced only very small deviations, on the order of 0.1 degrees. Therefore, simply allowing a shaker room to reach a steady state temperature before testing began

eliminated the temperature trend and any possible effects from a temperature change across a sine sweep.

Temperature testing in this section, as well as the subsequent data analysis, allowed for several important conclusions to be drawn:

- 1) Temperature has a definite effect on damping measurements for both modes of interest, and this effect is greater for mode 3 than it is for mode 4.
- 2) Reclamping the sample into the constraint blocks increases variability between runs. Further, it may mask other factors which are influencing system damping.
- 3) Temperature increases cause the constraint blocks to clamp more effectively. This, in turn, allows the sample to achieve higher strain values for a given input. Due to the improved clamping condition, total damping decreases and the measured Q value increases.
- 4) Temperature in a shaker room does not reach a steady state temperature over a period of time. This steady state temperature varies, depending on daily laboratory conditions.
- 5) Temperature changes over the course of a single run may affect the shape of the frequency response function found.
- 6) In order to negate the effects of a temperature trend, an experimenter can wait until the shaker room has reached a steady state temperature before beginning an experiment.

This experimentation has shown the effect of temperature trends, as well as a means for negating their effect on sensitive experimentation. Coupled with knowledge of

the constraint blocks and the lab environment, this allowed the experimenter to design an effective and efficient ANOVA experiment to study the effect of air pressure and associated interactions. However, before this experiment could be performed, the equipment required had to be tested. Further, factors directly affecting this equipment had to be evaluated in order to insure this experiment would be accurate.

Accelerometer Location and Bungee Cord Testing Results

Though comparatively brief, this testing was essential for designing an effective ANOVA experiment. Testing in this section focused on the usefulness of bungee cords in improving results, as well as control accelerometer placement. This section was also used to determine whether testing with the full pressure vessel-baseplate set-up could be performed on the 6,000 lbf shaker if required.

Before the accelerometer locations and bungee cords were tested, the set-up was run without any modifications. The new baseplate was attached to the shaker head, the uncoated sample was clamped into the constraint blocks, and the pressure vessel was attached. The same accelerometer used for all previous testing was installed 1” behind the constraint blocks on the baseplate, inside the pressure vessel. Testing for both modes in this condition showed that mode 3 had slight modal interference issues, but the results for mode 4 were skewed by extreme modal interference. The response produced for mode 4 was decidedly nonlinear, and yielded Q values which were inconsistent with expectations. Though high Q values were desirable on an uncoated specimen, these values were artificially inflated due to nonlinearity in the mode 4 response. The test runs

completed on this basic set-up were used as a control, and as a means for comparison when examining accelerometer location and bungee cord use.

As expected, mounting the full test set-up on the 6,000 lbf shaker had produced interference issues. The mounting condition of the baseplate and pressure vessel on the shaker head, as described previously, was the most likely cause for this interference. However, numerous tests were still performed in the system in order to seek out any other possible causes of this interference.

First, two different accelerometer locations were considered. It would either be placed directly on top of the constraint blocks or directly behind the constraint blocks. Locating the accelerometer behind the constraint blocks was preferable, because it would allow the sample to be clamped in place or switched out without the removal of the accelerometer. The accelerometer on top of the constraint blocks was a smaller and of a different make than the one mounted behind the blocks. As mentioned in Chapter III, this was the case because the larger accelerometer, mounted behind the blocks, would not fit in the open space on top of the blocks.

Testing for accelerometer locations was straightforward. The accelerometers were installed inside the pressure vessel in their respective positions, and each was used to control the excitation of the system on different runs. The results were analyzed, looking for any significant difference in the response obtained from the control accelerometers in different positions. A significant difference in the results would indicate, of course, that one of the accelerometer locations was better than the other. The actual results are shown below, which compare runs completed on the basic set-up to those where the small accelerometer on top of the blocks was controlling the system.

Table 34. Like Runs With and Without Bungee Cords

ACCEL LOCATION	INPUT g-LEVEL	MODE	PEAK FREQ (Hz)	Q VALUE	PEAK VELOCITY (mm/s)
BEHIND BLOCKS	1	3	1233.719	303.33	331.6
BEHIND BLOCKS	1	3	1234.235	299.78	333.6
ON BLOCKS	1	3	1230.185	329.48	430.1
BEHIND BLOCKS	4	3	1229.901	197.28	941.3
BEHIND BLOCKS	4	3	1230.385	213.33	913.8
ON BLOCKS	4	3	1226.951	229.3	1152
BEHIND BLOCKS	1	4	1627.268	1337.2	362.2
BEHIND BLOCKS	1	4	1627.468	1479.3	349.7
ON BLOCKS	1	4	1627.452	1355.9	303.3
BEHIND BLOCKS	4	4	1626.168	1049	1007
BEHIND BLOCKS	4	4	1626.402	1084	955.7
ON BLOCKS	4	4	1626.268	1121.4	928

The table above does not show any great departure from the initial results when the control accelerometer location was moved to the top of the blocks. The damping remained roughly the same in all cases, and the nonlinearity in mode 4 remained intact. It was hoped that directly controlling the sample via its mounting blocks would negate baseplate interference effects in mode 4, but this was not the case. Even when using this control location, the Q values remained artificially high for mode 4.

Allen, in his previous study, theorized that the pressure vessel handles might resonate at frequency coincidental with the 4th mode in the sample (2). In order to negate this effect, he attached bungee cords to the handles of the pressure vessel and connected them to the sturdy structure supporting the shaker table. It was reasonable to assume that the severe interference affecting the sample may have been due, at least in part, to the movement of these handles.

The next obvious step, therefore, was to test whether bungee cords were effective at eliminating or reducing the nonlinearity seen in mode 4. The effectiveness of the bungee cords at improving the mode 3 response was also tested. Two bungee cords were

attached to each pressure vessel handle, pulled taut, and then attached to the large, immobile shaker table stand. A total of three runs were completed with the bungees in place, and these runs were again compared to the results of tests run on the basic set-up. A table containing the results of these runs is shown below.

Table 35. Like Runs With and Without Bungee Cords

BUNGEE CORDS (Y/N)	INPUT g-LEVEL	MODE	PEAK FREQ (Hz)	Q VALUE	PEAK VELOCITY (mm/s)
N	1	3	1233.719	303.33	331.6
N	1	3	1234.235	299.78	333.6
Y	1	3	1233.052	290.09	366
N	4	3	1229.901	197.28	941.3
N	4	3	1230.385	213.33	913.8
Y	4	3	1229.868	215.11	970.5
N	1	4	1627.268	1337.2	362.2
N	1	4	1627.468	1479.3	349.7
Y	1	4	1627.252	1355.8	350.6

The table above indicates that the bungee cords had no effect on the system. While the values differ for each of the runs, none of the data above indicates a departure from the same basic response. The damping of the system was not significantly altered for mode 3, with Q values falling in line with those derived from non-bungee tests. In mode 4, the bungee cords had no effect in abating the nonlinearity. The mode 4 bungee cord test still produced a Q value inordinately high for the system, and the response showed the same jump phenomenon.

A brief analysis of the table above did an acceptable job of showing the ineffectiveness of bungee cords. However, it remained to be seen how the pressure vessel handles actually moved. Though the bungee cords had no effect on the response, it was possible that the handles were still displaying movement coincidental with the 4th mode of the sample.

A test sweep was performed in order to directly test how the pressure vessel handles moved during an experimental run. In this test, the control accelerometer on top of the constraint blocks, located inside the pressure vessel, controlled the movement of the system. A run from 1170-1700 Hz was performed at a sweep rate of 106 Hz/min and an input level of 1g. For this test, the laser vibrometer recorded the movement of the top center of a pressure vessel handle. This sweep would capture any movement of the handles in either of the modes of interest for the sample. The response from this sweep is shown below.

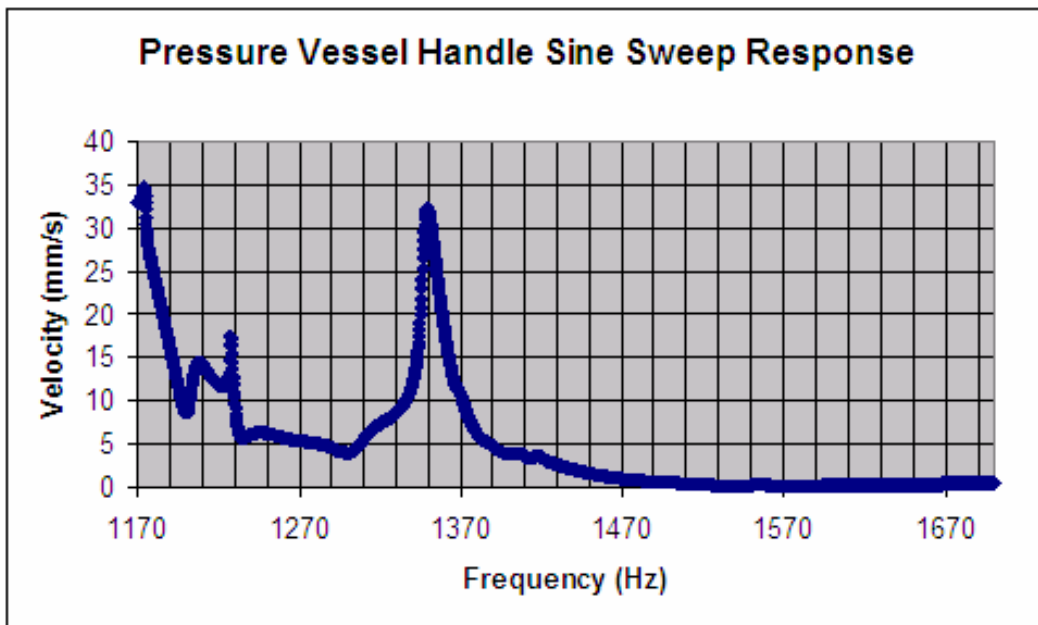


Figure 86. Pressure Vessel Handle Sine Sweep Response

The response above shows that the pressure vessel handles did indeed have resonances near the modes of interest for the sample. However, the movement associated with these modes did not coincide with the sample's mode 4. The handles experienced a strong response at 1350 Hz, but this was merely between modes 3 and 4 for the sample.

Movement of the handles at 1228 Hz coincided precisely with mode 3 of the sample. It is possible that this was a mode in the handles themselves, but could have also been the result of movement elsewhere in the structure. The velocity recorded at 1228 Hz was also only 17.6 mm/s. It seems unlikely that such a relatively small movement in the handles would have had an impact on the results for mode 3. Based on the results of this sweep, the pressure vessel handles could not have played a role in altering the modal response of the sample. This is why attaching bungee cords to them had no effect.

Two additional possibilities for reducing the modal interference in mode 4 included reducing the sweep rate and increasing the excitation level of the input. In order to test the sweep rate idea, the sweep rate was reduced and sweeps of mode 4 were run. At an input level of 1g, rates of 2 Hz/min, 0.8 Hz/min, and 0.4 Hz/min were used. The increased resolution afforded by these slower sweeps had no effect on the shape of the response. Increasing the input g-level for a constant sweep rate of 5 Hz/min also allowed for no improvement in mode 4. In mode 3, however, the increase in size of the sample response peak appeared to outpace surrounding peaks. However, these surrounding peaks were never a major source of interference.

Testing using the considerations in this section yielded several conclusions:

- 1) Bungee cords attached to the pressure vessel do not reduce modal interference in a system because the pressure vessel handles are not the source of this interference.
- 2) Increasing the input g-level is not a viable means for removing modal interference, as this interference generally grows proportionally.

- 3) Changing the location in the control accelerometer to the top of the constraint blocks does not lessen modal interference. Further, all results obtained for this position are effectively the same as for those obtained with the accelerometer placed behind the constraint blocks on the baseplate.
- 4) Mounting the pressure vessel and new baseplate to the 6,000 lbf shaker table causes extensive modal interference that cannot be negated through any means tested. This interference primarily affects mode 4 of the sample.

Because there was no apparent difference in the response for each accelerometer location, the location behind the constraint blocks was chosen for ANOVA testing. This was the case simply because it was a more convenient mounting location, and the accelerometer would not have to be removed every time a sample was clamped in place.

In ANOVA testing, the entire set-up would have to be mounted on the 18,000 lbf shaker in hopes of avoiding the interference issues seen in this section of testing. In order to better understand the causes of this modal interference, the entire set-up was ping tested while still mounted on the 6,000 lbf shaker. This was done so that any potentially interfering resonances in the system might be found, and possibly corrected, before beginning ANOVA testing.

Ping Testing Results

Ping testing was used to determine what resonant frequencies were at work within the pressure vessel-baseplate system. It was assumed that modal interference issues encountered in the previous section occurred because of the way the set-up must be mounted to the 6,000 lbf shaker table, as theorized and discussed previously in this

research. Ping testing would confirm that interfering modes were not endemic within the baseplate and pressure vessel themselves. If any potential sources of interference were found, this information would be used to make improvements to the equipment before mounting on the 18,000 lbf shaker table for ANOVA testing.

All ping testing was performed over a range of 0 to 2000 Hz, so as to encompass both modes of interest for the sample. Ping tests were performed on all locations on the set-up likely to cause interference issues. In ping testing, the accelerometer reading the response was placed in one of the locations being tested, while the hammer was always used to strike the top of the baseplate, outside the pressure vessel. The resulting frequency response functions derived from each ping test represented the transfer function between the two locations. These transfer functions highlighted modes present within the system. The baseplate was struck with a hammer because this was roughly the same location through which an excitation is delivered by a shaker table.

It is important to note that the amplitude between ping test figures cannot be compared. Because the magnitude of the input force was not recorded, the figures are only scaled arbitrarily. The first of these figures is the most applicable to ANOVA testing. It represents the response between the baseplate and the top of the constraint blocks, and is shown below.

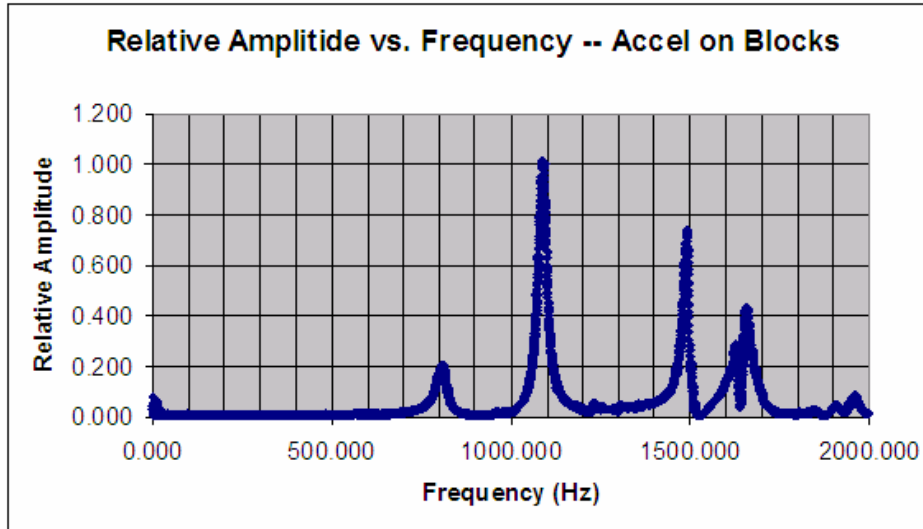


Figure 87. Ping Testing Between Constraint Blocks and Baseplate

In the figure above, several different peaks are recorded. One of these peaks occurred at a frequency of 1630 Hz, which was precisely the same as the peak frequency for mode 4 of the sample. This ping test shows that this interfering mode, at 1630 Hz, existed between the baseplate and the constraint blocks when mounted on the 6,000 lbf shaker. The response shown in this ping test was necessarily dependent upon the way the baseplate was mounted to the shaker head. Therefore, it differed when the set-up was mounted on the 18,000 lbf shaker. The response shown in the ping test above implicated baseplate interference on the 6,000 lbf shaker as the source for the interference seen in the previous section.

The next ping test shows the relationship between the baseplate and the pressure vessel window. When measuring sample movement, the laser vibrometer had to pass a laser beam through this acrylic window. Concern was expressed over whether movement in the window would reflect or refract the laser beam. It was thought that a rapidly

oscillating window might disrupt the signal between the laser vibrometer and the sample.

The results of the ping test are shown below.

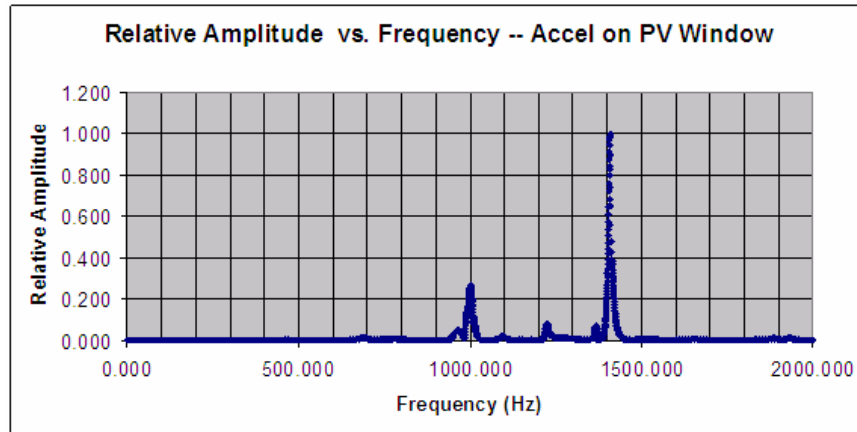


Figure 88. Ping Testing Between Pressure Vessel Window and Baseplate

The results above show a small peak at 1223 Hz, which was coincidental with mode 3 of the sample. There was no response peak for the window near the sample's 4th mode. Because there were no problems reading the sample response through the window, it was deemed unlikely the response seen at the window was of any concern.

Finally, ping testing was performed between the baseplate and one of the pressure vessel handles. The response below showed that the handles experienced a sharp resonance at 1220 Hz. Because the damping of these handles with bungee cords in previous testing had no discernable effect, it was determined that the handle resonance was not of concern. Additional ping testing results are contained in Appendix G.

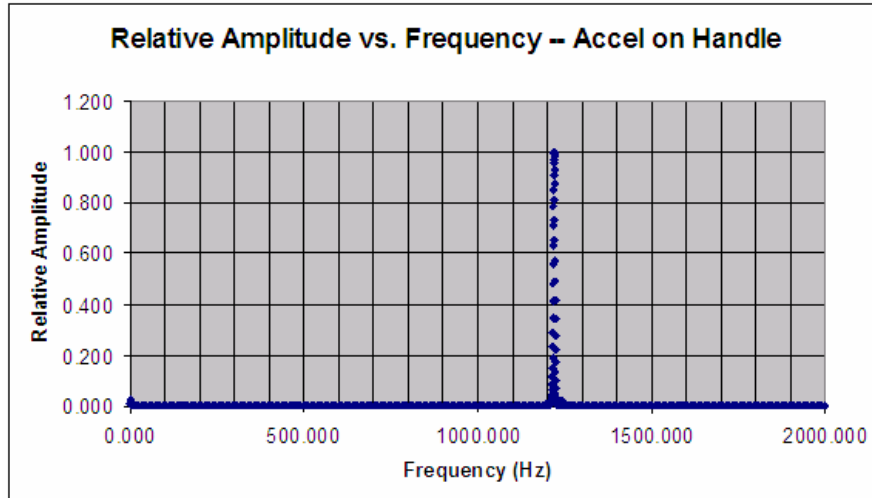


Figure 89. Ping Testing Between Pressure Vessel Handle and Baseplate

The conclusions which may be drawn from this section are brief, but consequential. They paved the way for ANOVA testing on the 18,000 lbf shaker.

- 1) Interference encountered in testing on the 6,000 lbf shaker was due to modal interference between the baseplate and the constraint blocks.
- 2) As suspected, the pressure vessel handles have a mode near the sample's mode 3. However, this mode has little or no effect on the damping measured for the sample.
- 3) The pressure vessel window experiences a mode near the sample's mode 3, but no effects on damping measurement due to this mode were present.

ANOVA Testing Results

The accuracy of ANOVA testing was dependent on knowing all of the major factors affecting damping in the system. In order to determine whether air damping had an effect, other sources of variation had to be accounted for and negated. The Ishikawa

diagram below shows all of the major factors influencing the measured damping of the system. This diagram was used in order to design ANOVA experiments which would produce valid results. This diagram could not have been completed without the knowledge provided by previous work and the conclusions derived from all previous sections of this study.

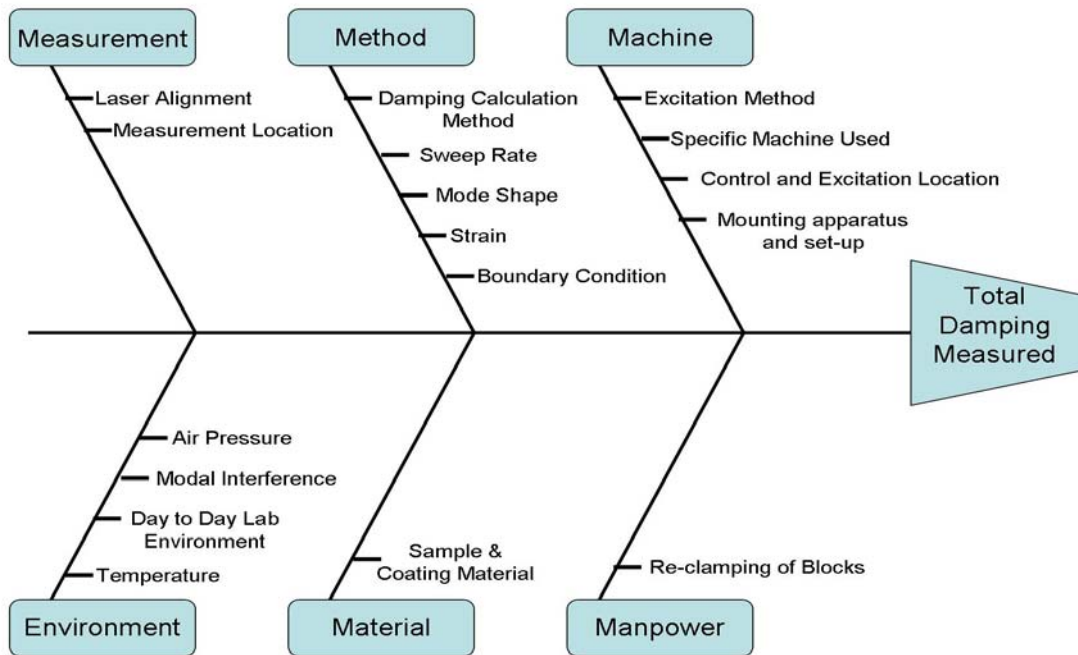


Figure 90. Ishikawa Diagram of Factors Affecting Damping

The factors used in this ANOVA experiment were mode shape, strain, and air pressure. Each replicate of the experiment was carried out in one day, and blocks were placed around each day of testing in order to negate the effect of day to day changes in the lab environment. The desired high and low settings for mode and air pressure were achievable for every run, but strain values were more problematic. Further details of the experimental design and statistical theory behind ANOVA are contained in Appendix A. Chapter III contains all design details for each ANOVA experiment in this section.

In ANOVA testing, the input g-level was adjusted before each run in an attempt to get the sample to oscillate at the desired strain level. Due to the nature of the set-up, it was not possible to hit this strain level precisely on each run. Therefore, strain values achieved within 8% of the value called for by the experiment were considered acceptable. Allowing small deviation in the strain values created more variation within strain treatments, and added to the overall noise of the system. Runs which produced strains outside this range were not used for ANOVA analysis, but still contained valid data. They are included in the conventional analysis of ANOVA data following this section.

The tables in Appendix E of this document show the results of runs which were used in the ANOVA analysis of the samples. In the tables presented, the percent error between the desired strains and strains achieved are shown. The 8% criterion was only exceeded when an extremely small and elusive strain value of 20 microstrain was required. The overall average error between desired and achieved strain values was only 3.76%.

The first ANOVA experiment was, perhaps, the most telling in its results. It tested the uncoated sample in order to determine the significance of air damping and its interactions with mode shape and strain level. This ANOVA experiment, and all others, were designed and analyzed using Stat-Ease Design Expert ® software, version 6.0.9.

The table below shows the resulting damping values for the first ANOVA experiment, along with the run order. The table also shows the three factors under consideration in the experiment, along with the letters assigned to those factors. Note the blocks used below are placed around full replicates in the experiment.

Table 36. Uncoated Sample ANOVA Design and Response

Std	Run	Block	Factor 1 A:mode	Factor 2 B:air pressure torr	Factor 3 C:strain microstrain	Response 1 Q value
13	1	Block 1	2nd Bend	5	500	261.91
22	2	Block 1	Two Stripe	741	500	578.49
16	3	Block 1	Two Stripe	5	500	795.45
4	4	Block 1	Two Stripe	5	150	822.51
10	5	Block 1	Two Stripe	741	150	496.36
1	6	Block 1	2nd Bend	5	150	464.07
7	7	Block 1	2nd Bend	741	150	454.91
19	8	Block 1	2nd Bend	741	500	234.03
11	9	Block 2	Two Stripe	741	150	639.3
8	10	Block 2	2nd Bend	741	150	481.98
20	11	Block 2	2nd Bend	741	500	243.53
17	12	Block 2	Two Stripe	5	500	783.01
14	13	Block 2	2nd Bend	5	500	267.66
5	14	Block 2	Two Stripe	5	150	802.48
23	15	Block 2	Two Stripe	741	500	568.33
2	16	Block 2	2nd Bend	5	150	455.52
15	17	Block 3	2nd Bend	5	500	290.87
18	18	Block 3	Two Stripe	5	500	815.23
9	19	Block 3	2nd Bend	741	150	438.83
24	20	Block 3	Two Stripe	741	500	571.56
6	21	Block 3	Two Stripe	5	150	783.02
12	22	Block 3	Two Stripe	741	150	537.19
21	23	Block 3	2nd Bend	741	500	262.59
3	24	Block 3	2nd Bend	5	150	501.78

Using these results, an ANOVA analysis was performed. This analysis began by determining which factors and interactions were significant by using a half normal plot. In this type of plot, the experimenter marks terms which lie off the best-fit line as significant. The terms which are apart from this best fit line have experimental contrasts which do not correspond to a normal distribution. Essentially, they are defying the odds and are, therefore, likely to be having an effect. The triangles represent unused degrees of freedom from the replicates. In the Design Expert ® software, pure error from the replicates is used to create these triangles and help guide the selection of significant factors.

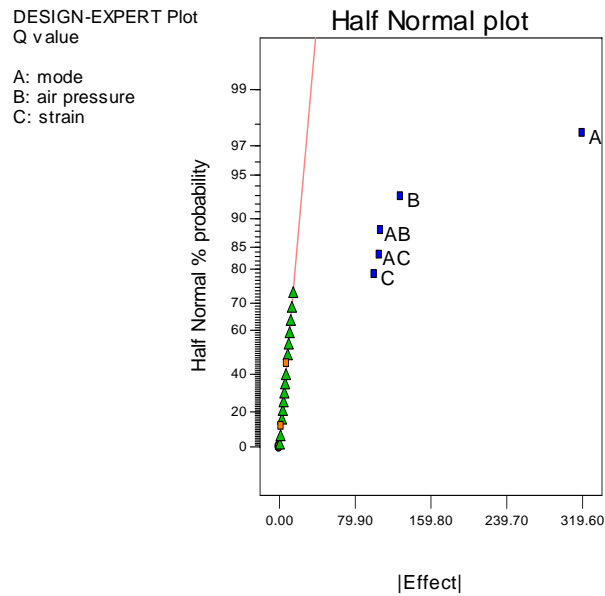


Figure 91. Uncoated Sample ANOVA Design and Response

In the half normal plot above, all of the factors and two interactions are significant. As expected, mode shape and strain (factors A and C, respectively), were determined to be significant. Strain's significance in damping of the uncoated sample was due to the strain dependence within the constraint blocks. Air pressure (factor B) was also determined to be significant in determining the damping of the sample. Interestingly, the interaction between mode shape and strain (interaction AC) and the interaction between mode shape and air pressure (interaction AB) were also significant. Interaction ABC, representing all three factors, and the interaction between air pressure and strain (interaction BC) were not found to be of sufficiently high significance.

The results of this ANOVA experiment are presented more fully in the ANOVA table below. The Design Expert ® software used the factors and interactions shown to be

significant in the half normal plot in the figure above, and computed the below table. This table was calculated using the equations and techniques shown in Appendix A.

Table 37. Uncoated Sample ANOVA Table

Response: Q value
 ANOVA for Selected Factorial Model
 Analysis of variance table [Partial sum of squares]

Source	Sum of Squares	DF	Mean Square	F Value	Prob > F	
Block	1181.231	2	590.6156167			
Model	907480.3	5	181496.0683	200.5924	< 0.0001	significant
A	545239.4	1	545239.4061	602.6075	< 0.0001	
B	98356.49	1	98356.487	108.7052	< 0.0001	
C	60530.17	1	60530.166	66.89893	< 0.0001	
AB	68750.72	1	68750.7217	75.98443	< 0.0001	
AC	66962.03	1	66962.02684	74.00753	< 0.0001	
Residual	14476.8	16	904.8001818			
Cor Total	923138.4	23				

The Model F-value of 200.59 implies the model is significant. There is only a 0.01% chance that a "Model F-Value" this large could occur due to noise.

Std. Dev. 30.0799 Adj R-Squared 0.979391

Statistical significance is a tool to show, with a large degree of certainty, whether or not a certain factor was affecting a system. In all of the ANOVA tables shown, the “Prob > F” column is the probability of obtaining the F value shown if the null hypothesis were true. Recalling that the null hypothesis states that all factors are insignificant, this column represents the probability of an insignificant factor causing the responses found. Thus, if the “Prob > F” is 0.0001, there is a 99.99% chance that factor was significant. The smaller the decimal, the greater the certainty that factor was

significant. The threshold for factor significance in this study, in the software, and in general practice is 95% (or “Prob > F” less than or equal to 0.05).

This table confirms that all of the factors chosen in the half normal plot were, in fact, significant in determining the damping response. The adjusted R-squared value of 0.979391 is very close to 1, also testifying to the adequacy of the model for this system. The “Prob > F” value is, essentially, an α value for each factor in the table above. Note that for each and every one of the factors and interactions included in the ANOVA table, this α indicated a greater than 99.99% chance they were influencing the results.

The final step in verifying the results of this experiment was to look at the diagnostic plots. These plots were used to determine whether the experiment was performed properly, and whether there were any trends in the data which may indicate a problem. The first of these plots is the normal plot of residuals, which appears roughly linear for valid experiments. The plot below shows that the residuals are normally distributed. That is, the residuals of the response from the experiment lie roughly along a line which indicates a normal distribution.

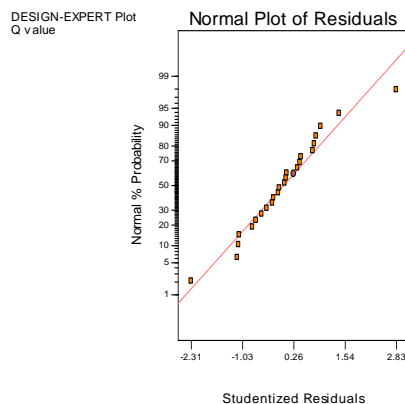


Figure 92. Uncoated Sample Normal Plot of Residuals

Two more diagnostic plots are shown below. In each of these plots, the desired effect is a random distribution of that data points. In the residuals versus run plot, no time trend is present in the data. The residuals versus predicted plot also shows the desired random distribution, which indicates the data was taken properly.

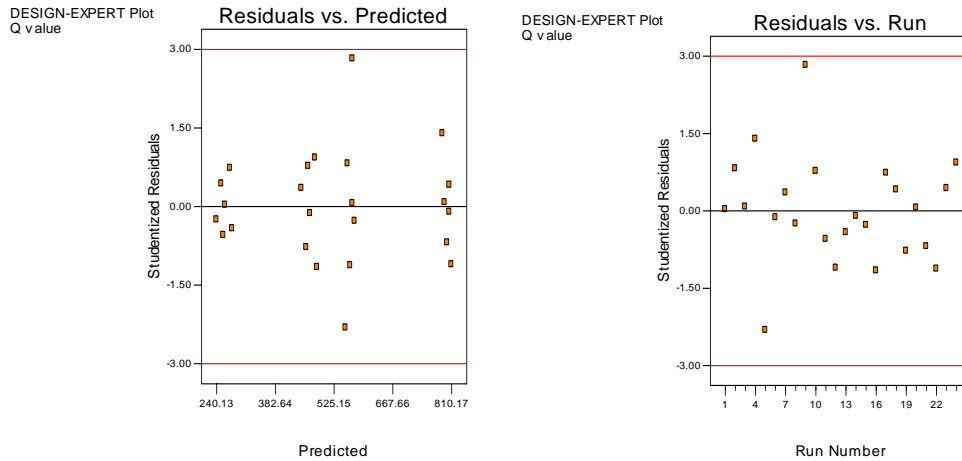


Figure 93. Uncoated Sample Residuals vs. Predicted and Residuals vs. Run

Following the tests above using the uncoated sample, the coated sample was used in an identical experiment. The only difference between the two experimental designs was the randomized run order. The table below shows the experimental design and resulting damping values for these tests.

Table 38. Coated Sample ANOVA Design and Response

Std	Run	Block	Factor 1 A:mode	Factor 2 B:air pressure torr	Factor 3 C:strain microstrain	Response 1 Q value
10	1	Block 1	two stripe	741	150	199.45
19	2	Block 1	2nd bend	741	500	125.84
16	3	Block 1	two stripe	5	500	161.36
7	4	Block 1	2nd bend	741	150	187.75
4	5	Block 1	two stripe	5	150	390.58
13	6	Block 1	2nd bend	5	500	146.78
1	7	Block 1	2nd bend	5	150	258.45
22	8	Block 1	two stripe	741	500	197.2
17	9	Block 2	two stripe	5	500	143.56
8	10	Block 2	2nd bend	741	150	235.86
11	11	Block 2	two stripe	741	150	284.19
14	12	Block 2	2nd bend	5	500	127.89
5	13	Block 2	two stripe	5	150	346.57
2	14	Block 2	2nd bend	5	150	259.64
20	15	Block 2	2nd bend	741	500	187.87
23	16	Block 2	two stripe	741	500	157.75
24	17	Block 3	two stripe	741	500	142.73
21	18	Block 3	2nd bend	741	500	122.89
3	19	Block 3	2nd bend	5	150	204.81
18	20	Block 3	two stripe	5	500	163.22
9	21	Block 3	2nd bend	741	150	188.97
15	22	Block 3	2nd bend	5	500	151.68
6	23	Block 3	two stripe	5	150	298.6
12	24	Block 3	two stripe	741	150	280.03

These results were used to develop a half normal plot. This plot shows that all three factors were once again significant. The interaction between air pressure and strain (interaction BC) and the interaction between mode shape and strain (interaction AC) were both deemed significant as well. While interaction AB was significant for the uncoated sample, it was not determined significant in this case. Additionally, interaction BC was not significant for the uncoated experiment, but proved significant in this experiment.

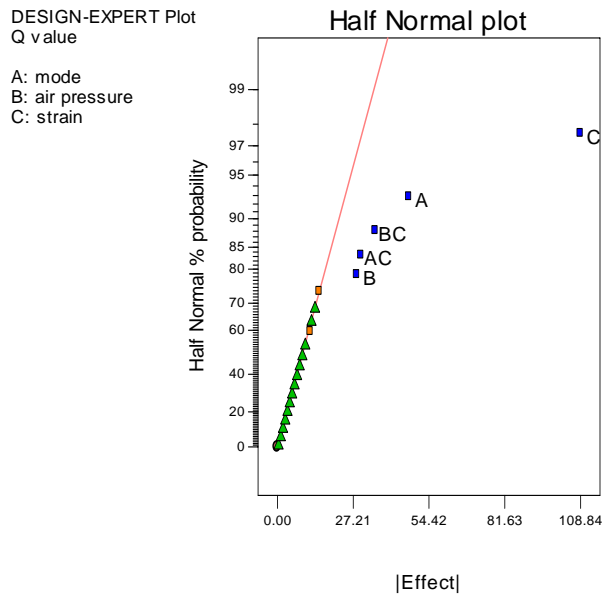


Figure 94. Coated Sample Half Normal Plot

The ANOVA table below shows that the factors and interactions chosen in the half normal plot were significant. The “Prob>F” column contains values which are higher than there were in the case of the coated sample, though still sufficiently small to maintain at least 95% significance for all factors chosen. Additionally, the adjusted R-squared value is lower than it was for testing on the uncoated sample. The data for the coated sample contains more noise. ANOVA assumes a linear behavior in the factors, and the nonlinearities introduced into the system by the sample coating introduce nonlinear behavior. The analysis is able to cope with this behavior, but it manifests itself in data which contains more noise.

Table 39. Coated Sample ANOVA Table

Response: Q value

ANOVA for Selected Factorial Model

Analysis of variance table [Partial sum of squares]

Source	Sum of Squares	DF	Mean Square	F Value	Prob > F	
Block	2296.737	2	1148.368267			
Model	102218.6	5	20443.72255	19.23546	< 0.0001	significant
A	13386.4	1	13386.399	12.59524	0.0027	
B	4890.901	1	4890.900504	4.60184	0.0476	
C	71082.32	1	71082.3157	66.88123	< 0.0001	
AC	5432.148	1	5432.147704	5.111099	0.0381	
BC	7426.85	1	7426.849838	6.98791	0.0177	
Residual	17005.03	16	1062.814126			
Cor Total	121520.4	23				

The Model F-value of 19.24 implies the model is significant. There is only a 0.01% chance that a "Model F-Value" this large could occur due to noise.

Std. Dev. 32.60083 Adj R-Squared 0.812796

The diagnostic plots below attest to the validity of the data used in this model.

The normal plots of residuals shows that the residuals were normally distributed. Both the residuals versus run and the residuals versus predicted plots show randomly distributed data, discounting the presence of any time trend or measurement error.

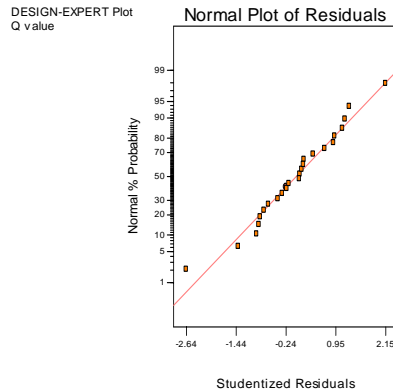


Figure 95. Coated Sample Normal Plot of Residuals

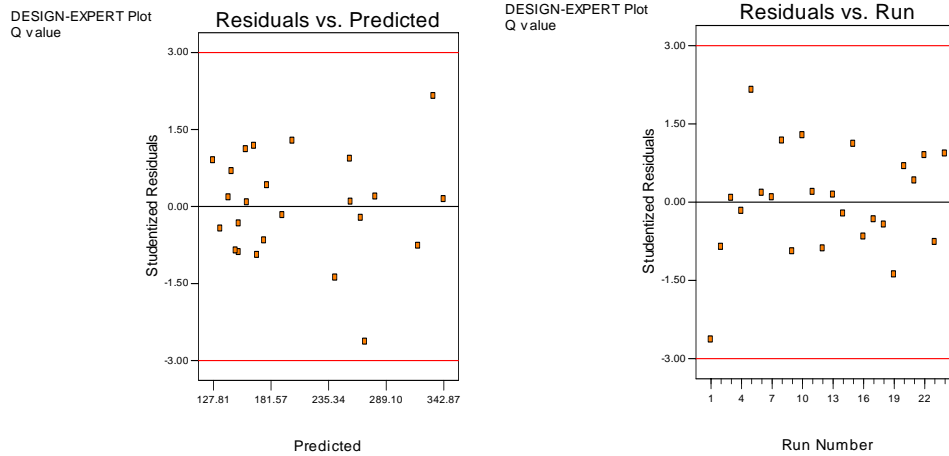


Figure 96. Coated Sample Residuals vs. Predicted and Residuals vs. Run

Additional ANOVA experiments were run on the coated sample as well. These experiments were designed to better understand how damping affected each of the modes both individually, and at different strain levels. The interaction between mode shape and air pressure was clearly significant in the uncoated sample, but not important for the coated sample. Testing for the significance of air pressure at individual mode shapes was implemented to verify whether mode 3 or 4 had an impact on the significance of air damping. Because the interaction between air pressure and strain was found to be significant for this sample, the strain levels used were changed in order to further investigate this effect.

The first of these additional experiments investigated mode 4 at the same strain and pressure settings used in the previous experiment. The 2^2 experimental design is shown below along with the responses that were found.

Figure 97. Coated Sample Mode 4 Experiment Design and Response

Std	Run	Block	Factor 1 A:pressure torr	Factor 2 B:strain microstrain	Response 1 Response 1 Q Value
10	1	Block 1	741	500	132.157
11	2	Block 1	741	500	143.57
4	3	Block 1	741	150	217.03
5	4	Block 1	741	150	227.46
1	5	Block 1	5	150	258.28
2	6	Block 1	5	150	274.05
6	7	Block 1	741	150	214.1
12	8	Block 1	741	500	173.13
3	9	Block 1	5	150	251.36
9	10	Block 1	5	500	164.18
7	11	Block 1	5	500	159.2
8	12	Block 1	5	500	161.59

These results were used to develop a half normal plot. In this experiment, both strain, and air pressure were found to be significant. The interaction between strain and air pressure, however, was not. Selection of the interaction as a significant factor is plausible given the layout of the half normal plot. However, the F value determined via ANOVA for the interaction indicates it is not significant.

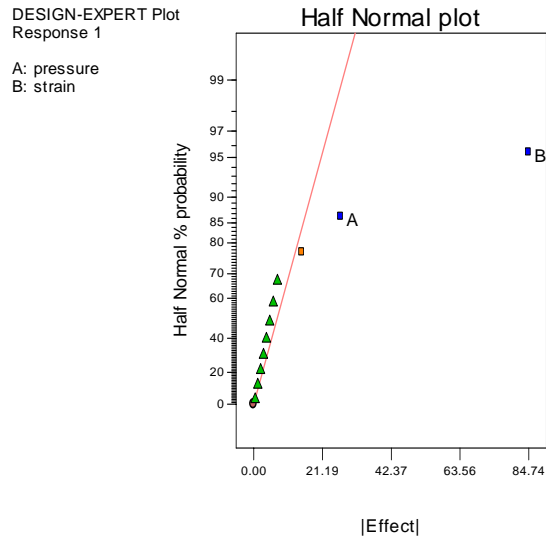


Figure 98. Coated Sample Mode 4 Experiment Half Normal Plot

The results from this half normal plot lead to the formation of the ANOVA table below. This table shows the insignificant interaction (interaction AB) in the “lack of fit” category, as discussed in Appendix A’s explanation of ANOVA. This table supports the conclusions of the large ANOVA experiment for the coated sample, which also indicated that the interaction between air pressure and strain was insignificant.

Table 40. Coated Sample Mode 4 Experiment ANOVA Table

Response: Q value
ANOVA for Selected Factorial Model
Analysis of variance table [Partial sum of squares]

Source	Sum of Squares	DF	Mean Square	F Value	Prob > F	
Model	23709.51	2	11854.75352	55.11936	< 0.0001	significant
A	2165.803	1	2165.802614	10.07002	0.0113	
B	21543.7	1	21543.70443	100.1687	< 0.0001	
Residual	1935.668	9	215.0742163			
Lack of Fit	659.8905	1	659.8905141	4.137966	0.0764	not significant
Pure Error	1275.777	8	159.4721791			
Cor Total	25645.17	11				

The Model F-value of 55.12 implies the model is significant. There is only a 0.01% chance that a "Model F-Value" this large could occur due to noise.

Std. Dev. 14.66541 Adj R-Squared 0.907748

The results of this experiment were examined in the diagnostic plots below. In the normal plot of residuals, the normal distribution of the data appeared to be questionable. Therefore, an analysis was performed within the Design Expert program to determine whether a transform of the data was required. It was determined that the data was satisfactory in linear form and required no transform. However, the results of this small ANOVA test were still considered uncertain. The residuals versus predicted plot

also shows that the predicted value was linked to the residuals found. As such, this ANOVA experiment was not used in the formation of conclusions regarding air pressure and damping.

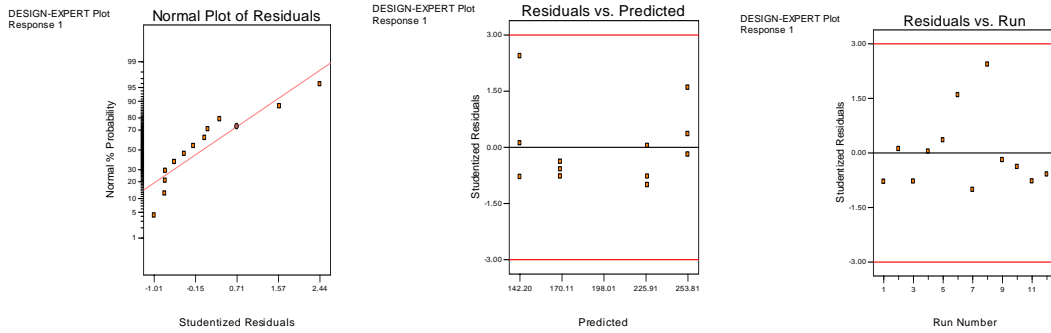


Figure 99. Coated Sample Mode 4 Experiment Diagnostic Plots

The next additional ANOVA experiment was again performed at mode 4 of the coated sample. The experiment was identical to the experiment just described, except that the strain levels used were changed in order to better understand how the sample performed at different strain levels. The design and responses found are shown below.

Table 41. Coated Sample Mode 4 Experiment (New Strain Levels) Design and Response

Std	Run	Block	Factor 1 A:pressure torr	Factor 2 B:strain microstrain	Response 1 Response 1 Q value
10	1	Block 1	741	325	190.61
12	2	Block 1	741	325	192.82
9	3	Block 1	5	325	255.91
8	4	Block 1	5	325	225.26
3	5	Block 1	5	20	589.45
1	6	Block 1	5	20	599.88
7	7	Block 1	5	325	250.86
5	8	Block 1	741	20	432.28
6	9	Block 1	741	20	437.18
2	10	Block 1	5	20	653.91
4	11	Block 1	741	20	581
11	12	Block 1	741	325	188.41

These responses and the experimental design were again used to develop a half normal plot. This plot shows that both air pressure and strain were once again significant, while the interaction between the two was once again insignificant. This is fully consistent with the other ANOVA experiment for mode 4, but not large ANOVA experiment for the coated sample.

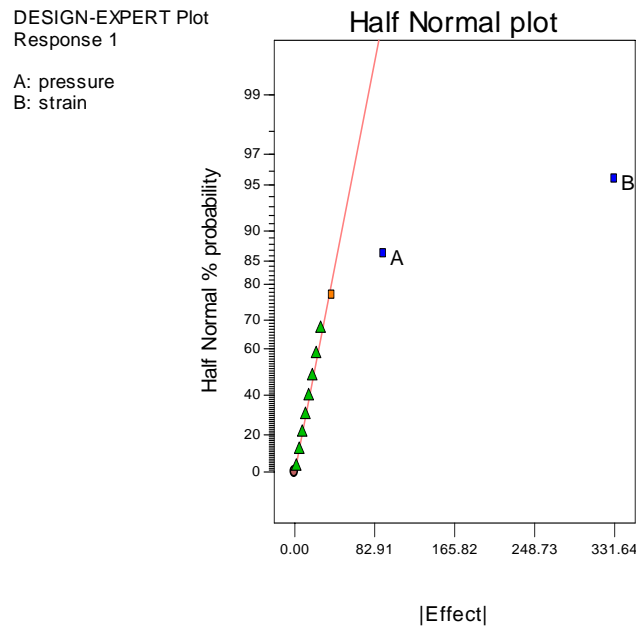


Figure 100. Coated Sample Mode 4 Experiment (New Strain Levels) Half Normal Plot

The ANOVA table below confirms that air pressure and strain were significant. It also shows that the interaction was once again relegated to the “lack of fit,” where it was included in the experimental error. The adjusted R-squared value of 0.93 shows that the model accounted for nearly all variation within the data. The high R-squared values seen throughout ANOVA testing are a testament to ability of the experiment to isolate sources of damping, and apply them to a statistical model.

Table 42. Coated Sample Mode 4 Experiment (New Strain Levels) ANOVA Table

Response: Q value

ANOVA for Selected Factorial Model

Analysis of variance table [Partial sum of squares]

Source	Sum of Squares	DF	Mean Square	F Value	Prob > F	
Model	355433.3	2	177716.6354	73.61357	< 0.0001	significant
A	25481.32	1	25481.31841	10.55484	0.0100	
B	329952	1	329951.9524	136.6723	< 0.0001	
Residual	21727.65	9	2414.183053			
Lack of Fit	4508.176	1	4508.175675	2.094455	0.1859	not significant
Pure Error	17219.47	8	2152.433975			
Cor Total	377160.9	11				

The Model F-value of 73.61 implies the model is significant. There is only a 0.01% chance that a "Model F-Value" this large could occur due to noise.

Std. Dev. 49.13434 Adj R-Squared 0.92959

The diagnostic plots below illustrate that there were problems with this experiment. The residuals appear to have a normal distribution, but the other two plots do not show the desired random distribution of data. In both of these plots, the “megaphone effect” is present, where values on the right side of the plot have a wider distribution. As such, the results of this small ANOVA experiment were also considered uncertain. Results from this small experiment were also not considered when drawing conclusions.

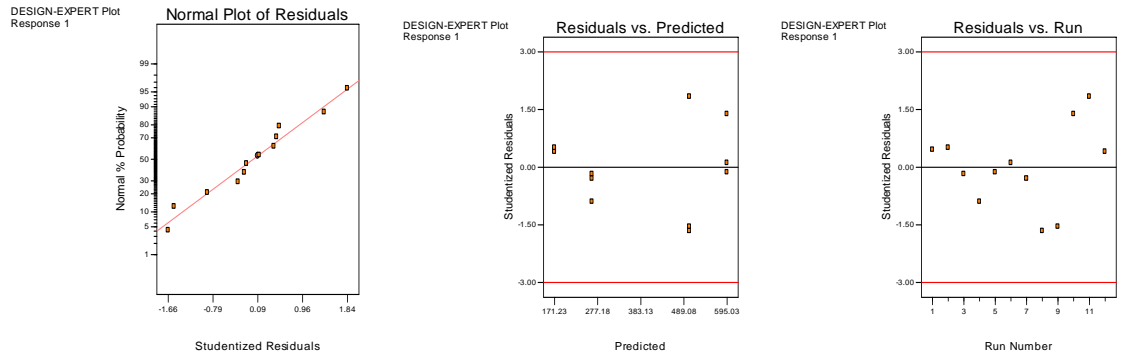


Figure 101. Coated Sample Mode 4 Experiment (New Strain Levels) Diagnostic Plots

The final ANOVA experiment was performed at mode 3 of the coated sample. This experiment also used the new high and low settings for strain. The high and low strain level settings were the same as those used in the experiment immediately above. In fact, this experiment design was identical to the one given above except it was carried out for mode 3. The experiment design used served the dual purpose of testing how mode 3 alone responded to air pressure, while also testing how mode 3 responded to different strain levels than were used in the large ANOVA experiment. The design and response to this experiment are shown below.

Table 43. Coated Sample Mode 3 Experiment (New Strain Levels) Design and Response

Std	Run	Block	Factor 1 A:pressure torr	Factor 2 B:strain microstrain	Response 1 Q value
8	1	Block 1	5	325	182.83
12	2	Block 1	741	325	139.43
1	3	Block 1	5	20	347.48
5	4	Block 1	741	20	358.41
7	5	Block 1	5	325	171.02
3	6	Block 1	5	20	330.76
10	7	Block 1	741	325	145.17
2	8	Block 1	5	20	324.11
11	9	Block 1	741	325	155.72
4	10	Block 1	741	20	334.88
6	11	Block 1	741	20	345
9	12	Block 1	5	325	162.52

This design, as all those which came before, was used to create a half-normal plot. From this plot, strain (factor B) and the interaction between air pressure and strain (interaction AB) were determined to be significant. Air pressure alone (factor A), sat along the line indicating a normal distribution and, consequently, non-significance. It was only selected as a factor in order to support model hierarchy. That is, because the interaction including factor A was significant, the main effect A had to be included in the ANOVA model. The half normal plot below shows both factors and their interaction selected.

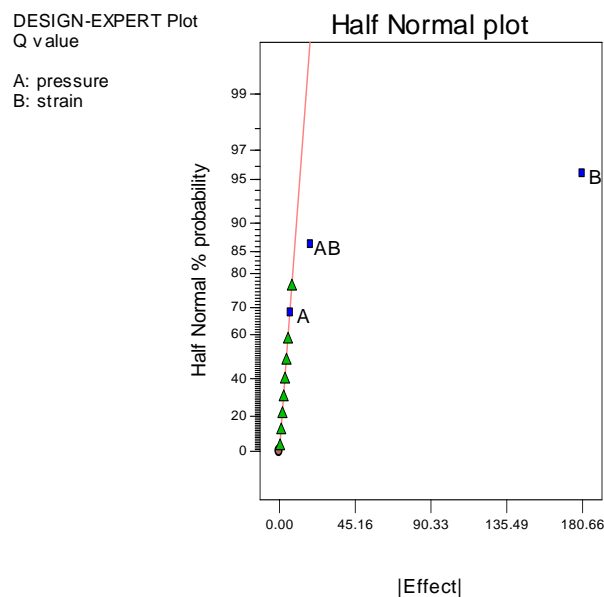


Figure 102. Coated Sample Mode 3 Experiment (New Strain Levels) Half Normal Plot

The ANOVA table below shows that factor A was statistically insignificant. Though main effects usually dominate in the arena of significance, it is not unheard of for an interaction to be significant while a main effect is not. The result below is perhaps the

most interesting in this section, because it shows that air pressure was not a significant factor for mode 3 of the coated sample at the strain levels used.

Table 44. Coated Sample Mode 3 Experiment (New Strain Levels) ANOVA Table

Response: Q value

Hierarchical Terms Added after Manual Regression

A

ANOVA for Selected Factorial Model

Analysis of variance table [Partial sum of squares]

Source	Sum of Squares	DF	Mean Square	F Value	Prob > F	
Model	99091.51	3	33030.50485	289.3523	< 0.0001	significant
A	134.0677	1	134.067675	1.174454	0.3101	
B	97912.3	1	97912.30021	857.7269	< 0.0001	
AB	1045.147	1	1045.146675	9.155647	0.0164	
Pure Error	913.2259	8	114.1532333			
Cor Total	100004.7	11				

The Model F-value of 289.35 implies the model is significant. There is only a 0.01% chance that a "Model F-Value" this large could occur due to noise.

Std. Dev. 10.68425 Adj R-Squared 0.987444

Finally, the validity of the data used was inspected via the use of the diagnostic plots. In the plot of residuals versus predicted values, the center of the plot was empty. This is the case because, due to the nature of the design, none of the Q values fell into the middle range of values. None of the plots below displayed irregularities which aroused the concern of the experimenter.

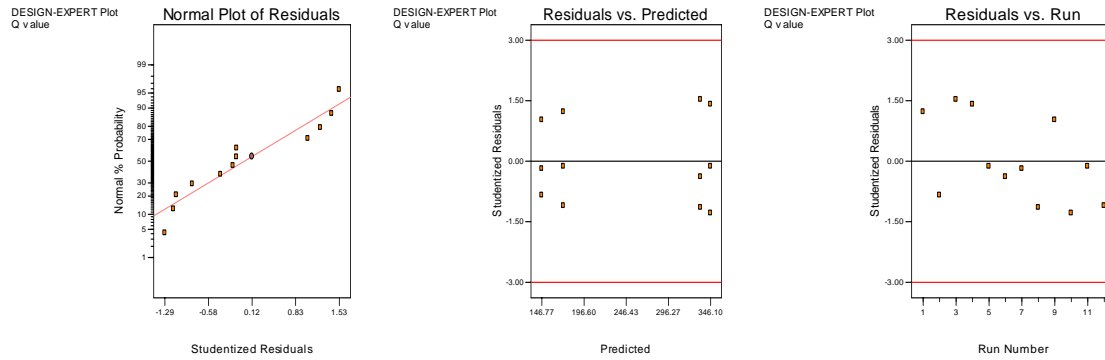


Figure 103. Coated Sample Mode 3 Experiment (New Strain Levels) Diagnostic Plots

This section of testing showed, via a detailed statistical analysis, that air pressure had an effect on the damping of a cantilevered sample. In the uncoated sample, this pressure also had an effect through interactions with mode shape. In the coated sample, air pressure was again significant, and had an effect through its interaction with strain level. An additional experiment at the coated sample's 3rd mode showed that air pressure was insignificant at this mode, while the interaction between strain and air pressure was significant. Significance, in this study, meant that there was at least a 95% certainty the factor or interaction was having an effect on the system.

Because of the high threshold for certainty, some factors may have an effect, but not be included in the results as significant. The reasoning for this ties into the Appendix A explanation of ANOVA, where experimenters do not desire to metaphorically imprison the innocent by rejecting a potentially valid null hypothesis. Strong conclusions regarding the behavior of this system, and the effects of air pressure on damping, can be drawn from tests that are backed up by a strict system of significance. However, the results will have more meaning, and can be more easily interpreted, if they are also

analyzed in a conventional manner. This allows for a strong marriage of statistical certainties and trends spotted through observation.

Conventional Analysis of ANOVA Testing Results

The plots presented in this section show the data derived from ANOVA testing. All data collected during that testing is included in these plots, including data for runs with strain values which were unusable for analysis in the previous section. The plots provide insight into the behavior of the samples both in a vacuum and at atmospheric pressure. The plots allow the reader and the experimenter to draw conclusions about the results, while the previous ANOVA analysis provides a backbone for those conclusions. This is the strength of ANOVA testing- it allows concrete conclusions to be drawn through the interpretation of experimental data.

The first plot shown is for the uncoated sample in its 3rd mode. The plot shows strong strain dependence in damping. As strain increased, damping also increased (*i.e.* Q value decreased). This was consistent with previous the previous conclusion that there existed a strain dependence within the constraint blocks, as a bare sample should not have displayed strain dependence in damping. More to the point, the plot shows that damping levels for the sample at both near-vacuum and atmospheric pressure were roughly the same.

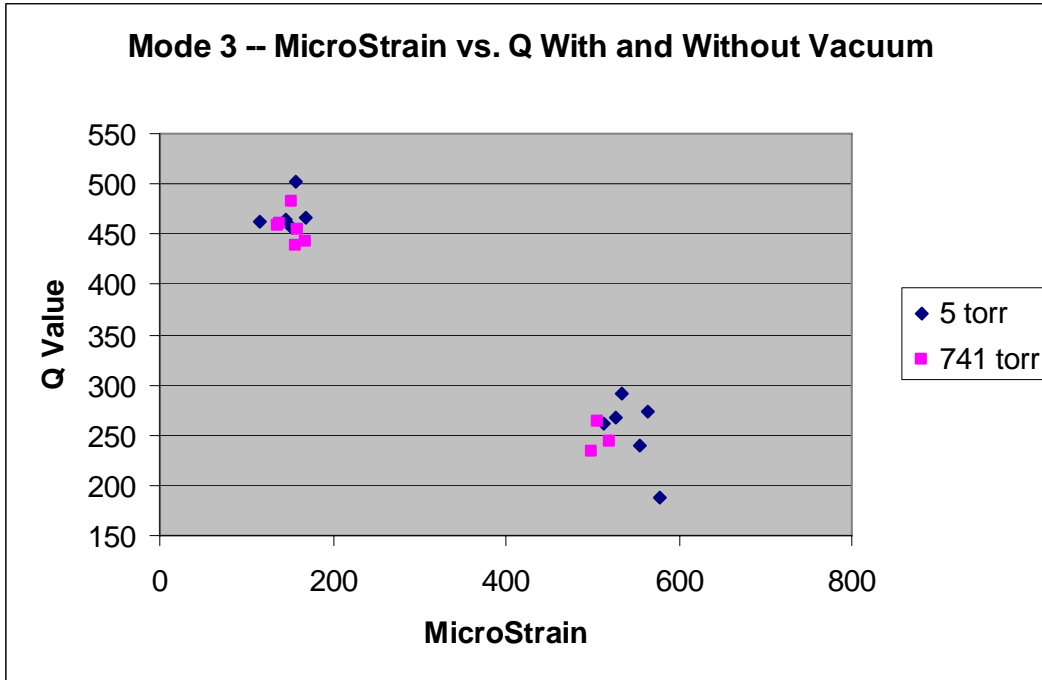


Figure 104. Uncoated Sample Mode 3 Damping at two Pressure Levels

The second plot, below, represents the 4th mode of the uncoated sample. It shows a far lesser strain dependence. This makes sense, since the constraint blocks did not have to “work” as hard to hold a sample oscillating such that the maximum displacement is at the tip. The sample was therefore less dependent on constraint block performance for this mode. This plot also showed a clear change in Q value due to air pressure. At near-vacuum levels, Q value was increased by an average of 30.8% over atmospheric pressure tests.

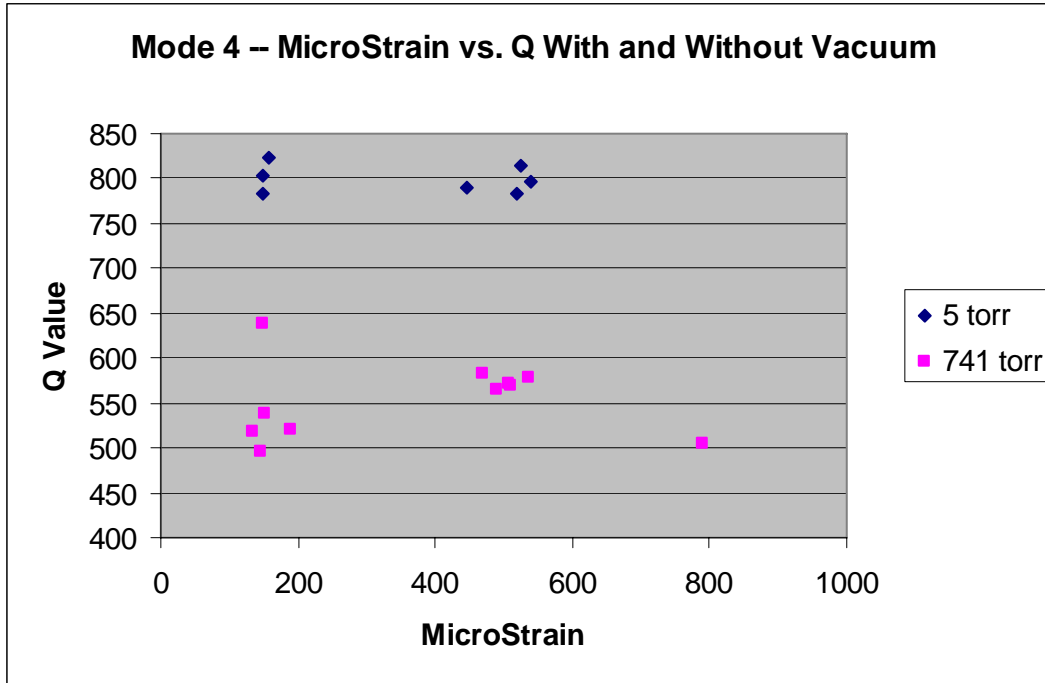


Figure 105. Uncoated Sample Mode 4 Damping at two Pressure Levels

Between the two uncoated plots, the interactions confirmed by ANOVA have been discussed. ANOVA shows that there are significant interactions between mode and air pressure, as well as between mode and strain. The mode-pressure interaction came about because pressure had a large impact on mode 4, but was shown to have virtually no impact on mode 3. The significance of the mode-strain interaction was highlighted by the plots above, which show a strain dependence in mode 3 that was all but absent in mode 4. It was also true that the same strain level at different modes produced very different Q values.

The plots for the coated samples contain about 40 more data points than the uncoated sample plots. This is because these plots contain all the data for the 4 different ANOVA tests performed on the coated sample. The coated sample displayed more

complicated behavior than the uncoated sample, and more tests were required to draw conclusions about its behavior. Even though the results from additional small ANOVA experiments were questionable, the data itself was perfectly valid for conventional plots.

The next plot shows the damping versus strain values for mode 3 of the coated sample. In this plot, it can be seen there was once again no clear difference in damping between runs at near vacuum and atmospheric pressure. As expected, damping in the coated sample was higher than for the uncoated sample. This was certainly due to the damping characteristics of the mag spinel coating. Strain dependence in both the coating and constraint blocks no doubt contributed to the strain dependence in damping seen below.

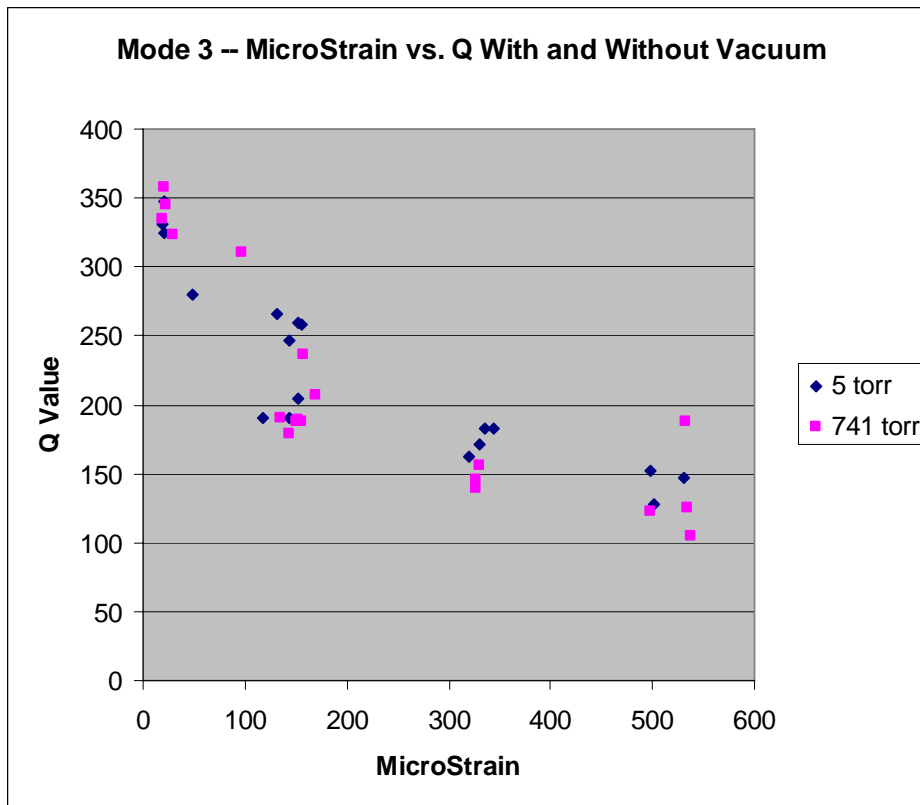


Figure 106. Coated Sample Mode 3 Damping at two Pressure Levels

Finally, the next plot shows the 4th mode for the coated sample. Through the use of multiple data points, this plot shows that runs at near vacuum yielded lower damping. Unlike in the uncoated sample, a strain dependence in damping was also observable in this mode. In the plot, it appears as though the effect of pressure on damping may have been strain dependent. At lower strain levels, it appears as though there was a larger margin between runs at the two different air pressures. As strain increased, the margin between the two sets of runs dissipated.

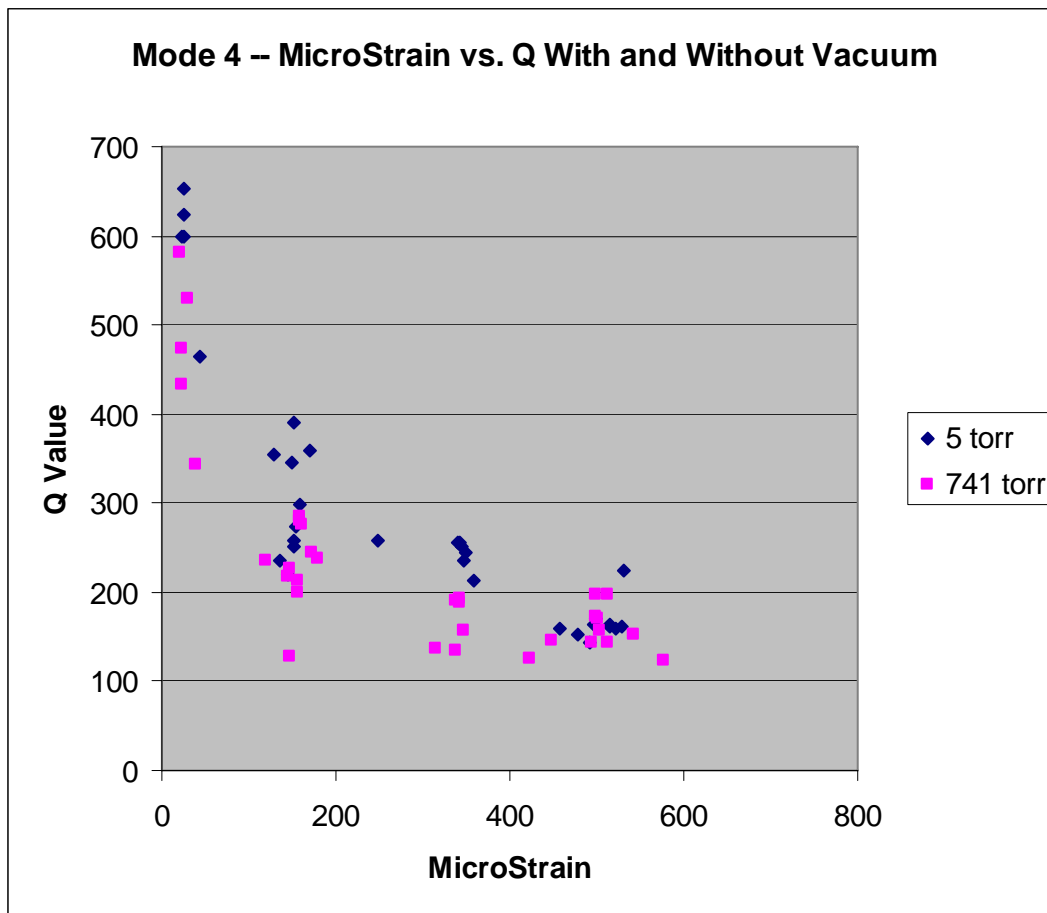


Figure 107. Coated Sample Mode 4 Damping at two Pressure Levels

The interactions and significant factors illustrated by ANOVA for the coated sample are present in the conventional plots above. Obviously, air pressure, strain level, and mode shape all have an impact. ANOVA confirms that the mode-strain interaction has an effect as well, though this effect is also intuitive given the nature of the system. For different combinations of mode and strain in a strain dependent specimen clamped into strain dependent blocks, it makes sense that the damping will change. The air pressure-strain interaction was less obvious. In looking it at mode 4 plot, this effect looked probable. ANOVA, however, confirmed that this effect was present in the large experiment. The air damping-mode interaction was not shown to be significant in the large ANOVA experiment for the coated sample, but that does not preclude the possibility. The ANOVA experiment targeting the 3rd mode showed that air pressure was not significant in that case, which is reflected in the plot above. It also implied that the effect of air pressure was mode dependent with the coated sample as well.

The plots in this section for the uncoated sample are fully consistent with the results found by Allen in his experimentation. The data from his study also indicated the presence of air damping in mode 4, while data for air damping in mode 3 was more difficult to interpret. In Allen's study, it was not necessary to strictly control the strain levels seen by the sample. Further, data for multiple tests at the same high and low levels for air pressure was not taken, since his study focused on a full range of air pressures. As such, the data contains a large amount of statistical noise and ANOVA could not be applied to it after the fact.

Appendix B uses data on the peak frequencies from each run to show general frequency trends in the results. These trends are organized by mode, of course, and

sample. The plots in Appendix B show how pressure affected the peak frequencies for each mode and sample.

Plots in Appendix C show data from the coated and uncoated samples plotted together. These plots highlight the difference in performance between the two samples, illustrating the overall greater damping of the coated sample and how the samples reacted differently to air pressure.

Plots in Appendix D show a few of the frequency response functions found in air pressure testing. Response curves at each mode and air pressure are shown for the coated and uncoated samples. The response curves illustrate the raw results, and allow the reader to see how exactly air pressure influenced the measured response of the system.

Finally, overall conclusions regarding ANOVA testing are reserved for Chapter V, since ANOVA testing on air pressure and its interactions represents the primary focus of this study. These conclusions are presented along with relevant conclusions regarding other factors found to influence damping.

Air Horn Testing of Free-Free-Free-Free Condition Results

Testing performed with the free condition set-up provided an alternative means for determining the damping in coated and uncoated Ti-6Al-4V plates. Through the use of the set-up described in Chapter III, the experimenter was able to determine damping levels for the plates over a range of strains between 0.1 and 2.2 microstrain, with displacements less than 1000 nm. These strain values equate to small displacements in the samples, making direct comparison to the samples used in the constraint blocks impossible. Larger strain value could not be achieved due to limitations in the equipment.

The air horn could only be placed so close to the sample before the sample's oscillations would cause it to impact the horn and ruin the results. Further, the volume of the air horn could only be increased until the signal from the controlling computer was clipped.

The mode shapes displayed by the free-free plates were of the same size and shape as those on the cantilevered samples. The results of testing in this set-up sidestepped many of the factors which lead to excess damping in the cantilevered set-up. Given the similarities in the samples and the more efficient boundary condition, this testing provided new insight into the performance of the mag spinel coating. The higher Q values afforded by this set-up allow for better calculations of the damping contributed by the coating.

Damping Evaluation Testing Results

The first step in the evaluation of damping in these samples was to insure that rigid body motion was not occurring. Rigid body motion in the samples would interfere with the displacement caused by the air horn excitation, and thus make accurate measurements of data impossible. The half-bandwidth method of damping measurement used requires a resonant peak, and the presence of rigid body oscillation would cause erroneous measurements that would distort the shape of the peak.

Checking for rigid body motion in the samples was an easy process. When mode shape verification was performed on each of the samples, the chirps used in excitation swept a range from 0 to 2500 Hz for the coated sample and 0 to 4000 Hz for the uncoated sample. The frequency response plots produced showed all resonant peaks across this range for each sample, as well as the large irregularity caused by rigid body motion in the

plate. In both cases, this irregularity occurred at the beginning of the frequency scale and dropped off exponentially as frequency increased. The irregularity was present at a frequency of 0 Hz, and pervaded through the first two modes in both the coated and uncoated sample. Because it began at 0 Hz and continued through two mode shapes (which were experimentally verified), it was determined that this irregularity must have been a rigid body effect.

Because the modes of interest were 4th and 7th in line, the effect of rigid body motion dissipated before these resonant peaks were reached. The figures below show the response plots from the scans of each sample, the modes of interest, and the rigid body effect. In these plots, velocity is plotted in dB versus frequency.

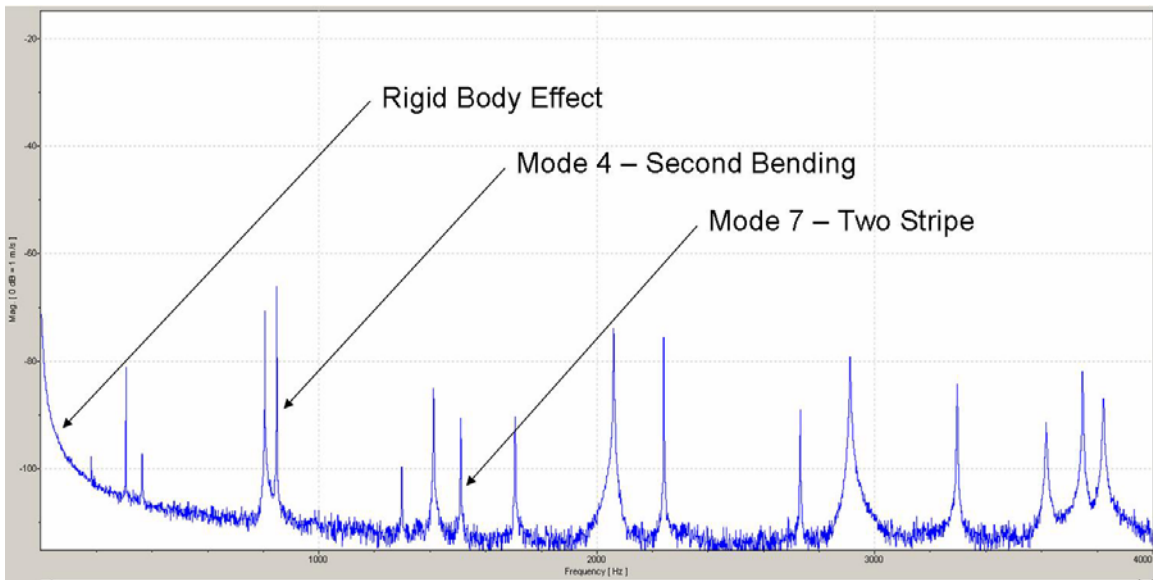


Figure 108. Rigid Body Effect in Uncoated Free Condition Sample

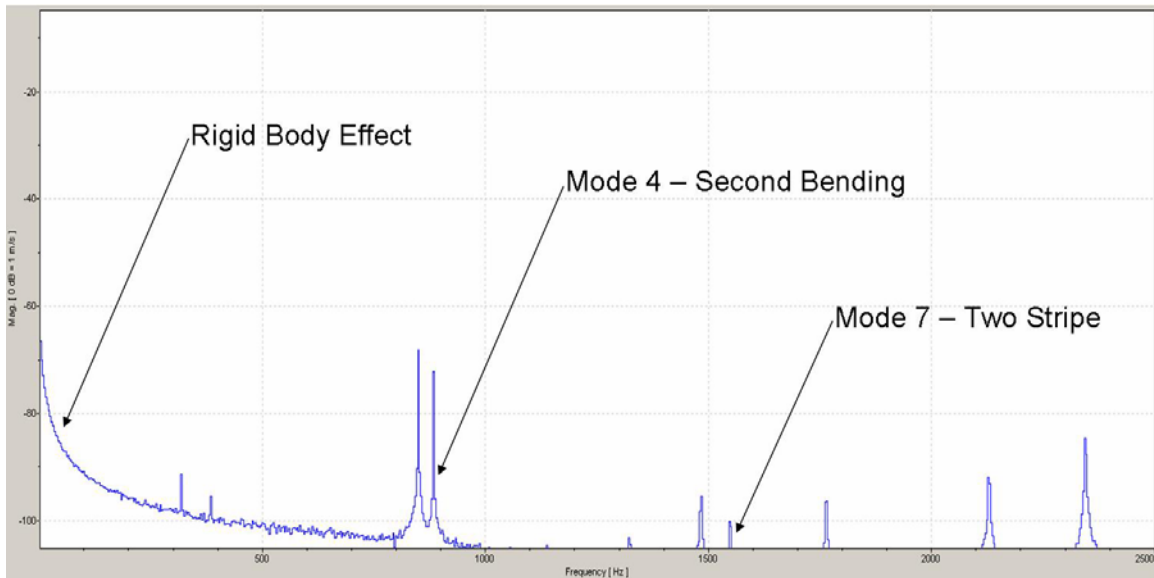


Figure 109. Rigid Body Effect in Coated Free Condition Sample

The next step was to test the means for determining damping. As already stated, damping was found using the half-bandwidth method. This method requires good resolution in recording the resonant peaks, otherwise it will result in inaccurate calculations. The resolution used in this study ranged from 20 mHz to 40 mHz, and was always the best allowed by the software used. The bandwidth used was as small as possible while still encompassing the resonant peak in question, be it for mode 4 or mode 7. Complete details on the set-up are provided in Chapter III.

The figure below shows one of the resonant peaks from an experimental run in this testing. It is the 7th mode of the uncoated sample, and was captured at a resolution of 40 mHz. The markers along the line represent data points derived from 5 averages at each of 4 symmetric measurement points. The data collection software was used to interpolate in between these points and generate a smooth curve. Curves for each

experimental run, like the one presented here, were used to calculate the damping data for this testing.

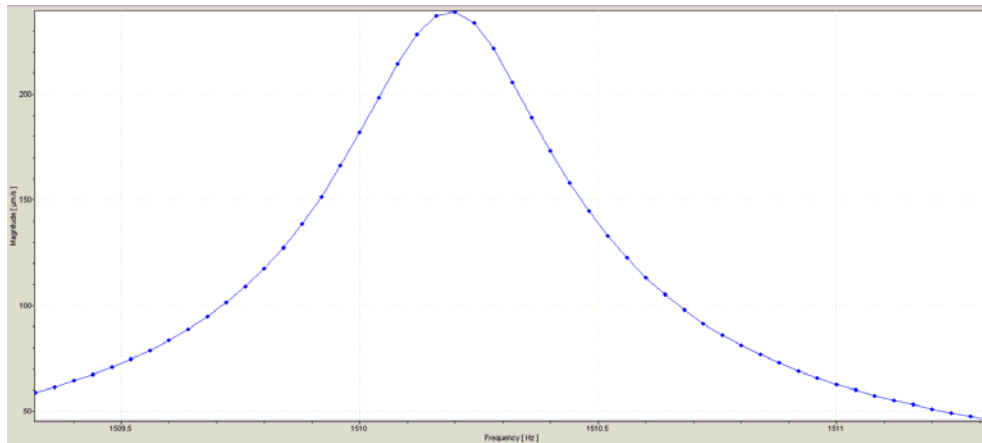


Figure 110. Example Experimental Result for Uncoated Sample, Mode 7

Free condition testing of plates produced Q values much higher than those seen using the cantilevered testing. Although the displacements achieved were very small, the results are promising. In the plot below, the damping performance of the two samples was compared for mode 4. In this second bending mode, the coated sample displayed significant damping, with an average reduction in Q value of 78.7%.

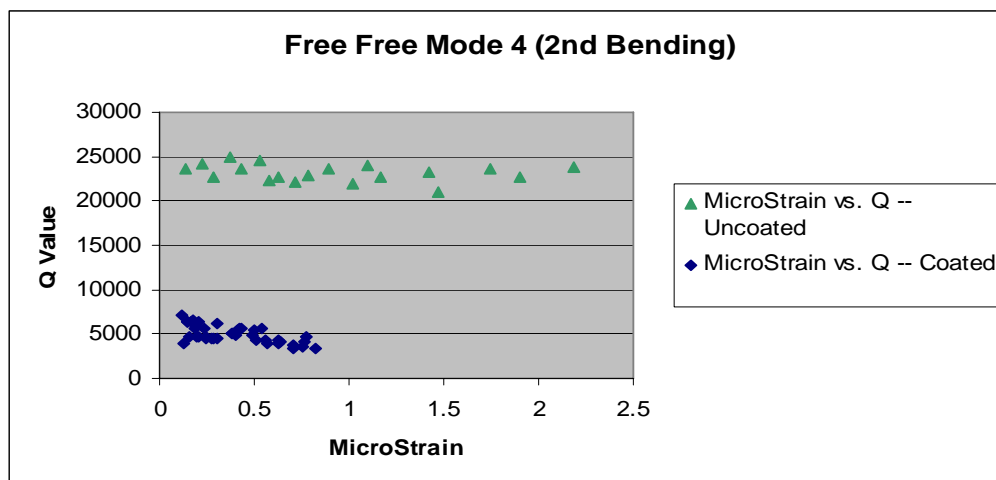


Figure 111. Free Condition Damping Results, Mode 4

The next plot shows the results of free condition testing in Mode 7. In this mode, the reduction in Q value introduced by the coating was less. The average Q value was reduced by only 48.2% in this case. It is notable, however, that the damping in the uncoated plate was initially higher than in the previous case. This was a higher mode and therefore naturally damped out more quickly.

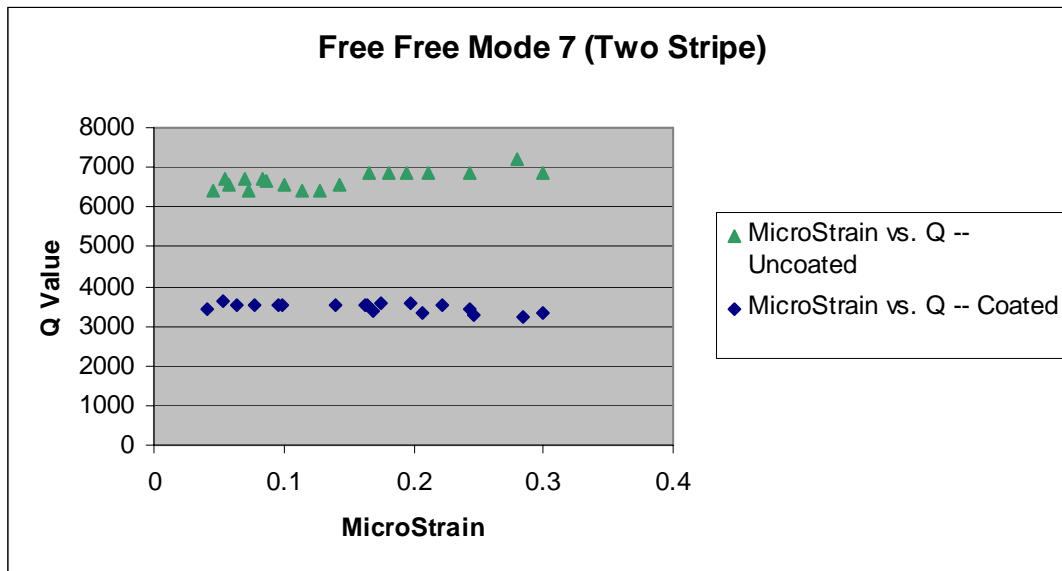


Figure 112. Free Condition Damping Results, Mode 7

The following two figures show data for the coated plate in both modes re-plotted alone, allowing the scale to be increased so that trends in the data were more visible. Overall, the coated sample in both modes showed strain dependence. As strain increased, the Q value decreased. This corresponded, of course, to an increase in damping as strain rose. This strain dependence, as mentioned, was characteristic of the mag spinel material.

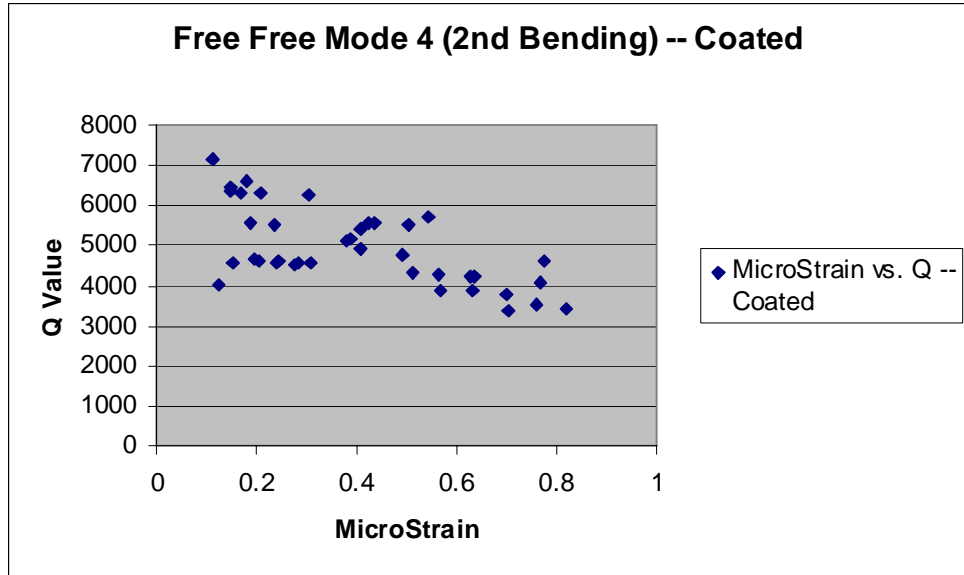


Figure 113. Free Condition Damping Results, Coated Sample, Mode 4

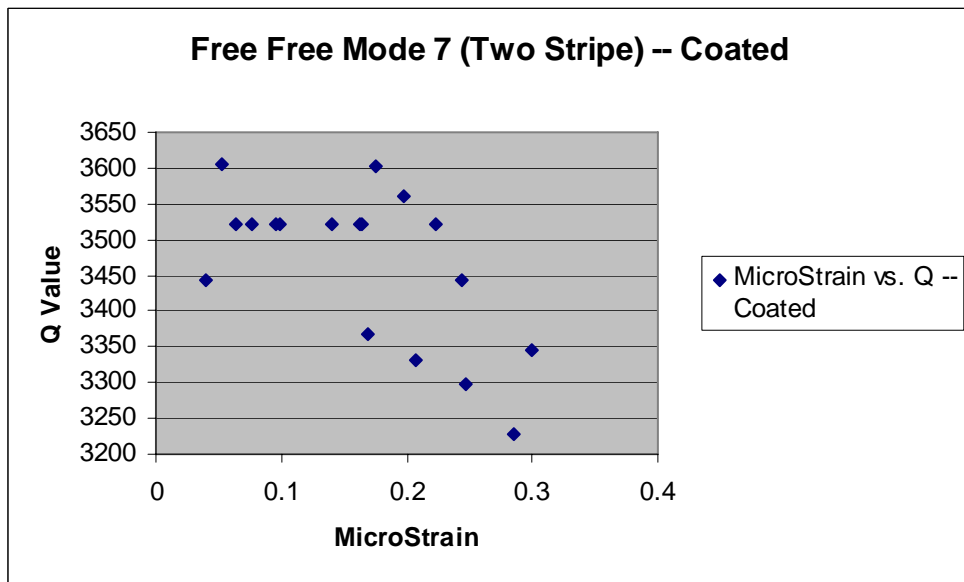


Figure 114. Free Condition Damping Results, Coated Sample, Mode 7

In both of the plots above, the data only shows a very general downward trend. The data does not form a neat line or curve. This was due to the numerous small changes

which were performed on the experimental set-up over the course of testing. During testing, the set-up was moved to make way for other experiments. Stretching in the tape supporting the sample required re-adjustment of the stands. The laser had to be re-planed (or recalibrated) to the sample whenever the sample was moved slightly. Additionally, small deviations in the placement of the air horn excitation would change the input condition and, therefore, the results. Every effort was made to negate these changes, but they still caused variations in the data. Every change that was made was recorded, however, so each run could be grouped according to a common set-up, where no changes were made.

The following 2 plots represent a color coding of the 2 plots shown above. The data points have been coded according to when adjustments to the experiment were made. Therefore, groups of runs with completely common set-up appear as the same color. In the plots below, trends in the behavior of the coated sample are more evident. While still not perfect, the data more clearly highlights the strain dependence in the material. The data shows that changes imparted on a set-up introduce a bias, shifting the range of responses either up or down.

In these plots below, it is noteworthy to mention that smooth trends in the data are more easily spotted for mode 7. In fact, fewer runs were performed on this mode because the data was more consistent, and more runs were not needed to further define the trends. It is possible that the higher mode is less susceptible to changes in the experimental set-up.

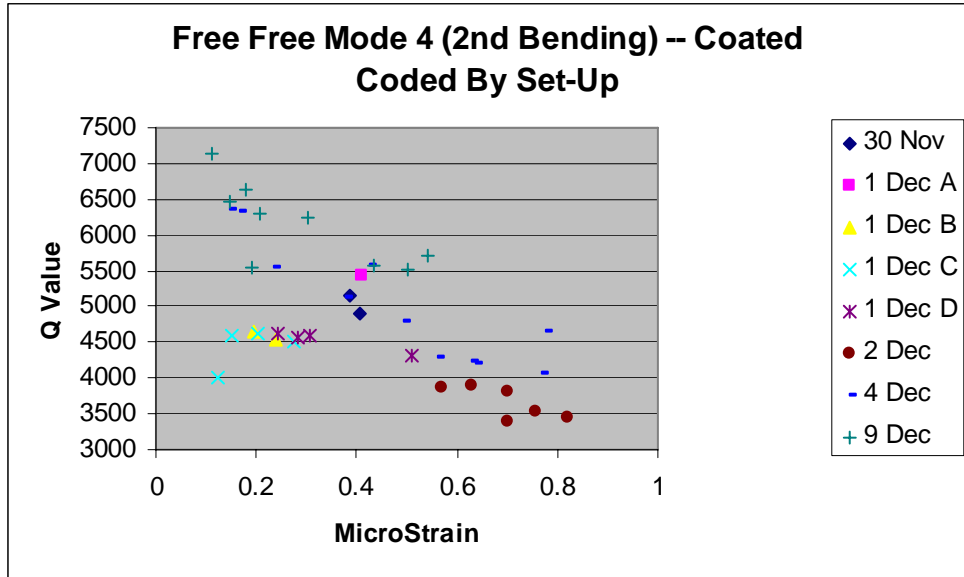


Figure 115. Free Condition Damping Results, Coated Sample, Mode 4, Color Coded

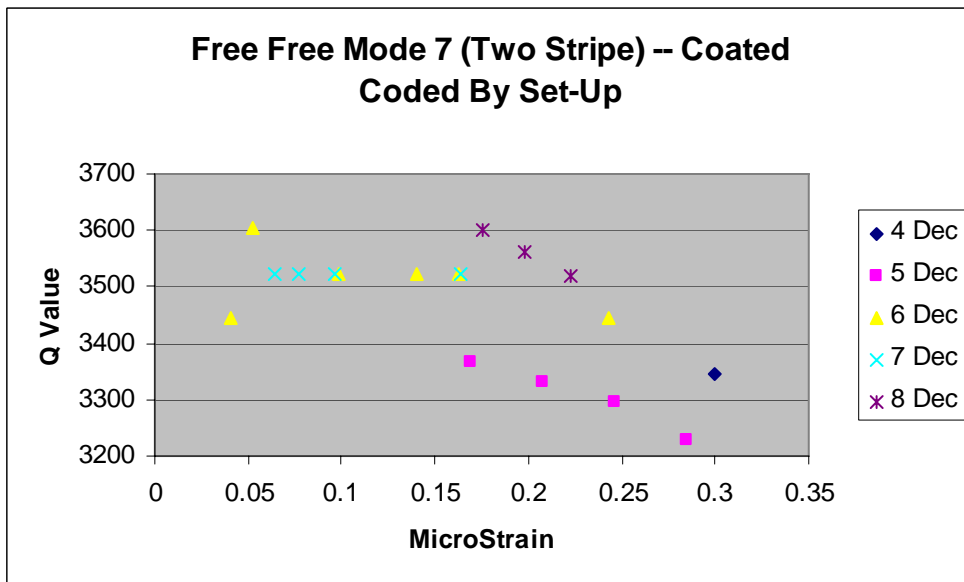


Figure 116. Free Condition Damping Results, Coated Sample, Mode 7, Color Coded

This section has shown that much lower damping may be achieved by using a different boundary condition in testing. While all Q values for the second bending and two-stripe modes resided in the hundreds for cantilevered testing, Q values upwards of

20,000 were found for the uncoated plate in this set-up. Loss mechanisms, such as the constraint blocks, were removed from the equation in this damping evaluation technique. The free condition testing set-up was by no means perfect, but it did offer another alternative for evaluating the effectiveness of coatings on plates. Conclusions regarding this section are enumerated in Chapter V of this study.

V: Conclusions and Recommendations

Conclusions

The conclusions garnered from this study are numerous, and will help to better characterize damping in nonlinear ceramic coatings in the future. The findings of this study highlight major factors affecting damping measurements, while simultaneously offering solutions to combat these factors. The effect of air pressure on damping was studied using a statistical approach, allowing the experimenter to speak with confidence about the nature of air damping and how it affects vibrating plates. Further, a new approach for comparing damping in vibrating plates was also tested.

The first set of conclusions deals with several factors affecting the measurement of total damping within a system. Throughout this study, various factors which affect the measured damping were experimentally determined. Some of these factors are universal, while others apply specifically to equipment used for this study. The conclusions regarding these factors are shown here:

- 1) The constraint blocks used in this study perform in a strain-dependent manner. This effect is more prevalent for the second bending mode, which has its highest strain nearer the sample root.
- 2) Reclamping the constraint blocks between runs produces poor repeatability, especially for the 4th mode of the cantilevered sample.
- 3) The constraint blocks show varying movement across the upper surface. The clamped condition is non-uniform, and this condition changes each time

sample is reattached to the blocks via torqued bolts. Repeatability worsens when the sample is reattached between runs.

- 4) The use of jack bolts, which cants the top block forward onto the sample root, does increase repeatability. They do this by impinging on the sample more tightly across the entire edge, thus reducing the disparity in movement across the top of the constraint blocks.
- 5) The performance of the constraint blocks and the damping seen from the sample is temperature dependent. For the entire temperature range observed, Q values increased as temperature increased. The clamped condition effectively improved for relatively modest temperature increases.
- 6) The effect of a temperature time trend can be avoided by allowing the room used for testing to heat to a steady state temperature. A constant temperature greatly improves repeatability between subsequent runs and makes it easier to consistently attain desired displacements in the sample.
- 7) Baseplate modal interference can be avoided by using a thicker, more rigid baseplate. Interference issues still prevail, however, when a large mass is placed on an unsupported portion of the baseplate.

It is important to note that even conclusions relating to specific pieces of equipment have widespread merit. For example, other experimenters designing constraint blocks for their own damping measurements might wish to take the failings of this study's blocks into account.

The next set of conclusions deals specifically with the effect of air pressure on damping. While it has a definite impact on the system, the exact nature of this air pressure effect has previously appeared ambiguous. Results from this study better characterized the effect of air pressure and its interactions with other factors. These results made use of a specifically designed statistical experiment.

- 1) For the uncoated sample, air pressure is clearly significant for mode 4 but the results for mode 3 were unclear. Statistical results showed a 99.99% probability that the interaction between air pressure and mode was significant. It can be concluded that for this sample, air damping is significant for the two-stripe mode, but not for the second bending mode. The air pressure-mode interaction shows that air damping is mode dependent.
- 2) Increased variation between runs and nonlinear trends in the results cause the degree of certainty afforded by ANOVA testing to drop for coated samples. However, valid results may still be produced. These results may also be used in concert with standard plots.
- 3) For the coated sample, the effect of air damping is still significant, to a certainty of 95.24%. However, the difference in Q value is far less for the coated sample. For mode 4 in this study, a near-vacuum condition increased the average Q value by only 26.14% at 150 microstrain and 6.97% at 500 microstrain.
- 4) The damping of the coated sample is dependent on the interaction between air pressure and strain. This was determined with a certainty of 98.33% in the large ANOVA test. As strain increases, the relative effect of air damping gets

smaller. This trend, confirmed by ANOVA, is not shown conclusively in a conventional plot alone due to the variations in the data. Data from the smaller ANOVA tests did conflict with this conclusion, but the small ANOVA experiments at mode 4 were both deemed unreliable based on their diagnosis plots.

- 5) Mode dependence is also present for air damping in the coated sample, although it is far less visible due than in the uncoated sample due to increased variation within the data. Air pressure was found to be significant for all tests at mode 4, but testing at mode 3 did not yield an air pressure significance of at least 95%. This, coupled with the appearance of the plotted data, makes it clear that air damping is mode dependent here as well.

The mode dependence of rectangular plates in air damping can also be seen in results produced by Allen, for both a cantilevered and free condition uncoated sample. In his work, air damping had a definite effect on the two-stripe mode, and a questionable effect on the second bending mode. The results of this study, in combination with Allen's results provide for a strong conclusion regarding this effect. His results show that the effect observed is not unique to this study.

The last set of conclusions deals with the free condition testing of coated and uncoated plates. Testing in this section of the study provided some conclusions, but worked mostly as a proof-of-concept experiment.

- 1) Damping values may be determined for a free condition plate using the half-bandwidth method. The repeatability of these values is highly dependent on

the experimental set-up, and could be improved with better resolution in the software. Allowing the software to interpolate between data points creates a smooth curve if better resolution is unavailable, though this solution is not ideal.

- 2) Averaging data from symmetric data collection points is an effective means of generating response plots and minimizing noise in the data. The use of averages also helps the experimenter to both spot and negate unwanted movement in the plate.
- 3) Rigid body movement in a free condition plate would be a problem for the study of lower modes, but the effect dissipates as frequency increases. This allows for the study of higher order modes, such as those observed in this study.
- 4) The high Q values obtained via this method (up to 20,000) allude to how much damping is introduced by the clamp for the cantilevered samples. Use of a free condition eliminates clamp losses and allows for a better characterization of the effectiveness of coatings, such as mag spinel.

Recommendations

In light of the conclusions above, many possibilities exist for improving the study of damping in nonlinear materials. It is clear that the constraint blocks used currently provide an unsatisfactory platform for the determination of damping. This problem could be rectified if the amount of damping lost to the clamp was known.

In this study, the effectiveness of the constraint blocks could not be compared to the free condition because of the vast difference in strain levels attainable between the samples. In order to make a comparison, and determine a baseline for losses due to the clamp, a sample in the constraint blocks could be excited with an acoustic air horn. If a free condition sample were then excited in the same manner, some comparison could be made at like strain levels. As mentioned previously, the similarities between the samples and their mode shapes make this comparison interesting. While the centerline node of the free condition sample will necessarily differ from a cantilevered condition, it is felt that the similarities are enough to make the comparison worthwhile.

It seems more prudent, though, to simply design a new system for making damping comparisons. The lack of repeatability in the blocks makes them undesirable, even if the damping they introduced was known. Repeatability could be improved, of course, if beams were tested instead. A clamp for a beam would have less opportunity for a non-uniform clamping surface, due to its smaller width. This, however, would defeat the purpose of determining damping properties for plates.

Another possibility is to use an actual turbine engine blade and mount in testing coatings. Coated and uncoated blades could be compared, with any losses to the mount representative of what is to be expected in the operational environment. If this was not an option, blocks similar to the current constraint blocks could be designed with stronger jack bolts. This might increase the amount of force holding the sample in place and, therefore, increase both repeatability and performance.

In looking for sources of damping on these new cantilevered set-ups, ANOVA might once again be employed in order to determine significant factors. In order to

ascertain damping at different pressures indicative of an operational environment, testing might also have to be carried out at various pressures. This would, of course, depend on the mode shape, strain level, and the coating used. The use of more runs would allow trends in the data to emerge more clearly as well, and help to negate the effects of variation which are inherent in damping measurements.

Finally, damping could also be evaluated using plates in a free condition. These plates would have to be less massive than the ones used in this study, in order to attain higher displacements. The set-up of the experiment would have to be strictly controlled as well, in order to maintain repeatability and generate clear trends in the results. Additionally, the study of modes should be limited to those outside the reach of rigid body motion in the sample if at all possible. Otherwise, the rigid body effect would have to be removed from the data before damping could be determined.

Further analysis of air pressure effects could also be performed. Testing at air pressures greater than atmospheric pressure would better highlight the effects of air damping. Further, higher pressures might better replicate the environment inside a turbine engine. Additionally, a “smoker” could be used to show how different mode shapes affect the movement of air. This might help to explain why the impact of air pressure on measured damping varies with mode shape.

Appendix A: ANOVA Theory

This appendix is designed to provide the reader with a full explanation of ANOVA theory. While the main text of this study provides brief descriptions of terms and techniques used, this section has been written to show in detail both how ANOVA works and how it is applied. ANOVA is, of course, rooted in basic statistics. Therefore, this explanation of ANOVA will begin by reviewing a few terms.

The null hypothesis, commonly symbolized as H_0 , is the default assumption at the beginning of a statistical study. In ANOVA, the null hypothesis is that all treatments are equal, with no difference in variance between them assumed. The alternative hypothesis, or the default when the null hypothesis is proven false, is that there is change in variation between treatments. Therefore, the null hypothesis assumes factors are insignificant, while the alternative hypothesis states that they are significant. A Type I error occurs when an experiment proves the null hypothesis false, when it is in fact true. Assuming that suspects in a court of law are innocent until proven guilty, an example of a Type I error would be convicting a man of a crime, even though he is actually innocent (16). A Type II error occurs when the experiment fails to reject the null hypothesis, when the null hypothesis is in fact false. Using the same court case metaphor as above, a Type II error would be finding the man innocent, even though he was actually guilty. Type I errors are typically considered worse than Type II errors. As such, the probability of a Type I error is more often utilized in experimentation.

The probability of a Type I error is assigned to the variable α . This term is closely related to the degree of certainty within an experiment, as shown by the equation below.

$$\text{Percent Certainty} = (1 - \alpha) * 100 \quad (\text{A.1})$$

Therefore, in order to disprove the null hypothesis with 95% certainty, an α of 0.05 must be used. In order to attain 99% certainty in this cause, an α of 0.01 must be used. The value for α is typically chosen before an experiment is designed and run.

In ANOVA, there are several relevant terms which must be understood. A factor is something in the experiment which is being changed. It is a, essentially, a variable. The specific settings or values assigned to a factor are its treatments, where the number of treatments used is a . A replicate is generated each time the entire experiment is repeated, where the number of replicates is symbolized as n . The response is the output of the experiment, or what is being measured and recorded.

In all equations given pertaining to ANOVA, treatments are denoted by the letter i , where i represents the specific treatment from $1 \dots a$. Replicates are denoted by j , where j represents the replicate in question from $1 \dots n$. The values and associated equations which form the backbone of ANOVA are given below (15). Note that in the equations below, the dot represents either all treatments or all replicates, depending on its position.

$$\text{Treatment Sum } y_{i\bullet} = \sum_{j=1}^n y_{ij} \quad (\text{A.2})$$

$$\text{Treatment Mean } \bar{y}_{i\bullet} = \frac{y_{i\bullet}}{n} \quad (\text{A.3})$$

$$\text{Treatment Variance} \quad S_i^2 = \frac{\sum_{j=1}^n (y_{ij} - \bar{y}_{i\cdot})^2}{n-1} \quad (\text{A.4})$$

$$\text{Grand Sum} \quad y_{\cdot\cdot} = \sum_{i=1}^a \sum_{j=1}^n y_{\cdot j} \quad (\text{A.5})$$

$$\text{Grand Mean} \quad \bar{y}_{\cdot\cdot} = \frac{y_{\cdot\cdot}}{n} \quad (\text{A.6})$$

The formulations above are immediately useful in explaining how ANOVA handles signal and noise measurements, which in turn leads back to how ANOVA determines significance. The total sum of squares (SS) deviation from the grand mean is partitioned into the sum of squares from the treatments, and the sum of squares from the error, as shown below. Drawing from the equations above, this partition can be expressed mathematically as well.

$$\text{SS}_{\text{Total}} = \text{SS}_{\text{Treatments}} + \text{SS}_{\text{Error}} \quad (\text{A.7})$$

$$\sum_{i=1}^a \sum_{j=1}^n (y_{ij} - \bar{y}_{\cdot\cdot})^2 = n \sum_{i=1}^a (\bar{y}_i - \bar{y}_{\cdot\cdot})^2 + \sum_{i=1}^a \sum_{j=1}^n (y_{ij} - \bar{y}_{i\cdot})^2 \quad (\text{A.8})$$

The total number of runs required for an experiment is the product of the number of treatments, a , and the number of replicates, n . This total number of runs is given by N . The total degrees of freedom (DOF) in an experiment is one less than the value of N . These degrees of freedom are delegated to the treatments and the error as shown below, both symbolically and mathematically.

$$\text{DOF}_{\text{Total}} = \text{DOF}_{\text{Treatments}} + \text{DOF}_{\text{Error}} \quad (\text{A.9})$$

$$(N-1) = (a-1) + (N-a) \quad (\text{A.10})$$

When ANOVA compares the two sources of variation, it compares the mean square (MS) of the treatments to the mean square of the error. The mean square of the treatments represents the average variation between treatments, while the mean square of the error represents the average variation within the treatments (16). The formulas for these means are very straightforward.

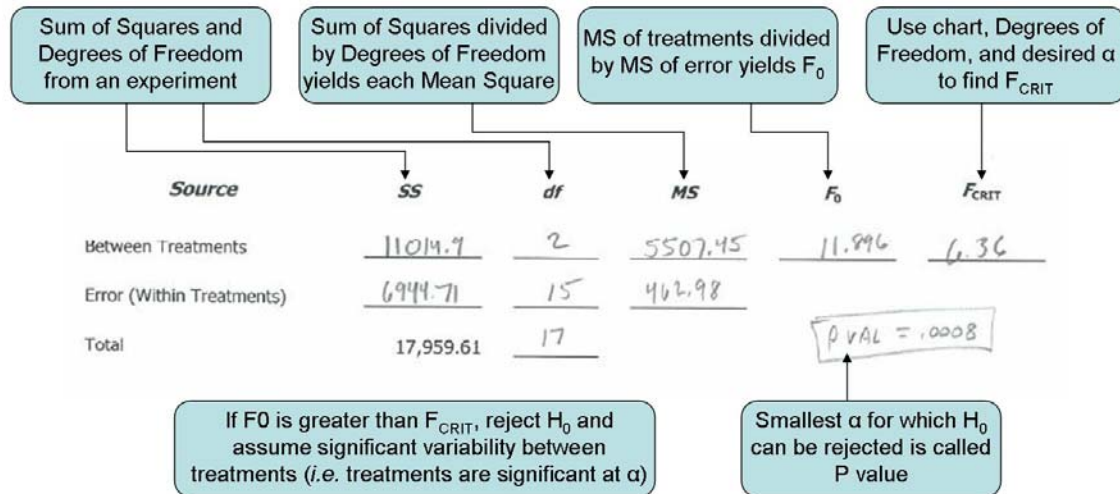
$$\text{MS}_{\text{Treatments}} = \text{SS}_{\text{Treatments}} / \text{DOF}_{\text{Treatments}} = \text{SS}_{\text{Treatments}} / (a-1) \quad (\text{A.11})$$

$$\text{MS}_{\text{Error}} = \text{SS}_{\text{Error}} / \text{DOF}_{\text{Error}} = \text{SS}_{\text{Error}} / (N-a) \quad (\text{A.12})$$

The ANOVA statistic, written as F_0 , is then the ratio given by $\text{MS}_{\text{Treatments}}$ over MS_{Error} . In order to determine whether the variation between the treatments is significant, F_0 must be greater than the critical F value, written as F_{Crit} . The value for F_{Crit} is found in a published chart, which is organized by desired α , $\text{DOF}_{\text{Treatments}}$, and $\text{DOF}_{\text{Error}}$. If the value found experimentally for F_0 is greater than the given value F_{Crit} , then the variation between treatments is found to be significant at the desired level of certainty (15). The null hypothesis is, therefore, rejected.

ANOVA tables present the results of an experiment in a concise manner, showing information about how the experiment was run and, ultimately, which factors were found significant. The figure below shows a basic sample ANOVA table along with how it

should be calculated and interpreted. Each column or category is derived from an equation which has been discussed.



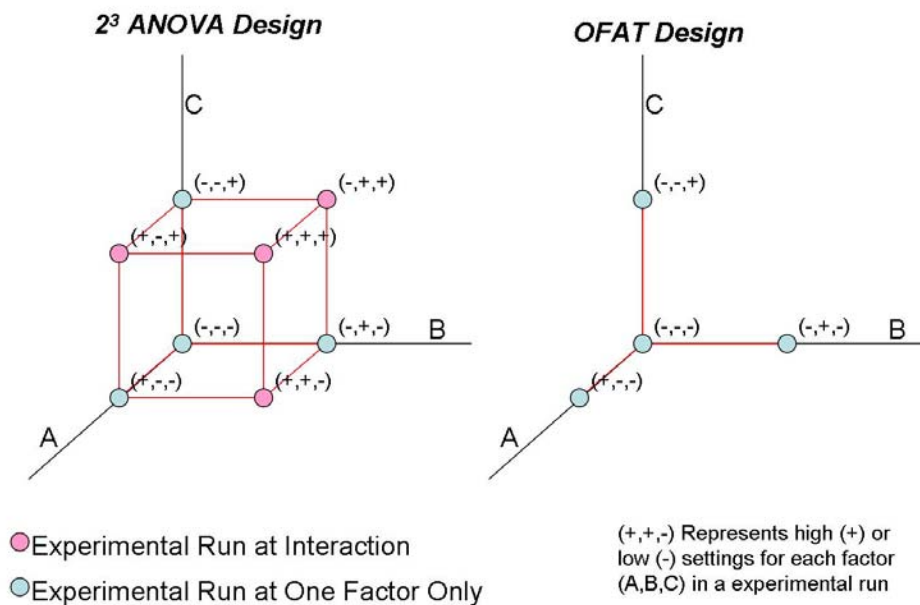
Appendix Figure A 1. Sample ANOVA Table [Adapted From (16)]

Many experiments are performed using one factor at a time (OFAT) testing. This has the advantage of being easy to do, but is woefully inadequate when an experimenter wishes to evaluate multiple factors in an efficient and effective manner. OFAT testing yields a higher α than ANOVA testing and often requires more tests (16). Further, OFAT testing does not allow for interactions between factors to be studied. For example, assume an experimenter is studying three factors: A, B, and C. If he only changes one of these factors at a time, he will never know what happens when changes occur in both A and B, or what happens when all three of them are changed. By only testing one factor at a time, he can never know if the interaction between factors is in itself significant.

ANOVA is used when there are multiple factors under consideration (15). Since this study looks at 3 factors, this explanation will continue in considering ANOVA with 3

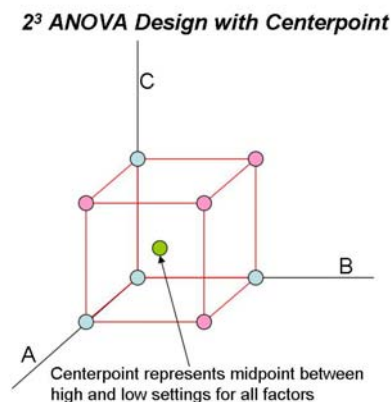
factors. In ANOVA, the factors are tested at 2 levels, arbitrarily labeled as high and low. These levels can be numerical, where they actually do correspond to a high and low number, or categorical. The use of the high level for any given factor is signified by a plus sign (+), while the low level setting is signified by a minus sign (-).

Consider the three factors A, B, and C in the figure below. The origin of the coordinate system represents a low level (-) for all of the factors. Each axis represents a factor. A point on that axis would, therefore, represent a high setting for that factor. Points off the axes represent high settings for multiple factors. Note that the diagram representing OFAT testing has 4 fewer data points. Those missing data points correspond to multiple high settings, which illustrates how OFAT testing ignores all of the possible interactions between factors.



Appendix Figure A 2. ANOVA versus OFAT Experimental Design

ANOVA designs are typically done at 2 levels – a high and a low level – for good reason. Namely, a design at two levels greatly reduces the number of experiments required (16). A design at 2 levels for k factors is defined as a 2^k design. In a 2^k design, there are 2^k experimental runs required per replicate. Therefore, for a 3 factor design, there would be $2^3 = 8$ runs required per replicate. If three levels were included per factor, this experiment would become a 3^k design. With 3 factors, there would then be $3^3 = 27$ runs required per replicate. The 2 level design does assume a linear response between the 2 levels, but this is usually a good assumption. In addition, centerpoints may be added to a 2^k design in order to check for curvature. These centerpoints represent a setting halfway between the high and low settings for all factors. If curvature is found to be significant, then the experiment can be modified in order to account for this nonlinearity. For example, points on the face of the cube or outside of the original design may be added in subsequent experiments in order to better model what is occurring. The figure below shows the ANOVA 2^3 cube with a centerpoint added.



Appendix Figure A 3. ANOVA Design with Centerpoint

In order to design and run a 2^k experiment, it is first necessary to create a design matrix. The design matrix shows the factor settings (high or low) for all of the factors, as well as the resultant levels for the interactions. In creating this matrix, the runs required are listed in numerical order on the left side. The plusses and minuses are then assigned to each of the factors by column. Starting with minus, the settings alternate every run for factor A. For factor B, the settings alternate every 2 runs, and every 4 runs for factor C. If there were more than 3 factors, this pattern of doubling would continue. The plus or minus setting for each interaction at each run is determined by multiplying the signs for each factor concerned in that run's row. The column designated "name" simply names each run according to which main factors have a high setting in that row. The first run will always have all low settings, and is, by convention, named [1]. The design matrix below represents 1 replicate for a 2^3 design. If there were more than 1 replicate, this matrix would simply be repeated for each replicate desired.

Appendix Table A 1. Basic ANOVA Experimental Design

RUN	A	B	C	AB	AC	BC	ABC	NAME
1	-	-	-	+	+	+	-	[1]
2	+	-	-	-	-	+	+	a
3	-	+	-	-	+	-	+	b
4	+	+	-	+	-	-	-	ab
5	-	-	+	+	-	-	+	c
6	+	-	+	-	+	-	-	ac
7	-	+	+	-	-	+	-	bc
8	+	+	+	+	+	+	+	abc

If the experiment laid out in the matrix above were being performed, the run order in this design matrix would be randomized. Randomization is done in order to combat the effects of changes over time (15). For example, a change in the lab environment

halfway through testing could make factor C look very significant because of the way runs were assigned above. If the runs were randomized, however, that change would not have any more effect on factor C than the other factors, and the variance imparted (as compared to the first half of the runs) would be diffused throughout the experiment.

The change in the lab environment mentioned would be due to what is termed a nuisance factor. A nuisance factor is something that is known to affect the experiment, but is not in itself being tested as a factor. Nuisance factors may or may not be controlled, depending on how the experiment is designed.

Another way to combat nuisance factors in the lab environment is through the use of blocking. Randomization helps to negate the effects of nuisance factors affecting an experiment, but blocking is also essential. If nuisance factors affecting the experiment are changing, then different runs will yield different results in accordance with these changes. These changes will cause the variation between treatments to skew, altering the true significance of the factors in question. The extra variation introduced also adds to the noise of the system and reduces the overall ability of the experiment to produce a result that reflects reality. In blocking, sets of runs which contain homogenous experimental conditions are grouped together (15). Thus, runs completed with like experimental conditions find themselves in the same block. These blocks are analyzed separately within an ANOVA model, in order to negate the effects of known nuisance factors.

It is important to note that blocks are only effective against known nuisance factors. If a nuisance factor is unknown, then there is, of course, no way to divide the runs in to blocks based on this factor. If the nuisance factor cannot be controlled, then an

analysis of covariance is the preferred option. Given a known and controlled nuisance factor, however, blocking is a highly effective technique in dealing with that factor.

There are several examples of nuisance factors which lend themselves to experimental blocking. For example, consider an experiment where 2 different operators control 2 different machines being studied. The experiment would have to be designed so that blocks were placed around each operator, as the individual traits and skill of the operators would affect the overall variability. Another example of a nuisance factor conducive to blocking would be the different aircraft used if, perhaps, 2 different air-to-air missiles were being compared (16).

Another important note about blocking is that it should be done, if possible, for entire replicates of an experiment at a time. This saves time and avoids complications. Consider the example above with the 2 operators on the 2 machines being compared. Say there are 2 additional factors being tested besides the machines, making this a 3 factor experiment. As a 2^3 experiment, there are 8 runs in each replicate. If each operator performs a set of runs, then each replicate is a block. The experiment is sound, and will produce valid results.

What if the operators trade off in operating the equipment within a replicate, though? It is still possible to group runs by operator and block them, but chances are that some information about the experiment has been lost. When nuisance factors change within a replicate, they can change just as factors change, or close to it, and alter results again. If a factor's or interactions' high or low levels are matched by a block, then that factor or interaction is said to be confounded with blocks (15). When a term is confounded, there is no way to say whether its significance is due to the effect of the

factor or the blocking itself. If the 2 operators in the example always used the same machine, there would be no way of knowing whether the machines had a significant effect, or if it was just the effect of the operator causing that difference. The figure below shows just one example of confounding in an experimental block design.

RUN	A	B	C	AB	AC	BC	ABC	NAME	OPERATOR
1	-	-	-	+	+	+	-	[1]	Operator 1 (Block 1)
2	+	-	-	-	-	+	+	a	Operator 2 (Block 2)
3	-	+	-	-	+	-	+	b	Operator 1 (Block 1)
4	+	+	-	+	-	-	-	ab	Operator 2 (Block 2)
5	-	-	+	+	-	-	+	c	Operator 1 (Block 1)
6	+	-	+	-	+	-	-	ac	Operator 2 (Block 2)
7	-	+	+	-	-	+	-	bc	Operator 1 (Block 1)
8	+	+	+	+	+	+	+	abc	Operator 2 (Block 2)

↑

Each operator alternates, so the blocks also alternate. Block 1 then corresponds to all low (-) values for factor A, while Block 2 corresponds to all high (+) values. The effect of A is therefore masked, or confounded, by blocks and cannot be determined

Appendix Figure A 4. ANOVA Experimental Design Confounded by Blocks

As mentioned, it is preferred to avoid confounding if at all possible by blocking full replicates. This does place restrictions on randomization, because the runs can only be randomized within the blocks (15). However, it is preferable to losing data on the factors involved. If it is necessary to block within replicates, the experiment should be designed so that the highest order interaction is confounded. The principle of sparsity of effects states that the lowest order factors and interactions usually dominate the effect on an experiment (16). Therefore, it makes sense to confound the highest order effects if something has to be lost. The figure below shows the best way to confound a 2^3 experiment, if it was required. Note that the interaction ABC is confounded with blocks.

RUN	A	B	C	AB	AC	BC	ABC	NAME	OPERATOR
1	-	-	-	+	+	+	-	[1]	Operator 1 (Block 1)
2	+	-	-	-	-	+	+	a	Operator 2 (Block 2)
3	-	+	-	-	+	-	+	b	Operator 2 (Block 2)
4	+	+	-	+	-	-	-	ab	Operator 1 (Block 1)
5	-	-	+	+	-	-	+	c	Operator 2 (Block 2)
6	+	-	+	-	+	-	-	ac	Operator 1 (Block 1)
7	-	+	+	-	-	+	-	bc	Operator 1 (Block 1)
8	+	+	+	+	+	+	+	abc	Operator 2 (Block 2)

Blocks are set here so that they coincide with the high/low settings of interaction ABC

Appendix Figure A 5. ANOVA Experimental Design Properly Confounded

It is possible to design and run experiments which consist of fractions of a full design. These are called factorial designs. These designs are an excellent way to minimize the number of experiments required and eliminate factors during experimentation (16). They are also especially useful when resources are limited. However, they were not utilized in this study and will not, therefore, be elaborated on here.

Once the experiment has been run and the responses recorded, an analysis of the ANOVA results must begin. This analysis begins by computing the contrasts for each factor and interaction. Each run will have a response, which is some numerical value. The design matrix, as shown previously, contains a matrix of + and – settings for each factor and interaction at each run. The contrast for each factor is the sum of responses where that factor was at its high setting, minus the sum of responses where that factor was at a low setting. For interactions, it works the same way. Whether the response from each run is added or subtracted depends on whether the design matrix shows that run to be + or -. The figure shows example computations of contrast in a 2^3 design matrix.

RUN	A	B	C	AB	AC	BC	ABC	NAME	RESPONSE
1	-	-	-	+	+	+	-	[1]	12.0
2	+	-	-	-	-	+	+	a	13.2
3	-	+	-	-	+	-	+	b	11.0
4	+	+	-	+	-	-	-	ab	12.5
5	-	-	+	+	-	-	+	c	18.1
6	+	-	+	-	+	-	-	ac	17.0
7	-	+	+	-	-	+	-	bc	22.8
8	+	+	+	+	+	+	+	abc	19.0

$$\text{Contrast}_A = (13.2+12.5+17.0+19.0) - (12.0+11.0+18.1+22.8)$$

$$\text{Contrast}_{AB} = (12.0+12.5+18.1+19.0) - (13.2+11.0+17.0+22.8)$$

Sum of responses at high (+) setting for each factor or interaction minus sum of responses at low (-) setting yields its contrast

Appendix Figure A 6. Example ANOVA Contrast Computation

Once the contrasts for each factor and interaction are computed, they are used to find the main effect. The contrast for each term is converted to an estimate for the main effect in accordance with the equation below.

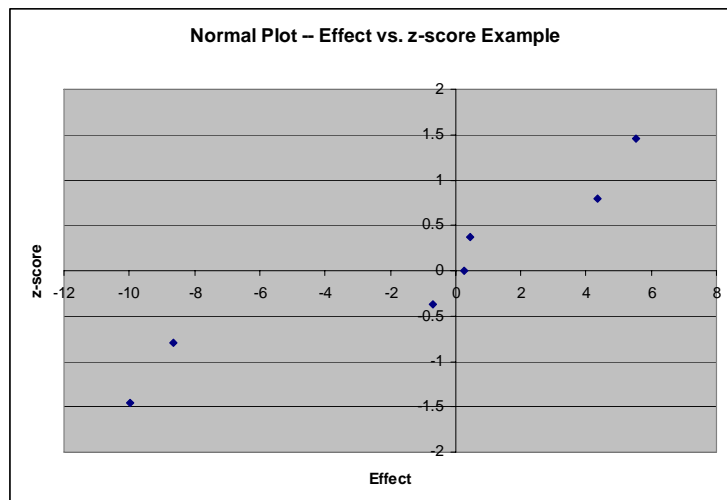
$$\text{Main Effect} = \frac{\text{Contrast}}{n2^{k-1}} \tag{A.13}$$

The main effects are then plotted on a normal plot or a half normal plot. A half normal plot is simply the absolute value of a normal plot, which makes it easier to interpret data (16). In order to plot these effects, they are first sorted by ascending order. In this order, they are numbered. Each number, corresponding to a data point, can be used to calculate the percentile. This percentile can, in turn, be used to find a z-score from a chart. A normal plot may present the effects plotted against either percentiles or studentized results (*i.e.* z-scores). The table below gives example values for the effect, and shows the generation of percentiles and z-scores. The accompanying figure shows the effects plotted versus the z-scores found in the table, creating a normal plot. The

table and plot are, of course, representative of a 2^3 design. Below, p represents the number of factors and interactions.

Appendix Table A 2. Data for Normal Plot (16)

Factor	Effect	Data Point h	Percentile $(h-0.5)/p$	z-score
B	-9.99	1	0.0714	-1.46
AC	-8.64	2	0.214	-0.79
ABC	-0.7	3	0.357	-0.37
BC	0.27	4	0.5	0
AB	0.46	5	0.643	0.37
C	4.35	6	0.786	0.79
A	5.55	7	0.929	1.46



Appendix Figure A 7. Example Normal Plot

In creating the normal or half normal plot, the main effect can either be the dependent or independent variable. This plot is important because it shows where the main effects for each factor or interaction fall in relation to normal probability. Because the probability has been normalized, normal probability is represented by a straight line

which passes through the origin. The path of the straight line is generally shown by the placement of the factors and interactions, as shown in the figure above. Factors or interactions whose main effects are farther away from a “best fit” line are the ones which are significant. If a factor or interaction has a main effect which is not on or near this line, that factor does not correspond to normal probability distribution. This implies that the factor in question is actually influencing the result of the experiment. Removing the non-normal (*i.e.* significant) main effects from the normal plot will create a better “best fit” line.

The normal plot is a handy tool for deciding which factors may be significant before an ANOVA table is generated. Significant factors and interactions can be singled out, in order to have the mean squares calculated. Non-significant factors can be added to the error term, under a category titled “Lack of Fit.” Removing insignificant factors from the analysis before an ANOVA table is generated can save time, but insignificant factors will also stand out on the table if left in place.

The ANOVA table, appearing earlier in this section, shows that each factor used, and each interaction between factors, will generate its own $MS_{\text{Treatments}}$. This value is compared to the overall MS_{Error} in order to determine if that factor or interaction is significant, as discussed previously. All of the significant factors together form a model which represents the system. Factors which prove insignificant can be dropped from the resulting model and thrown in to the error at this point, if required. Essentially, the insignificant factors are considered to be only noise. Removing factors which are insignificant strengthens the new model, and thus the results of the experiment. By dropping the insignificant factors, the degree of certainty which can be satisfied by the

experiment is increased. Further, any follow-on experiments will not have to consider the dropped factors. One of the primary uses of ANOVA is, in fact, to determine which factors potentially affecting an experiment are important.

There is an important caveat to dropping factors, however. Insignificant factors which are part of a higher order interaction should not be dropped. For example, if factor C proves insignificant, but interaction AC is significant, then factor C should not be dropped from the model. The requirement to keep the components of significant interactions is referred to as hierarchy.

It can be mathematically shown whether the employment of experimental blocks is significant in an ANOVA design as well. If blocks can be proven significant, it shows that they were essential in producing the correct results. If blocks prove insignificant, they can be removed from the experimental analysis. The number of degrees of freedom assigned to the blocks is equal to one less than the number of blocks, b . Blocks are proven significant in the same manner as any other factor (16). The SS_{Blocks} is computed and divided by the DOF_{Blocks} to produce the MS_{Blocks} . The MS_{Blocks} divided by the MS_{Error} yields F_0 for the blocks, which is compared to an F_{Crit} pulled from a chart. If the blocking ANOVA F value is greater than F_{Crit} , then blocking is considered significant.

After an analysis has been completed, and the significant factors determined, the remaining step is to verify the adequacy of the ANOVA model. This is done primarily by looking at residuals of the results versus various other dynamics. The residuals of the results are merely the difference between the observed and expected value for each response. For each response, the residual is the response minus the mean of this

treatment. This is shown mathematically in the following equation, where the residual is symbolized by e .

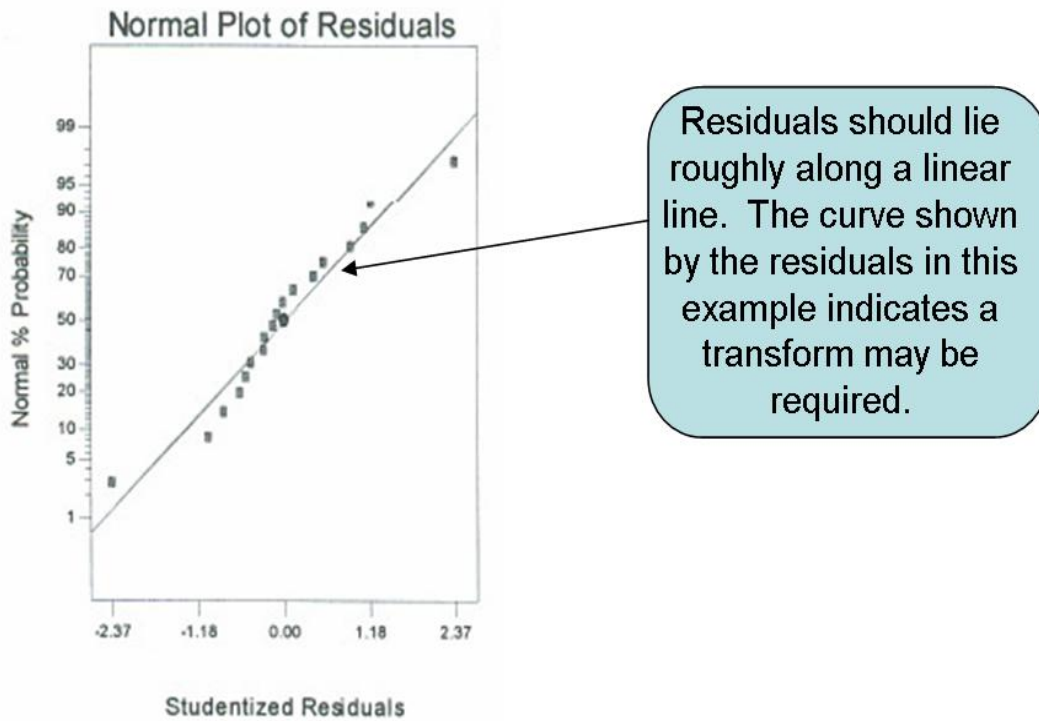
$$e_{ij} = y_{ij} - y_{i\bullet} \quad (\text{A.14})$$

This residual can be standardized such that it represents the number of standard deviations from the observed to the predicted value. The standardized residual is represented by d .

$$d_{ij} = \frac{e_{ij}}{\sqrt{MS_{Error}}} \quad (\text{A.15})$$

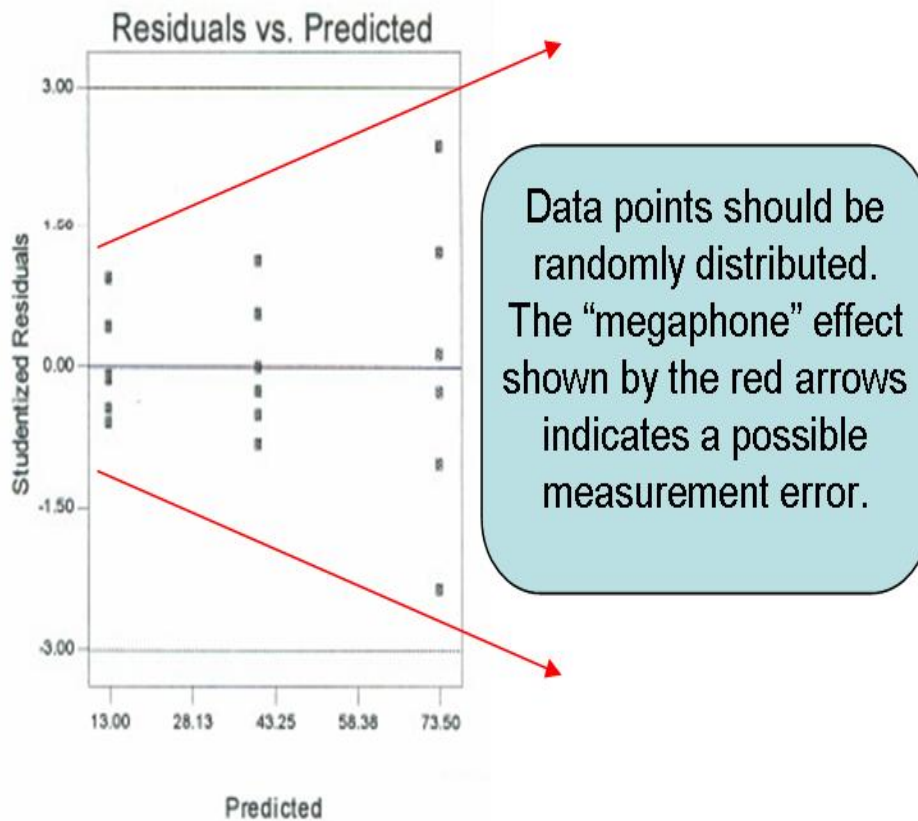
The residuals are plotted versus normal distribution, predicted values, and run order in order to validate the results of the experiment (16). Each of these plots reveals something about the results of the study, and may indicate a problem with the way in which it was conducted.

In the normal plot of the residuals, the residuals are plotted versus their normal distribution in the exact same manner as the effects were plotted. In this plot, the residuals should line up roughly along a line, indicating a normal distribution. If the residuals do not attain this normal distribution, a transform on the responses may be required. For example, a poorly fit normal plot may imply that the responses should be re-analyzed after a log conversion. An example of a normal plot of residuals is shown below. Here, a transform may be required to improve results, but since the data lies close to the line it is probably acceptable in its current form.



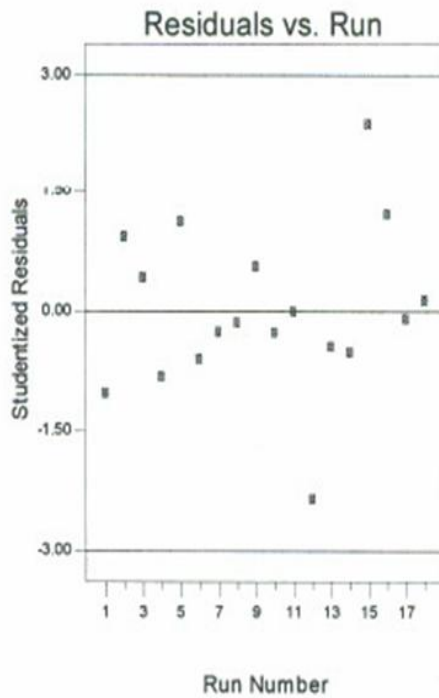
Appendix Figure A 8. Example Normal Plot of Residuals [Adapted from (16)]

When the residuals are plotted against their predicted values, it is desirable to see no discernable pattern. The residuals should be randomly distributed about all of their predicted values, resembling a shotgun blast. If a pattern emerges, it may mean there is a problem with the measurement devices in use. For example, a trend showing that the distribution of residuals continually increases (or decreases) on the plot might indicate the measurement device loses precision at certain settings. A sample of a residuals versus predicted plot is also given here.



Appendix Figure A 9. Example Residuals vs. Predicted Plot [Adapted from (16)]

Finally, the integrity of the experiment is verified by plotting the residuals versus the run order. Again, it is desired to see no pattern. The residuals should be randomly distributed as the runs progress. If a pattern emerges, it suggests that a time trend is at work influencing the results. A common pattern is the “megaphone effect”, where the residuals either continually grow or decrease in magnitude throughout the experiment. The plot below is an example of a residuals versus run plot.



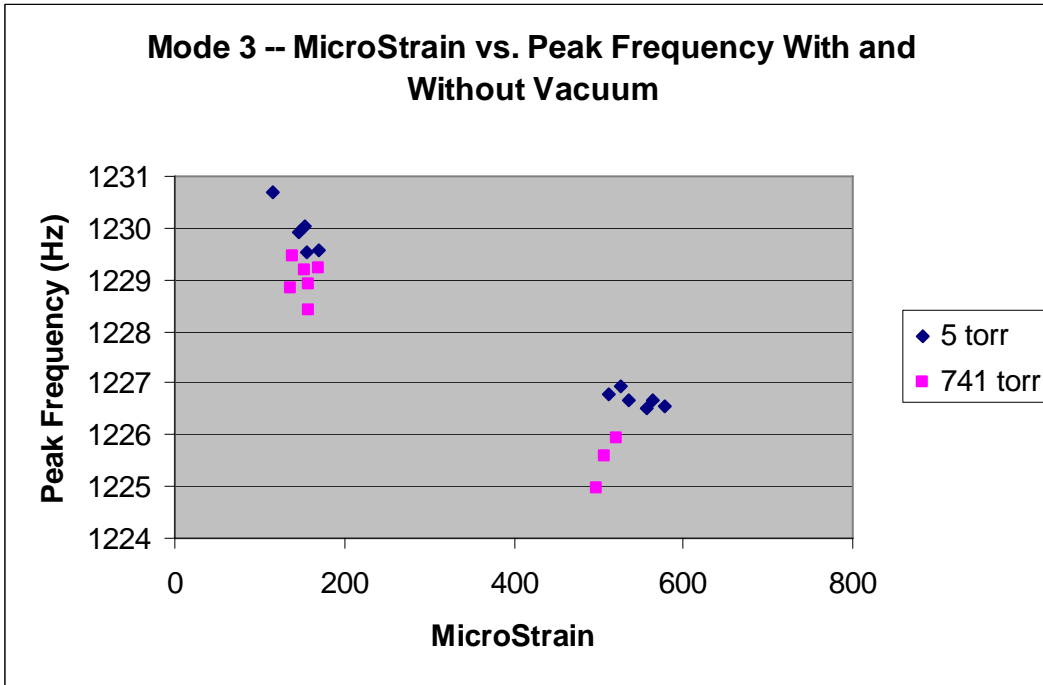
Data points should be randomly distributed. The “shotgun blast” look of this example plot shows the desired random distribution

Appendix Figure A 10. Example Residuals vs. Run Plot [Adapted from (16)]

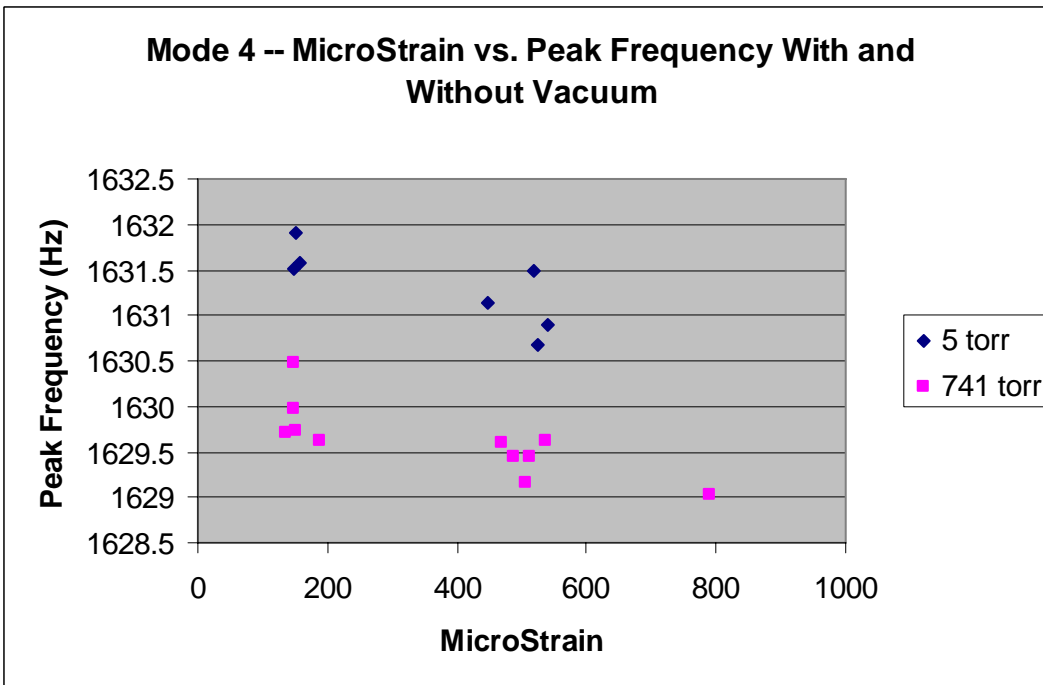
The ability of the model to account for all noise in the system is given by a term designated R. The closer this term gets to 1, the better the experimental model, and the better the results. In a traditional R term, adding factors to the experiment will increase the value of R, even if the model is not any better (15). In order to compensate for this, an adjusted R term is used instead. The equation for the adjusted R is shown below.

$$R_{adj}^2 = 1 - \frac{SS_{Error} / DOF_{Error}}{SS_{Total} / DOF_{Total}} \quad (\text{A.16})$$

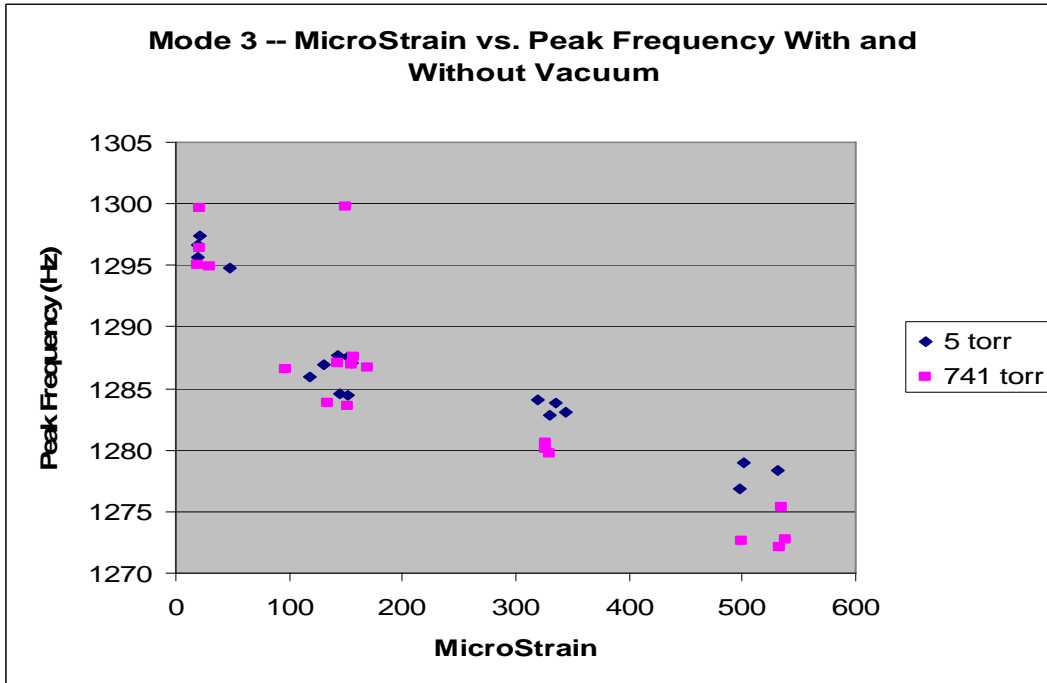
Appendix B: Peak Frequency Plots from Air Pressure Testing



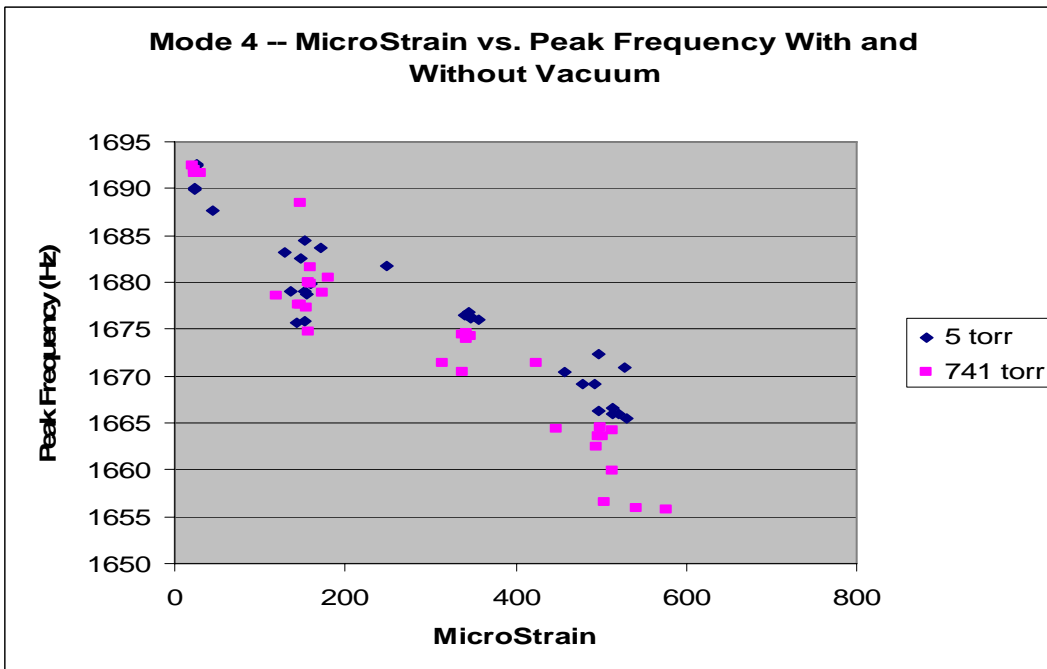
Appendix Figure B 1. MicroStrain vs. Peak Frequency for Uncoated Sample, Mode 3



Appendix Figure B 2. MicroStrain vs. Peak Frequency for Uncoated Sample, Mode 4

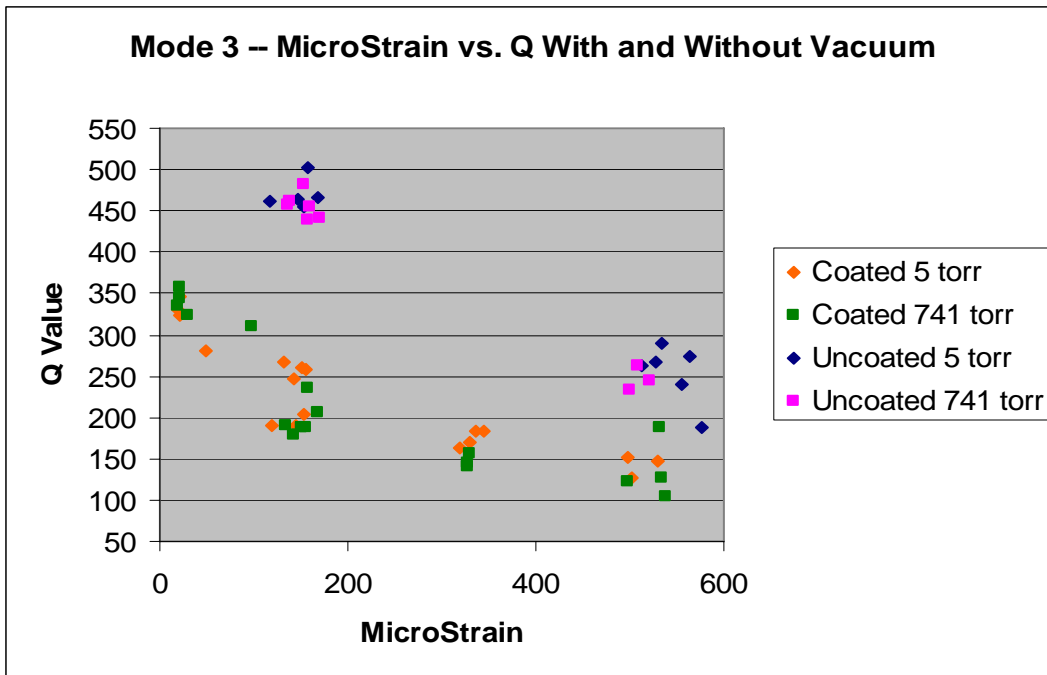


Appendix Figure B 3. MicroStrain vs. Peak Frequency for Coated Sample, Mode 3

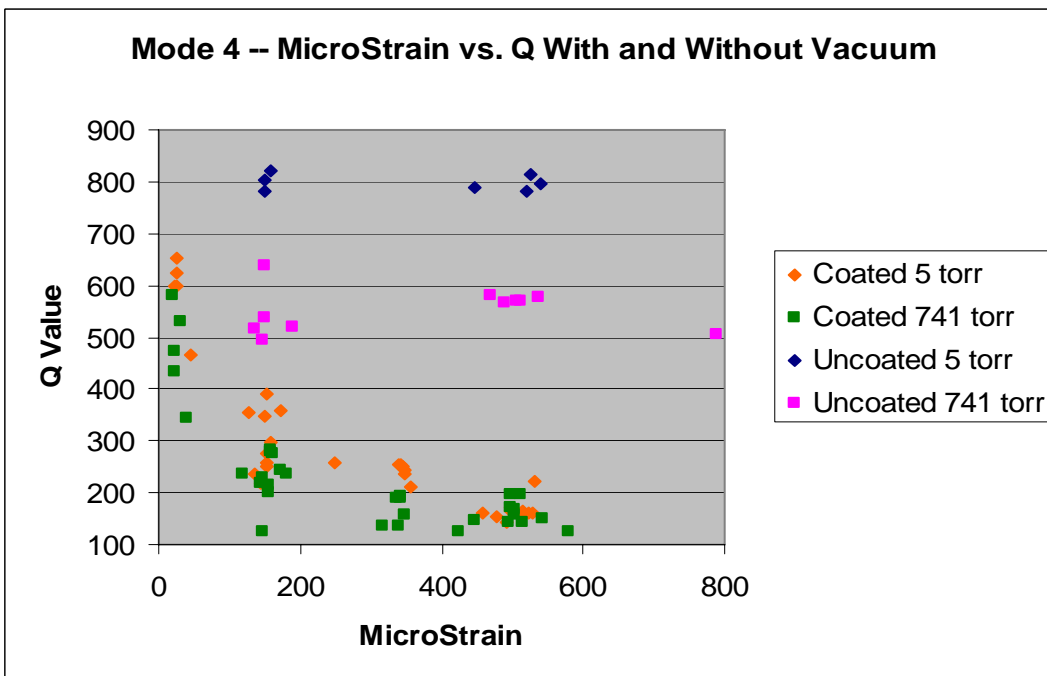


Appendix Figure B 4. MicroStrain vs. Peak Frequency for Coated Sample, Mode 4

Appendix C: Combined Coated and Uncoated Plots from Air Pressure Testing

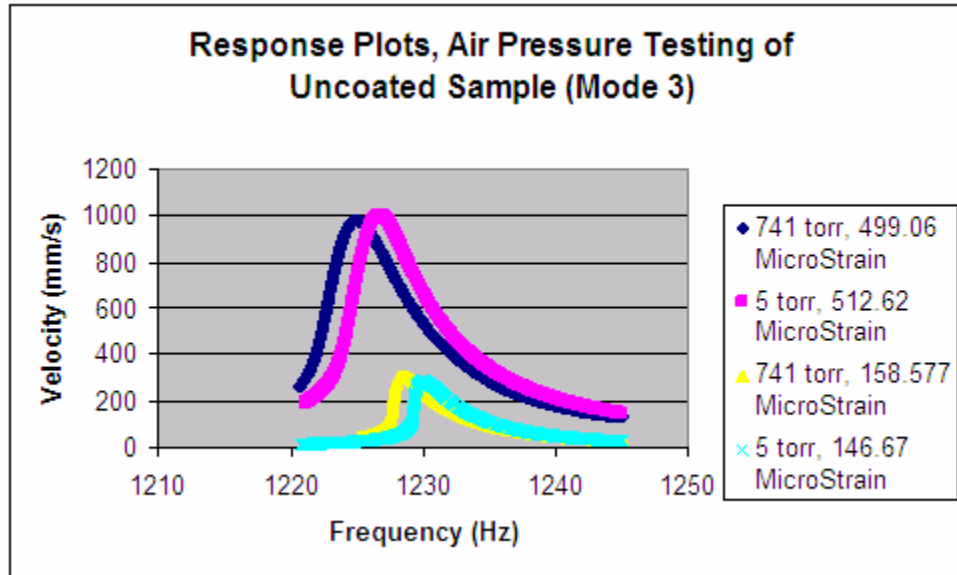


Appendix Figure C 1. Coated and Uncoated Strain vs. Q Value, Mode 3

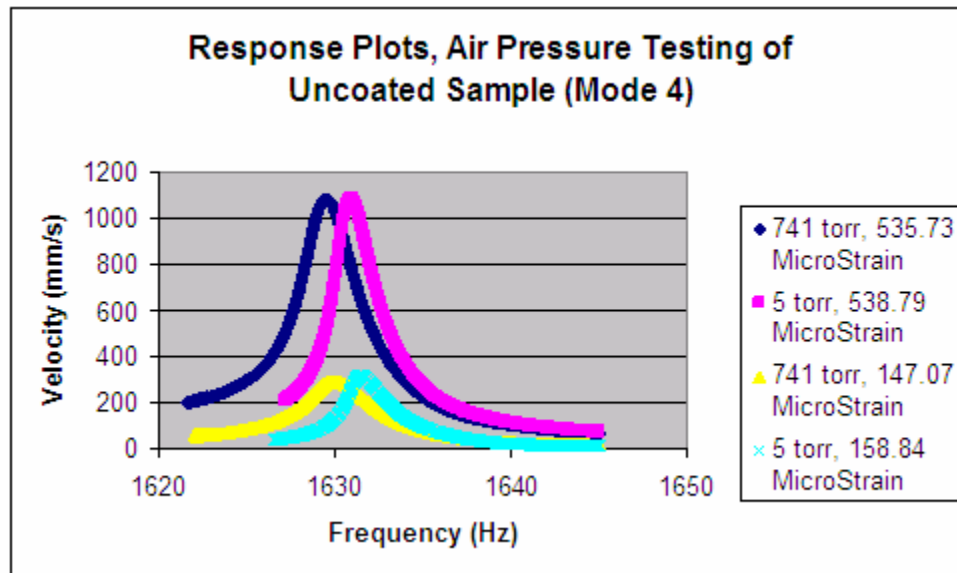


Appendix Figure C 2. Coated and Uncoated Strain vs. Q Value, Mode 3

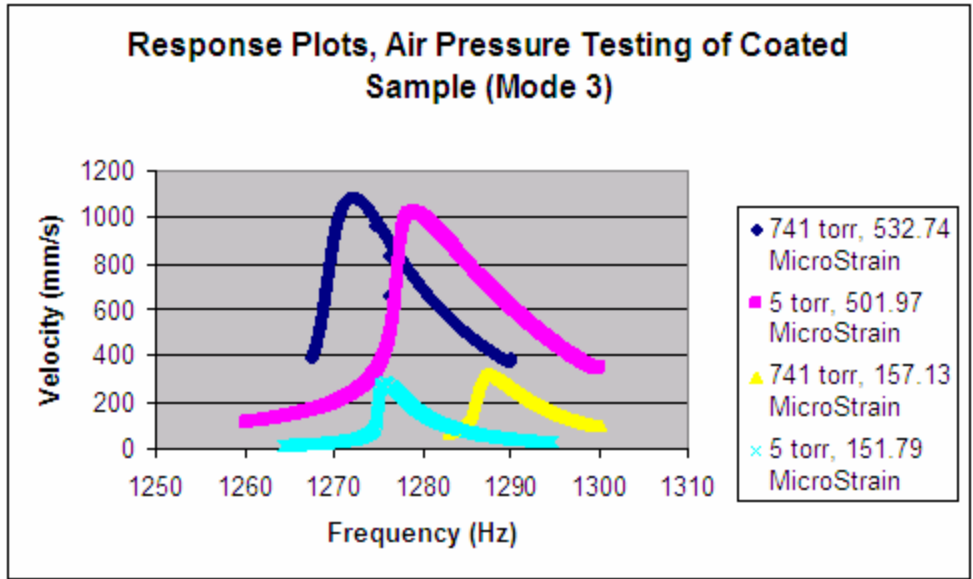
Appendix D: Typical Response Plots from ANOVA Testing



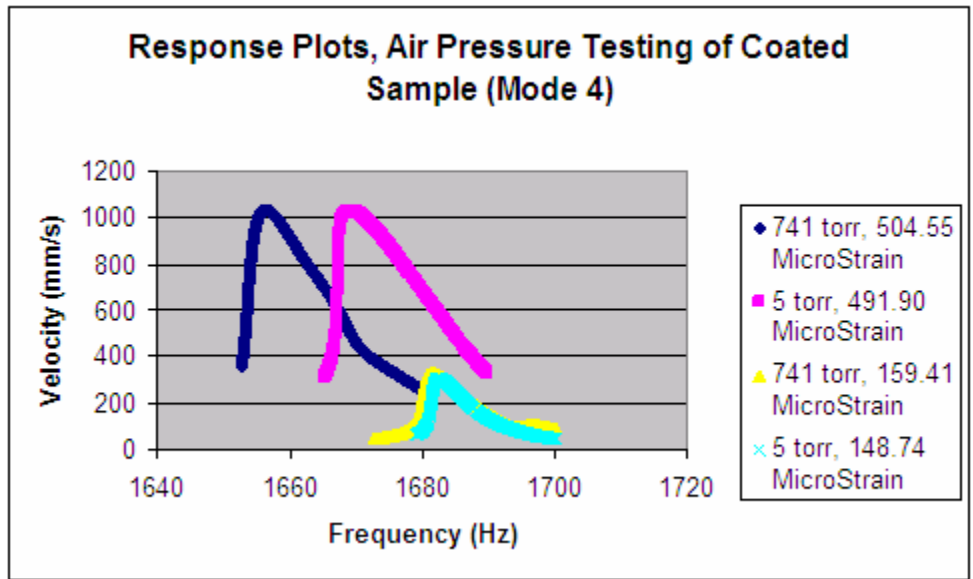
Appendix Figure D 1. Typical Responses for Uncoated Sample (Mode 3)



Appendix Figure D 2. Typical Responses for Uncoated Sample (Mode 4)



Appendix Figure D 3. Typical Responses for Coated Sample (Mode 3)



Appendix Figure D 4. Typical Responses for Coated Sample (Mode 4)

Appendix E: Data from ANOVA Testing with Strain Error

Appendix Table E 1. Results and Strain Error for Runs Used in ANOVA (Uncoated)

UNCOATED SAMPLE

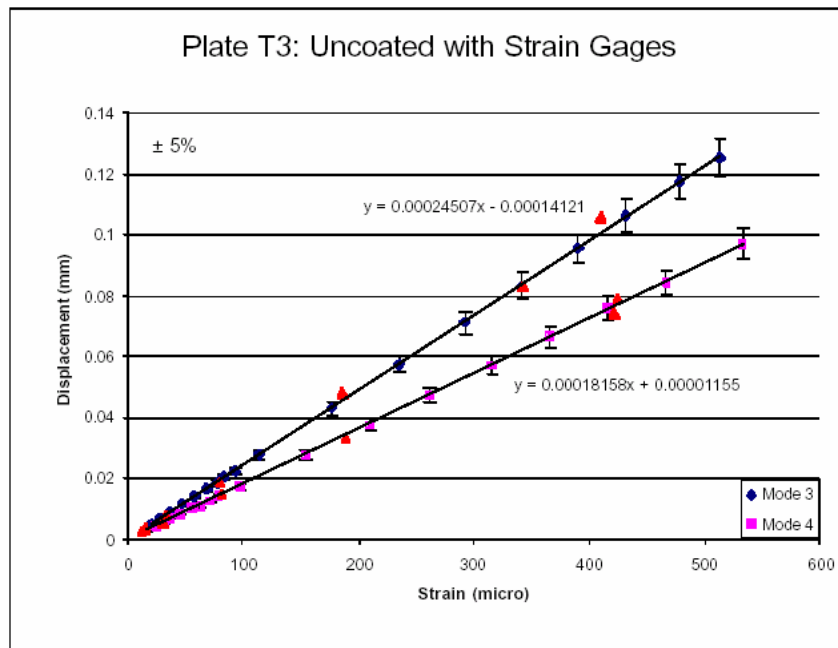
MODE	PRESSURE (torr)	MICROSTRAIN	Q VALUE	PEAK FREQ (Hz)	DESIRED STRAIN	% ERROR
3	5	512.62	261.91	1226.768	500	2.46
3	5	146.63	464.07	1229.902	150	2.30
3	5	526.84	267.66	1226.935	500	5.09
3	5	152.76	455.52	1230.052	150	1.81
3	5	534.61	290.87	1226.685	500	6.47
3	5	156.91	501.78	1229.519	150	4.40
3	741	158.577	454.91	1228.402	150	5.41
3	741	499.06	234.03	1224.951	500	0.19
3	741	152.36	481.98	1229.185	150	1.55
3	741	520.63	243.53	1225.935	520	0.12
3	741	158	438.83	1228.902	150	5.06
3	741	507.5	262.59	1225.568	500	1.48
4	5	538.79	795.45	1630.902	500	7.20
4	5	158.84	822.51	1631.569	150	5.57
4	5	519.73	783.01	1631.486	500	3.80
4	5	149.87	802.48	1631.902	150	0.09
4	5	524.46	815.23	1630.669	500	4.66
4	5	149.413	783.02	1631.519	150	0.39
4	741	535.73	578.49	1629.619	500	6.67
4	741	147.07	496.36	1629.969	150	1.99
4	741	149.51	639.3	1630.485	150	0.33
4	741	511.43	568.33	1629.452	500	2.23
4	741	507.05	571.56	1629.152	500	1.39
4	741	151.07	537.19	1629.735	150	0.71

Appendix Table E 2. Results and Strain Error for Runs Used in ANOVA (Coated)

COATED SAMPLE

MODE	PRESSURE (torr)	MICROSTRAIN	Q VALUE	PEAK FREQ (Hz)	DESIRED STRAIN	% ERROR
3	5	530.66	146.78	1278.314	500	5.78
3	5	154.76	258.45	1287.003	150	3.08
3	5	501.97	127.89	1279.002	500	0.39
3	5	151.79	259.64	1287.503	150	1.18
3	5	152.63	204.81	1284.482	150	1.72
3	5	497.44	151.68	1276.793	500	0.51
3	5	344.16	182.83	1283.052	325	5.57
3	5	20.76	347.48	1297.452	20	3.66
3	5	330.56	171.02	1282.818	325	1.68
3	5	19.34	330.76	1295.652	20	3.41
3	5	20.29	324.11	1296.636	20	1.43
3	5	319.49	162.52	1284.119	325	1.72
3	741	533.85	125.84	1275.36	500	6.34
3	741	155.74	187.75	1286.982	150	3.69
3	741	157.13	235.86	1287.565	150	4.54
3	741	532.74	187.87	1272.127	500	6.15
3	741	498.59	122.89	1272.586	500	0.28
3	741	151.76	188.97	1283.565	150	1.16
3	741	327.22	139.43	1280.568	325	0.68
3	741	20.78	358.41	1296.42	20	3.75
3	741	327.34	145.17	1280.101	325	0.71
3	741	329.41	155.72	1279.668	325	1.34
3	741	19.35	334.88	1295.053	20	3.36
3	741	21.69	345	1299.637	20	7.79
4	5	528.79	161.36	1670.919	500	5.44
4	5	151.93	390.58	1684.503	150	1.27
4	5	491.9	143.56	1669.106	500	1.65
4	5	148.74	346.57	1682.592	150	0.85
4	5	496.7	163.22	1666.356	500	0.66
4	5	158.62	298.6	1679.794	150	5.43
4	5	151.94	258.28	1679.002	150	1.28
4	5	153.89	274.05	1678.773	150	2.53
4	5	152.22	251.36	1675.918	150	1.46
4	5	531	223.28	1665.502	500	5.84
4	5	513.84	164.18	1665.94	500	2.69
4	5	521.6	159.6	1666.023	500	4.14
4	5	514.61	161.59	1666.606	500	2.84
4	5	341.55	255.91	1676.418	325	4.85
4	5	340.58	255.26	1676.435	325	4.57
4	5	23.48	598.45	1690.003	20	14.82
4	5	24.44	599.88	1689.953	20	18.17
4	5	345.82	250.86	1676.802	325	6.02
4	5	24.88	653.91	1692.414	20	19.61
4	741	512.767	197.2	1659.96	500	2.49
4	741	156.68	199.45	1674.688	150	4.26
4	741	159.41	284.19	1681.648	150	5.90
4	741	504.55	157.75	1656.502	500	0.90
4	741	494.95	142.73	1662.44	500	1.02
4	741	157.6	280.03	1680.03	150	4.82
4	741	498.71	197.8	1664.52	500	0.26
4	741	513.13	143.57	1664.148	500	2.56
4	741	145.31	217.03	1677.668	150	3.23
4	741	147.72	227.46	1677.668	150	1.54
4	741	155.48	214.1	1677.252	150	3.52
4	741	498.51	173.13	1663.585	500	0.30
4	741	337.61	190.61	1674.385	325	3.74
4	741	342.42	192.82	1674.535	325	5.09
4	741	22.5	432.28	1691.639	20	11.11
4	741	23.45	473.18	1691.926	20	14.71
4	741	20.7	581	1692.489	20	3.38
4	741	342.06	188.41	1673.918	325	4.99

Appendix F: Comparison of Strain Calculation Techniques



Appendix Figure F 1. Blackwell Experimental Displacement/Strain Relationship (4)

The strain/displacement relationship above was experimentally determined by Blackwell during a study using the same uncoated sample. It was found by placing strain gauges on the uncoated sample at the positions of maximum strain for each mode, and plotting these strains versus the corresponding displacements seen by the sample. Note that for each mode, the relationship between displacement and strain is linear.

In this appendix, the experimentally determined relationship above is compared to the FEA-derived strain/displacement proportion used in this study. The tables below show comparisons for several runs of the uncoated sample at various displacements for each mode. In all cases, the displacements were determined based on the peak velocity and peak frequency of the run. Experimentally determined values were found using the

linear equations in the above plot. FEA values were found using the strain/displacement proportion discussed in Chapter I.

Appendix Table F 1. FEA vs. Experimental - Differences in Strain Calculated (Mode 3)

MODE 3

RUN #	VELOCITY (mm)	FREQUENCY (Hz)	DISPLACEMENT (mm)	EXP STRAIN (microstrain)	FEA STRAIN (microstrain)	% DIFF
382	1131	1226.568	0.146754392	599.4026262	577.5537935	3.64510127
396	311	1228.402	0.040293965	164.9943897	158.5774172	3.88920646
410	1047	1226.685	0.135841904	554.8745807	534.6075564	3.65254151
419	308	1229.519	0.039869024	163.2604315	156.905056	3.89278376
316	186	1234.368	0.023982167	98.43463874	94.38212599	4.11695801
318	682	1230.485	0.088212104	360.5227662	347.1598698	3.70653331
28	1015	1238.426	0.130441599	532.8388159	513.3545871	3.65668345
30	63.1	1245.577	0.00806267	33.47566197	31.73074325	5.21249952

Appendix Table F 2. FEA vs. Experimental - Differences in Strain Calculated (Mode 4)

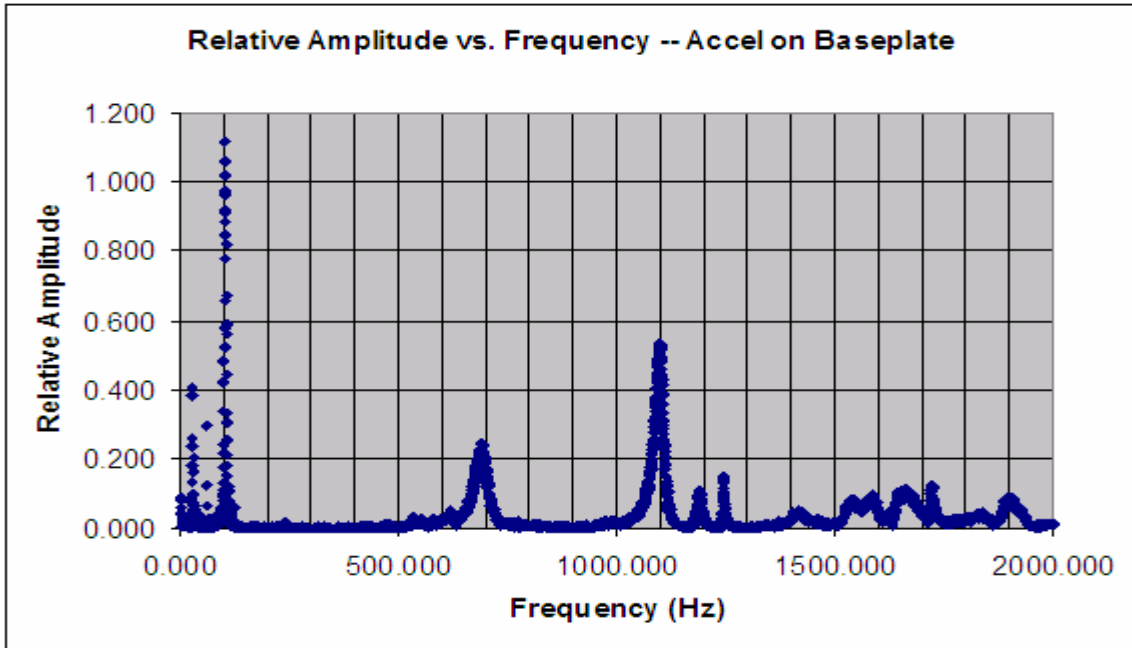
MODE 4

RUN #	VELOCITY (mm)	FREQUENCY (Hz)	DISPLACEMENT (mm)	EXP STRAIN (microstrain)	FEA STRAIN (microstrain)	% DIFF
398	301	1630.485	0.02938122	161.7450689	149.5081576	7.5655446
403	1047	1631.486	0.102137086	562.427226	519.7308931	7.59144134
411	1056	1630.669	0.103066668	567.5466332	524.4611285	7.5915356
416	304	1629.735	0.029687712	163.4329861	151.0677612	7.56592974
317	398	1627.902	0.038911229	214.2288738	198.0022007	7.57445658
319	1173	1627.002	0.114744019	631.8563107	583.8820543	7.59258958
29	1183	1622.377	0.116052125	639.060329	590.5384309	7.59269444
31	185.2	1625.602	0.018132049	99.7934751	92.26605658	7.54299668

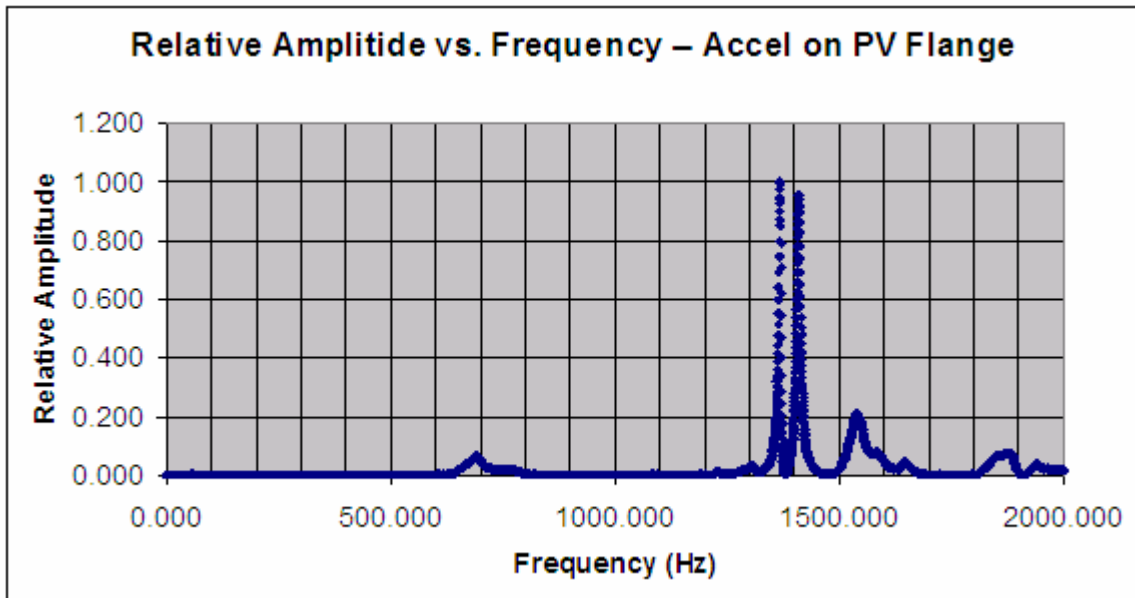
The tables above show that the percent difference in strain calculations does not exceed 5.22% for mode 3, and remains near 7.59% for mode 4. The values for strain determined by the experimental data are consistently higher than the FEA-derived values. However, the FEA-derived values also remain consistently close to the experimental values over the entire range of displacements seen in this study. Based on this data, it was decided that the FEA strain/displacement proportions were acceptable for use in this study.

The use of FEA strain/displacement proportions for samples in the free condition was especially valuable, since no experimental data for a strain relationship existed. The close relationship between experimental data and FEA data shown above served as justification to use FEA proportions in determining strain on the free condition samples.

Appendix G: Additional Ping Testing Results



Appendix Figure G 1. Baseplate to Baseplate Ping Test Results



Appendix Figure G 2. Baseplate to Pressure Vessel Flange Ping Testing Results

Bibliography

1. Adekeye, K. S. and Kunert, J. *On the Comparison of Run Orders of Unreplicated 2^{k-p} Designs in the Presence of a Time-Trend*. Fachbereich Statistik, Universität Dortmund, Dortmund, Germany.
2. Allen, K. S. *Evaluation Techniques for Determining Damping Mechanisms on Titanium Plates*. MS Thesis, AFIT/GAE/ENY/05-M01. Department of Aeronautics and Astronautics, Air Force Institute of Technology (AU), Wright-Patterson AFB OH, March 2005.
3. Baker, W.E., Woolam W.E., and Young D. “Air and Internal Damping of Thin Cantilever Beams”, *International Journal of Mechanical Sciences*, 9: 743-766 (1967).
4. Blackwell, C. M. *The Evaluation of the Damping Characteristics of a Hard Coating on Titanium*. MS Thesis, AFIT/GAE/ENY/04-M03. Department of Aeronautics and Astronautics, Air Force Institute of Technology (AU), Wright-Patterson AFB OH, March 2004.
5. Cobb, R. G. Air Force Institute of Technology, Printed Class Material on Vibration Damping and Control, December 2005.
6. Cowles, B.A. “High Cycle Fatigue in Aircraft Gas Turbines – an Industry Perspective”, *International Journal of Fracture*, 80: 147-163 (1996).
7. Edwins, D.J. “Damping Measurements”, *Encyclopedia of Vibration*, pp. 332-335. San Diego, CA: Academic Press, 2001.
8. Garrison, B, “High Cycle Fatigue (HCF) Science and Technology Program Report”, AFRL-PR-WP-TR-20012010, Feb. 2001.
9. Hoover, T. M. *An Electromagnetic Tool for Damping and Fatigue Analysis*. MS Thesis, AFIT/GSS/ENY/04-04. Department of Aeronautics and Astronautics, Air Force Institute of Technology (AU), Wright-Patterson AFB OH, March 2004.

10. Ivansic, F. T. and Palazotto, A.N. “Experimental Considerations for Determining the Damping Effects of Hard Coatings”, *Journal of Aerospace Engineering*, 18: 8-17 (2005).
11. Ivansic, F. T. *The Effect of a Hard Coating on the Damping and Fatigue Life of Titanium*. MS Thesis, AFIT/GAE/ENY/03-12. Department of Aeronautics and Astronautics, Air Force Institute of Technology (AU), Wright-Patterson AFB OH, March 2003.
12. “Material Properties”, *Matweb, Material Property Data*, September, 2005, www.matweb.com.
13. Meirovitch, L. *Elements of Vibration Analysis*. Boston: McGraw-Hill, 1986.
14. *Metallic Materials and Elements for Aerospace Vehicle Structures, MIL-HDBK-5J*. Department of Defense Handbook, 31 January 2003.
15. Montgomery, D. C. *Design and Analysis of Experiments*. 5th ed. New York: John Wiley & Sons, Inc., 2003.
16. Ness, G. United States Air Force Academy, Printed Class Material and Computer Files on Statistical Design and Analysis of Experiments, May 2004.
17. Patsias, S., Byrne, A., and Shipton, M. “Hard Damping Coatings: Optimization of Damping Effectiveness by Controlling the Deposition Parameters”, *Proceedings, 9th National Turbine Engine High Cycle Fatigue Conference*, Pinehurst, NC, March 2004.
18. Patsias, S., and Robin, W. “Hard Damping Coatings: Material Properties and F.E. Prediction Methods”, *Proceedings, 8th National Turbine Engine High Cycle Fatigue Conference*, Monterey, CA, April 2003.
19. Patsias, S., Saxton, C., and Shipton, M. “Hard Damping Coatings: An Experimental Procedure for Extraction of Damping Characteristics and Modulus of Elasticity”, *Materials Science and Engineering, A 370*: 412-416 (2004).

20. Ritchie, R.O., Boyce, B.L., Campbell, J.P., Roder, O., Thompson, A.W., and Mulligan, W.W. "Threshold for High Cycle Fatigue in a Turbine Engine Ti-6Al-4V Alloy", *International Journal of Fatigue*, 21: 653-662 (1999).
21. Shen, M.-H. H. "Development of a Free Layer Damper Using Hard Coatings", *Proceedings, 7th National Turbine Engine High Cycle Fatigue Conference*, West Palm Beach, FL, May 2002.
22. Shipton, M. and Patsias, S. "Hard Damping Coatings: Internal Friction as the Damping Mechanism", *Proceedings, 8th National Turbine Engine High Cycle Fatigue Conference*, Monterey, CA, April 2003.
23. Stephen, D.G. and Scavullo, M.A. "Investigation of Air Damping of Circular and Rectangular Plates, a Cylinder, and a Sphere", NASA TN, D-1865, April 1965.
24. Tarnopolsky, A.Z. "Aerodynamic Damping of Randomly Excited Plates in Stationary and Moving Air", *Journal of Sound and Vibration*, 253: 795-805 (2002).
25. Torvik, P. J., Patsias, S., and Tomlinson G.R. "Characterizing the Behavior of Hard Coatings: Comparisons from Two Methodologies", *Proceedings, 7th National Turbine Engine High Cycle Fatigue Conference*, West Palm Beach, FL, May 2002.
26. Torvik, P. J. "Determining Material Properties of Nonlinear Damping Materials from System Response Data", *Proceedings, 8th National Turbine Engine High Cycle Fatigue Conference*, Monterey, CA, April 2003.
27. Torvik, P. J. "Review of Damping Data from Mg Spinel Coated Plates", 18 March 2003.
28. Ungar, E. E. "Damping Materials", *Encyclopedia of Vibration*, pp. 327-331. San Diego, CA: Academic Press, 2001.
29. Wertz, J. R. and Larson, W. J. (Editors). *Space Mission Analysis and Design*. 3rd ed. El Segundo, CA: Microcosm Press, 1999.

REPORT DOCUMENTATION PAGE				<i>Form Approved OMB No. 074-0188</i>	
<p>The public reporting burden for this collection of information is estimated to average 1 hour per response, including the time for reviewing instructions, searching existing data sources, gathering and maintaining the data needed, and completing and reviewing the collection of information. Send comments regarding this burden estimate or any other aspect of the collection of information, including suggestions for reducing this burden to Department of Defense, Washington Headquarters Services, Directorate for Information Operations and Reports (0704-0188), 1215 Jefferson Davis Highway, Suite 1204, Arlington, VA 22202-4302. Respondents should be aware that notwithstanding any other provision of law, no person shall be subject to a penalty for failing to comply with a collection of information if it does not display a currently valid OMB control number.</p> <p>PLEASE DO NOT RETURN YOUR FORM TO THE ABOVE ADDRESS.</p>					
1. REPORT DATE (DD-MM-YYYY) 23-03-2006		2. REPORT TYPE Master's Thesis		3. DATES COVERED (From - To) Aug 2004 - Mar 2006	
4. TITLE AND SUBTITLE Evaluation of Factors Contributing to Damping of Coated and Uncoated Titanium Plates				5a. CONTRACT NUMBER	
				5b. GRANT NUMBER	
				5c. PROGRAM ELEMENT NUMBER	
6. AUTHOR(S) Lee, Dustin W., 2 nd Lieutenant, USAF				5d. PROJECT NUMBER	
				5e. TASK NUMBER	
				5f. WORK UNIT NUMBER	
7. PERFORMING ORGANIZATION NAMES(S) AND ADDRESS(S) Air Force Institute of Technology Graduate School of Engineering and Management (AFIT/EN) 2950 Hobson Way, Building 641 WPAFB OH 45433-7765				8. PERFORMING ORGANIZATION REPORT NUMBER AFIT/GA/ENY/06-M06	
9. SPONSORING/MONITORING AGENCY NAME(S) AND ADDRESS(ES) Dr. Charles Cross AFRL/PRTS 1950 5 th Street Bldg. 252 WPAFB OH 45433-7251 DSN: 656-5530				10. SPONSOR/MONITOR'S ACRONYM(S)	
				11. SPONSOR/MONITOR'S REPORT NUMBER(S)	
12. DISTRIBUTION/AVAILABILITY STATEMENT APPROVED FOR PUBLIC RELEASE; DISTRIBUTION UNLIMITED.					
13. SUPPLEMENTARY NOTES					
14. ABSTRACT High Cycle Fatigue (HCF) is the leading cause of component failure in gas turbine engines today, which poses great risk to aircraft, engines, and their crews. Mitigation of HCF effects has become a priority topic, and the damping benefits of hard coatings are being reevaluated for this purpose. Research was conducted to further understanding of damping measurements on these coatings. This study continues work to characterize the damping effects of a magnesium aluminate spinel (mag spinel) coating applied to a titanium plate via vibration testing. Two different plate sizes were evaluated in a clamped-free-free-free condition and a free-free-free-free condition, respectively. In both the clamped and free studies, the second bending and two-stripe mode shapes were identified and studied. Clamped specimens were tested in order to determine various factors affecting damping. Using these factors, it was shown that air damping has a statistically significant impact on damping, where the impact is dependent on mode shape. The amount of damping introduced by the air was, however, minute compared to the losses introduced by the constraint blocks. Testing on free condition specimens explored another possible method to obtain a damping comparison between coated and uncoated samples with fewer damping losses.					
15. SUBJECT TERMS Vibration, High Cycle Fatigue, Damping, Fatigue, Titanium, Magnesium Aluminate Spinel, Resonance, Resonance Frequency, Resonance Mode, Finite Element Analysis, Air Damping, ANOVA					
16. SECURITY CLASSIFICATION OF:			17. LIMITATION OF ABSTRACT UU	18. NUMBER OF PAGES 260	19a. NAME OF RESPONSIBLE PERSON Dr. A. N. Palazotto (ENY)
a. REPOR T U	b. ABSTRAC T U	c. THIS PAGE U			19b. TELEPHONE NUMBER (Include area code) (937) 255-3636, e-mail: Anthony.Palazotto@afit.edu